6-4-2024

A Pilot Study Comparing Muscle Activation and Kinematic Parameters Between Professional and Non-Professional Tennis Players

Anton S. Petrenko

A Pilot Study Comparing Muscle Activation and Kinematic Parameters Between Professional and Non-Professional Tennis Players

Anton Sergeyevich Petrenko

A Thesis Submitted to the Graduate Faculty of

GRAND VALLEY STATE UNIVERSITY

In

Partial Fulfillment of the Requirements

For the Degree of

Master of Science in Engineering, Biomedical Engineering

Padnos College of Engineering and Computing

April 2024

Approval Page

GRAND VALLEY STATE UNIVERSITY

The signatories of the committee below indicate that they have read and approved the thesis of **Anton Sergeyevich Petrenko** in partial fulfillment of the requirements for the degree of **Master of Science in Biomedical Engineering**.

4/25/2024

Dr. Yunju Lee, Thesis committee chair — Date

4/23/2024

Dr. Samhita Rhodes, Committee member — Date

4/25/24

Dr. Sunghwan Joo, Committee member — Date

Accepted and approved on behalf of the Padnos College of Engineering and Computing

Dean of the College

4/25/2024

Date

Accepted and approved on behalf of the Graduate Faculty

Trista Bergerud

Dean of The Graduate School

6/4/2024

Date

Acknowledgements

I am deeply grateful to Dr. Yunju Lee for her unwavering support and encouragement throughout this endeavor. Her guidance has been invaluable in navigating the complexities of this research journey. Additionally, I extend my heartfelt thanks to Dr. Samhita Rhodes for generously sharing her wealth of knowledge, which proved instrumental in implementing and executing this study. I would also like to that Dr. Sunghwan Joo for all his recommendations for the revision of this manuscript. I am indebted to my fiancée, Teresa Cameon, for her unwavering support, attentive listening, and ingenious contribution of creating a smaller research vest, which greatly facilitated data collection. Furthermore, I am thankful to my family for their steadfast support and for instilling in me the values of perseverance and determination, especially as we embarked on the journey of immigrating across the ocean. I extend my gratitude to all the participants who generously donated their time and effort to contribute to this research endeavor. Lastly, I would like to acknowledge the School of Engineering Graduate Program for their provision of space, equipment, and funding, which were essential for the successful execution of this study. Their support has been invaluable in bringing this research to fruition.

Abstract

Tennis, a widely played sport across various age and skill groups, prompts continual skill improvement among competitive players seeking a competitive edge. This study explores two approaches for enhancing playing style: motion capture (MoCap) and surface electromyographic (sEMG) signals. The study addresses a gap in simultaneous examination of MoCap and entire dominant leg muscle activation, particularly concerning the influence of skill level and gender on various tennis strokes. To fill this void, the research records and analyzes MoCap and dominant leg sEMG data during serves and strokes on both court sides. The hypothesis posits differences in muscle activation and body mechanics between professional and non-professional players, as well as between male and female players. Recording employed XSENS MVN MoCap and an EMG system with WinDaq Pro Data Acquisition software. MoCap and sEMG data were recorded at rates of 60 Hz and 1200 Hz, respectively, focusing on seven target muscles on the dominant side. Gel-type electrodes were strategically placed on the skin for sEMG data collection and full body XSENS sensors were placed according to guidelines. Following comprehensive warm-up, baseline readings and various tennis strokes were recorded on both court sides. Data processing and analysis were conducted in MATLAB, encompassing filtering, rectification, interpolation, and visualization. The study's findings contribute valuable insights into the relationship between motion and muscle activity in tennis, shedding light on skill-level and gender-related distinctions in player performance.

Table of Contents

List of Tables

List of Figures

Abbreviations

MoCap	Motion Capture
sEMG	Surface electromyography
IMUs	Inertial measurement units
Hz	Hertz
BNC	Bayonet Neill–Concelman
V	Volt
LEDs	Light emitting diodes
R	Resistance
Ω	Ohms
°	Degrees
De	Deltoid
GM	Gluteus maximus
BF	Biceps femoris
RF	Rectus femoris
VM	Vastus medialis
GaM	Gastrocnemius medialis
TA	Tibialis anterior
cm	Centimeters
kg	Kilograms
PCB	printed circuit board

Chapter 1 – Introduction

1.1 Introduction

Tennis is a popular sport played by individuals of diverse ages and skill levels. Competitive tennis players strive to enhance their performance and gain an edge over their opponents. Two technologies, Motion Capture (MoCap) and Surface Electromyography (sEMG), hold potential to yield significant insights into tennis performance.

Motion capture technology (MoCap) digitally tracks and records movements of living beings or objects by using infrared or depth-sensitive cameras with reflective markers or inertial measurement units (IMUs) [1-4]. The data obtained from MoCap might be analyzed to diagnose and rectify kinematic errors that hinder performance [5].

Surface electromyography (sEMG) is a technique that records the electrical activity produced in muscle fibers after stimulation by innervating motor neurons [11]. The signal provided by this study technique enables the assessment of muscle activation patterns and identification of areas where muscle activation can be optimized for different strokes [6].

1.2 Purpose

The objective of this research is to elucidate the differences between professional and non-professional tennis players, including male and female sexes, in terms of muscle activation patterns and kinematic parameters during forehands, backhands, and serves. The study findings will be used to develop more effective training programs, thereby improving performance analysis and coaching techniques for tennis players of all levels. Similarly, the field of sports science will be advanced as the findings from this study will contribute valuable data and knowledge to the understanding of human movement and performance in tennis.

1.3 Research Question

How do muscle activation and body mechanics differ between professional and non-professional tennis players, and between male and female tennis players?

1.4 Significance

This study will improve understanding of shot performance in male and female expert and non-expert level athletes. It will also enhance comprehension of the body mechanics, force generation, and accuracy exhibited by advanced tennis players in contrast to those at intermediate or beginner levels. This knowledge can be applied to develop more effective training programs for less experienced players, potentially mitigating injuries and enhancing their performance.

Chapter 2 – Review of Literature

2.1 Motion Capture (MoCap) and Surface Electromyography (sEMG) in Tennis Performance Analysis

2.1.1 Motion Capture (MoCap)

2.1.1.1 MoCap Systems

As a form of recreation and even competition, tennis can be played by individuals across a wide range of ages and skill levels. These players, especially those in the competitive sphere, are constantly looking for improvements in their skills to give themselves an edge over their opponents. One way to find improvements in playing style comes from the use of motion capture (MoCap) or kinematics. MoCap involves digitally tracking and recording the movements of objects or living beings in space using either reflective markers coupled with an infrared camera system, depth sensitive cameras, or inertial measurement units (IMUs) [1-4]. Data obtained from the MoCap system is then analyzed and used to improve the efficiency of the athlete by making performance-enhancing modifications [5].

For MoCap, two systems are generally used as the gold standard for accuracy and reliability of data: Vicon (Oxford Metrics, Oxford, UK) and Qualisys (Qualisys AB, Goteborg, Sweden) [6]. Both systems require at least eight cameras that must be specifically set up and calibrated, often in a laboratory setting as shown in Figure 1. Not only that, but the subject who is being recorded must also have numerous reflective markers placed on specific locations on the body. After the markers are placed, the individual can then perform the activity that is being analyzed.

Figure 1. Example of Vicon system with reflective markers on subjects as well as camera and laboratory set up [21]

2.1.1.2 Advantages of IMUs

However, despite the number and orientation of the cameras as well as the number of markers placed, some markers can become obstructed and therefore not recorded. Analysis without all the markers captured at all times can become challenging. For example, among all the markers that need to be placed on the subject's body, two need to be placed on both anterior, superior iliac spines (ASIS). If the subject is then tasked with performing any variation of a squatting motion, the markers placed on the ASIS become obstructed for a certain amount of time. With those markers absent, analysis of certain parameters cannot be completed for the time that the markers were absent.

For these reasons, in recent years, there has been a trend toward using IMUs for MoCap. The typical IMU is compact and light enough to be secured with surgical tape to the subject or placed in a special uniform that houses all the sensors and can be worn by the subject. Along with their portability and unobtrusiveness, IMUs can be used for MoCap of athletes in their

natural training environment rather than in a laboratory setting without any impedance to motion [7]. Because these sensors do not require a camera system, none of the sensors can become obstructed during any prescribed exercise. An example of the typical XSENS setup can be seen in Figure 2.

Figure 2. Example of typical XSENS setup with IMU sensors shown in orange [22]

2.1.1.3 MoCap Applications in Tennis

Numerous studies have been conducted involving the use of IMUs in the analysis of tennis. For example, one study using XSENS IMU sensors found that with a greater knee angle and higher knee extension, the pre-impact racket velocity increased as shown in the bottom image of Figure 3 by the blue line being substantially higher than the red line [8]. Using the information obtained from this study, beginner and intermediate tennis players have a mechanism by which they can increase their serve speed.

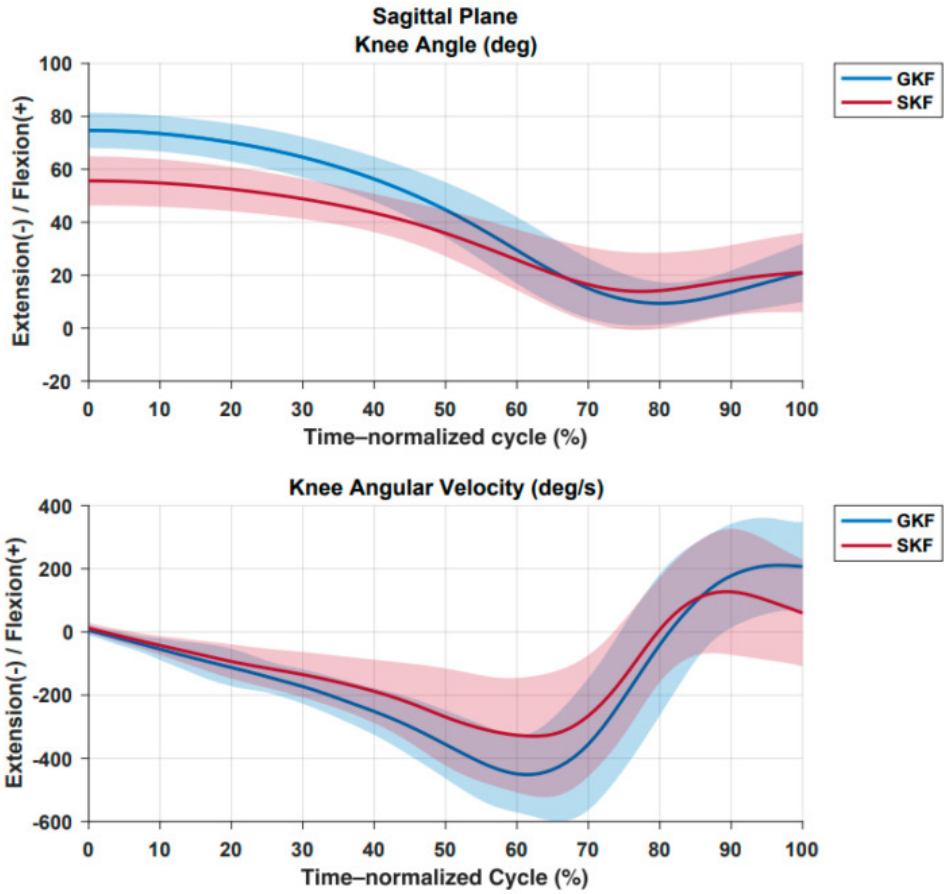

Figure 3. The top graph illustrates knee angle, while the bottom graph shows knee angular velocity. The solid lines represent mean values, and the shadows indicate standard deviation. The blue lines represent the greater knee flexion group (GKF), while the red lines represent the smaller knee flexion group (SKF). The serve cycle was time normalized between the events "maximum knee flexion" and "racket-ball impact" [8].

Another study also using XSENS IMU sensors found that highly skilled players have greater motor control consistency with differences visible only in shoulder alignment to the baseline [9]. This is shown in Figure 4 by the overlaid red and black lines which depict cross-court and inside-out returns. The red and black lines are overlaid in every instance except for trunk base line rotation and shoulder rotation. From this data, tennis players or coaches can predict the direction of their opponent's forehand return by observing the opponent's shoulder or trunk alignment.

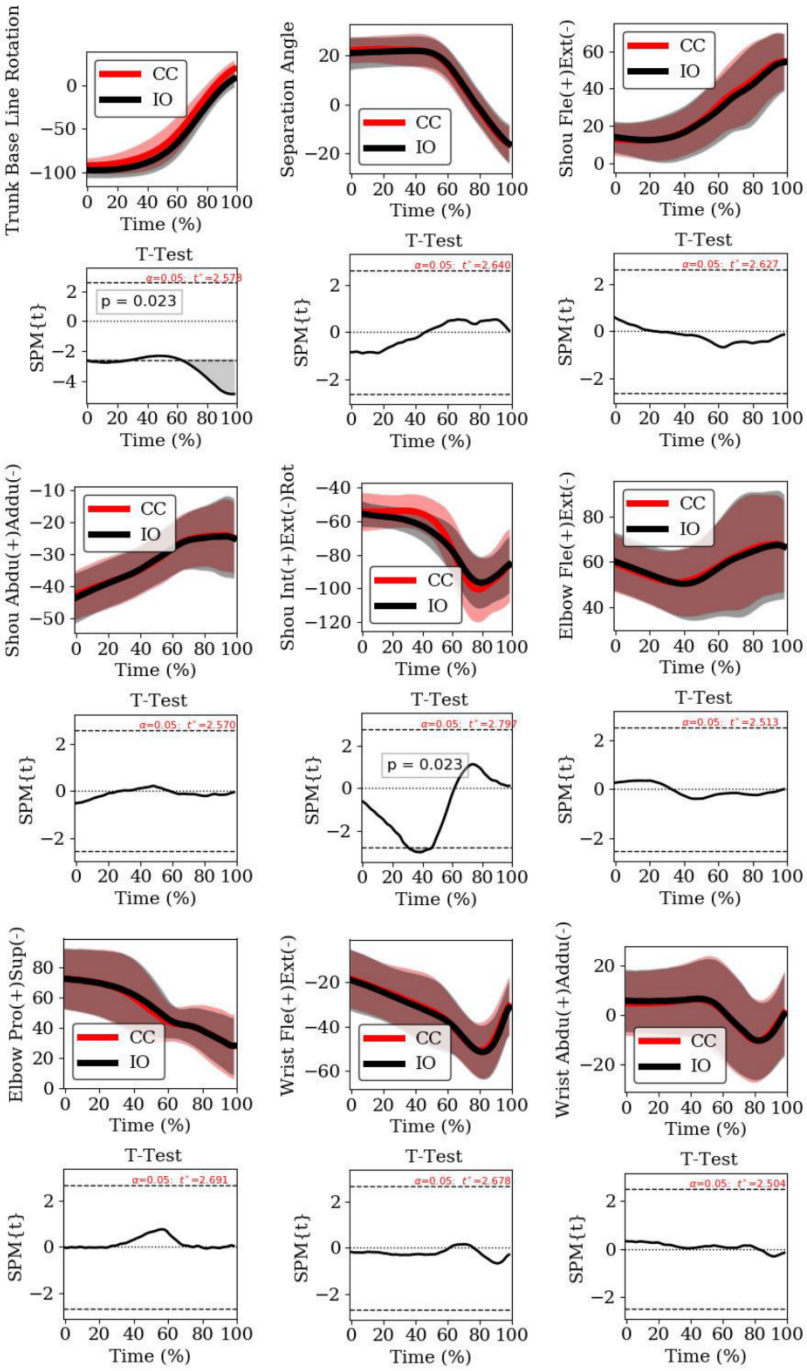

Figure 4. One-dimensional statistical parameter mapping analysis assessed joint angles for cross-court (red line) and inside-out (black line) directions. Parameters included trunk baseline rotation, separation angle, shoulder and elbow movements, as well as wrist flexion/extension and abduction/adduction. Threshold test values (t*) are denoted by horizontal dashed lines, with statistically significant differences marked in grey shaded regions [9].

Furthermore, Buthe et al. found that through the placement of three IMUs, one on the racket and two on the dorsal surface of either foot, a predictive algorithm could be developed that tells what kind of shot was taken with 95% accuracy [10]. Subsequently, a virtual assistant can be set up that not only visualizes when each step during tennis play occurs but also when each shot happens thereby guiding improvements in the timing of shots. Implementing all these studies allows an expert player or trainer to make improvements in the body angles during play, in anticipation or disguising of shots, and in timing of steps.

2.1.2 Surface Electromyography (sEMG)

2.1.2.1 sEMG Principles

Another way for finding improvements in playing style involves looking at the surface electromyographic (sEMG) signals of muscles. The sEMG signal shows the electrical activity generated in muscle fibers after excitation by innervating motor neurons; in essence, how much of and how long a particular muscle is active [11]. Examples of wireless and wired EMG systems can be seen in Figure 5.

Figure 5. Examples of wireless and wired EMG systems. Shown on the left is the Noraxon EMG system and on the right is the MLS EMG system [23-24]

2.1.2.2 sEMG Studies in Tennis

To this end, several sEMG studies have been performed on tennis players. One study using Liberty Technology electrodes found the importance of abdominal and low back exercises after sEMG electrodes were connected to the rectus abdominus, the external oblique, the internal oblique, and lumbar erector spinae muscles while the subject performed three different types of serves [12]. This study also looked at the timing of the different trunk muscles activation during the serves as seen in Figure 6, thereby giving the beginner or intermediate player an aiming point for which muscles should be activated before, during, and after a serve.

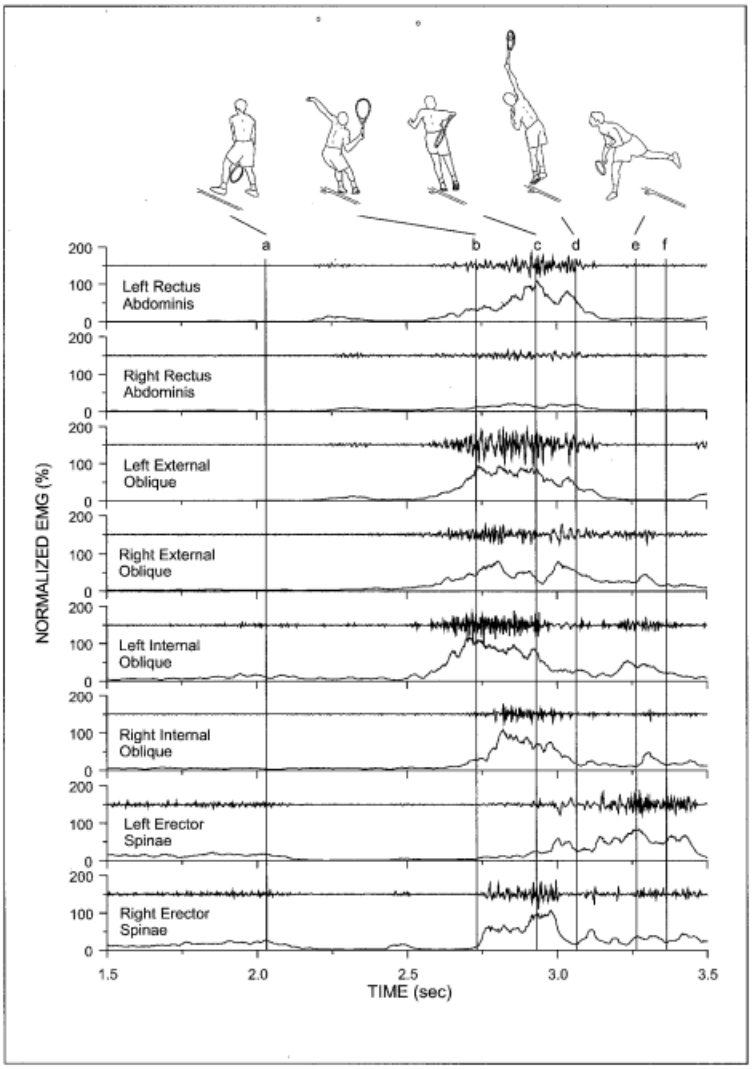

Figure 6. Raw and rectified EMG data collected from a topspin trial. Depicted by vertical lines are (a) beginning of the ascending windup, (b) end of ascending windup, (c) end of descending windup, (d) ball impact, (e) landing, and (f) end of the follow-through phase [12]

A similar study by Knudson & Blackwell using the Noraxon EMG system illustrated non-significant differences in muscle activation between open and square stance forehand drives as shown by the non-significant EMG depictions in Figure 7 [13]. Again, this serves as a useful tool for expert-level players or coaches as to which muscles to target for open and square stance forehand drives.

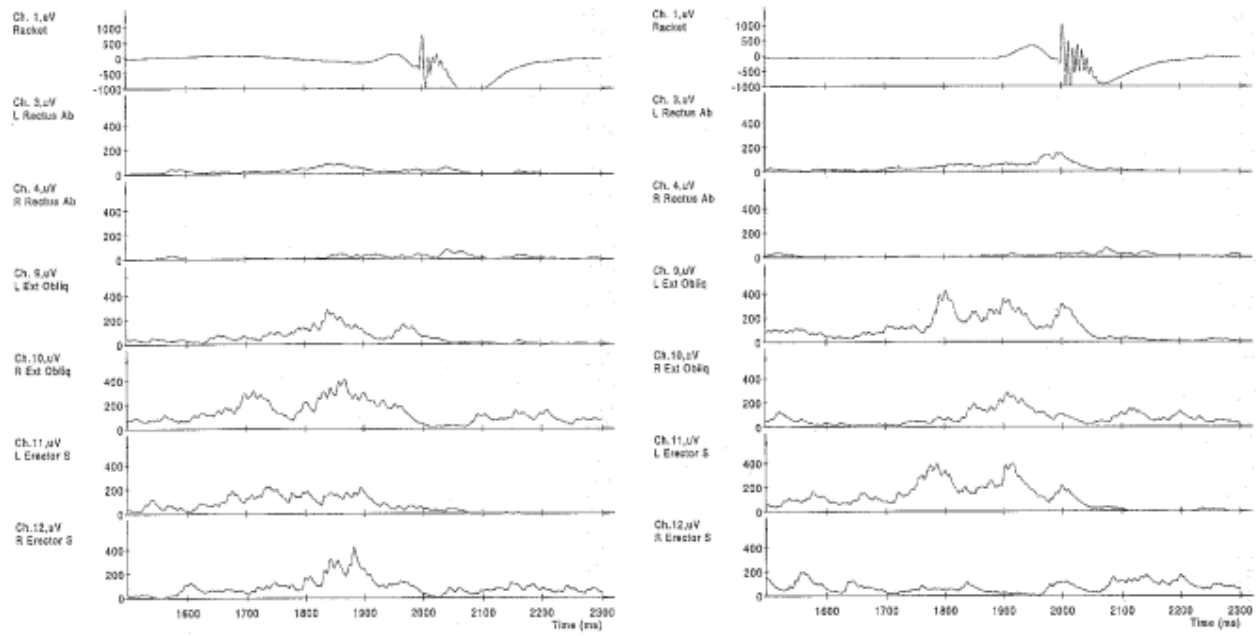

Figure 7. On the left: typical impact and rectified EMG signals of the muscles for the square stance forehand. On the right: typical impact and rectified EMG signals of the muscles for the open stance forehand.

A very interesting study was done by Girard et al. in 2005 using the Bagnoli EMG system. Three sEMG electrodes were connected to each leg on the vastus lateralis, vastus medialis, and gastrocnemius lateralis after which subjects were tasked with serving with the maximum power relative to the ability of the player. The study concluded that the timing of muscle activation between elite-level players as compared to their lower-level counterparts illustrated a higher level of neuromuscular coordination that generated a more forceful lower-limb drive [14]. This is shown by earlier activation for all the muscles studied in the elite-level player as compared to the beginner-level player in Figure 8. Using the results of this study, beginner and intermediate level players can know which muscles to activate as well as the timing of activation to have more powerful tennis shots.

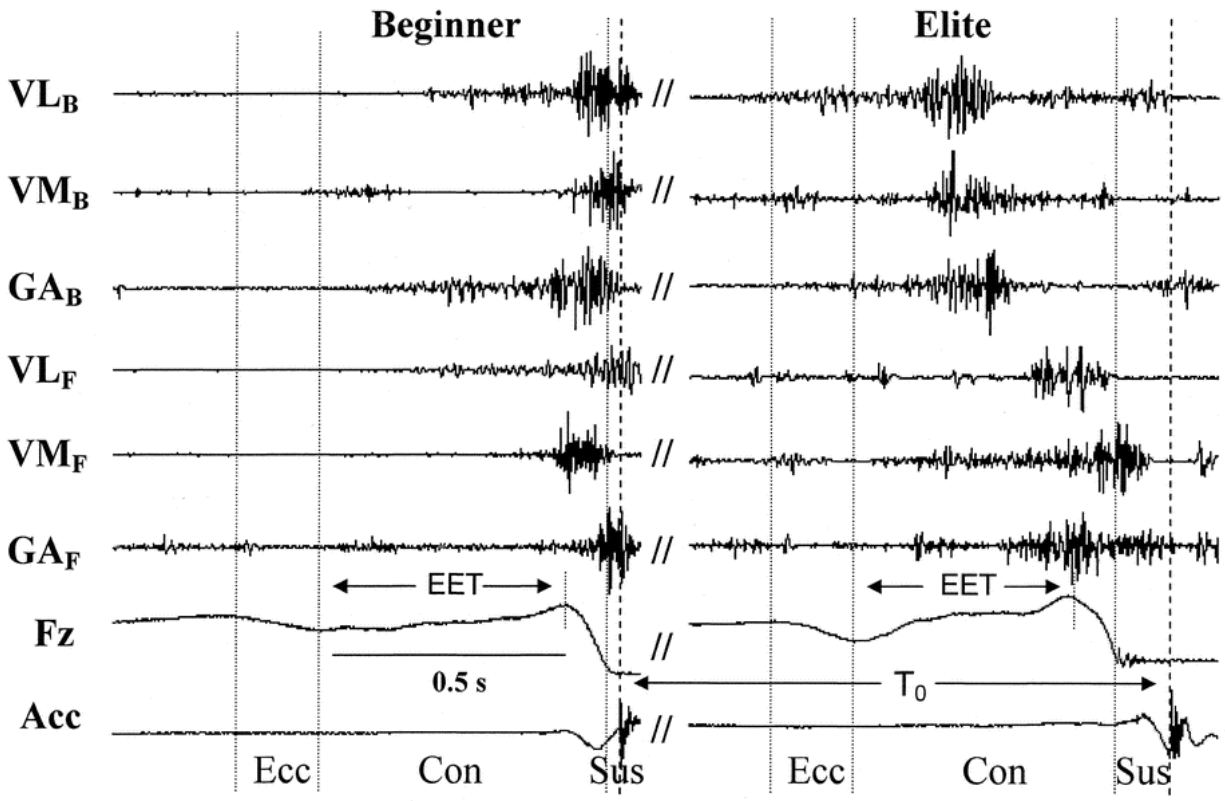

Figure 8. Electromyograms of successful performance of a beginner and elite participant. VL_B , back vastus lateralis; VM_B , back vastus medialis, GN_B , back gastrocnemius lateralis; VL_F , front vastus lateralis; VM_F , front vastus medialis; GN_F, front gastrocnemius lateralis; Fz, vertical ground reaction force; Acc, accelerometer; EET, effective extension time; T_0 , time of impact between ball and racquet; Ecc, eccentric phase; Con, concentric phase; Sus, suspension phase [14]

2.1.2.3 sEMG and Kinematics Integration

While kinematics and sEMG signals are powerful analysis tools by themselves, their strength is greater when they are combined. Using both methods, powerful tools such as angular acceleration, linear acceleration, velocity, joint angles, force generation, and muscle activation and timing are combined. However, few studies exist that combine the two methods. When reviewing literature, at the time of this study's publication, only a couple studies were performed that combined the sEMG and kinematics data. One study by Chow et al. examined tennis serves by monitoring anatomical joint angles and sEMG signals of four trunk muscles [15]. The study

further reinforced the heavy involvement of lower trunk muscles as well as proper bending of the spine during service. Therefore, if training of the lower trunk muscles is ignored, the risk of spinal injury greatly increases. Another study used MoCap and sEMG electrodes to monitor knee kinematics and leg muscle activation during the tennis serve in a three-set match [16]. Fenter et al. demonstrated a reduction of maximum knee flexion angle during the serve and a decrease of EMG amplitudes in biceps femoris and rectus femoris muscles throughout a three-set tennis match indicating fatigue as the matches progressed [16]. As a result, beginner and intermediate level tennis players can know what specific areas to train.

2.2 Gap in the Literature

2.2.1 Lack of Comprehensive MoCap and sEMG Studies

Nonetheless, none of these studies examine MoCap and entire dominant leg muscle activation simultaneously. Even then, none of the mentioned studies look at the effects of skill level and sex on different types of serves and ground strokes. While some independent MoCap or sEMG studies have looked at the different skill levels and their effect on tennis performance, few studies have been done that combine MoCap and sEMG data while looking at these factors.

2.2.2 Need for Studies on Skill Level and Sex Differences

By combining MoCap and sEMG data, a more comprehensive understanding is gained of the biomechanics and muscle activity involved in tennis performance. This integrated approach enables the examination of how skill levels, ranging from novice to expert players, affect movement patterns and muscle engagement during various strokes, footwork, and overall gameplay. Understanding the interplay between skill level and biomechanical responses is crucial for tailoring training programs, injury prevention strategies, and optimizing performance

in tennis players. For instance, identifying specific movement patterns associated with higher skill levels can inform coaching strategies to enhance skill development in aspiring athletes.

Furthermore, the integration of MoCap and sEMG data can contribute valuable insights to sports science and technology, facilitating the development of advanced training tools and technologies. Coaches and athletes can utilize this information to refine techniques, address weaknesses, and design personalized training regimens based on individual biomechanical profiles. Therefore, combining MoCap and sEMG data in tennis performance studies fills a critical research gap, offering a more holistic understanding of the factors influencing player performance. This integrated approach holds promise for advancing sports science, improving training methodologies, and ultimately enhancing the overall performance of tennis athletes across different skill levels and sexes.

2.3 Current Study

2.3.1 Objectives

To address this lack of data, this study recorded and examined MoCap and dominant leg sEMG data during serves and return volleys on both right (deuce) and left (advantage) sides of the court. The aims of this study were to examine the relationship between MoCap and sEMG parameters during serves and return volleys as well as investigating the effects of skill level and sex on tennis performance.

2.3.2 Methodology

During this investigation, we concurrently gathered MoCap and dominant surface sEMG data as subjects executed serves, cross-court returns, and down-the-line returns on both sides of the court. Subsequently, a comparative data analysis was conducted.

2.3.3 Expected Outcomes

Upon the conclusion of this study, there will be an enhanced comprehension of the interactions between muscles and joints, elucidating their influence on tennis performance. Likewise, the research aims to pinpoint factors that enhance performance for tennis players across varying skill levels and genders.

Chapter 3 – Methodology

3.1 Instrumentation

To obtain simultaneous recording of MoCap and sEMG data, XSENS MVN MoCap (Movella., Enschede, Netherlands) with its own recording software and an EMG system (MA300, Motion Lab Systems, Inc., Baton Rouge, LA) with WinDaq Pro Data Acquisition (WinDaq) software were used.

Two different types of preamplifiers were used for capturing muscle activity: one with three snap connectors (MA-420, Motion Lab Systems, Inc., Baton Rouge, LA) and one with two snap electrodes (MA-422, Motion Lab Systems, Inc., Baton Rouge, LA). Each of the preamplifiers had two snap electrodes for muscle activity but the preamplifier with three electrodes had an extra electrode for common noise rejection.

3.2 Synchronization of signals

A major proponent of capturing MoCap and sEMG data at the same time is ensuring that the start and stop time of data collection are synchronized. While the XSENS system had a "Sync in" Bayonet Neill–Concelman (BNC) port that could start and stop recordings with a 0V to 5V rise and 5V to 0V drop, respectively, the MA300 system did not have any form of a "Sync in" port. However, through experimentation with the MA300 system and the WinDaq software, it was found that a trigger could be created by using the footswitch of the MA300 system, specifically by connecting power and ground to the "#1" or "Toe" ports as illustrated in Figure 9. It was found that when 5V were sent to the switch, the reading in WinDaq was 0V, but when 0V were sent, the reading in WinDaq was 2.5V. This is illustrated in Figure 10. Once these findings were confirmed, the wires going to the footswitch were secured with electrical tape.

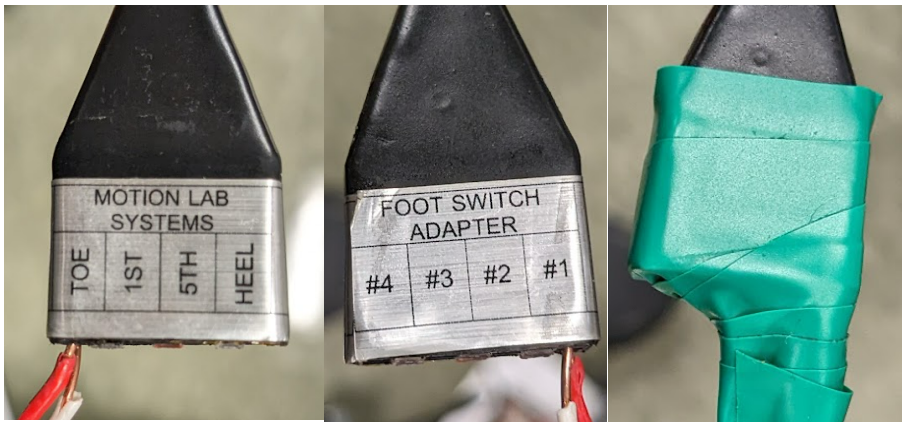

Figure 9. Foot switch adapter used as a trigger for start time in sEMG data capture

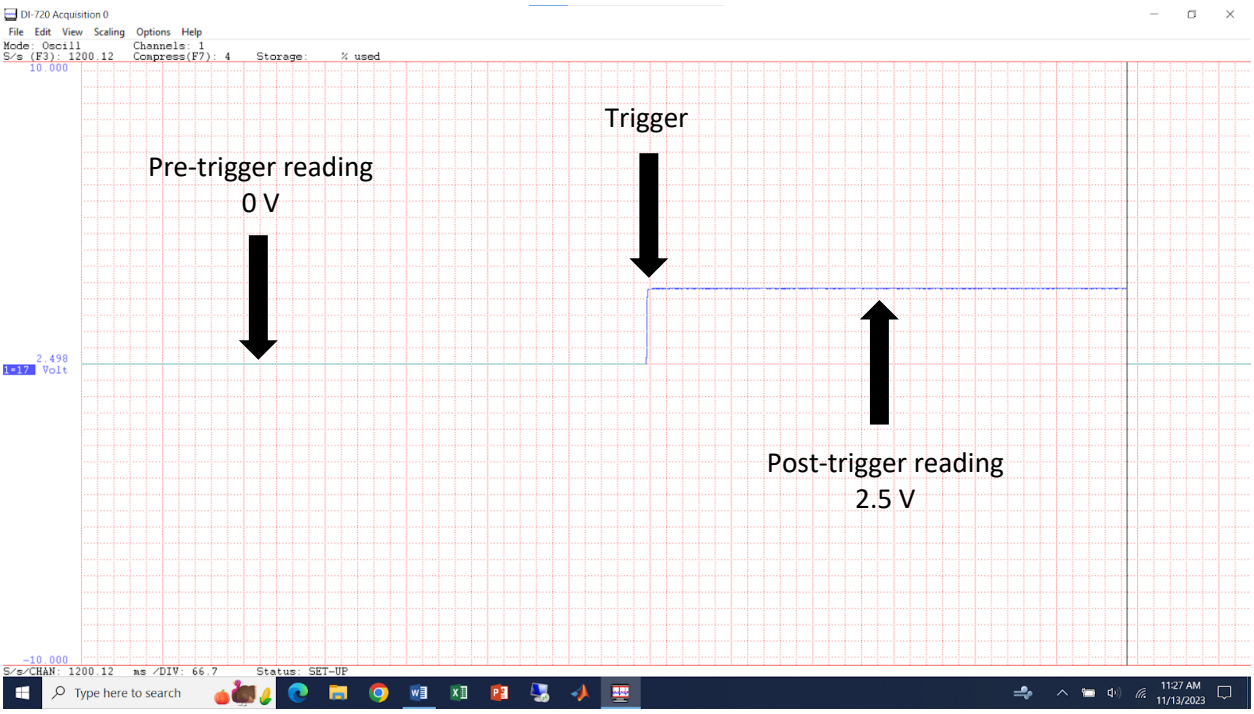

Figure 10. WinDaq reading of pre-trigger, trigger, and post-trigger voltage

In the WinDaq software, the duration of recording could be defined. Therefore, if the XSENS system received a start signal concurrently as the trigger was sent to the MA300 system and if the stop signal was delivered to the XSENS system at the same time that recording time was complete for the MA300 system, then the two systems would be perfectly synchronized.

3.2.1 Hardware

An Arduino Uno development board was chosen to accomplish the precise triggering of both XSENS and MA300 systems. To power the Arduino Uno, a 12V battery (EXP-1270, Expert Power), sent through a 5V regulator (L298N), was used. The 5V coming out of the regulator was connected to Arduino Uno and two light emitting diodes (LEDs), one blue (560LB7D) and one red (560MR2D) to denote the status of recording. Resistors were put in series with the LEDs whose minimum values were calculated according to Equations 1 and 2

$$R_{red\ LED} = \frac{V_s - V_f}{I_f} = \frac{5-2.2}{0.02} = 140\ \Omega \quad (1)$$

$$R_{blue\ LED} = \frac{V_s - V_f}{I_f} = \frac{5-3.2}{0.02} = 90\ \Omega \quad (2)$$

where V_s, V_f, and I_f represent supply voltage, forward voltage of the LEDs, and forward current of the LEDs, respectively. Thus, a standard value of 220Ω was chosen so that current would not be overdrawn. The LEDs were also placed in series with metal-oxide-semiconductor field-effect transistors (MOSFETs) (2N7000) so future iterations of code could account for dimming capabilities.

On the Arduino Uno, pins 3 and 7-10 were connected to the push-button switch, the BNC for the XSENS system, the footswitch for the MA300 system, the red LED, and the blue LED, respectively. All the connections from and to the Arduino Uno were made with 18-gauge, unstranded wire except for the footswitch. Because the footswitch is connected to the backpack unit of the MA300 system which will be attached to the subject during experimentation, the wire needs to be long and flexible so 18-gauge, stranded wire was used. Figure 11 depicts the schematic of the described hardware setup. Figure 12 shows the experimental setup.

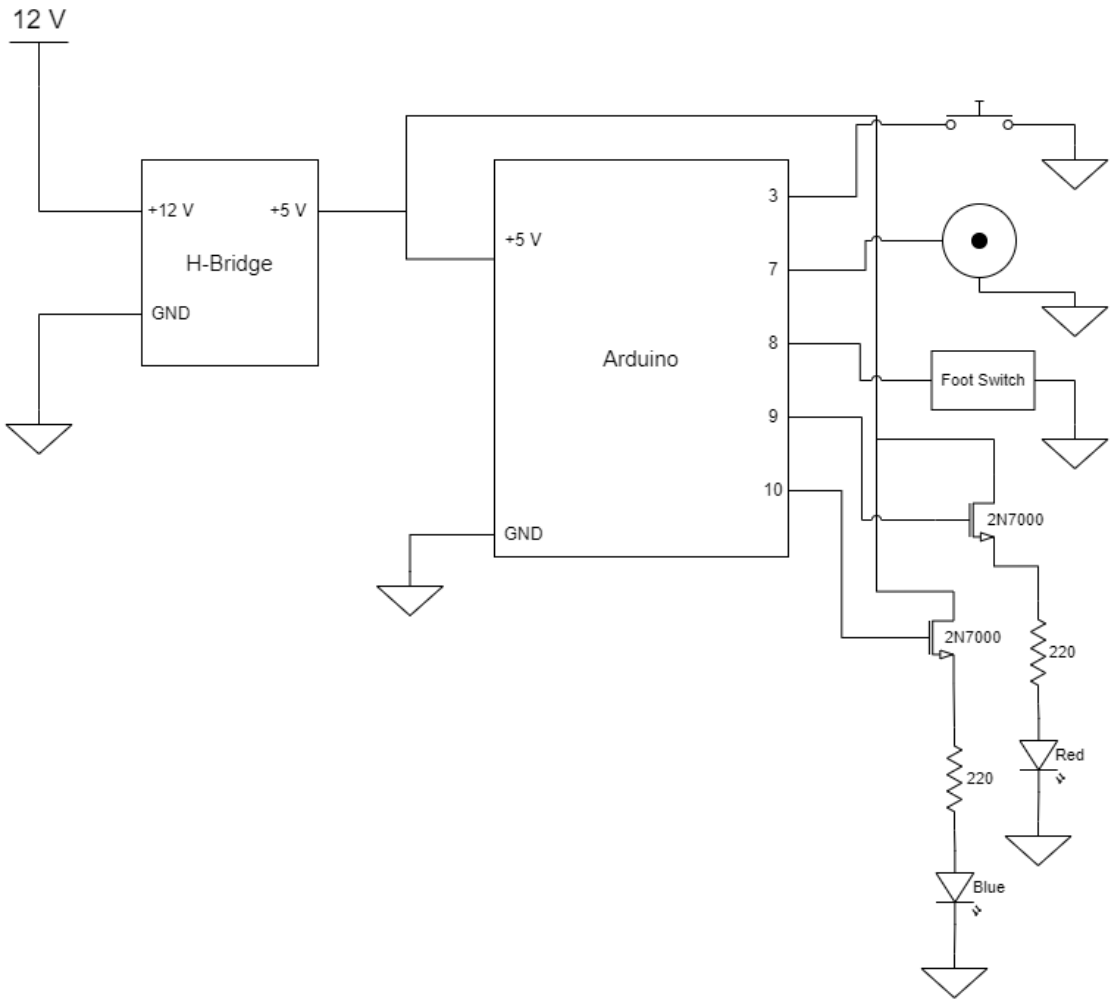

Figure 11. Schematic of the hardware setup for synchronization of systems

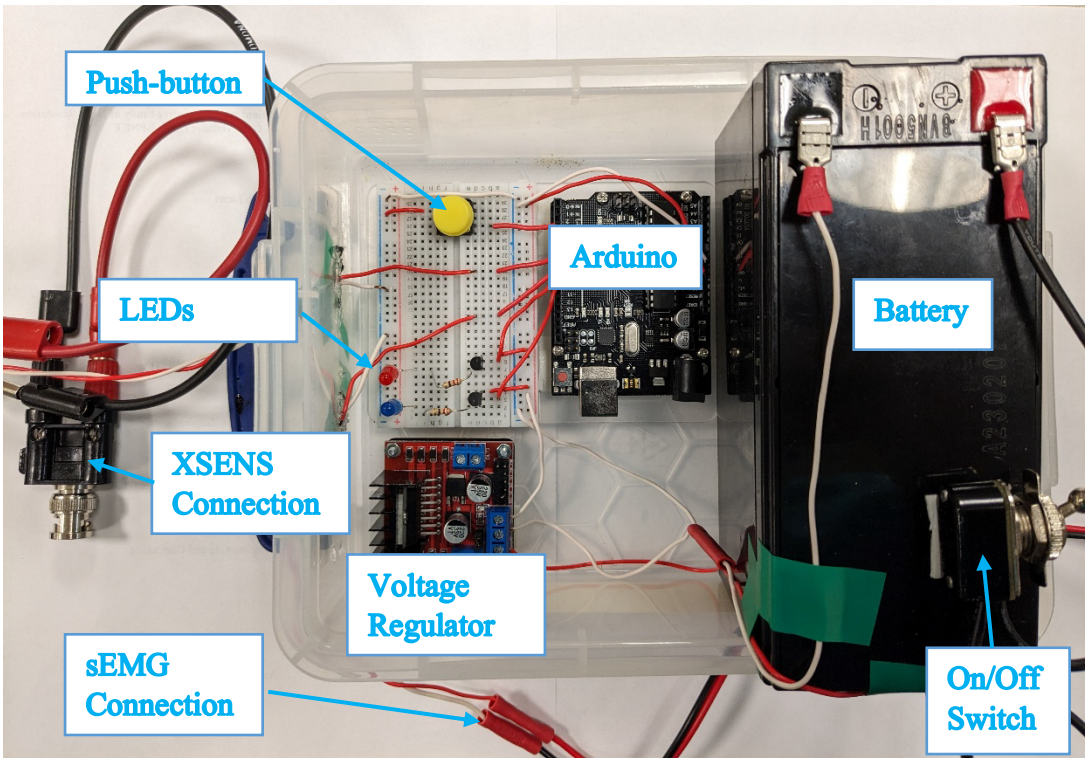

Figure 12. Experimental setup of switch for synchronization of systems

3.2.2 Software

Code was written using Arduino IDE 2.2.1 software. To begin, an enumerated state was declared with two statuses: “ON” and “OFF”. For the duration of recording, a time of 5 seconds (s) was chosen based on preliminary tests. From there, pin 3 was assigned as an input and pins 7-10 were assigned as outputs with the same connections as outlined in Section 2.2.1. Pin 3 was designated as a falling voltage interrupt pin and pulled up to 5V. This means that the interrupt would be triggered each time the voltage dropped to 0V from 5V. Subsequently, each time the button was pressed, the voltage on pin 3 would drop to 0V and the interrupt would be triggered. Inside of the interrupt was a single conditional which was comparing the status of the enumerated state; if the state was “OFF,” then it would be changed to “ON.”

Inside of the main loop was a set of conditionals comparing the status of the enumerated state. If the state was set to “OFF,” pins 7 and 10 would be set to “LOW” and pins 8 and 9 would

be set to “HIGH,” all of which denote that recording is not proceeding currently. If the state was set to “ON,” that is, if the button was pressed and the interrupt was triggered, pins 7 and 10 would be set to “HIGH” and pins 8 and 9 would be set to “LOW,” all of which denote that recording is proceeding currently. Then, the program would pause for a prescribed amount of time, in this case 5 s, and switch the enumerated state to “OFF.” Thus, the program would proceed until power supply was removed from the system. Figure 13 shows the flowchart of the program.

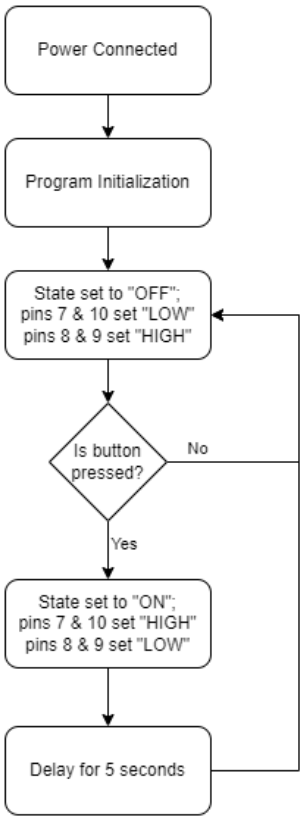

Figure 13. Flowchart of program for synchronization of switches

3.3 Participants

Participants were recruited and included in the study if they were between 18 and 50 years of age as well as being at least a beginner tennis player according to the Universal Tennis Rating Conversion chart. Conversely, participants were excluded from the study if they had

musculoskeletal injuries/impairments requiring surgical intervention within the past 12 months, had any musculoskeletal injuries/impairments of the spine, pelvis, and upper and lower extremities that required medical treatment within the past 12 months, were currently pregnant, were currently being treated for cardiopulmonary diseases, or have been diagnosed with a neurologic disorder such as Multiple Sclerosis or Parkinson's Disease. This is detailed in the informed consent form found in Appendix A. For the purposes of this study, professional skill was defined as a player having played in college and now being a coach. A player was considered non-professional if both of those conditions were not met.

Of the eight participants, two were of the professional skill level and six were of the non-professional skill level. Values are represented as mean ± standard deviation (SD). Both of the professional players were male with an average age of 22.5 ± 0.71 years, an average height of 180.7 ± 6.22 centimeters (cm), an average weight of 77.7 ± 5.52 kilograms (kg), a years played average of 13.5 ± 2.12 years, and a times played per year average of 260 ± 0.00. For the non-professional participants, two were male and four were female. Of the male non-professionals, the average age was 27.0 ± 4.24 years, the average height was 176.1 ± 7.42 cm, the average weight was 84.5 ± 7.85 kg, the years played average was 9.5 ± 0.71, and the times player per year average of 3.0 ± 2.83. For the female non-professionals, the average age was 29.0 ± 11.46 years, the average height was 161.7 ± 4.32 cm, the average weight was 57.2 ± 2.38 kg, the years played average was 10.0 ± 7.07, and the times player per year average of 80.3 ± 87.47. All the participants' demographics are recorded in Table 1.

Table 1. Participant demographics showing age, height in cm, weight in kg, years played, and number of times played per year of professional and non-professional males as well as non-professional females. There were no professional females in this study.

	Age	Height (cm)	Weight (kg)	Years played	Times Played (per year)
Male Pro (*n* = 2)[a]	22.5 ± 0.71	180.7 ± 6.22	77.7 ± 5.52	13.5 ± 2.12	260 ± 0.00
Male Non-Pro (*n* = 2)	27.0 ± 4.24	176.1 ± 7.42	84.5 ± 7.85	9.5 ± 0.71	3.0 ± 2.83
Female Non-Pro (*n* = 4)	29.0 ± 11.46	161.7 ± 4.32	57.2 ± 2.38	10.0 ± 7.07	80.3 ± 87.47

[a] All data is displayed as mean ± SD.

3.4 Experimental procedure

Before any experimentation was be conducted, the subject read and signed the informed consent form (IRB# 23-296-H-GVSU) that detailed the outline of trials. Then, measurements were taken of the subject including weight, height, arm span, etc. From there, electrodes were attached to the seven target muscles on the dominant side of the subject. Muscles of interest include the medial portion of the deltoid (De), the gluteus maximus (GM), the biceps femoris (BF), the rectus femoris (RF), the vastus medialis (VM), the gastrocnemius medialis (GaM), and the tibialis anterior (TA). Target locations of the muscles were identified according to the SENIAM guidelines, and the locations were shaved of hair after the skin was moistened with a damp, disposable, paper towel [17]. Figure 14 shows the placement of IMUs, the muscles of interest denoted by green circles, and the sensors used for analysis of swing cycle and ball contact by red arrows.

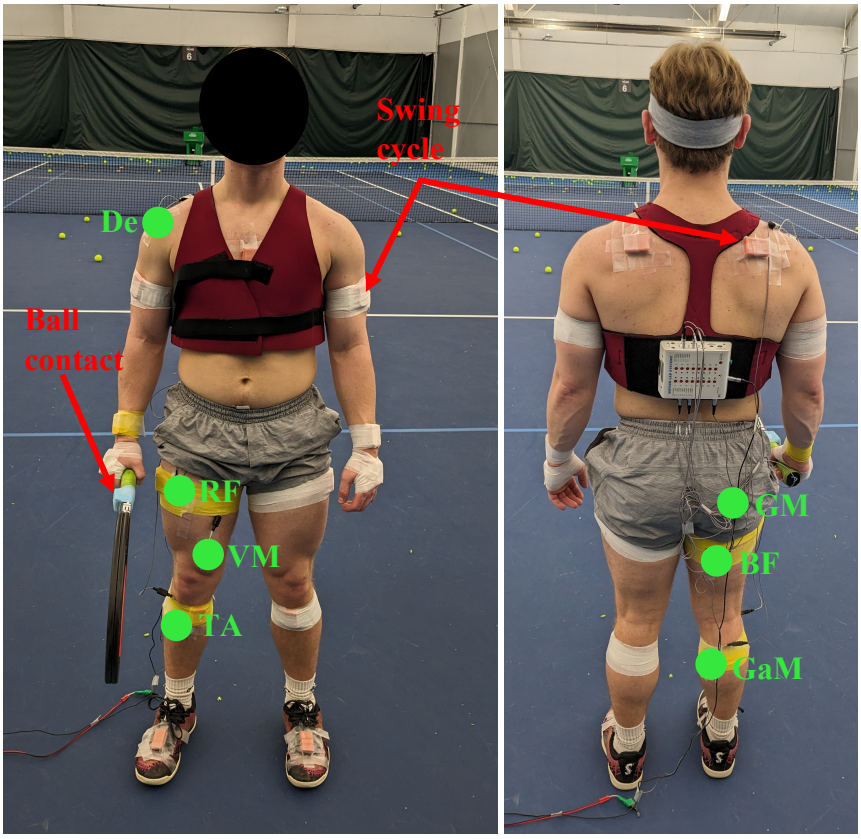

Figure 14. Typical set up of MoCap and EMG systems on subject. Shown in green circles and abbreviation are the muscle of interest. Shown by red arrows are the IMU sensors used for delineation of swing cycle and ball contact.

After the target locations were wiped dry and left for 1 minute, they were abraded with disposable alcohol wipes. Gel-type electrodes (GS-27) were placed directly on the skin, parallel to the muscle fibers, and secured with surgical tape to minimize movement artifact. Preamplifiers were then connected to the electrodes. Next, the subject was given a vest that held a backpack unit to which all the preamplifiers connected. The backpack unit had two sets of wires leaving: one going to the MA300 system and one going to the synchronization switch. Finally, after all the sEMG preamplifiers were placed on the subject, 17 XSENS sensors were placed on the subject ranging from the head to the foot and 1 XSENS sensor on the tennis racket. The sensors were placed in compliance with the manufacturer's recommendations [18]. After all the sensors

were placed, the subject was guided through motions to ensure all the sEMG preamplifiers were recording as well as an N-pose and walk calibration for the XSENS system [19].

After confirmation of the operability of all the sensors, the subject went through a self-directed warm-up. Then, the subject was guided through a set of tennis shots as depicted in Figure 15. It is important to note that Figure 15 shows the forehand and backhand shot types for a right-handed player. If the player was left-handed, the positions would be mirrored. For each set of tennis shots, the subject was allowed 3-5 warm up trials before recording began and continued until 10 successful trials were recorded. For the first part, the subject was guided to perform serves on both sides of the court with successful trials denoted as a ball landing in. For the second part, a ball machine was used that was placed on the opposite side of the net. The subject then returned balls cross court and down the line first with forehand and then with backhand strokes. Points were awarded based on the location of the ball return as shown in Figure 15. For example, if the subject returned the ball to the red shaded area during either the cross court or down the line return task, 3 points were awarded. No points were awarded if the subject missed all the areas. Trials were considered successful if a non-zero point value was ascribed.

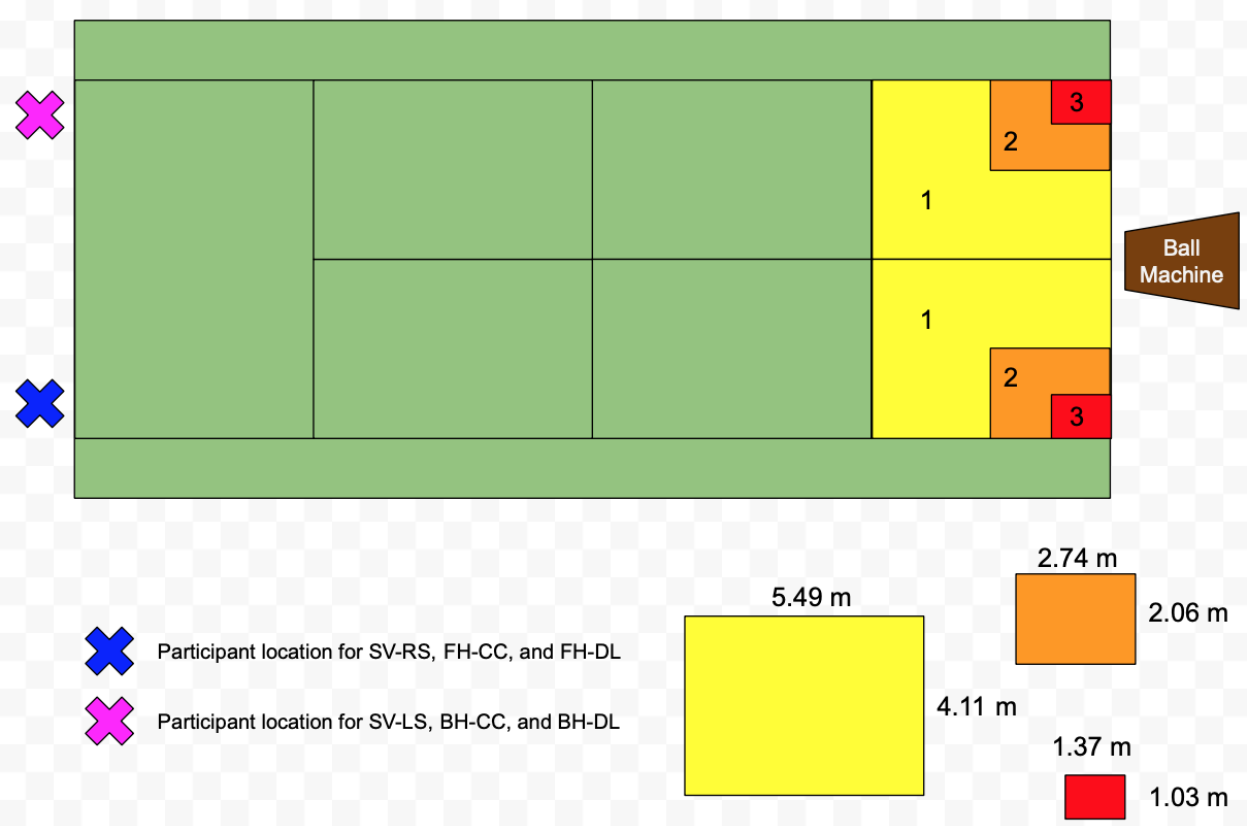

Figure 15. Down the line and cross court return depiction on the advantage side of the court. SV-RS, FH-CC, FH-DL, SV-LS, BH-CC, BH-LS stand for service on the right side, forehand cross court, forehand down the line, service on the left side, backhand cross court

3.5 Data processing

MoCap was recorded at a frequency of 60 Hz, while sEMG data was recorded at 1200 Hz. Following the completion of trials, both XSENS and sEMG data were exported into MATLAB (2023a), where the swing cycle was defined according to Section 3.6. The onset and cessation points of each swing cycle were synchronized in time by time matching XSENS data with sEMG data. sEMG data underwent band-pass filtering using a Butterworth 4th order high-pass filter (20 Hz cut-off frequency) and a Butterworth 4th order low-pass filter (500 Hz cut-off frequency). Subsequently, the sEMG data was rectified and a linear envelope was generated by applying a Butterworth 4th order low-pass filter (5 Hz cut-off frequency). No additional processing was applied to the XSENS data after recording. Both XSENS and filtered sEMG data

were interpolated to 100 points between the start and end of the swing cycle to show the percentage of that respective swing cycle.

3.6 Outcome measures

3.6.1 Swing cycle

3.6.1.1 Serves

To delineate the serve cycle, shoulder abduction and adduction of the dominant arm, given by the sensors shown in Figure 14, were used [20]. The abduction and adduction of the dominant shoulder joint obtained from XSENS data was plotted and the two lowest points just before and after the greatest shoulder abduction were chosen as the starting and ending points. Ten points were added to the ending point to incorporate muscle activity at the end of the serve cycle. These data points were recorded and stored for further analysis of data. Figure 16 shows dominant shoulder abduction and adduction of a typical serve. Shown in red are the points chosen for the start and stop of the serve cycle.

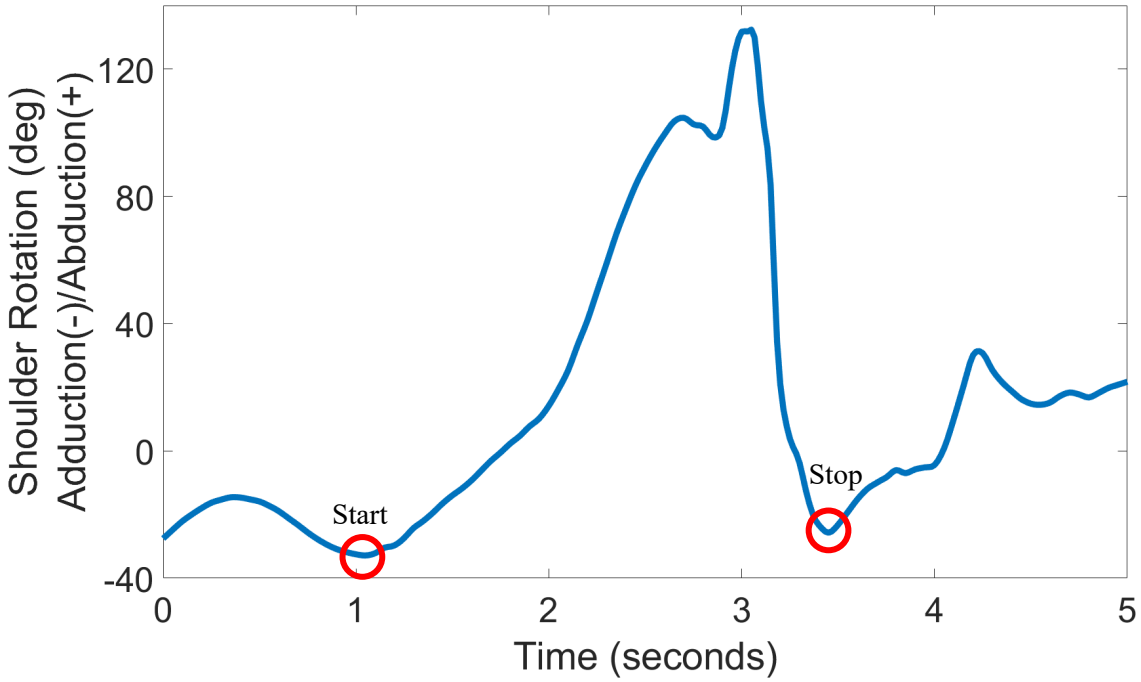

Figure 16. Dominant shoulder abduction and adduction with the red circles denoting points chosen for the start and stop of the serve cycle

3.6.1.2 Forehand strokes

Similar to the serve cycle, dominant shoulder abduction and adduction obtained from XSENS were plotted for forehand strokes. In this instance, the last point closest to 0 degrees of abduction and adduction before the greatest amount of abduction was chosen as the starting point. Ten points after the lowest adduction was selected as the end point of the forehand swing cycle. Figure 17 shows typical dominant shoulder adduction and abduction with the points chosen for the start and end of the forehand stroke marked in red.

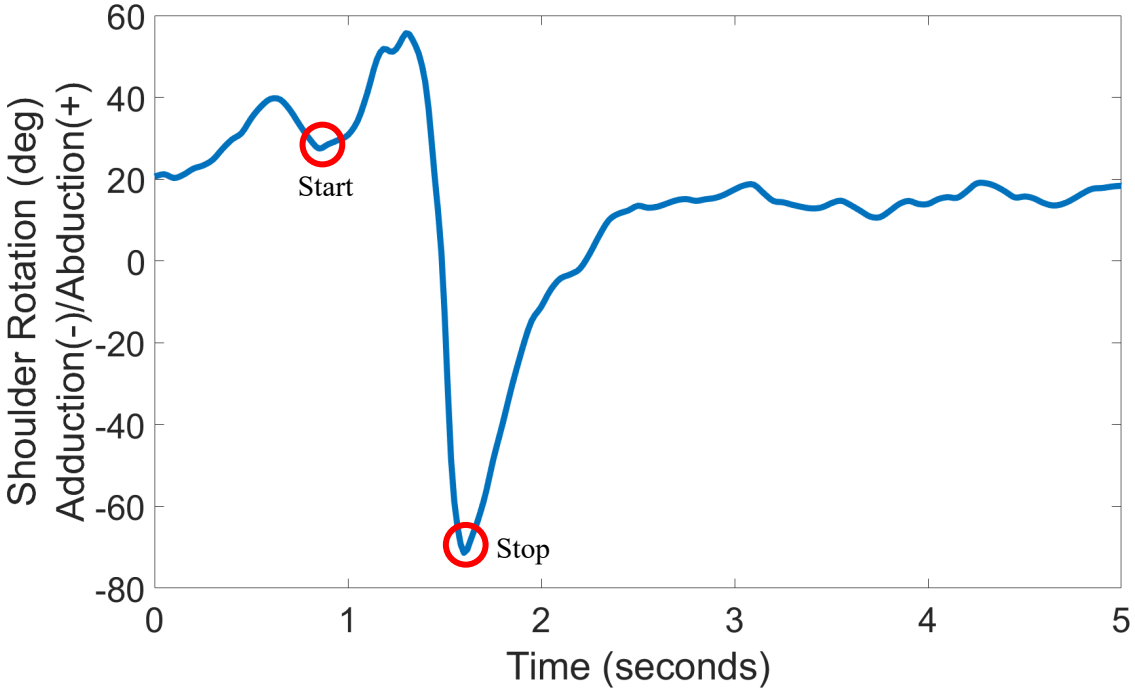

Figure 17. Dominant shoulder abduction and adduction with the red circles denoting points chosen for the start and stop of the forehand stroke cycle

3.6.1.3 Backhand strokes

Once again, dominant shoulder abduction and adduction were used to mark the start and stop of the backhand stroke cycle. The lowest point of adduction and the highest point of abduction were chosen as the starting and stopping points, respectively. As before, 10 points were added to the stopping point to help visualize muscle activity at the end of swing cycle. Figure 18 shows typical dominant shoulder abduction and adduction during backhand strokes with points for starting and stopping of the cycle shown in red.

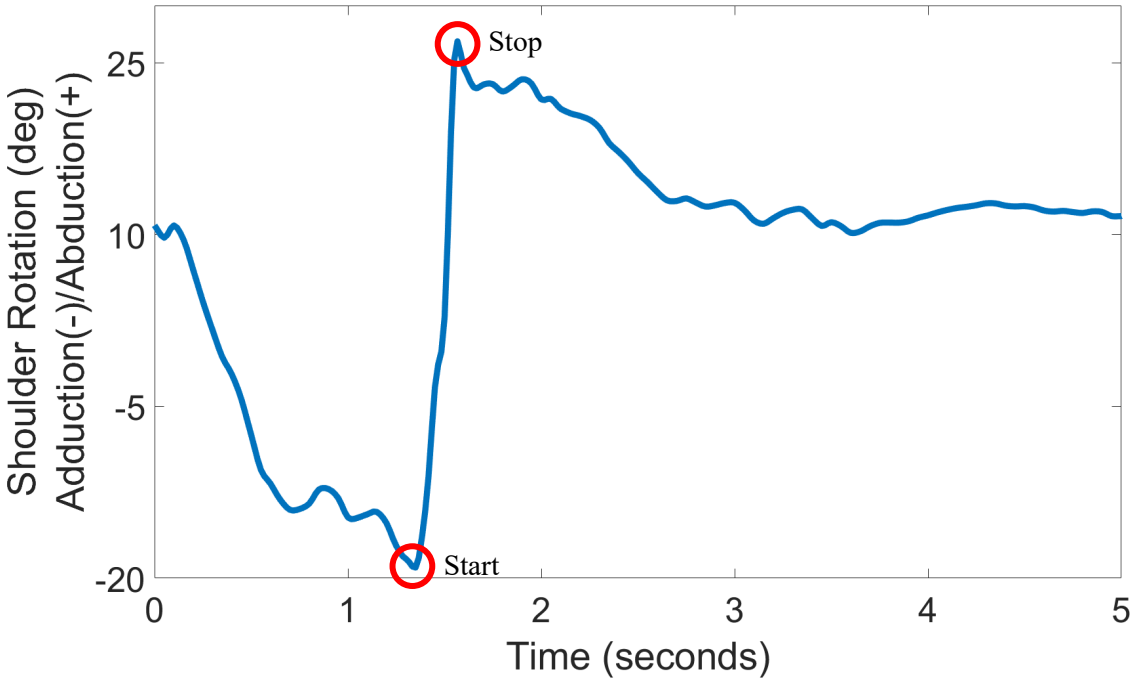

Figure 18. Dominant shoulder abduction and adduction with the points chosen for the start and stop of the backhand stroke cycle

After all the starting and ending points pertaining to the difference cycles were obtained, the points were time matched for the respective sEMG data. Data outside these starting and ending points were discarded. The data that remained was interpolated to 100 points to show percentage of a swing cycle.

3.6.2 Muscle activation

After sEMG data was obtained from the MA300 system, exported to MATLAB, and time matched with XSENS data, but before the sEMG data was filtered, Figure 19 shows typical muscle activation. In Figure 19, the top left image shows dominant shoulder kinematics, that is, abduction and adduction. The rest of the images show muscle activation.

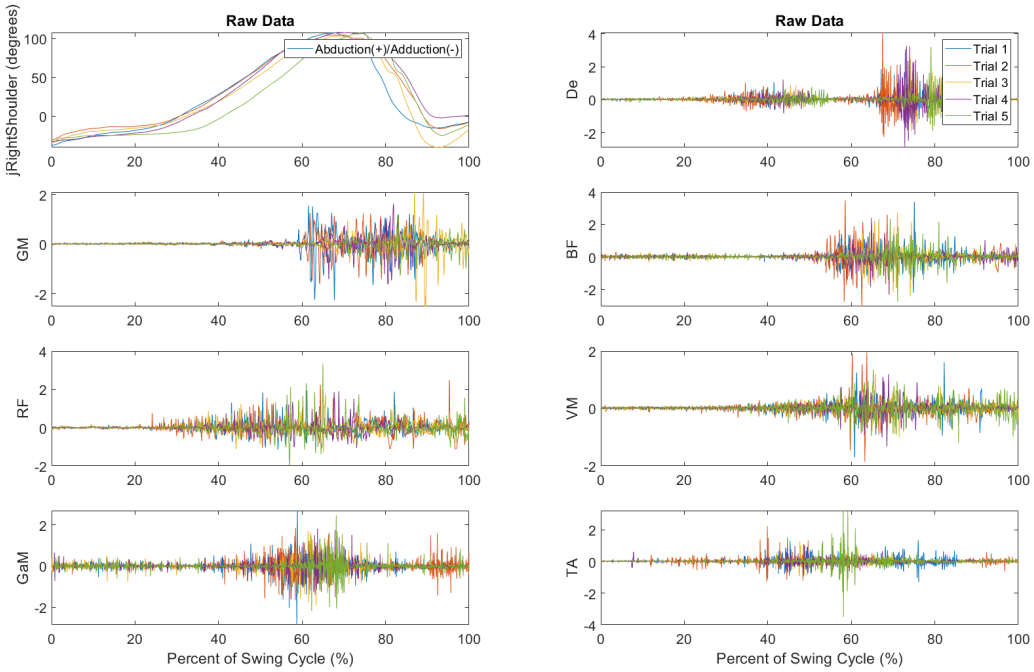

Figure 19. Unfiltered sEMG data of a typical participant

This wavering signal made it difficult to tell during which times the muscle was active and during which times the muscle was relaxed. However, after filtering and normalizing the muscle activity from each trial to that muscle's maximal contraction for the same trial, the activity of the muscles became more clear as seen in Figure 20.

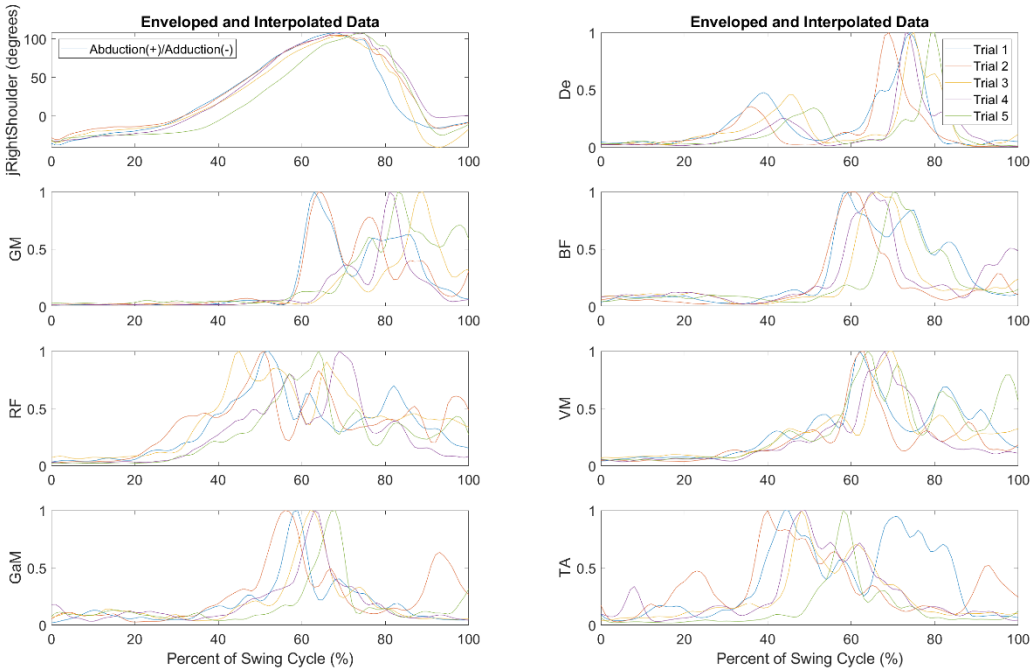

Figure 20. Filtered sEMG data of a typical participant

Therefore, for the purposes of this study, muscle activity was delineated as any measurement surpassing 20% of the maximum contraction value.

3.6.3 Ball contact

Based on preliminary studies, it was found that using the prop angular velocity in the z-direction shows the point of ball contact. The sensor that was used for prop angular velocity is shown in Figure 14.

3.6.3.1 Serves

For the serve cycle, it was found that the most negative point of angular racket velocity denoted ball contact. Shown in Figure 21 is typical racket angular velocity for the serve cycle with the point chosen for ball contact delineated by the red circle.

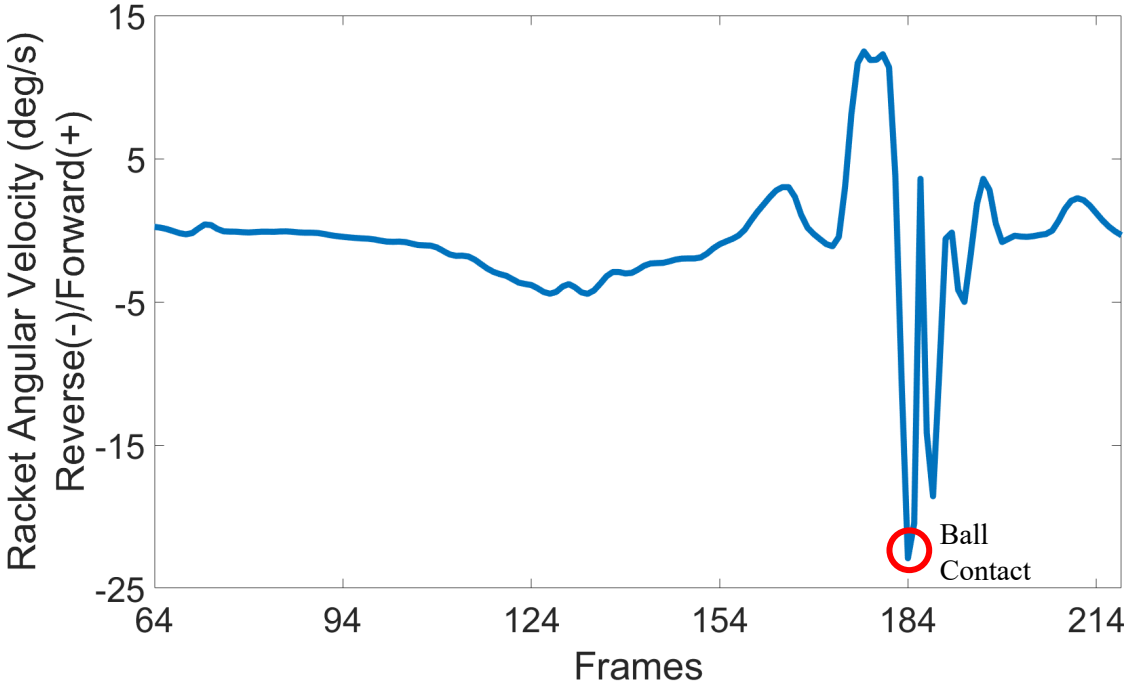

Figure 21. Prop angular velocity in the z-direction with red circle designating ball contact for the serve cycle

3.6.3.2 Forehand Strokes

During the forehand groundstroke cycle, it was discovered that the peak angular velocity of the racket coincided with the moment of ball contact. Figure 22 illustrates the typical racket angular velocity throughout the forehand stroke cycle, with the instance of ball contact marked by a red circle.

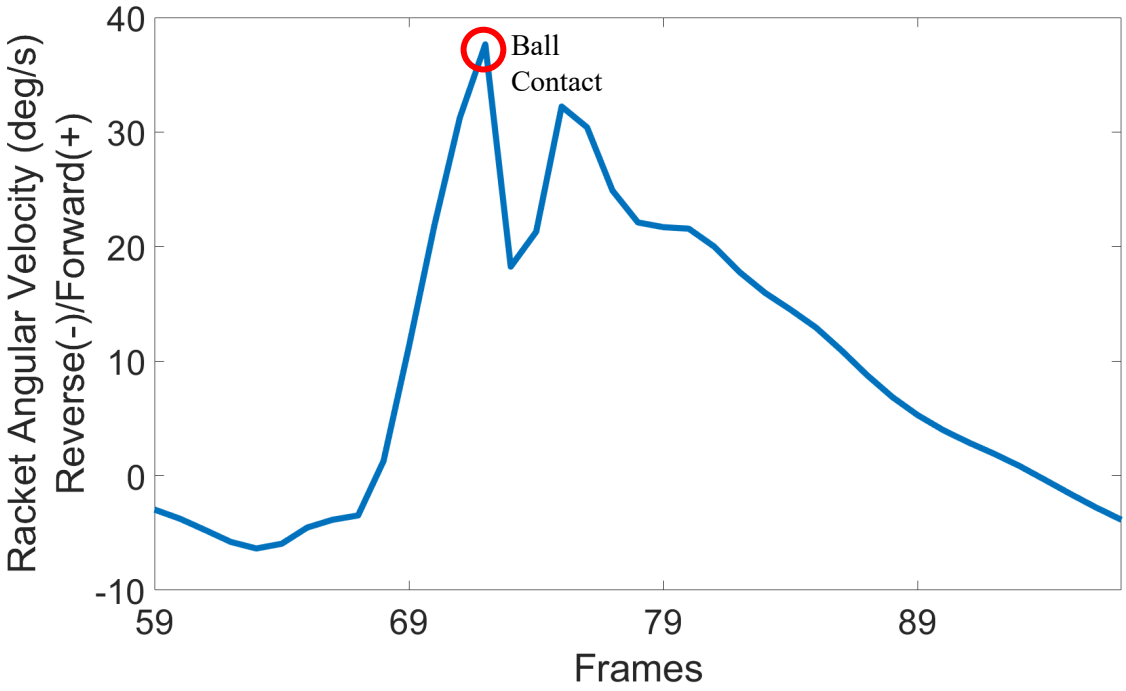

Figure 22. Prop angular velocity in the z-direction with red circle designating ball contact for the forehand stroke cycle

3.6.3.3 Backhand Strokes

Throughout the backhand groundstroke cycle, it was found that the lowest angular velocity of the racket aligned with the instant of ball contact. Occasionally, this moment did not precisely correspond to the most negative angular velocity. Therefore, the point just before a distinct upward peak of negative velocity was selected as the reference for ball contact. Figure 23 depicts the usual racket angular velocity during the backhand stroke cycle, with the point of ball contact highlighted by a red circle.

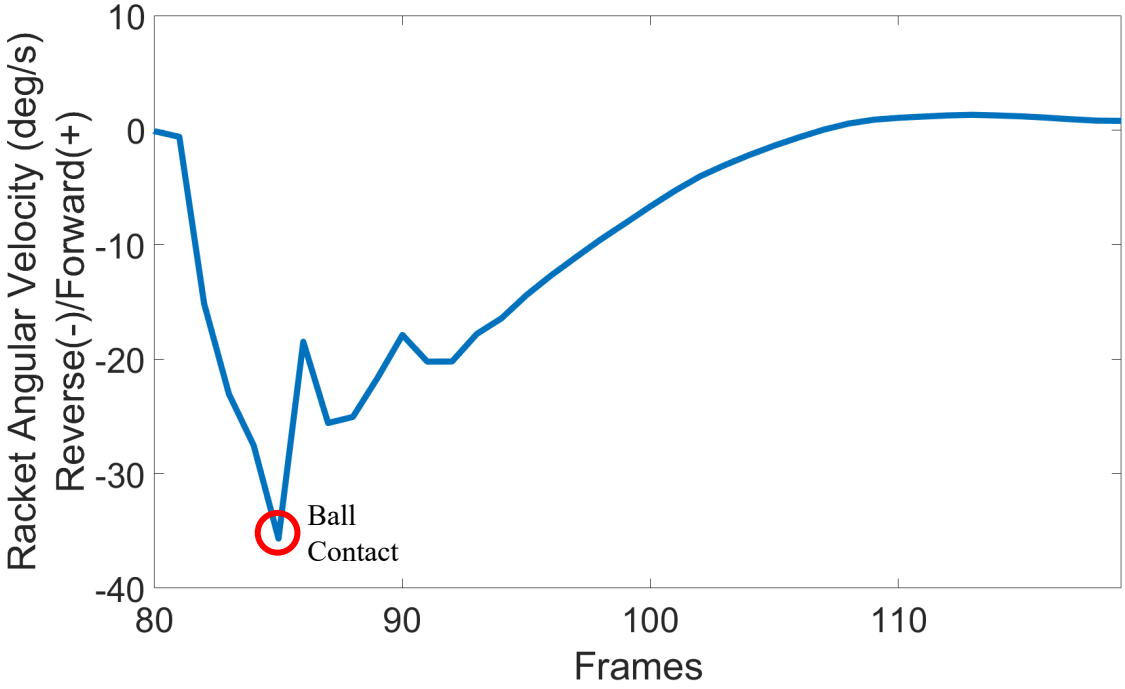

Figure 23. Prop angular velocity in the z-direction with red circle designating ball contact for the backhand stroke cycle

Chapter 4 – Results

Testing was performed, and the following results were obtained. As noted before, Figure 14 shows the typical setup of both EMG and XSENS systems on the subject. While this study did look at both MoCap and sEMG data, a greater emphasis was placed on the sEMG portion. However, Figures 24 and 25 highlight the major differences that were observed from the MoCap standpoint.

4.1 Kinematics

Figure 24 shows dominant shoulder rotation, specifically abduction and adduction, while subjects were performing a backhand groundstroke. Likewise, Figure 25 shows dominant shoulder rotation, internal and external, but during deuce side service. In each of the figures, the solid lines represent the means across five different trials while the shaded region depicts the standard deviation across those trials. The two averaged trials depicted in red are the professional tennis players while the two averaged trials depicted in blue are the non-professional tennis players. The solid black vertical line in Figure 24 and the respective colored vertical lines in Figure 25 show where ball contact occurred.

Comparing the professional and non-professional participants shows that the professional participants had greater total range differences between adduction and abduction when it came to backhand groundstrokes. The calculated angle ranges were 96.1° ± 10.1° for the professionals and 77.9° ± 47.9° for the non-professionals. This is visualized in Figure 24.

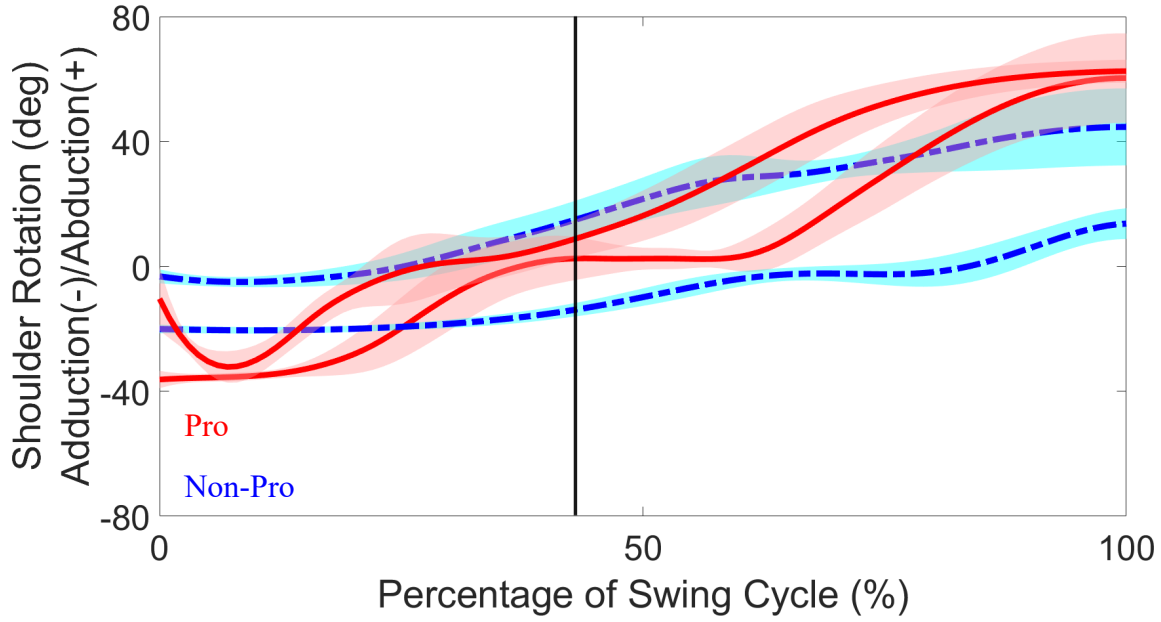

Figure 24. Dominant shoulder abduction and adduction during backhand groundstrokes for two professionals and two non-professionals

Likewise, comparing the professionals and non-professionals for tennis service shows that the professionals had greater values for both external (122.0° ± 8.4° vs. 113.3° ± 11.2°) and internal (66.4° ± 6.6° vs. 47.2° ± 39.5°) rotation of the dominant shoulder. This is depicted in Figure 25.

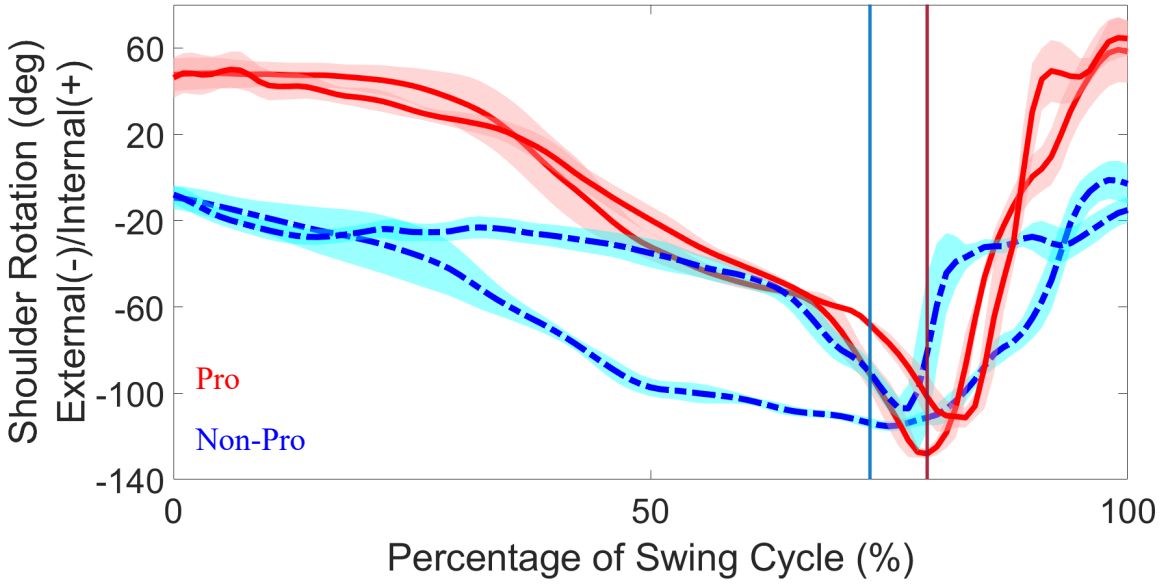

Figure 25. Dominant shoulder internal and external rotation during deuce side service for two professionals and two non-professionals

4.2 sEMG Data

The rest of the figures will be looking at the sEMG differences between professional and non-professional participants. The figures can be grouped together in groups of two, i.e. Figures 26 and 27 show data from the same task, that is either service, backhand groundstrokes, or forehand groundstrokes, but in this specific instance, it is the backhand cross-court task. The first figure in the set of two shows overlaid data from the professional participants while the second figure shows overlaid data from the non-professional participants. Each distinct color corresponds to a different subject from the trials. While there were more than two non-professional participants, only two are shown for better visualization. All of the non-professional players' data can be seen in Appendix B. Comparisons will be drawn from all subjects, not just those depicted in this section.

Similarly, all the figures have the same layout: the top left image displays the kinematics of the dominant shoulder, in this case the right shoulder, namely abduction and adduction.

Abduction is represented with the degrees in the shoulder joint increasing while adduction is represented by the degrees in the shoulder joint decreasing. From there, in a left to right and descending order, sEMG data is shown of the medial De, the GM, the BF, the RF, the VM, the GaM, and the TA. In all figures, the data is displayed from the start of the respective swing cycle to the end of the swing cycle. The data that is displayed is an average of three to five different trials taken from each participant with the dark line representing the average and the shaded region representing the standard deviation of the trials. Individual trial depictions can be seen in Appendix B. Furthermore, the swing cycles are delineated by vertical lines where each division corresponds to the XSENS MoCap figurine below the shoulder kinematics and EMG image. Important to note is that ball contact is depicted by a colored vertical line that corresponds to the subject whose data is overlaid.

4.2.1 Backhand Cross-Court Groundstrokes

Hence, Figures 26 and 27 present the backhand cross-court groundstrokes of two professional players and two non-professional individuals. Among the professionals, the backhand cross-court stroke initiated with a shoulder adduction angle of approximately 45° and concluded with a shoulder abduction angle of about 50°. Conversely, among the non-professionals, the initiation of the backhand cross-court stroke typically featured a lower shoulder adduction angle of around 25°, with the conclusion marked by a shoulder abduction angle of approximately 40° for most participants. Trials depicted in Appendix B highlighted in green (Figures B-93 and B-94) displayed a wider range of shoulder adduction and abduction, commencing around 50° of adduction and reaching nearly 100° of abduction. As the backhand cross-court swing cycle progressed, both among professionals and non-professionals, a general trend was observed where most muscles transitioned from a contracted state to a more relaxed

state, indicated by the downward trajectory of the solid lines in Figures 26 and 27. However, there were instances of latent muscle activation, notably exemplified by the subject represented by the green line in Figure B-94. Such deviations likely stem from diverse approaches to the backhand shot in comparison to the other participants. No major differences between muscled activation patterns and time of ball contact between professionals and non-professionals was observed with time of ball contact happening between 20-25% of the swing cycle for both groups.

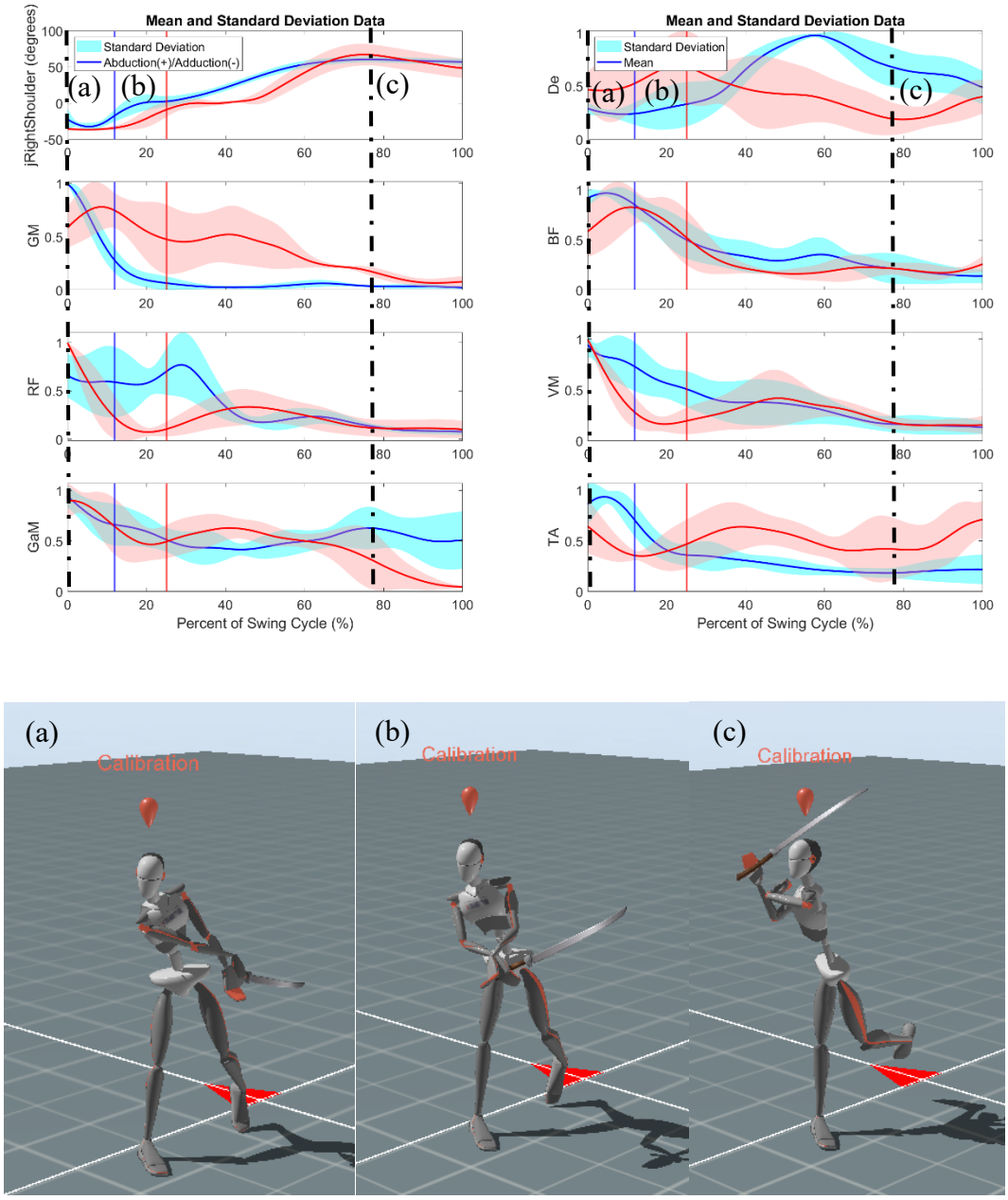

Figure 26. The graphs depict shoulder abduction and adduction, alongside sEMG data, recorded from professionals executing backhand cross-court groundstrokes. Vertical lines in the graphs indicate various stages of the groundstroke, as demonstrated by XSENS MoCap figurines. Two distinct colors denote two different subjects. The solid line represents the average of five trials, while the shaded region indicates the standard deviation across the same five trials.

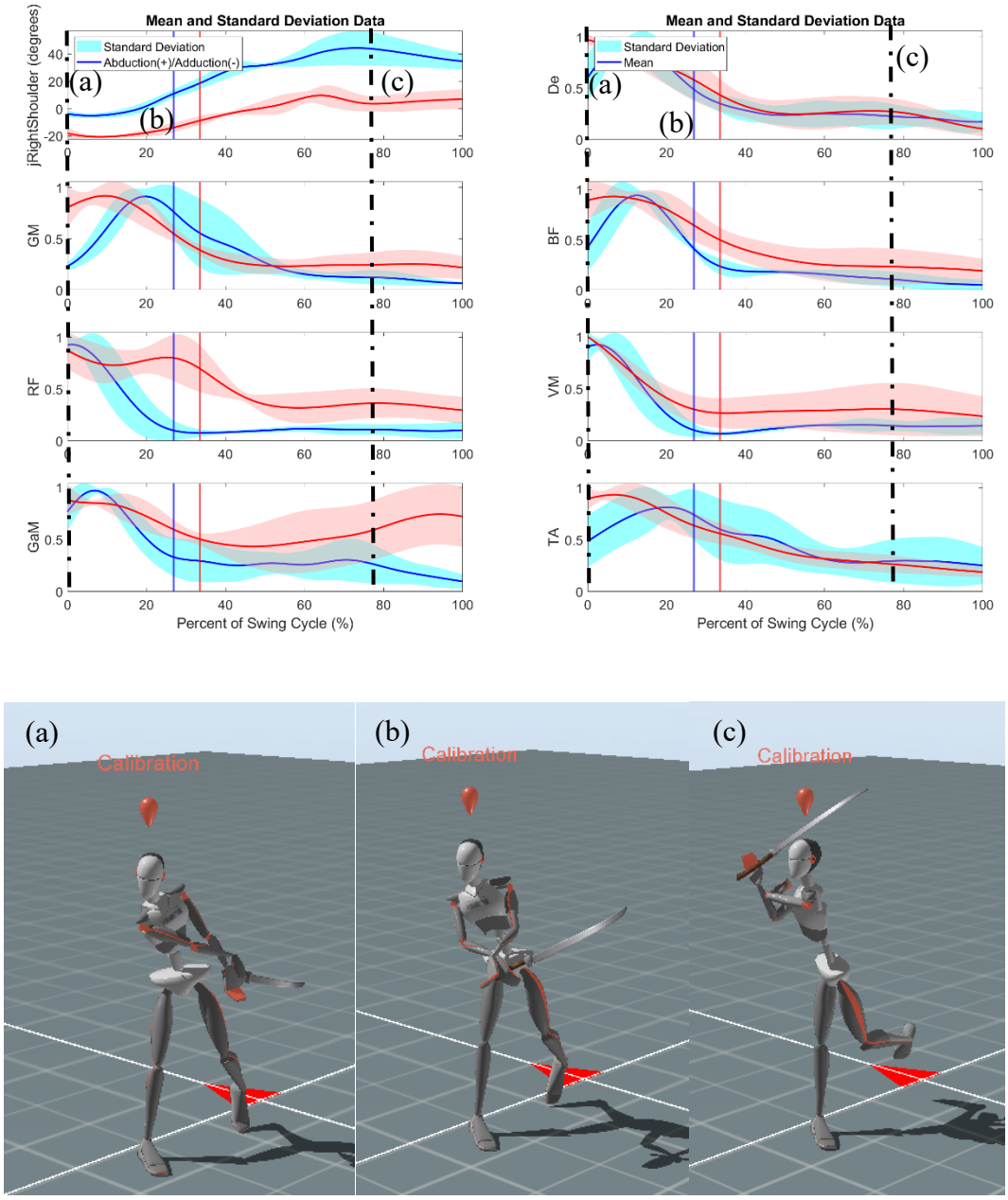

Figure 27. The graphs depict shoulder abduction and adduction, alongside sEMG data, recorded from non-professionals executing backhand cross-court groundstrokes. Vertical lines in the graphs indicate various stages of the groundstroke, as demonstrated by XSENS MoCap figurines. Two distinct colors denote two different subjects. The solid line represents the average of five trials, while the shaded region indicates the standard deviation across the same five trials.

4.2.2 Backhand Down-the-Line Groundstrokes

Figures 28 and 29 portray the backhand down-the-line groundstrokes executed by two professional players and two non-professional individuals. Similar to the observations in the backhand cross-court groundstrokes, among the professionals, the shoulder rotation spanned from approximately 35° of adduction to about 50° of abduction. In contrast, non-professionals exhibited a narrower range, with an average shoulder adduction of around 20° and an average shoulder abduction of about 30°. Additionally, akin to the patterns observed in the backhand cross-court groundstrokes, both among professionals and non-professionals, all measured muscles initially contracted and gradually relaxed as the shot unfolded. No significant disparities were noted in muscle activation patterns or timing of ball contact between professionals and non-professionals with time of ball contact happening between 20-25% of the swing cycle for both groups.

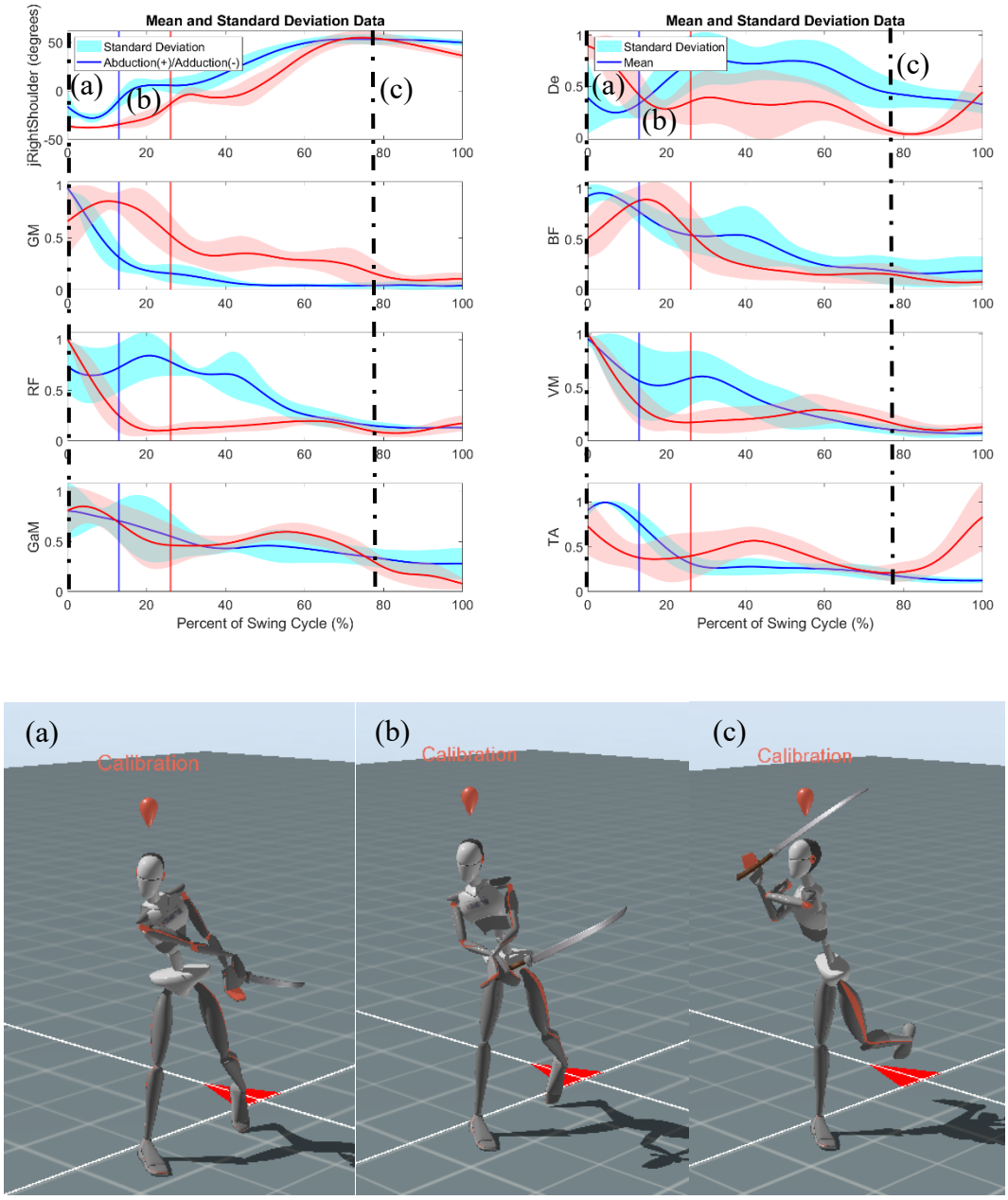

Figure 28. The graphs depict shoulder abduction and adduction, alongside sEMG data, recorded from professionals executing backhand down-the-line groundstrokes. Vertical lines in the graphs indicate various stages of the groundstroke, as demonstrated by XSENS MoCap figurines. Two distinct colors denote two different subjects. The solid line represents the average of five trials, while the shaded region indicates the standard deviation across the same five trials.

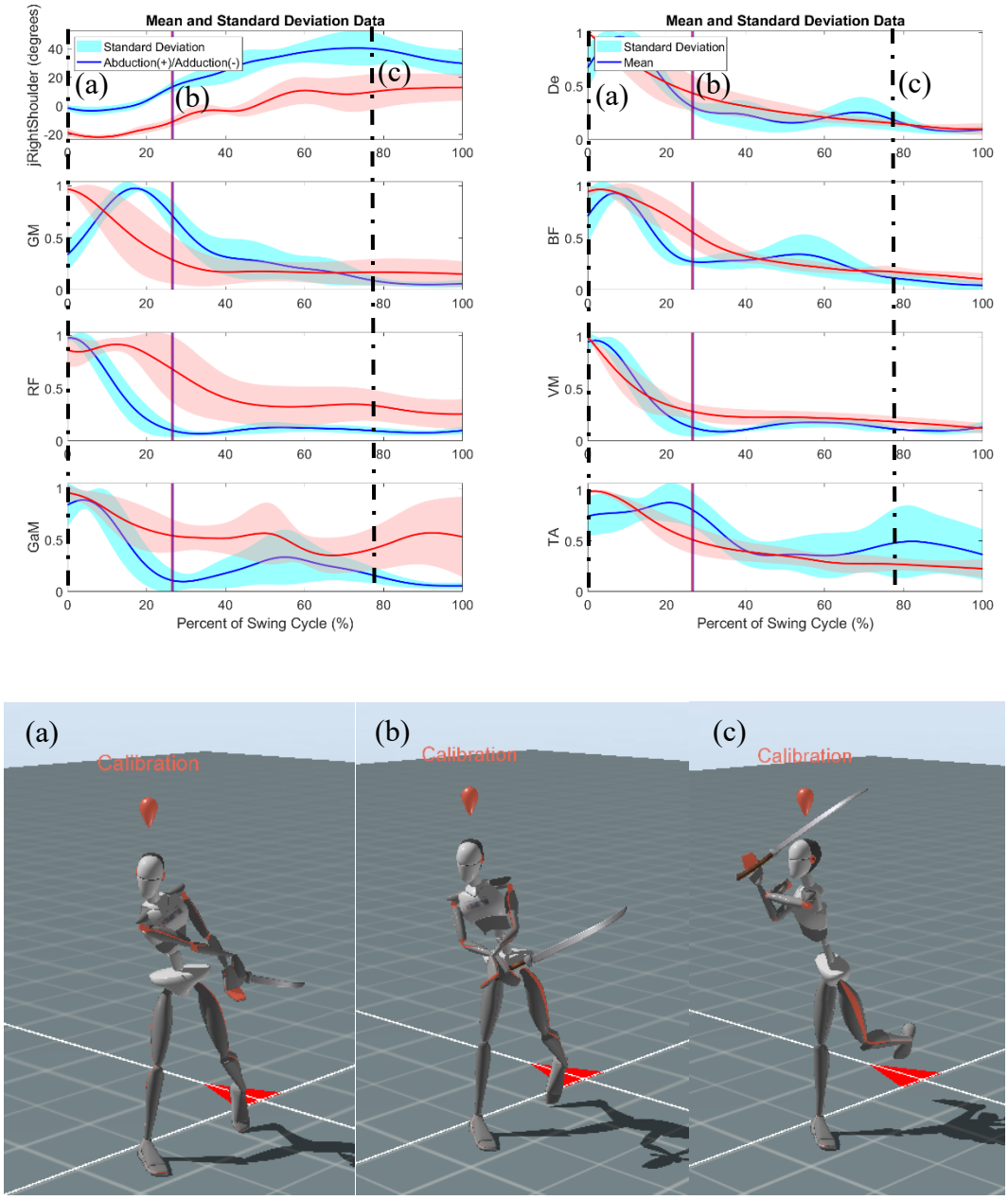

Figure 29. The graphs depict shoulder abduction and adduction, alongside sEMG data, recorded from non-professionals executing backhand down-the-line groundstrokes. Vertical lines in the graphs indicate various stages of the groundstroke, as demonstrated by XSENS MoCap figurines. Two distinct colors denote two different subjects. The solid line represents the average of five trials, while the shaded region indicates the standard deviation across the same five trials.

4.2.3 Forehand Cross-Court Groundstrokes

Figures 30 and 31 exhibit the forehand cross-court groundstrokes performed by two professional players and two non-professionals. Among the professionals, shoulder abduction initiates around the 40° mark and peaks at approximately 80° of shoulder adduction. Despite slight discrepancies in the phases of the professional players, the measured angles exhibit notable similarity. In contrast, the non-professionals demonstrate a wide variability in abduction and adduction angles. For most non-professionals, similar to professionals, shoulder abduction commences at approximately 40°. However, shoulder adduction ranges widely from 40° to about 200° among non-professional participants. Moreover, analyzing the muscle activity of professionals reveals early activation of the GM, BF, and GaM muscles before ball contact, with other muscle activity remaining relatively stable. In contrast, non-professionals exhibit no consistent major spike in muscle activity before ball contact, with all muscle activity remaining fairly constant. Lastly, the average timing of ball contact occurs later during the forehand groundstroke cycle for professionals (40% of swing cycle) compared to non-professionals (25% of swing cycle).

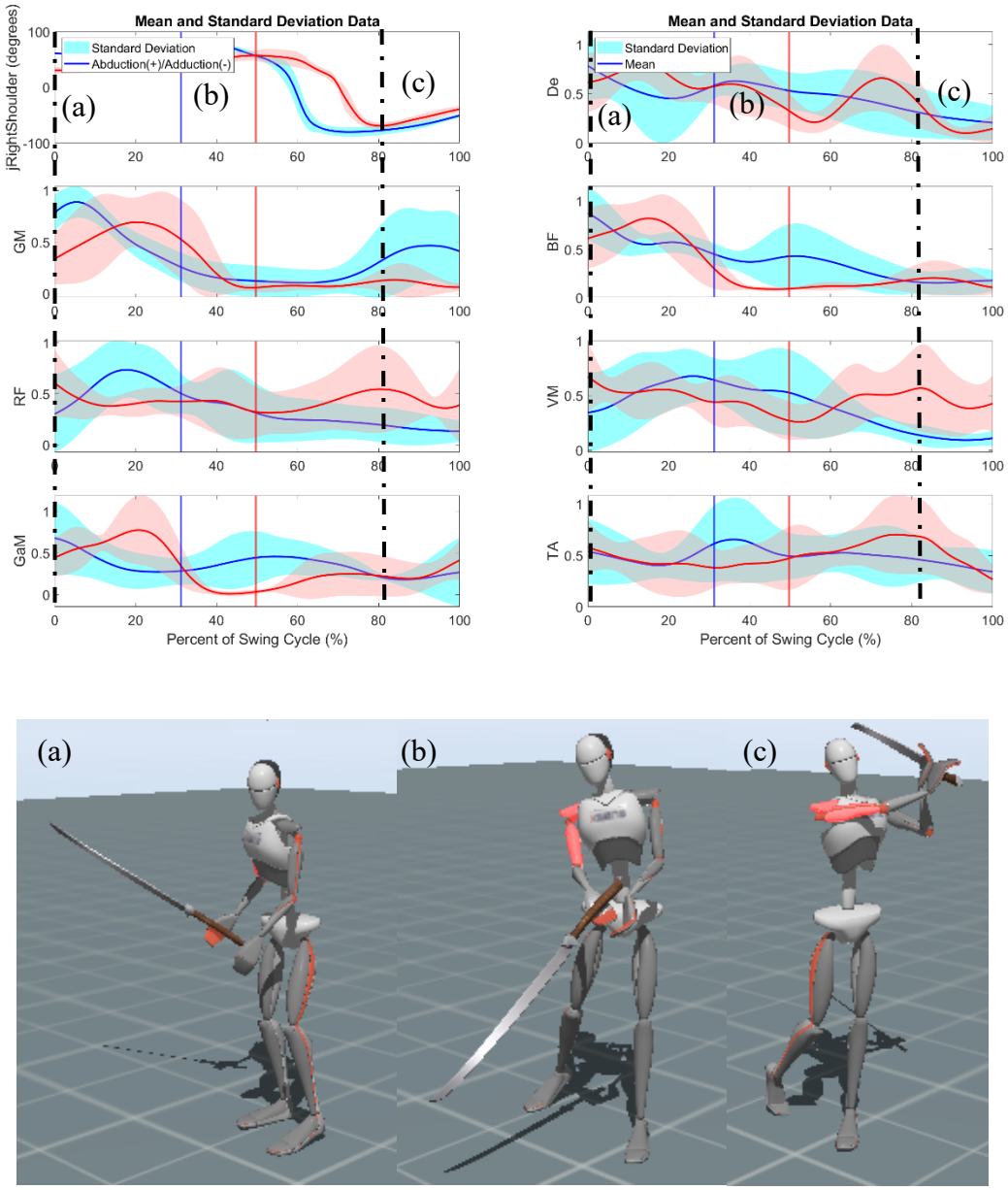

Figure 30. The graphs depict shoulder abduction and adduction, alongside sEMG data, recorded from professionals executing forehand cross-court groundstrokes. Vertical lines in the graphs indicate various stages of the groundstroke, as demonstrated by XSENS MoCap figurines. Two distinct colors denote two different subjects. The solid line represents the average of five trials, while the shaded region indicates the standard deviation across the same five trials.

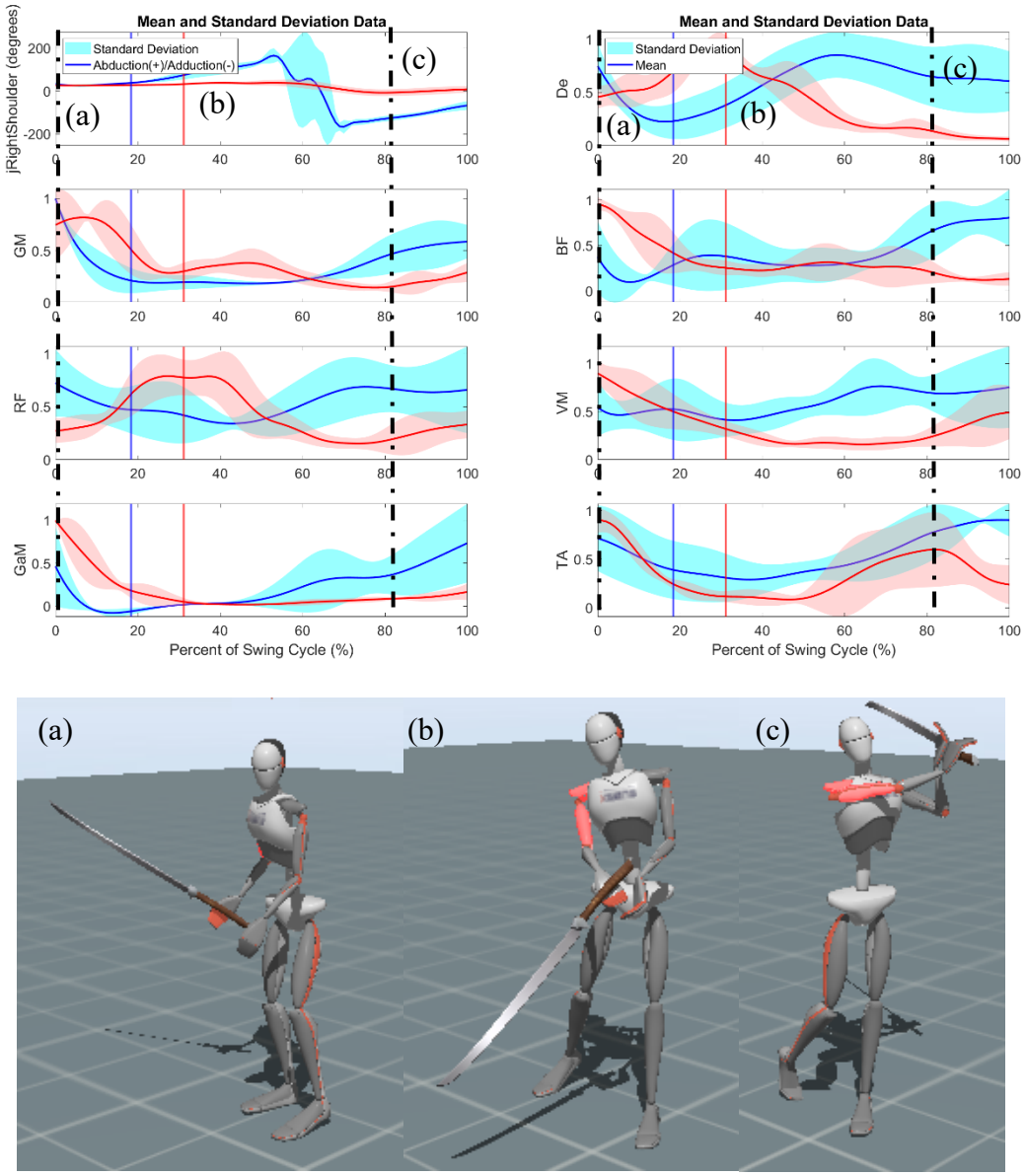

Figure 31. The graphs depict shoulder abduction and adduction, alongside sEMG data, recorded from non-professionals executing forehand cross-court groundstrokes. Vertical lines in the graphs indicate various stages of the groundstroke, as demonstrated by XSENS MoCap figurines. Two distinct colors denote two different subjects. The solid line represents the average of five trials, while the shaded region indicates the standard deviation across the same five trials.

4.2.4 Forehand Down-the-Line Groundstrokes

Figures 32 and 33 depict the forehand down-the-line groundstrokes performed by two professional players and five non-professional players. Almost the exact same trends are visible for the forehand down-the-line shots as for the forehand cross-court shots including the time of

ball contact. The ranges for the professionals is identical in this case while the ranges change only slightly for the non-professionals. Instead of an upper limit of 200° for shoulder adduction, the upper limit is closer to 175°. Lastly, similar muscle activation trends are seen as compared to the forehand cross-court shots for both the professional and non-professional players.

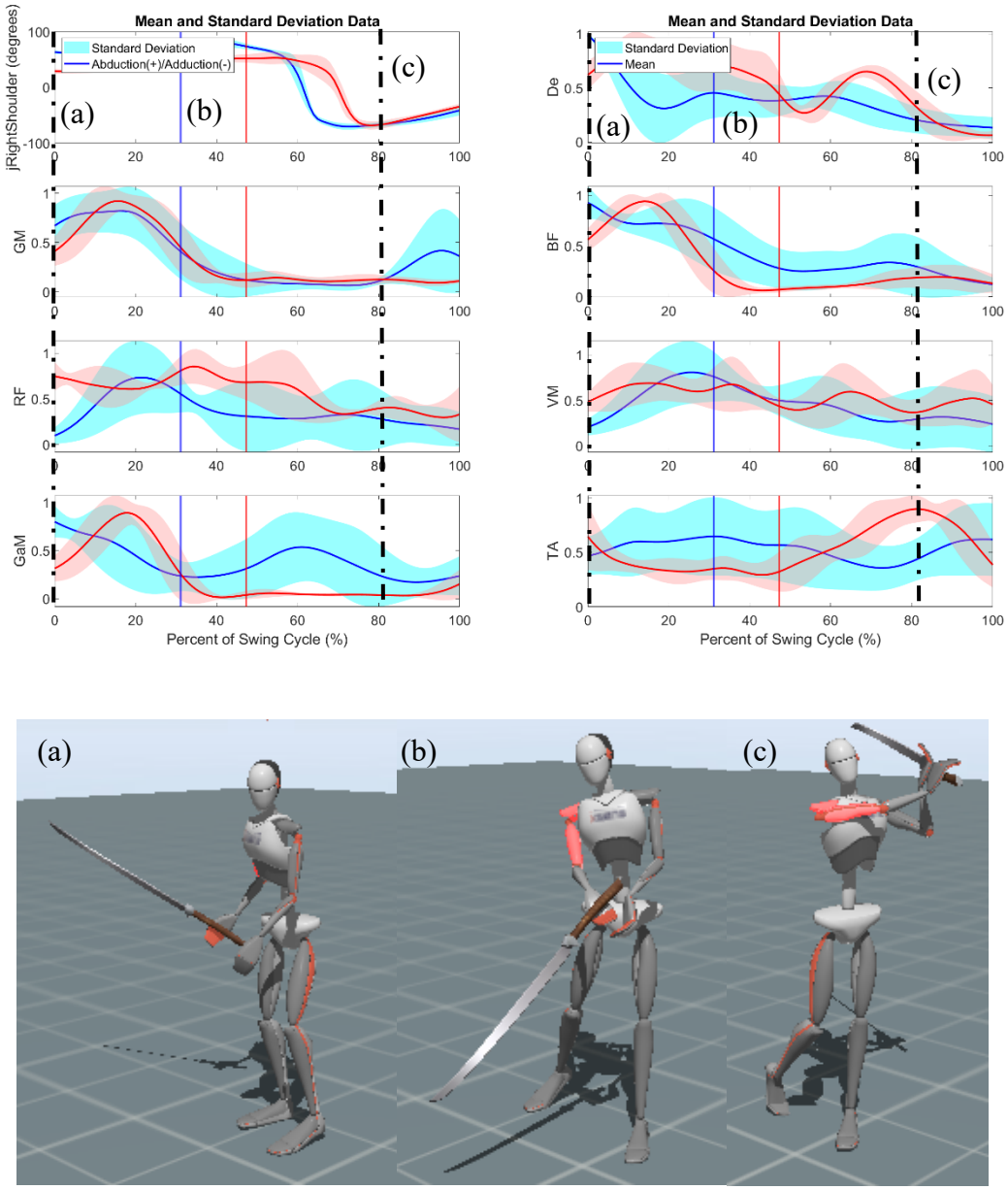

Figure 32. The graphs depict shoulder abduction and adduction, alongside sEMG data, recorded from professionals executing forehand down-the-line groundstrokes. Vertical lines in the graphs indicate various stages of the groundstroke, as demonstrated by XSENS MoCap figurines. Two distinct colors denote two different subjects. The solid line represents the average of five trials, while the shaded region indicates the standard deviation across the same five trials.

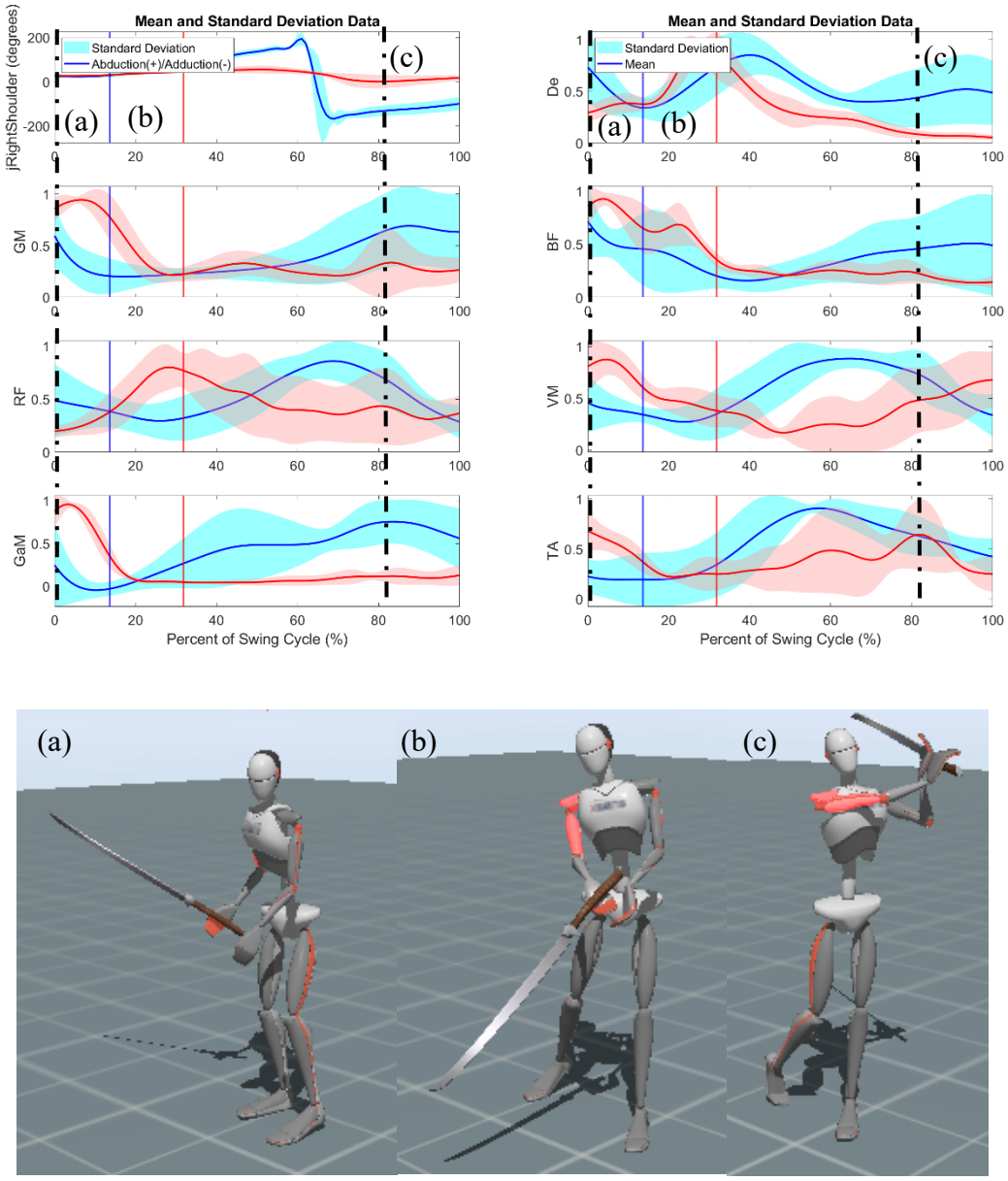

Figure 33. The graphs depict shoulder abduction and adduction, alongside sEMG data, recorded from non-professionals executing forehand down-the-line groundstrokes. Vertical lines in the graphs indicate various stages of the groundstroke, as demonstrated by XSENS MoCap figurines. Two distinct colors denote two different subjects. The solid line represents the average of five trials, while the shaded region indicates the standard deviation across the same five trials.

4.2.5 Deuce Side Serve

Figures 34 and 35 show the deuce side serve for two professional players and two non-professional players. Looking at the shoulder kinematics of the professional players, a very

similar trajectory is seen between both of the players: shoulder adduction begins at about 20°, extends to a shoulder abduction of about 120°, and ends at the starting point with a shoulder adduction of 20°. Conversely, looking at the non-professional players kinematics shows that shoulder adduction can begin anywhere in the range between 0°-50°, extend to a shoulder abduction between 80°-120°, and culminate with a shoulder adduction of 0°-50°.

Looking at the timing of muscle activation, a few more trends are noticeable. For both of the professional players, muscle activity remains very minimal before the trophy pose, depicted by the "(c)" designator, expect for the TA in one participant's data. However, in the non-professionals, muscle activity is at a higher level for all muscles before the trophy pose. Two bursts of De activation can be seen in both of the professionals and most of the non-professionals. One big similarity between the professional and non-professional players is the timing of peak muscular activation. For both groups, the peak activation for most of the big, driving muscles happens either right before or right around ball contact. One final difference to note between the professional and non-professional players is that ball contact happens at a slightly later time during the serve cycle for the professionals (80% of swing cycle) as compared to the non-professionals (75% of swing cycle).

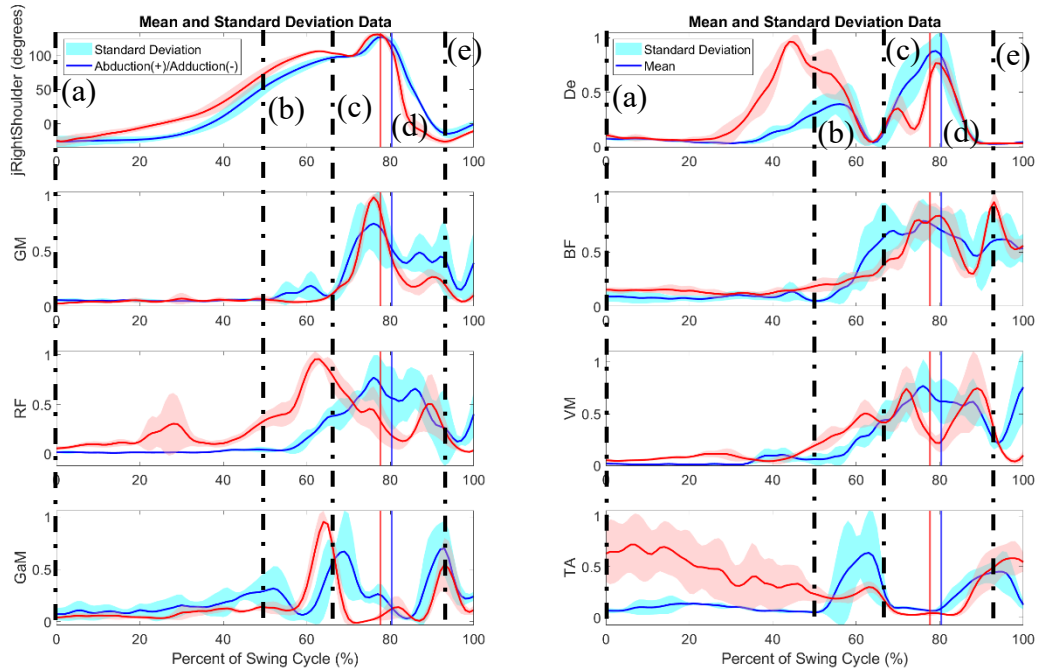

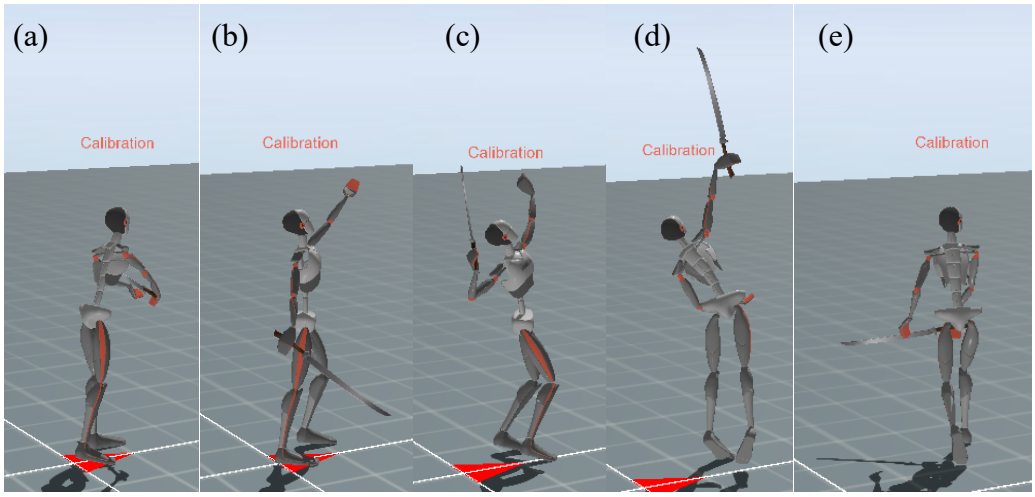

Figure 34. The graphs depict shoulder abduction and adduction, alongside sEMG data, recorded from professionals executing deuce-side serve. Vertical lines in the graphs indicate various stages of the serve, as demonstrated by XSENS MoCap figurines. Two distinct colors denote two different subjects. The solid line represents the average of five trials, while the shaded region indicates the standard deviation across the same five trials.

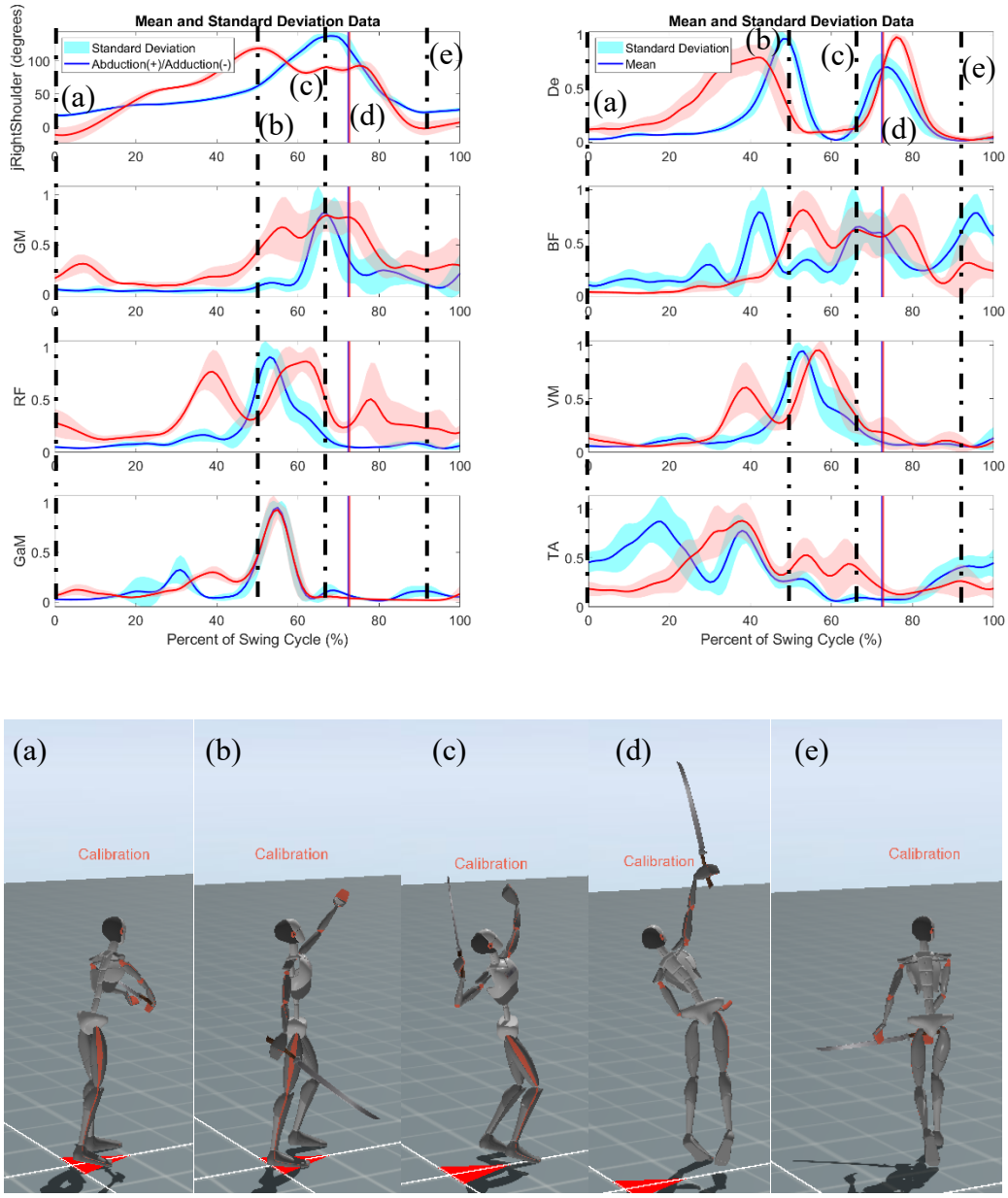

Figure 35. The graphs depict shoulder abduction and adduction, alongside sEMG data, recorded from non-professionals executing deuce-side serve. Vertical lines in the graphs indicate various stages of the serve, as demonstrated by XSENS MoCap figurines. Two distinct colors denote two different subjects. The solid line represents the average of five trials, while the shaded region indicates the standard deviation across the same five trials.

4.2.6 Advantage Side Serve

The final two figures, Figures 36 and 37, illustrate the advantage side serve. Similar patterns emerge in the shoulder kinematics of the advantage side serve as seen in the deuce side

serve. Shoulder adduction commences around 40°, extends to a shoulder abduction of about 120°, and concludes with a shoulder adduction of 20°. Similarly, the non-professional participants exhibit a broader range of shoulder adduction and abduction. Their shoulder adduction ranges from 10° to 50° at the start, extends to a shoulder abduction between 80° and 120°, and finishes between 0° and 30° of shoulder adduction.

The muscle activation trends also mirror those observed in the deuce side serve. Across nearly all participants, two peaks for the De are observed. Professional players consistently exhibit low muscle activation prior to the trophy pose, whereas non-professional players' muscle activity shows sporadic patterns. The peak contraction of muscles occurs either right before or at the point of ball contact for both professionals and most non-professionals. Another similarity between the deuce side and advantage side serves is that non-professionals make contact with the ball (75% of swing cycle) earlier in the swing cycle compared to professional players (80% of swing cycle).

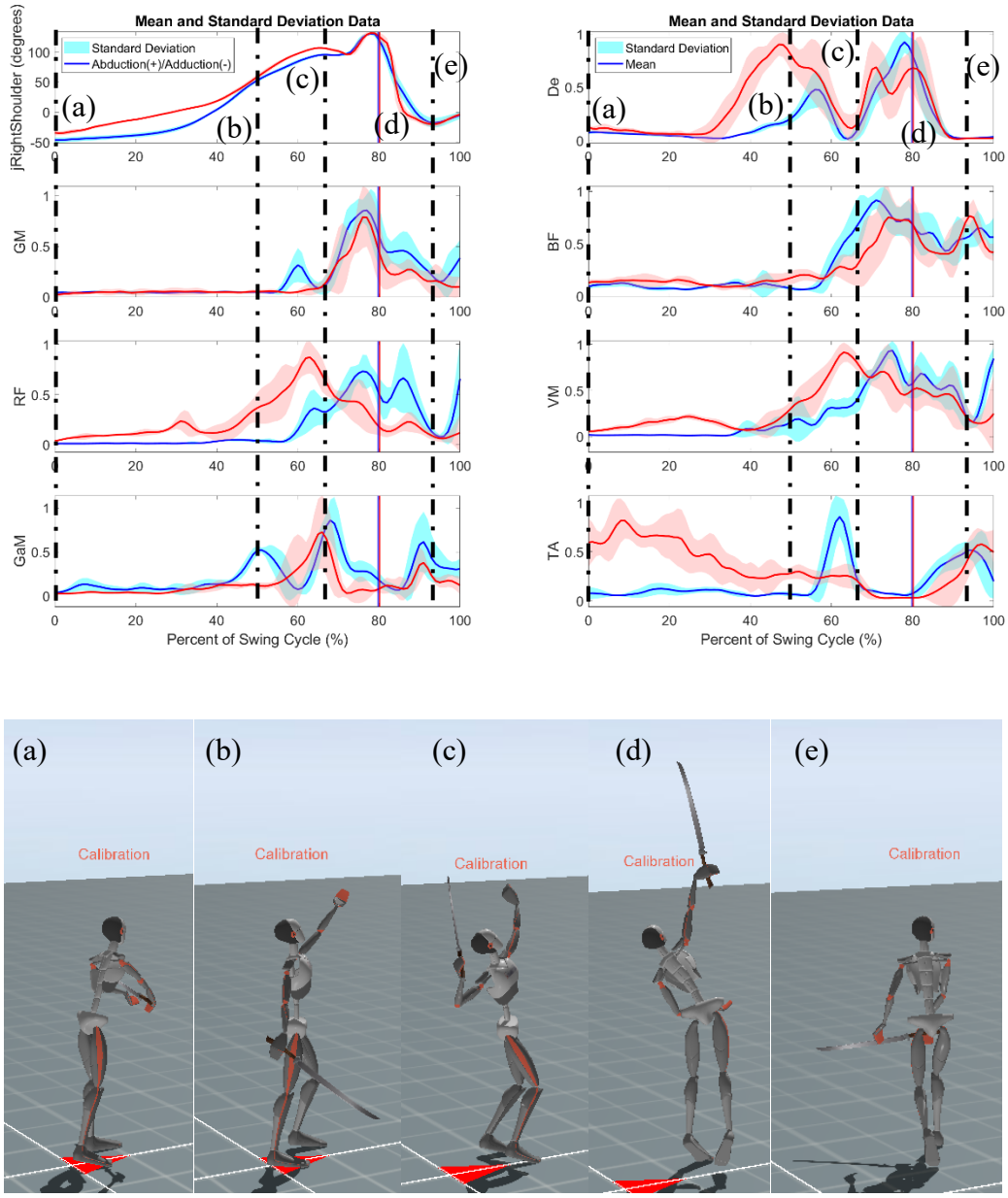

Figure 36. The graphs depict shoulder abduction and adduction, alongside sEMG data, recorded from professionals executing advantage-side serve. Vertical lines in the graphs indicate various stages of the serve, as demonstrated by XSENS MoCap figurines. Two distinct colors denote two different subjects. The solid line represents the average of five trials, while the shaded region indicates the standard deviation across the same five trials.

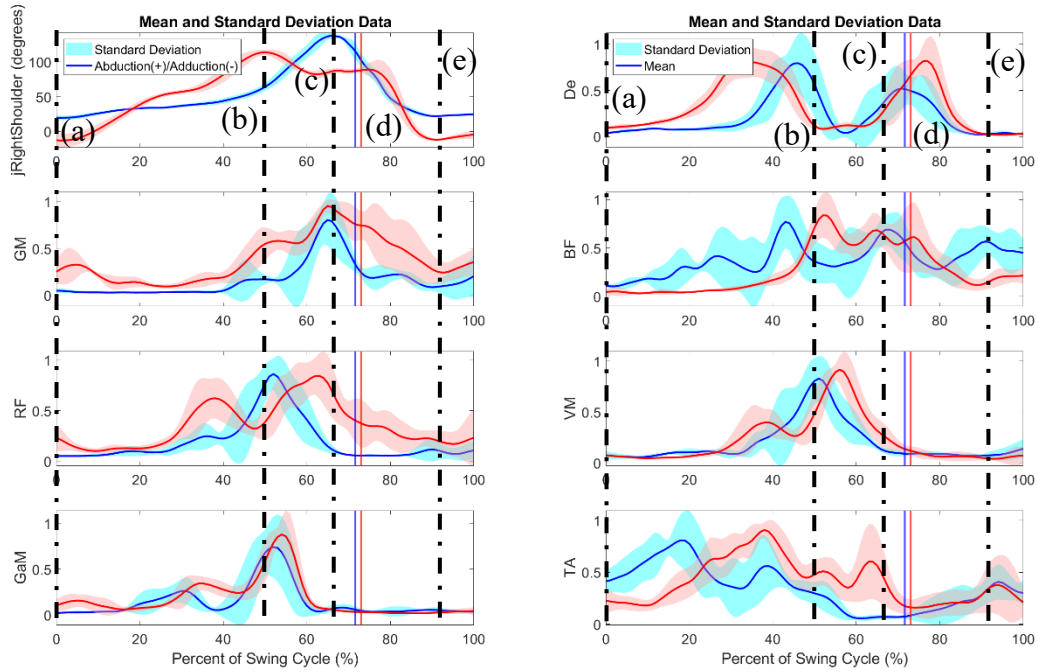

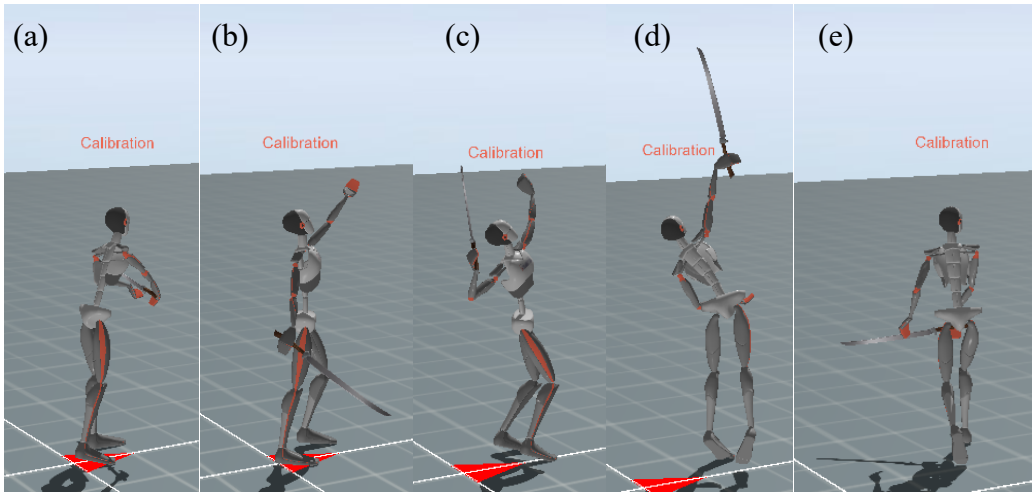

Figure 37. The graphs depict shoulder abduction and adduction, alongside sEMG data, recorded from non-professionals executing deuce-side serve. Vertical lines in the graphs indicate various stages of the serve, as demonstrated by XSENS MoCap figurines. Two distinct colors denote two different subjects. The solid line represents the average of five trials, while the shaded region indicates the standard deviation across the same five trials.

Chapter 5 – Discussion

5.1 Range of Motion

The study's small sample size notwithstanding sheds light on significant disparities between professional and non-professional tennis players, particularly regarding their biomechanics and range of motion during various shot types—forehands, backhands, and serves. The findings underscore several crucial insights. Firstly, it's evident that professional players exhibit a notably broader range of motion across all shot types compared to their non-professional counterparts, especially seen in Figures 24 and 25. These findings agree with the study performed by Hornestam et al. [8]. This expanded range of motion is indicative of enhanced flexibility, agility, and technical proficiency among professional players. Such capabilities enable them to execute shots with greater precision, power, and consistency, contributing to their overall performance superiority. The observed differences in range of motion underscore the importance of comprehensive training regimens tailored to enhance flexibility and mobility among aspiring tennis players. Emphasizing exercises aimed at improving joint flexibility, muscle elasticity, and overall body mobility can be instrumental in bridging the gap between amateur and professional skill levels in tennis.

Moreover, the study's findings emphasize the critical role of biomechanics in tennis performance. Professional players' ability to execute shots with a wider range of motion suggests optimal biomechanical efficiency, allowing them to generate maximum racket head speed and transfer kinetic energy effectively. This efficiency not only enhances shot power but also minimizes the risk of injury by ensuring proper technique and movement mechanics. Furthermore, the disparity in range of motion highlights potential areas of focus for non-professional players seeking to elevate their game. By incorporating targeted stretching routines,

flexibility exercises, and biomechanical drills into their training programs, amateur players can gradually expand their range of motion, refine their technique, and enhance their overall on-court performance.

5.2 Time of Ball Contact

Another significant contrast between professional and non-professional players lies in the timing of ball contact during their swings, particularly noticeable in forehands and serves. It appears that non-professional players tend to rush their shots, whereas professionals prioritize generating energy from the ground up before making contact. This distinction becomes especially apparent when comparing backhand down-the-line shots and forehand down-the-line shots.

In forehand down-the-line groundstrokes, professionals typically make contact with the ball at approximately 40% of their swing cycle as seen in Figure 32. However, non-professionals do so at around 20% as seen in Figure 33. This disparity underscores the difference in timing precision and energy transfer between the two groups. Additionally, prior to ball contact, professionals exhibit activation of three specific muscles—GM, BF, and GaM—all belonging to the posterior chain. This activation indicates a proper loading mechanism conducive to driving force towards the ball, consistent with previous research findings [14]. Conversely, non-professionals either show minimal activation of these muscles or activate them to a lesser extent, resulting in improper loading and premature ball contact. To enhance the understanding among professionals and non-professionals, Figure B-91 offers a useful visual aid. Within the illustration, the red line represents a typical professional, whereas the blue line represents a typical non-professional. Although the shoulder kinematics exhibit similar shapes, there are

significant disparities in muscle activation, particularly noticeable in the GM, BF, RF, VM, and GaM muscles.

Conversely, when comparing backhand down-the-line groundstrokes, the discrepancy in ball contact timing between professionals and non-professionals diminishes significantly. Both groups make contact at approximately 20% and 25% of their swing cycles, respectively, indicating a more synchronized timing approach. Moreover, both professional and non-professional players exhibit activation of the GM, BF, and GaM muscles prior to ball contact, suggesting a similar preparation for efficient shot execution. In this shot type, non-professionals emulate the muscle activation pattern observed in professionals, allowing for optimal priming of muscles and effective ball contact. For a clearer comparison of muscle activation patterns between professionals and non-professionals, Figure B-92 serves as a valuable tool. Similar to Figure B-91, the red line corresponds to a typical professional, while the blue line signifies a typical non-professional. Although the professional demonstrates a wider range of shoulder kinematics compared to the non-professional, the muscle activation remains highly similar across all muscles for both participants.

One possible explanation for the comparable timing of muscle activation observed in both professionals and non-professionals during the backhand groundstroke may stem from biomechanical constraints inherent to the body's movements. Specifically, the dominant shoulder's capacity for internal rotation in preparation for the backhand groundstroke may be limited. Additionally, effective execution of the shot requires the dominant foot to be firmly planted beforehand to generate power. Consequently, in order to complete the motion, tennis players of any skill level must engage the posterior chain muscles, push off with the dominant

foot, and drive towards the ball. This alignment of actions is evident in the data from both professional and non-professional players.

While professionals demonstrate a clear advantage in timing and muscle activation during forehands, the disparity diminishes in backhand shots. By understanding and emulating the techniques employed by professionals, non-professional players can improve their timing precision, energy transfer, and overall shot quality on the tennis court. Particularly with regards to forehands, non-professional players could enhance their performance by focusing on driving towards the ball and engaging their posterior chain muscles before making contact. Strengthening these muscles through targeted exercises, perhaps specific weight training, can help improve their ability to drive effectively towards the ball.

5.3 Consistency

This study yielded a surprising revelation regarding the consistency of performance between professional and non-professional tennis players, contrary to conventional expectations. Despite the vast discrepancy in experience and training hours between the two groups, the data analysis revealed comparable levels of consistency in their respective performances.

Conventionally, one might anticipate professional players to exhibit significantly higher levels of consistency, given their extensive practice and exposure to competitive play. However, the empirical evidence from this study challenges such assumptions, highlighting a remarkable parity in consistency between professionals and non-professionals.

This equivalence in consistency is prominently illustrated through the examination of standard deviations, represented by shaded regions in the figures. It is noteworthy that professional players demonstrated lower standard deviations in kinematic parameters compared to non-professionals, indicating a tighter performance distribution within the professional cohort.

However, the similarity in consistency becomes apparent when analyzing sEMG data. Despite the differing skill levels and training backgrounds, the standard deviation between professional and non-professional players in sEMG data remains strikingly similar. This finding underscores the unexpected similarity in muscle activation patterns and neuromuscular control mechanisms between professional and non-professional players, despite their divergent levels of proficiency. That is, all non-professionals have some professional tendencies.

Furthermore, this finding underscores the importance of considering both kinematic and physiological parameters when evaluating performance consistency in tennis players. While kinematic parameters may reflect technical proficiency and skill execution, sEMG data provides valuable insights into neuromuscular coordination and muscle activation patterns, offering a more holistic understanding of performance consistency. Therefore, while it is important to learn the specific technique of every different type of shot, it is more important to able to make adjustments and react accordingly.

One reason as to why the standard deviation is similar between the two groups is because of the consistency of the ball being thrown or launched by the ball machine. For service, it is nearly impossible to have the ball thrown the exact same way and to the exact same height. Similarly, despite the ball being launched from a ball machine for forehand and backhand groundstrokes, variations as to where and how the ball bounces can exist. Therefore, the player needs to adapt to the ball which can lead to different muscle activation at different time, resulting in a greater standard deviation.

Overall, while the study's limited sample size necessitates cautious interpretation, its findings underscore the significance of kinematics and sEMG data in distinguishing between professional and non-professional tennis players. By recognizing and addressing these

differences through tailored training interventions, aspiring players can strive towards narrowing the performance gap and realizing their full potential on the tennis court.

Chapter 6 – Conclusion and Future Directions

This study provides valuable insights into the disparities between professional and non-professional tennis players, particularly regarding biomechanics, timing, and performance consistency. Despite its limited sample size, the findings shed light on several key areas that influence on-court performance.

Firstly, the study highlights the pronounced differences in range of motion across various shot types, with professionals demonstrating superior flexibility, agility, and technical proficiency compared to non-professionals. These findings underscore the importance of tailored training regimens focused on enhancing flexibility and mobility among aspiring tennis players, thereby bridging the gap between amateur and professional skill levels.

Moreover, the study emphasizes the critical role of biomechanics in tennis performance, with professional players exhibiting optimal efficiency in energy transfer and technique execution. This efficiency not only enhances shot power but also minimizes the risk of injury, underscoring the importance of proper technique and movement mechanics in player development.

Furthermore, the analysis reveals significant disparities in the timing of ball contact during forehands and serves, with professionals demonstrating a more deliberate approach to energy generation from the ground up. However, this discrepancy diminishes in backhand shots, indicating potential areas for non-professionals to emulate professional techniques and improve their on-court performance.

Surprisingly, the study unveils a remarkable parity in performance consistency between professional and non-professional players, challenging conventional assumptions. While

professionals exhibit lower standard deviations in kinematic parameters, the similarity in sEMG data suggests unexpected similarities in muscle activation patterns between the two groups.

The study also highlights the importance of considering both kinematic and physiological parameters when evaluating performance consistency in tennis players. Variations in ball delivery from ball machines necessitate player adaptation, resulting in different muscle activation patterns and contributing to the observed standard deviation.

One potential avenue for future research in this study involves delving deeper into the analysis of surface electromyography (sEMG) data. While this study filtered the sEMG data and applied a linear envelope to visualize muscle activity, further exploration could entail more intricate analyses such as cross approximate entropy or cross-correlation calculations. These methods could provide insights into the interactions and coordination among muscles.

Another prospective direction for this study is the integration of a wireless EMG system. Although data collection using a wired EMG system was successful, managing the wires during experimentation presented challenges. Transitioning to a wireless system could potentially streamline data collection processes.

Additionally, a potential enhancement to this study could involve implementing a printed circuit board (PCB) for the synchronization switch instead of using a breadboard and individual components. Utilizing a PCB would securely hold all components in place, mitigating the risk of disconnection or instability during experimentation.

From the standpoint of analysis, another future direction would be the study between the one-handed and two-handed backhand. In the current study, both of the professional players and four of the non-professionals had a two-handed backhand. Upon observation, it was seen that the individuals who performed the backhand groundstroke with one hand had a greater shoulder

abduction and adduction range. While definitive conclusions could not be made from this study currently, as the sample size of the study increases, a more thorough analysis could be performed leading to more generalizations between one-handed and two-handed backhands.

In summary, while the study's limitations warrant cautious interpretation, its findings underscore the significance of kinematics and sEMG data in understanding and addressing performance disparities in tennis. By leveraging these insights and implementing tailored training interventions, aspiring players can strive towards narrowing the performance gap and realizing their full potential on the tennis court.

Appendices
Appendix A: Informed Consent Form

Informed Consent

Deciphering the Relationship Between Body Mechanics and Skill Level in Tennis Players

Researchers: Yunju Lee, PhD (principal investigator), Samhita Rhodes, PhD (co-investigator).

You are being asked to take part in a research study. The box below highlights key information about this research for you to consider when making a decision whether or not to take part. Carefully consider this information and the more detailed information provided below the box. Please ask questions about any of the information you do not understand before you decide whether to take part.

Key Information for You to Consider

- **Voluntary Consent**. You are being asked to volunteer for a research study. It is up to you whether you choose to participate or not. There will be no penalty or loss of benefits to which you are otherwise entitled if you choose not to participate or discontinue participation.
- **Purpose**. The purpose of this research is to capture your 3D motion when you are performing forehand, backhand, and overhead serve shots. We want to see how these measures compare between those who have beginner, intermediate, and advanced tennis experience.
- **Duration.** It is expected that testing will last 1.5-2 hours for a one-time session.
- **Procedures and Activities**
  - You will have selected physical measures taken, e.g., height, weight, etc.
  - You will have electromyographic (EMG) sensors placed onto your skin throughout your dominant side ranging from the shoulder to the lower leg.
  - You will have 17 sensors placed onto your skin throughout your torso, arms, and legs with an additional sensor on the base of your racket.
  - Your 3D motion will be calibrated by having you stand still and walk a short distance.
  - Your 3D motion including that of the racquet will be measured while you participate in the serve, forehand and backhand shot trials. We will assess your stroke type, accuracy of the shot, and the resultant velocity.
- **Risks.** Some of the foreseeable risks or inconveniences of your participation may include discomfort due to sensor and tape placement.
- **Benefits**. You may not receive immediate, direct benefit. With appropriate attention to managing risks, as noted above, benefits will not be affected.
- **Alternatives.** Taking part in this research is voluntary and the only alternative is to not take part.

Purpose
The purpose of this research is to record your joint angle placement, the resultant racquet velocity, and muscle activity during different styles of tennis shots. We want to see how these angles, velocities, and activity compare between beginner, intermediate, and advanced levels of tennis performance. This information may be used to prevent injury and improve training, performance, and rehabilitation.

Reasons for Invitation
You are asked to volunteer because we want to improve our understanding of shot performance in male and female beginner, intermediate, and advanced level athletes. To take part you will need to be medically and physically healthy.

Your eligibility will be determined by completing a self-assessment. Participants will be included if they: 1) are between 18 and 50 years of age and 2) are at least a beginner tennis player according to the Universal Tennis Rating Conversion Chart. Participants will be excluded if they 1) have musculoskeletal injuries/impairments requiring surgical intervention within the past 12 months, 2) had any musculoskeletal injuries/impairments of the spine, pelvis, and upper and lower extremities that required medical treatment within the past 12 months, 3) are currently pregnant, 4) are currently being treated for cardiopulmonary diseases, or 5) have been diagnosed with a neurologic disorder such as Multiple Sclerosis or Parkinson's Disease.

If you are a current varsity athlete, it is recommended you inform your coach and gain approval from your own institution to participate in this study.

Procedures
The testing session will take approximately 1.5-2 hours. You will be asked to wear a tee-shirt, shorts, and usual tennis shoes to be able to easily apply the sensors directly to skin.

Prior to data collection you will be asked some questions about your medical health history, age, and tennis experience, which will take about 10 minutes. Then some physical measures will be taken including weight assessment, height, and extremity length measurements which will be completed in 10 minutes.

A total of 17 motion sensors will be secured (using straps, elastic adhesive tape, and surgical tape) on your head, trunk, pelvis, arms, and legs. The 12 sensors placed on the arms, hands, legs, and feet will be stabilized with elastic adhesive tape around the extremity. The 4 sensors of the trunk (2 on shoulder blades, 1 on low back, and 1 on middle of chest) will be secured using surgical tape. The 1 sensor for the head will be secured using elastic adhesive tape or a headband if preferred. All sensors will be secured directly onto the skin to ensure the accuracy of the device measurements, aside from the head and feet sensors. The devices shall be placed as to not cause harm or interfere with the individual's natural movement.

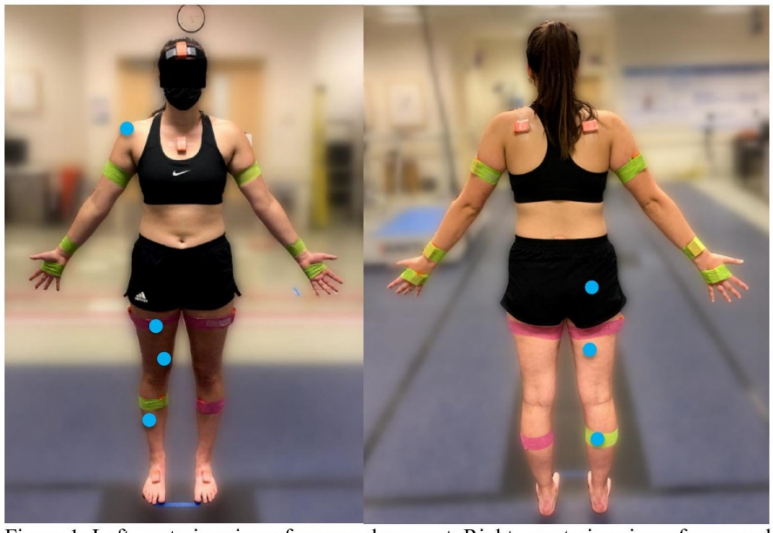

Figure 1: Left - anterior view of sensor placement. Right - posterior view of sensor placement. A total of 17 sensors are placed on the individual, 1 more sensor will be applied to the racquet. The blue circles indicate the locations of EMG sensors assuming the subject is right-side dominant.

Before we place the EMG electrodes, we will clean the skin over the middle part of the muscles we are interested in with alcohol swabs. We may need to shave the area first, and then we will gently rub it with mini-alcohol swabs

to make it clean and thoroughly dry. Before shaving, skin will be moistened with a damp, disposable, paper towel to minimize discomfort during shaving. After shaving, the area will be wiped dry and a period of 1 minute will elapse before gentle rubbing with alcohol wipes. We will then place gel-type EMG sensors directly on your skin and secure them with surgical tape to minimize movement artifact. We will shave any hair from the area around the electrodes, if necessary, to make it less uncomfortable when we remove the tape. Otherwise, we will use alcohol swabs to dissolve the adhesive on the tape as we remove it. To place the electrodes, we will rub the target area for 5 seconds with mini-alcohol swabs. We will place the electrodes approximately parallel to the direction of the muscle fibers. We will check the accuracy of the electrode placement by having you perform various movements and by feeling the muscles. We will place electrodes on one shoulder muscle (the medial deltoid) and several muscles in the hip (gluteus maximus), thigh (biceps femoris, rectus femoris, vastus medialis), and shin (gastrocnemius medialis, tibialis anterior). To ensure privacy for the placement of electrodes on sensitive areas of the body, a private location will be used near the tennis court.

XSENS sensor placement will be performed by two trained researchers on the tennis court where the study will take place. Both male and female researchers will be available to perform sensor placement if the participant has a preference. To secure the 4 trunk sensors directly onto the skin, the participant's tee-shirt will need to be temporarily removed. If participants prefer to remain fully clothed, they have the option to decline the removal of the shirt and the sensors will be secured tightly over the shirt with elastic adhesive tape and surgical tape.

Testing will take place on a standard tennis court on the GVSU campus. When weather does not permit testing on an outdoor court, testing will proceed at an indoor court. You will be asked to perform a series of shots including forehand, backhand, and serve while targeting cross court and down the line targets. A ball shooter will be located on the opposite side of the court for ball distribution. Participants will go through a self-directed warm up for 5 minutes. You will have 3 to 5 practice shots for each position, then 3 total trials for each will be assessed. For each shot, data will be collected of the joint angles of the upper and lower extremities, the velocity of the racquet, and the accuracy of the shot placement. We will use the video cameras to record the movement of the balls and shots. Data will be recorded for a total of 18 shots.

After we complete data collection of tasks, we will take a few minutes to check the data. Following our data checks, the sensors will be removed. The participant is requested to attend this single session lasting approximately 1.5-2hrs.

Risks
Other risks involved with this project are not expected but may include a mild muscle or joint strain.
Electronic data will be collected and/or stored for this research project. As with any use of electronic means to store data, there is a minimal risk that data could be lost or stolen.

Compensation for Harm
Emergency first aid will be provided to you, and you will be referred to an appropriate medical care center. Any costs for additional medical care that may be required are your responsibility and that of your medical insurance company.

Benefits to Society
A better understanding of the body mechanics, force generation, and accuracy of advanced tennis players as compared to intermediate or beginner level players. This may be used to prevent injury and improve training, performance, and rehabilitation in the less experienced tennis athletes.

Privacy and Confidentiality
Your name will not be given to anyone other than the research team. All information collected from you or about you is for the sole purpose of this research study and will be kept private to the fullest extent allowed by law. In very rare cases specially authorized university or government officials may be given access to our research records for purposes of protecting your rights and welfare, or to make sure the research was done properly.
Identifying data will be linked to data as long as the study remains active but will be stored separate from actual

data. This will be done so the possibility of linking the identifiers to the actual data will be decreased. Digital data will not be destroyed. All digital data will be stored in password protected computers in the Biomechanics and Motor Performance Laboratory (BMPL) at GVSU. This room is secured 24 hrs/day, 7 days/wk. and can be accessed only by students and faculty with GVSU Public Safety approved access cards.

After the study is over
After the study is over the research team will keep your research data to use for future research (with GVSU IRB approval). Future research will only use previously collected, but not analyzed data. Your name and other information that can directly identify you will be kept secure (BMPL) and stored (locked cabinets) apart from the research data collected as part of the project.

Research Study Results
If you wish to learn about the results of this research study you may request that information by contacting Yunju Lee (leeyun@gvsu.edu).

Payment
At this time, there is no compensation for volunteering in this study.

Payment for Research Related Injuries
In the unlikely event of minor injury, first aid will be provided. If the injury is not caused by the negligence of the primary investigator of the study, further medical care will continue under the direction of your physician in accordance with your own particular financial arrangement.

Removal from Study
Your decision to voluntarily withdraw from this study will be accepted without question.

Agreement to Participate
By signing this consent form below you are agreeing to the following:

- The details of this research study have been explained to me, including what I am being asked to do and the anticipated risks and benefits;
- I have had an opportunity to have my questions answered;
- I am voluntarily agreeing to take part in the research as described on this form;
- I may ask more questions or quit taking part at any time without penalty.

Print Name: _____

Sign Name (in ink): _____

Date Signed:_____

Contact Information
If you have any questions about this study you may contact: Yunju Lee, PhD,
PHONE: 616-331-6043; E-MAIL: leeyun@gvsu.edu.

If you have any questions about your rights as a research participant, please contact the **Office of Research Compliance & Integrity** at Grand Valley State University, 1 Campus Drive, Allendale, MI. Phone: 616-331-3197. E-mail: rci@gvsu.edu.

This research protocol has been approved by the Institutional Review Board at Grand Valley State University. File No. 23-296-H

Appendix B: Supplemental Figures

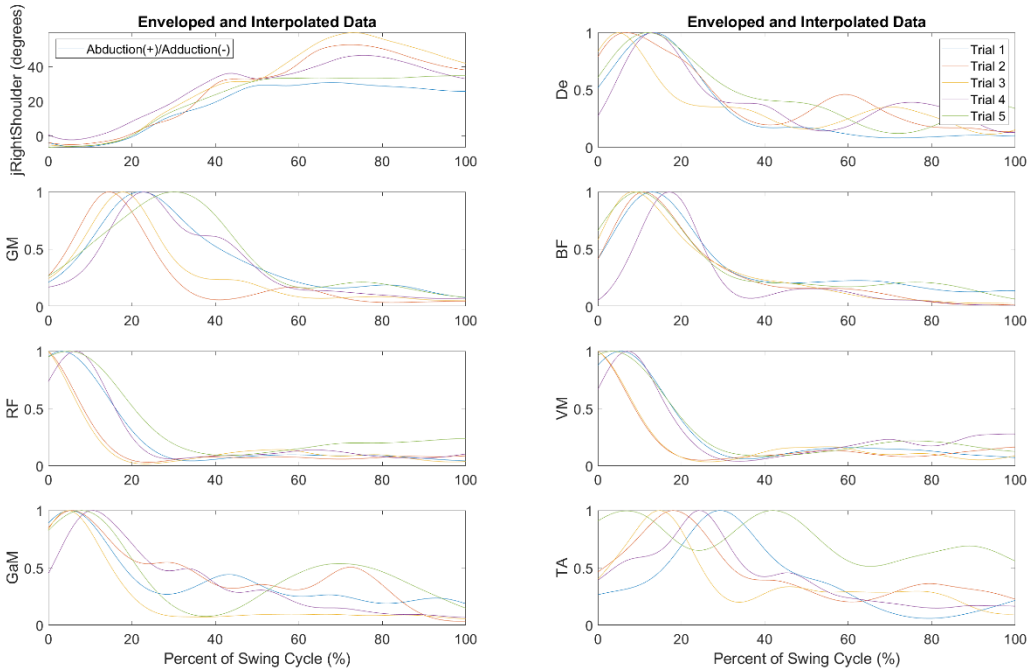

Figure B-1. TX08 individual backhand cross-court groundstrokes

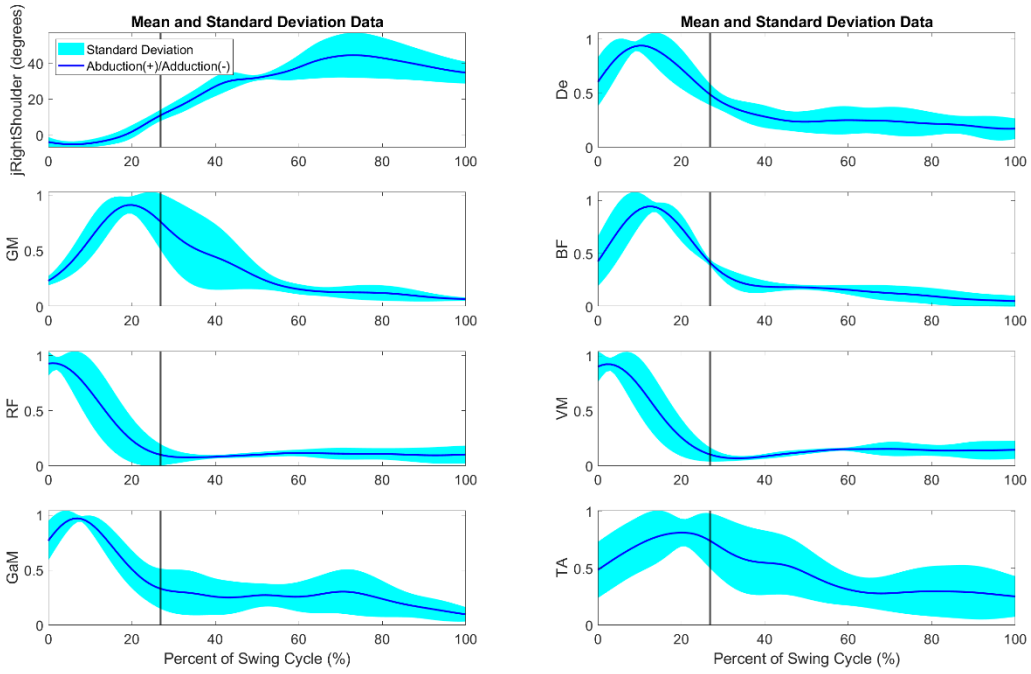

Figure B-2. TX08 averaged backhand cross-court groundstrokes with ball contact shown by vertical line

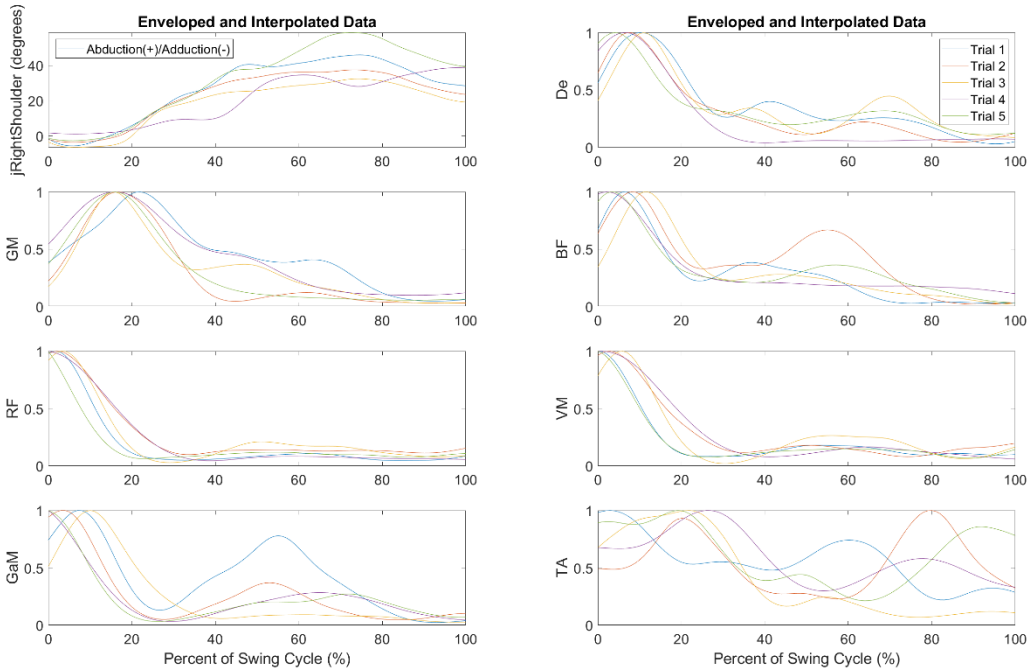

Figure B-3. TX08 individual backhand down-the-line groundstrokes

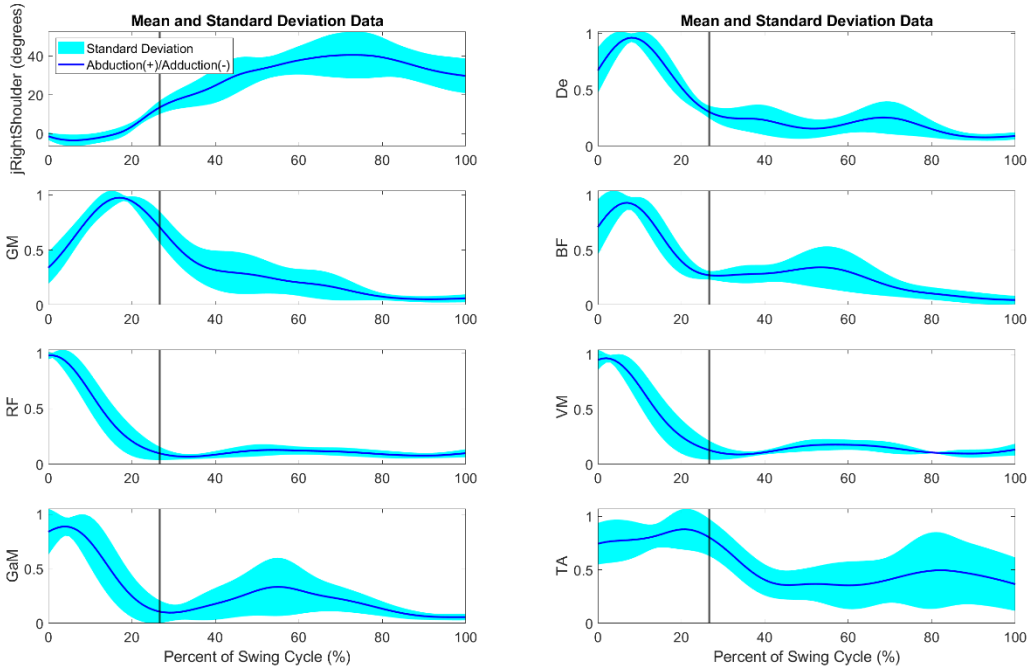

Figure B-4. TX08 averaged backhand down-the-line groundstrokes with ball contact shown by vertical line

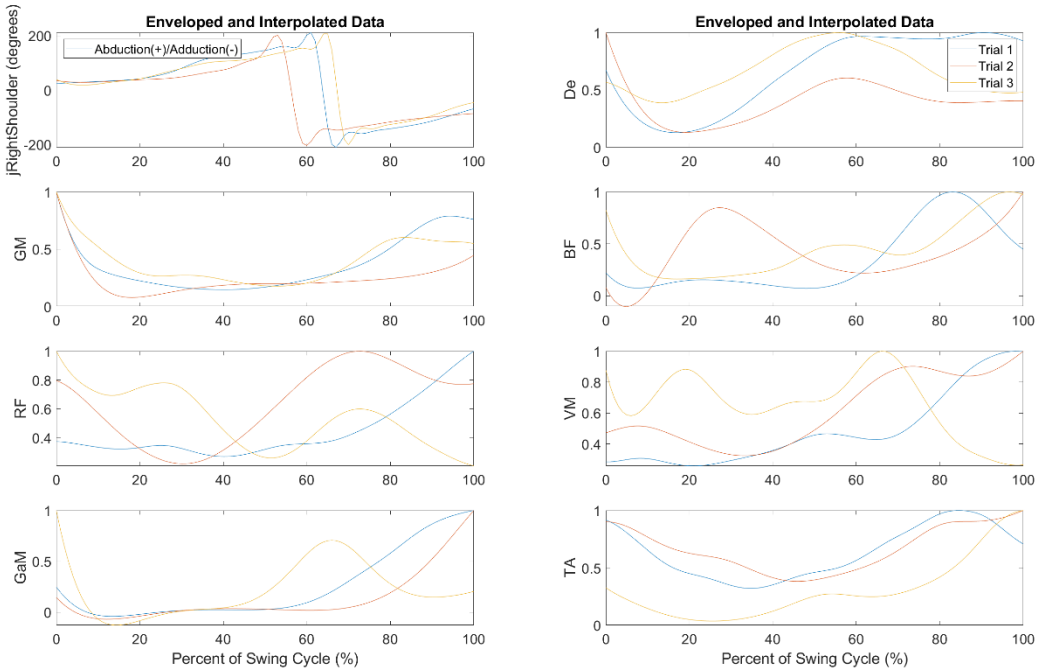

Figure B-5. TX08 individual forehand cross-court groundstrokes

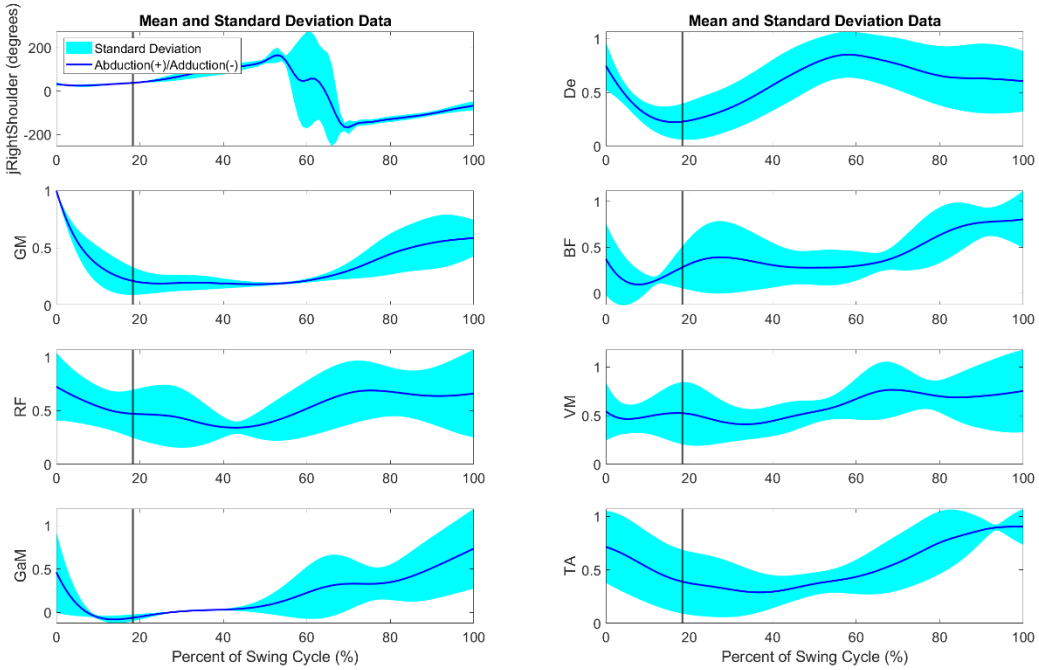

Figure B-6. TX08 averaged forehand cross-court groundstrokes with ball contact shown by vertical line

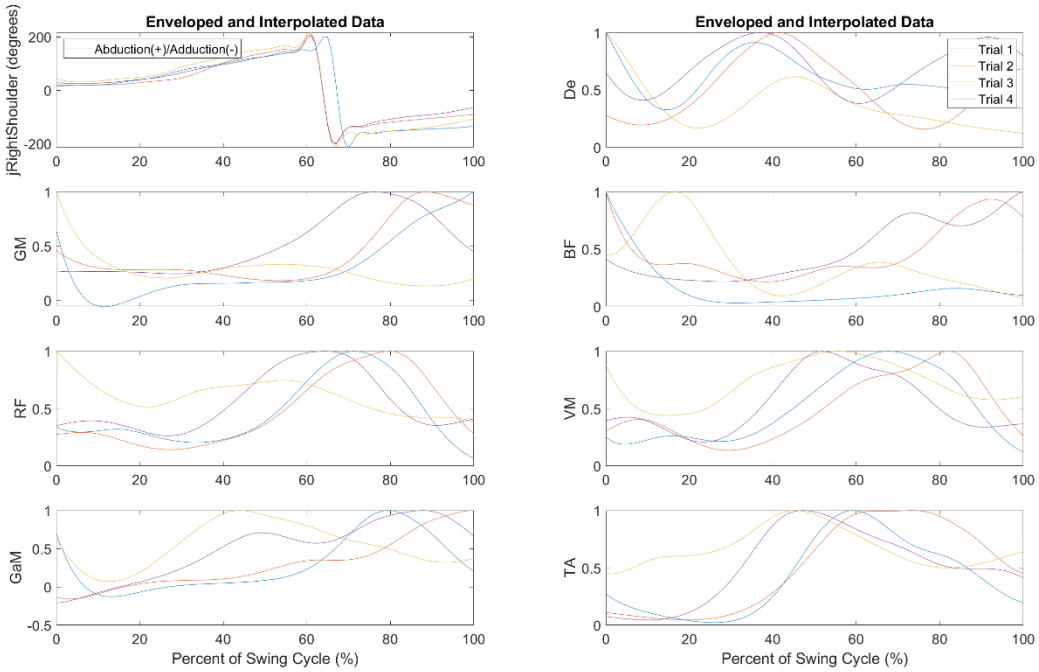

Figure B-7. TX08 individual forehand down-the-line groundstrokes

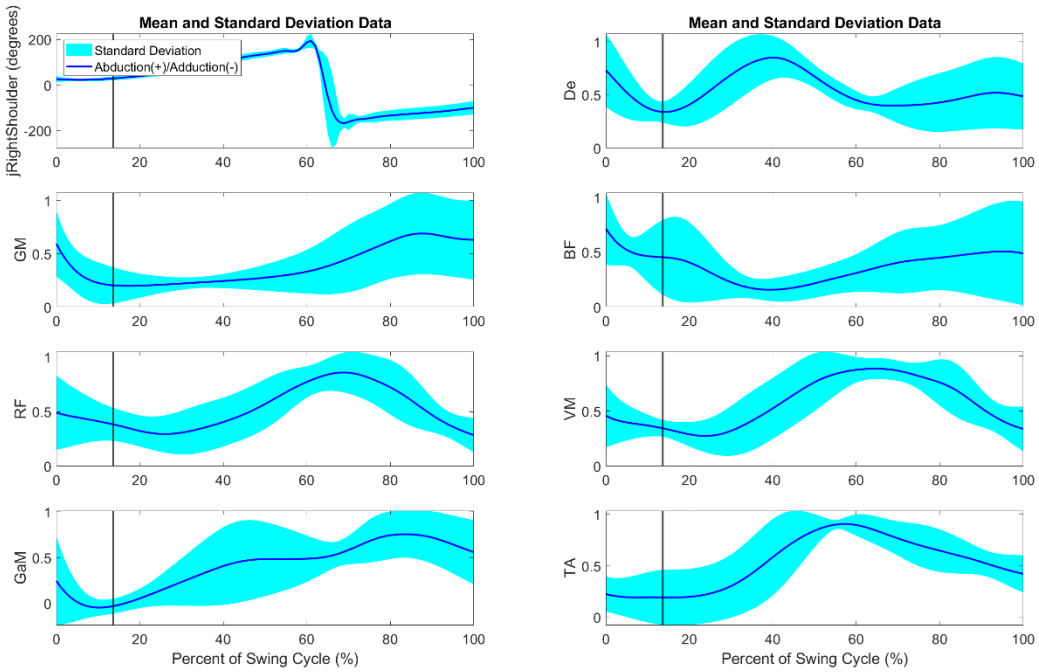

Figure B-8. TX08 averaged forehand down-the-line groundstrokes with ball contact shown by vertical line

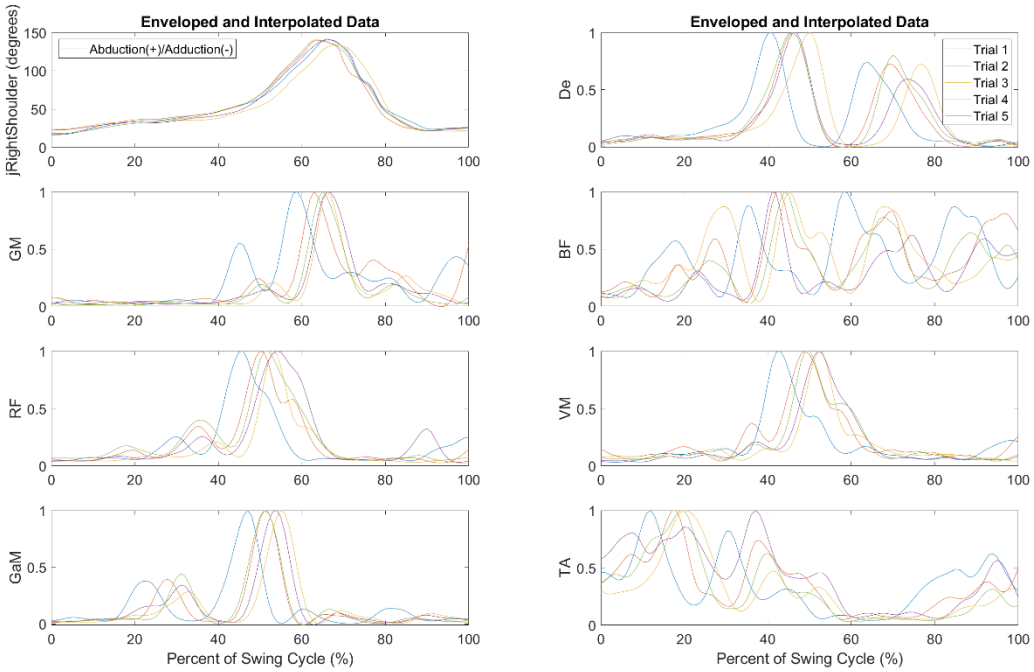

Figure B-9. TX08 individual advantage side serves

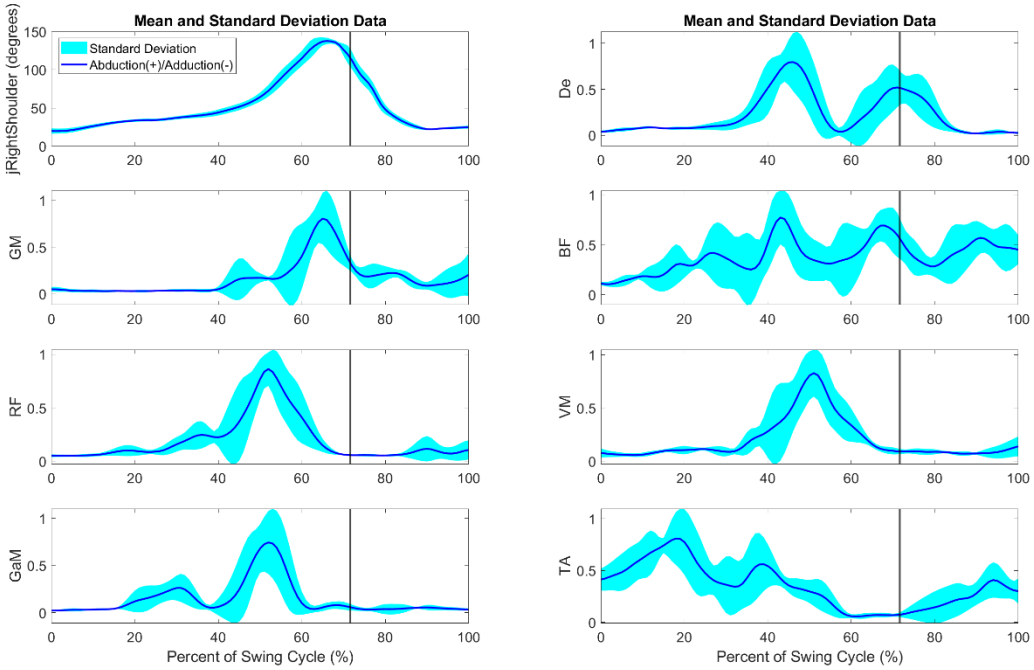

Figure B-10. TX08 averaged advantage side serves with ball contact shown by vertical line

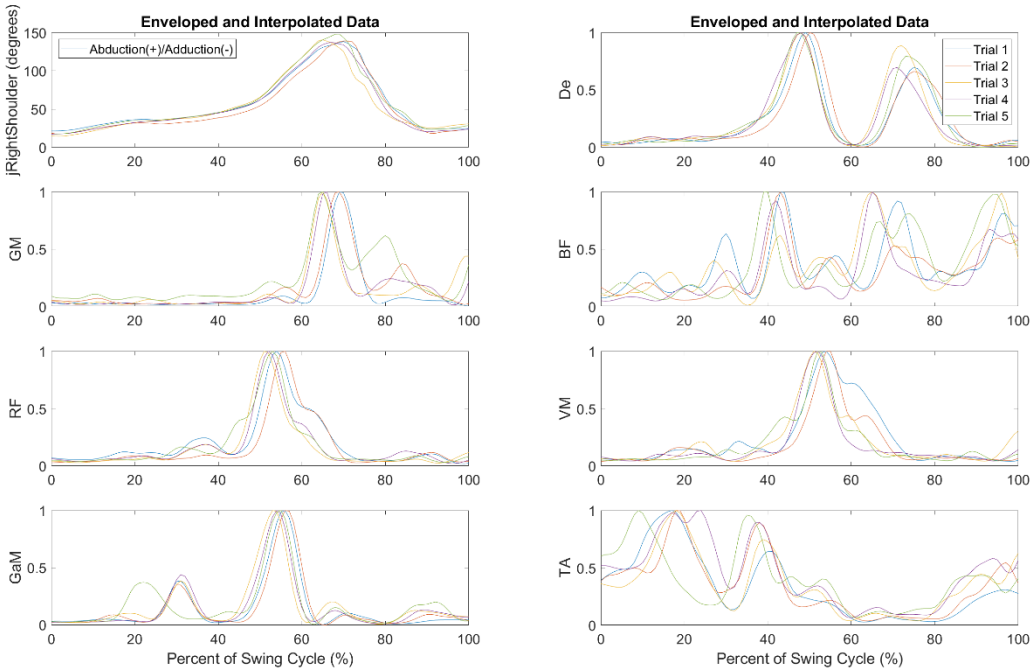

Figure B-11. TX08 individual deuce side serves

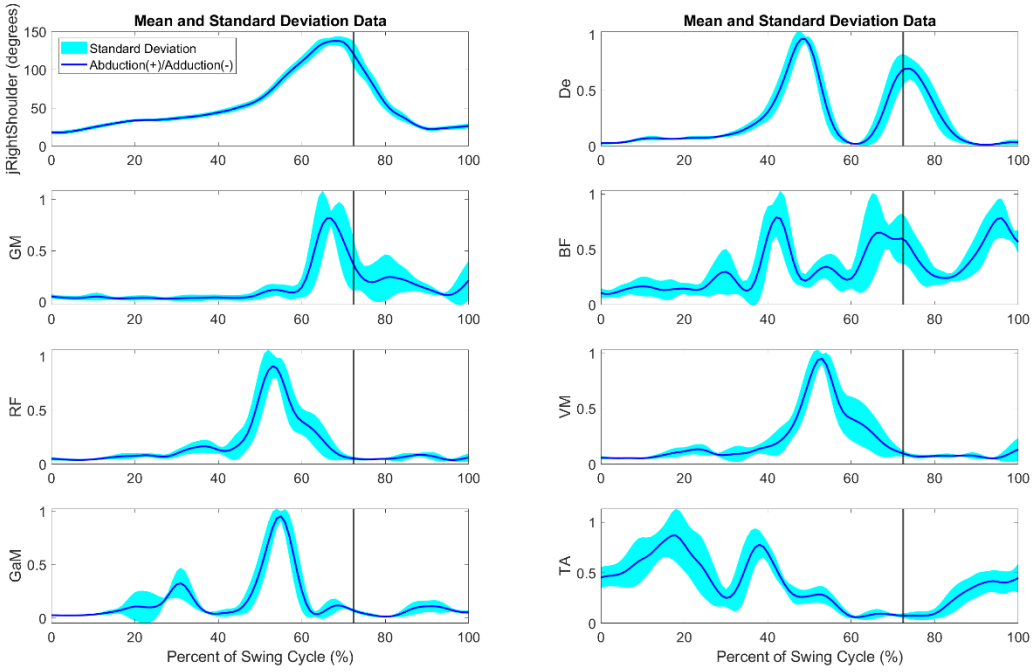

Figure B-12. TX08 averaged deuce side serves with ball contact shown by vertical line

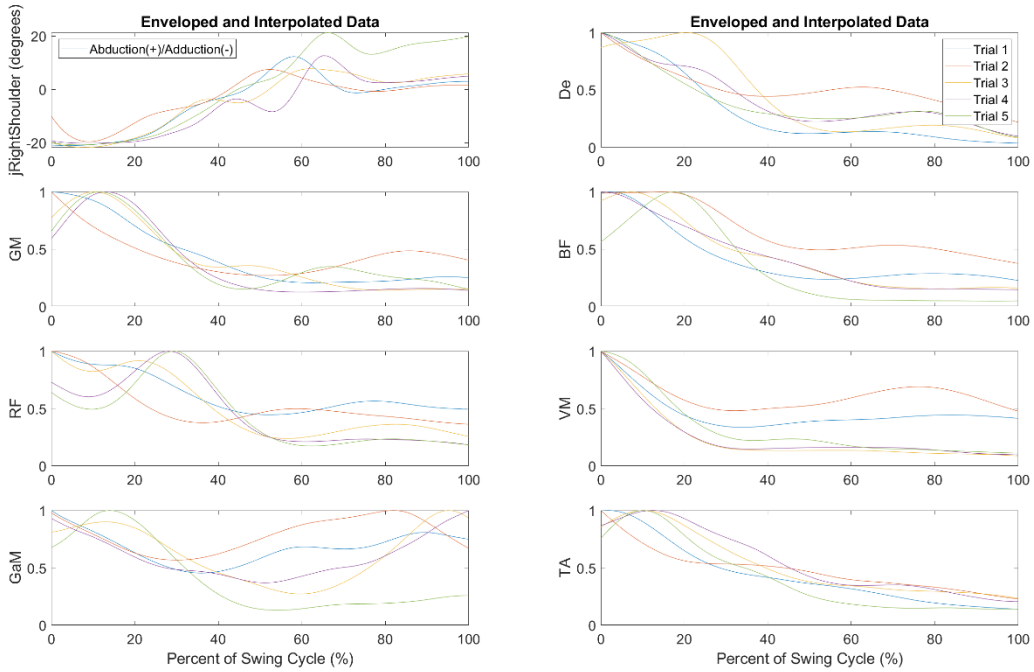

Figure B-13. TX10 individual backhand cross-court groundstrokes

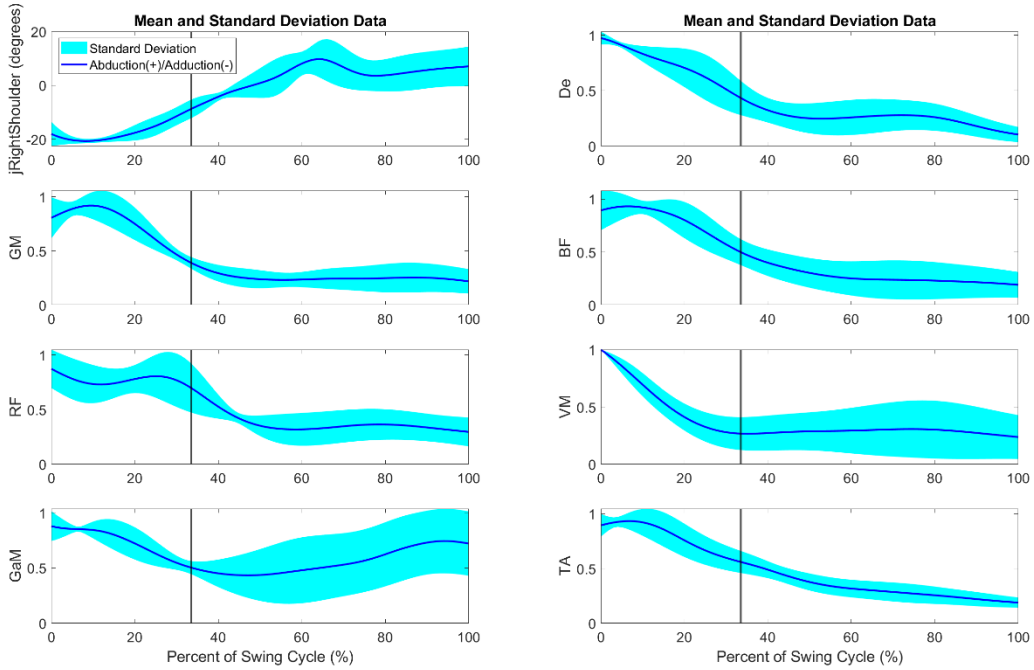

Figure B-14. TX10 averaged backhand cross-court groundstrokes with ball contact shown by vertical line

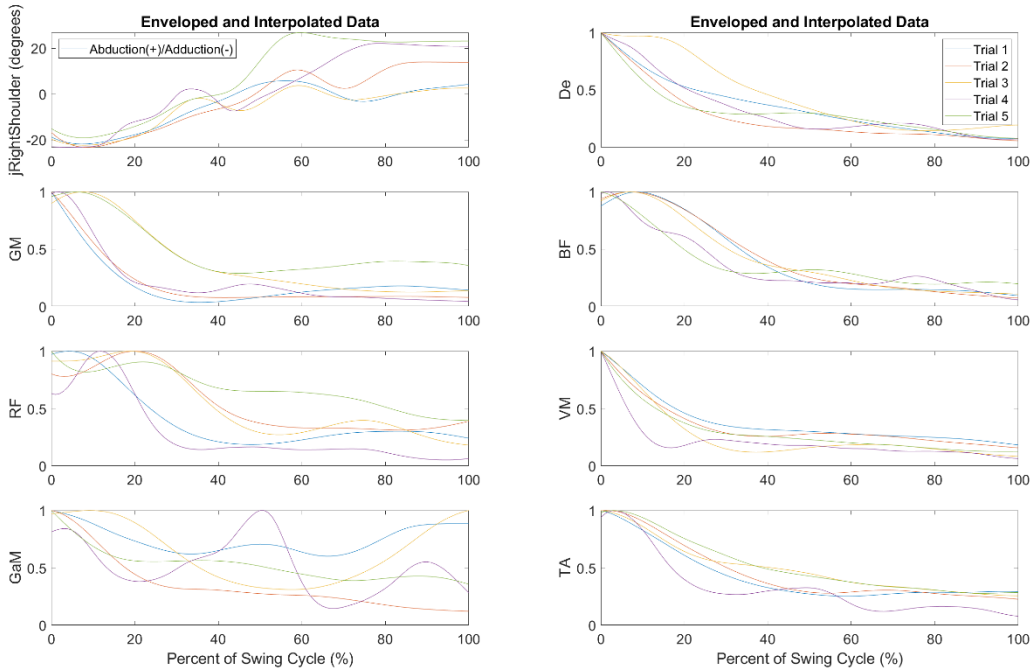

Figure B-15. TX10 individual backhand down-the-line groundstrokes

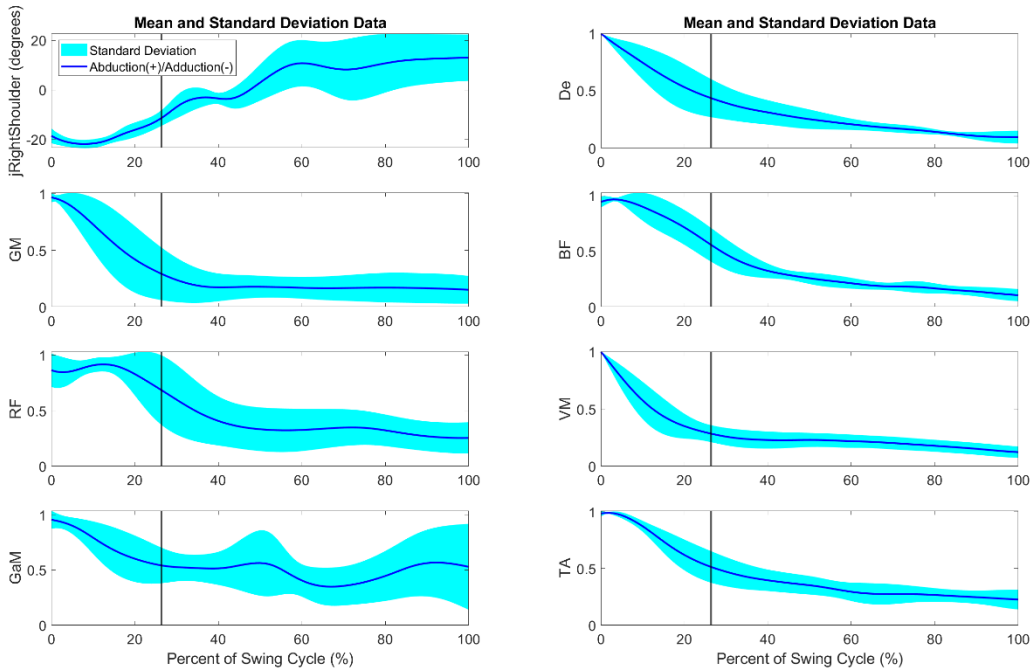

Figure B-16. TX10 averaged backhand down-the-line groundstrokes with ball contact shown by vertical line

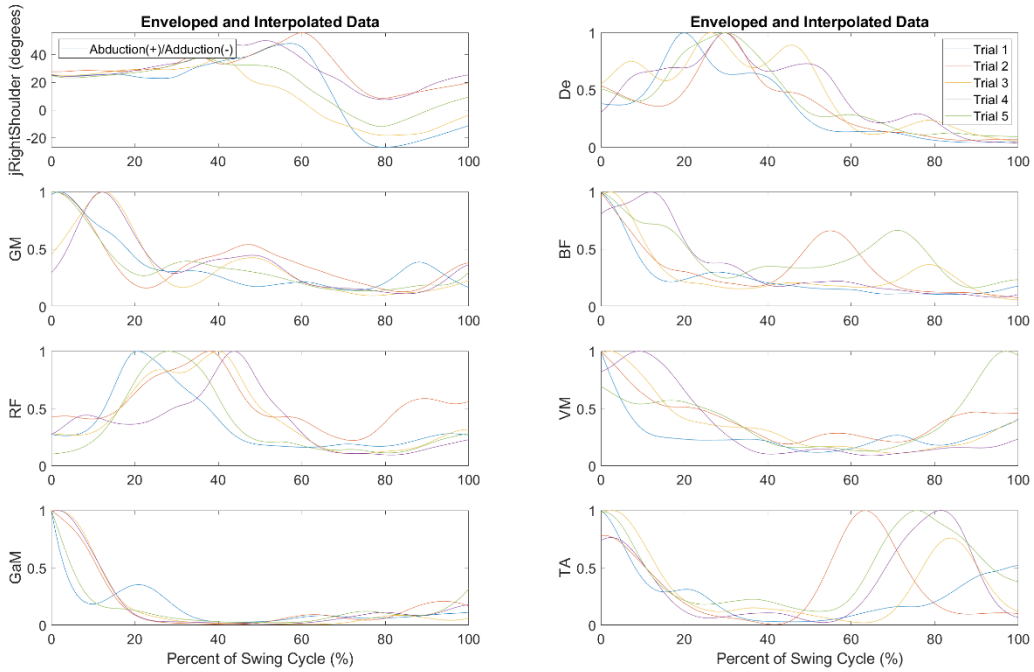

Figure B-17. TX10 individual forehand cross-court groundstrokes

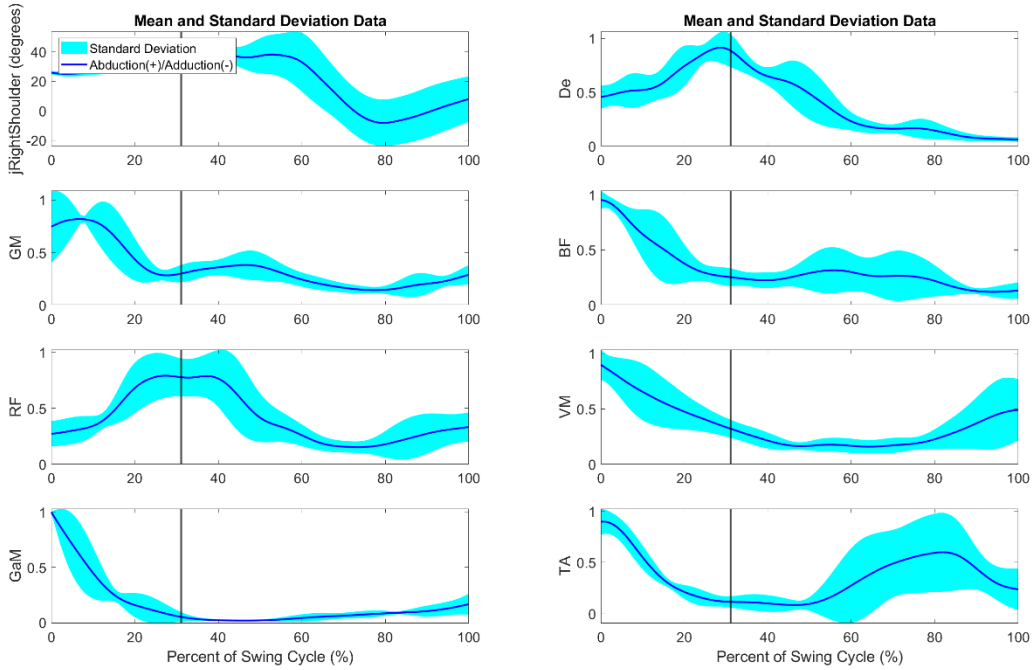

Figure B-18. TX10 averaged forehand cross-court groundstrokes with ball contact shown by vertical line

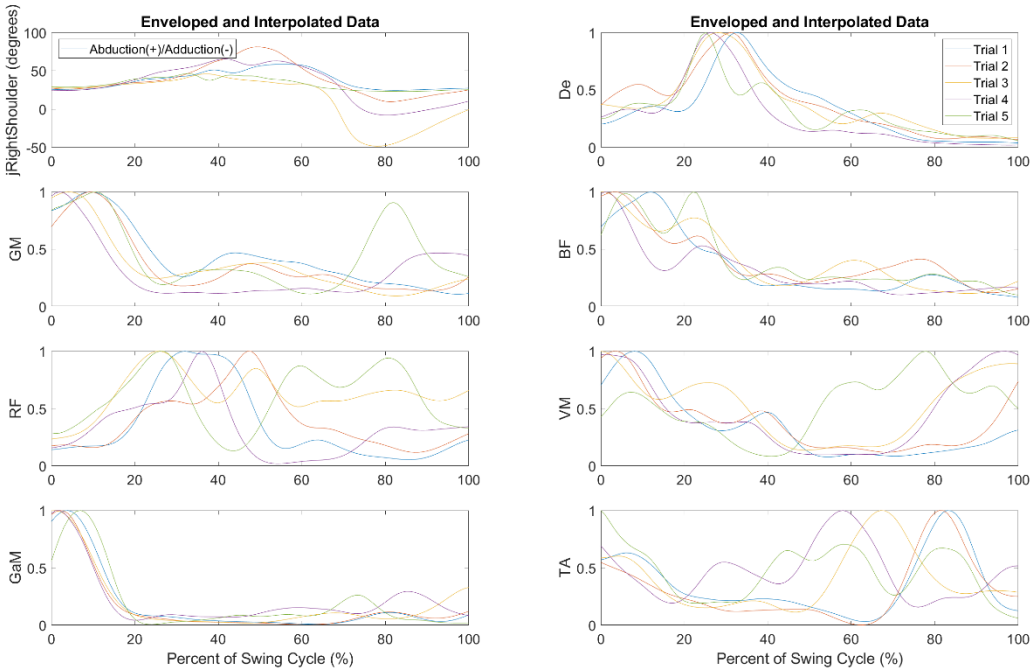

Figure B-19. TX10 individual forehand down-the-line groundstrokes

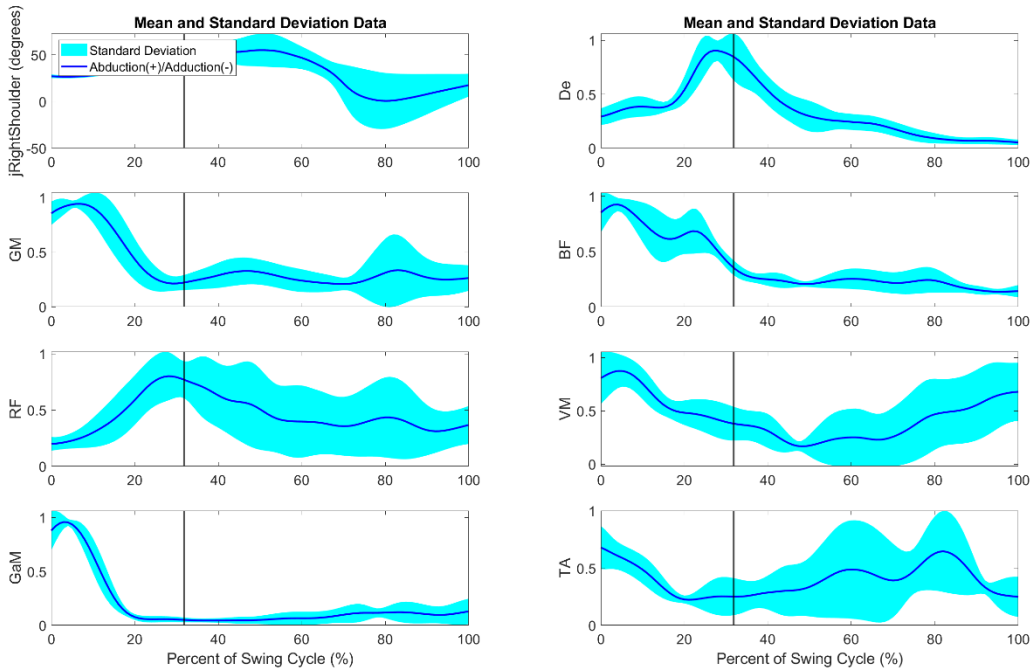

Figure B-20. TX10 averaged forehand down-the-line groundstrokes with ball contact shown by vertical line

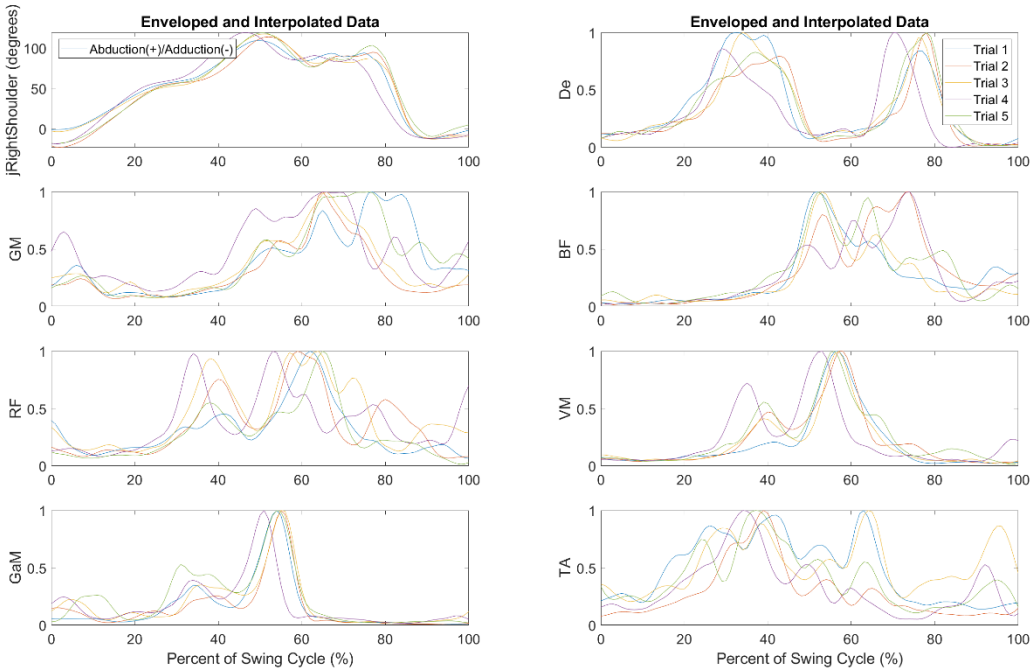

Figure B-21. TX10 individual advantage side serves

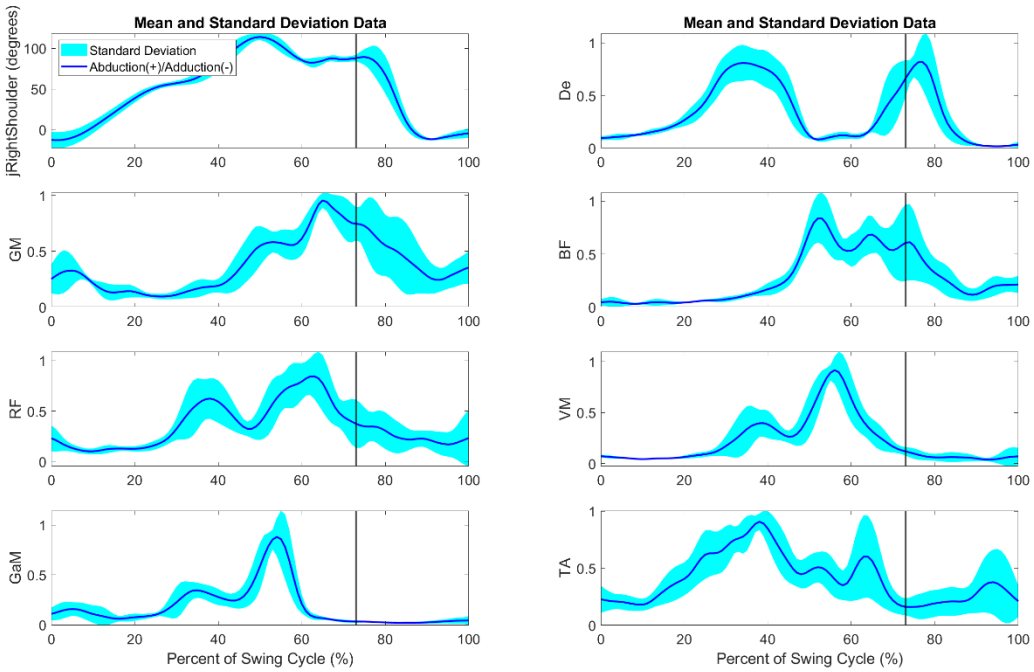

Figure B-22. TX10 averaged advantage side serves with ball contact shown by vertical line

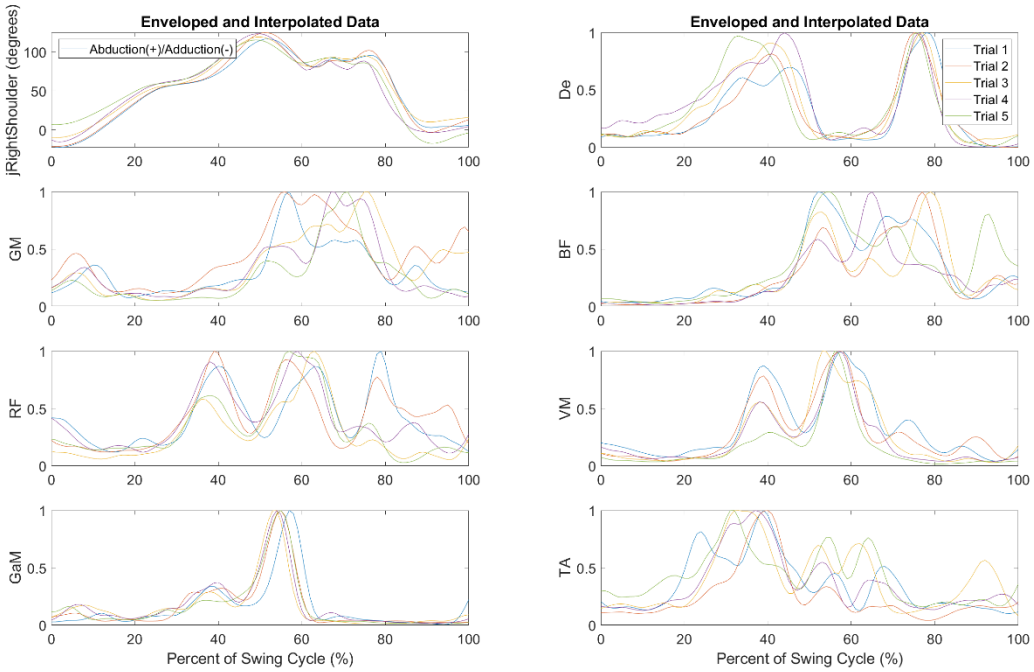

Figure B-23. TX10 individual deuce side serves

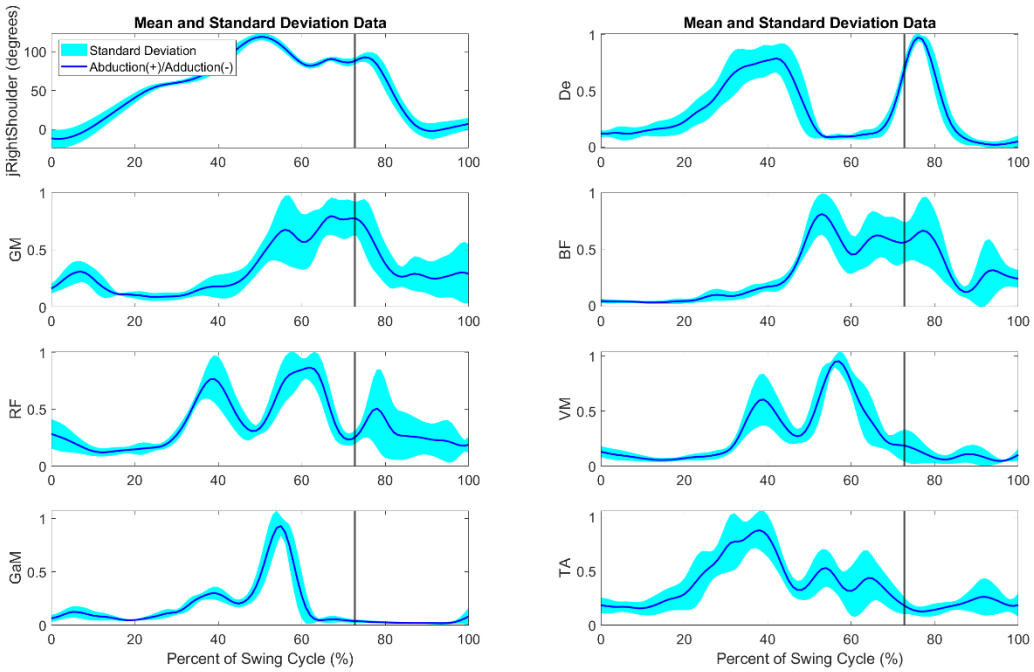

Figure B-24. TX10 averaged deuce side serves with ball contact shown by vertical line

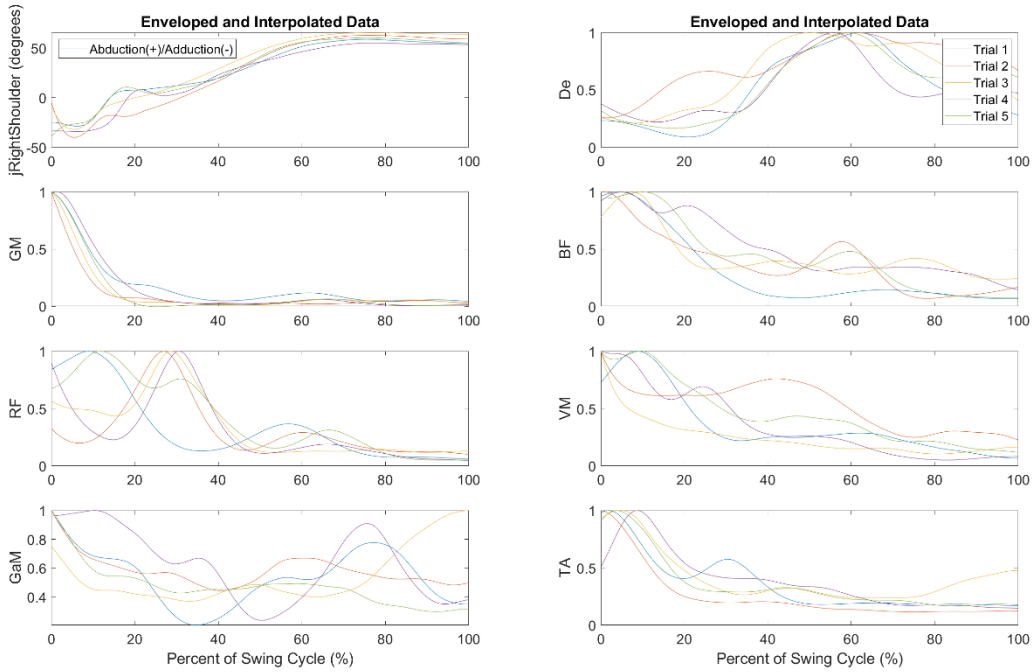

Figure B-23. TX11 individual backhand cross-court groundstrokes

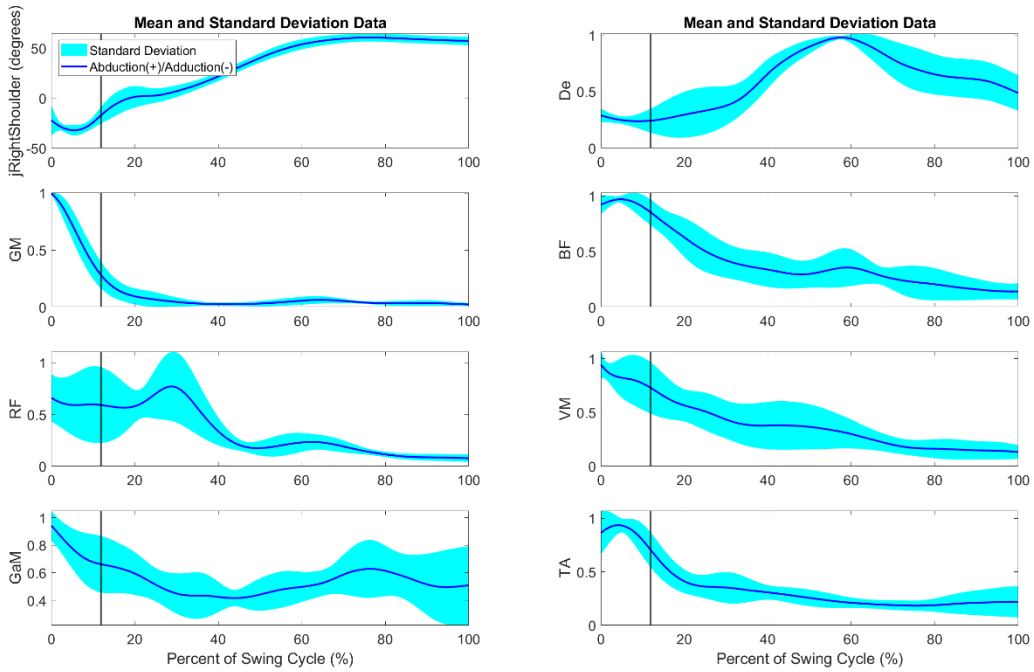

Figure B-24. TX11 averaged backhand cross-court groundstrokes with ball contact shown by vertical line

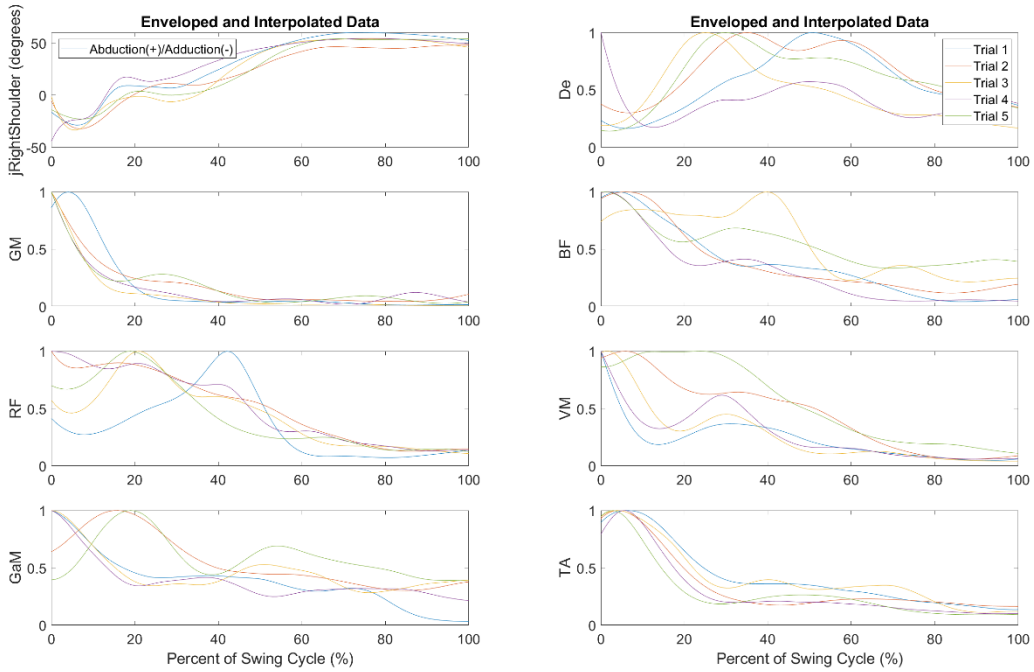

Figure B-25. TX11 individual backhand down-the-line groundstrokes

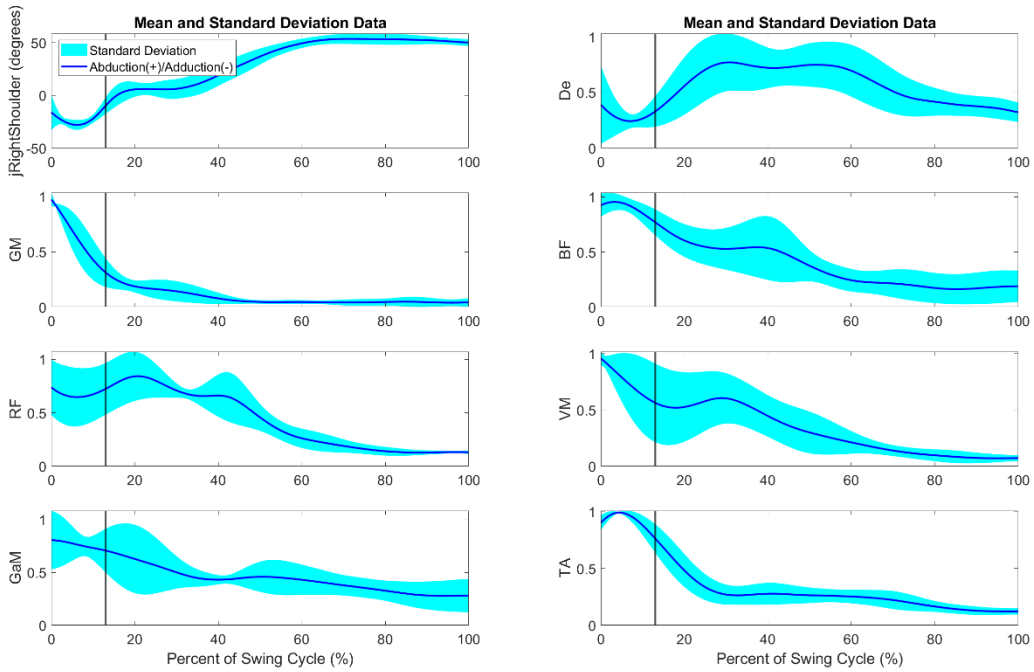

Figure B-26. TX11 averaged backhand down-the-line groundstrokes with ball contact shown by vertical line

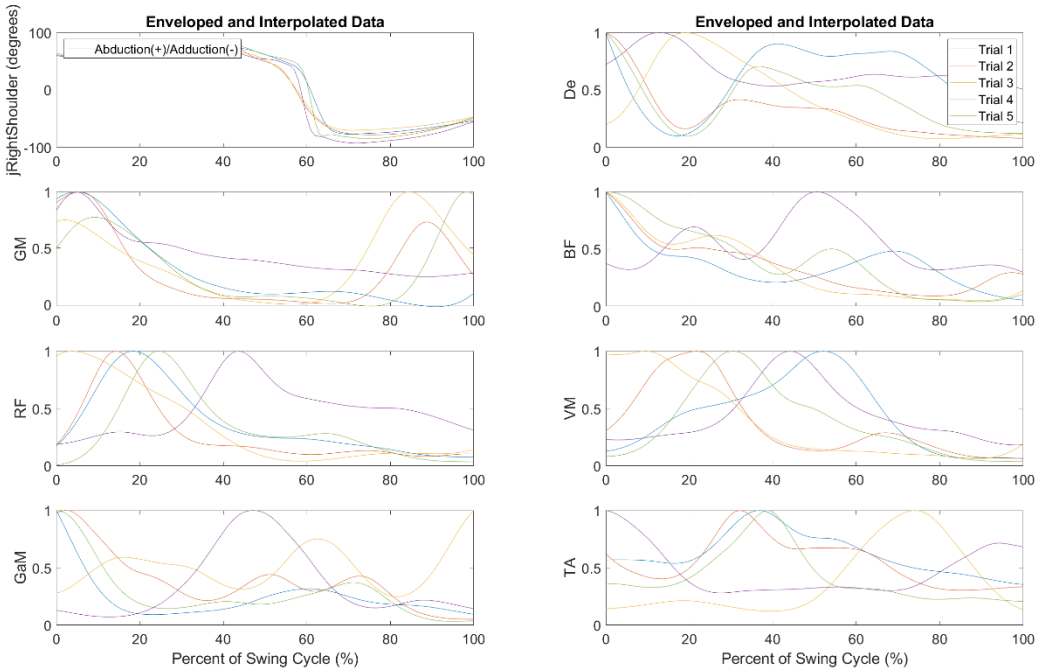

Figure B-27. TX11 individual forehand cross-court groundstrokes

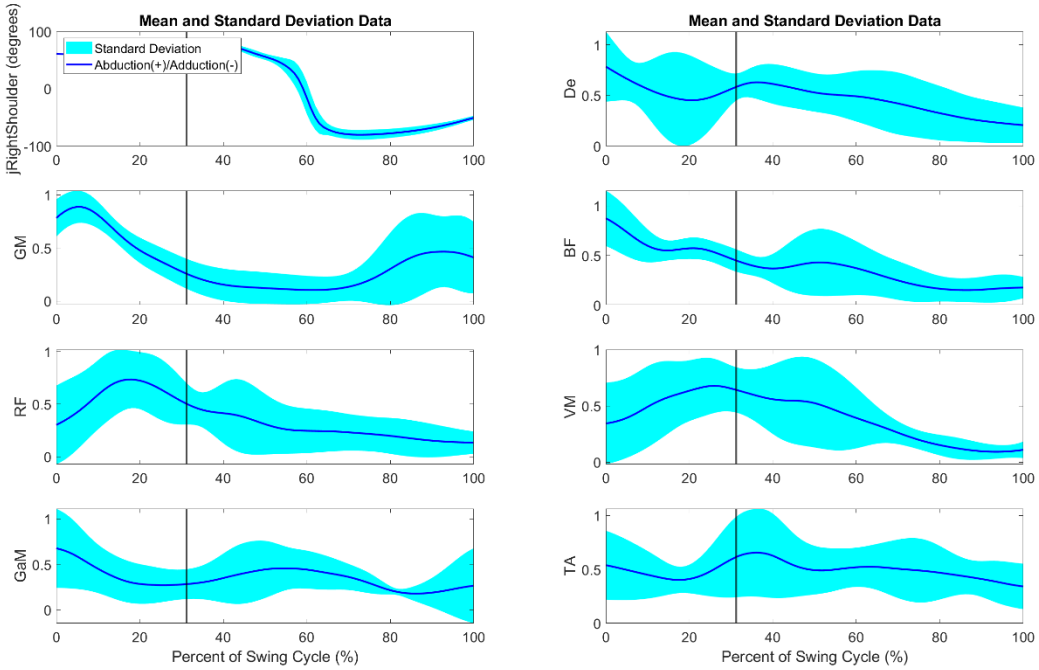

Figure B-28. TX11 averaged forehand cross-court groundstrokes with ball contact shown by vertical line

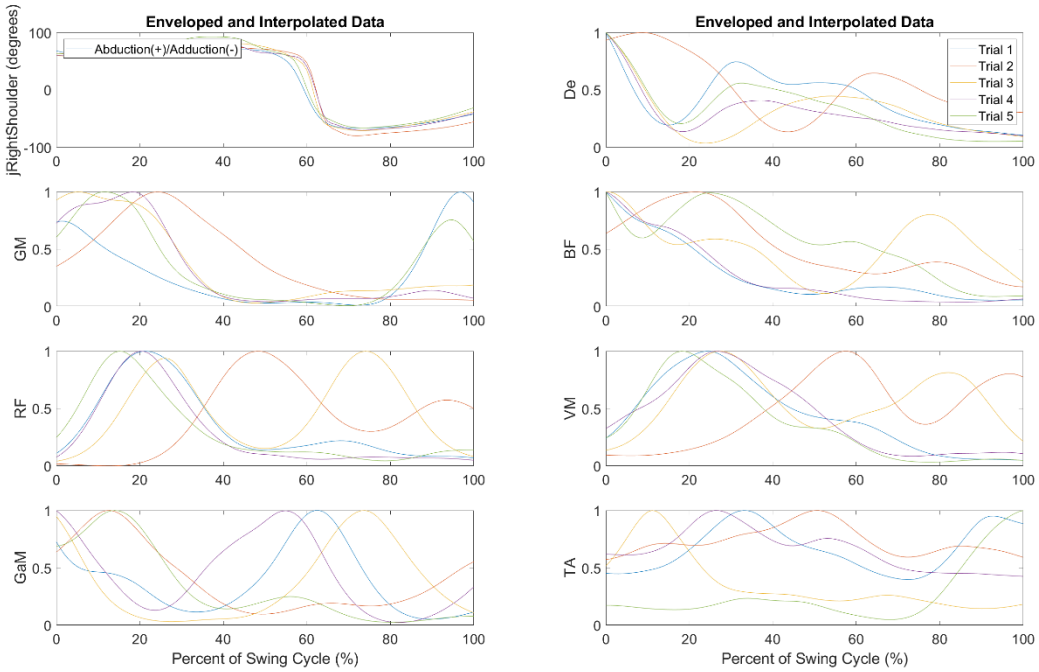

Figure B-29. TX11 individual forehand down-the-line groundstrokes

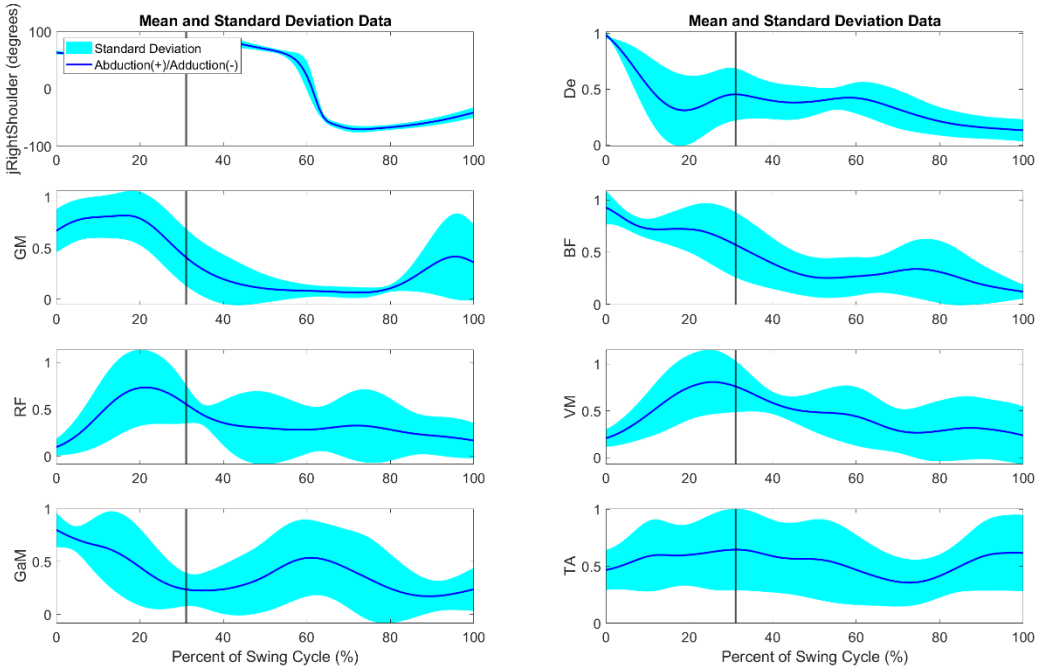

Figure B-30. TX11 averaged forehand down-the-line groundstrokes with ball contact shown by vertical line

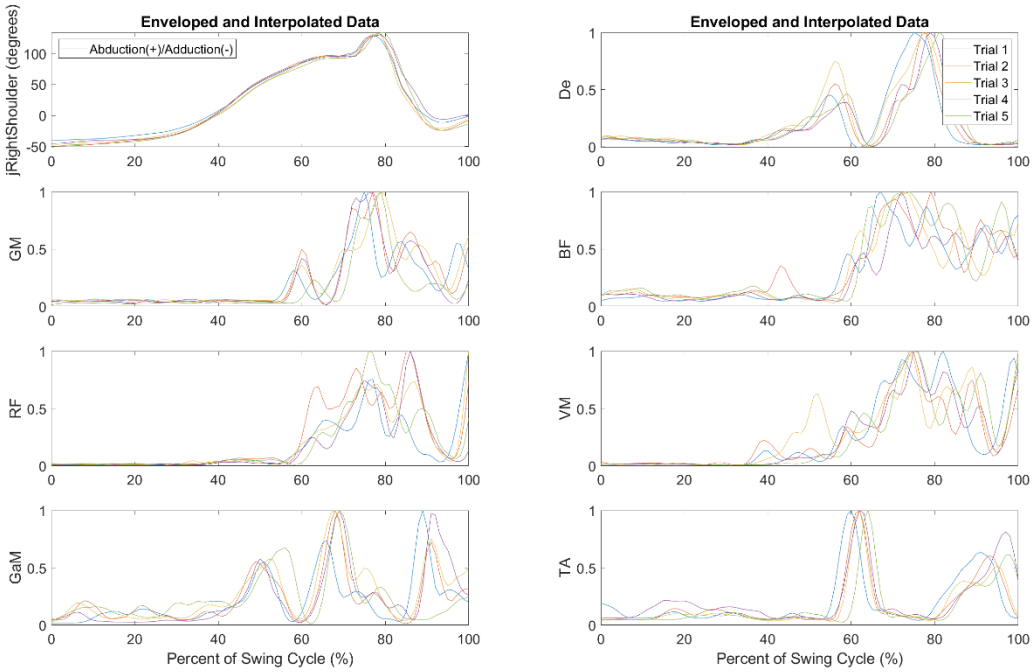

Figure B-31. TX11 individual advantage side serves

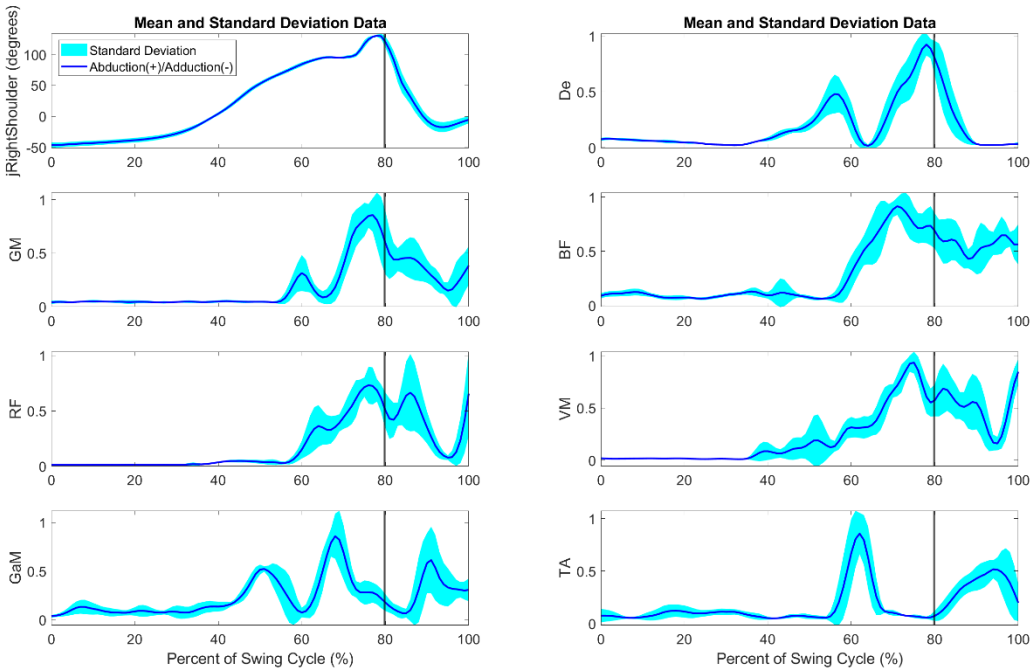

Figure B-32. TX11 averaged advantage side serves with ball contact shown by vertical line

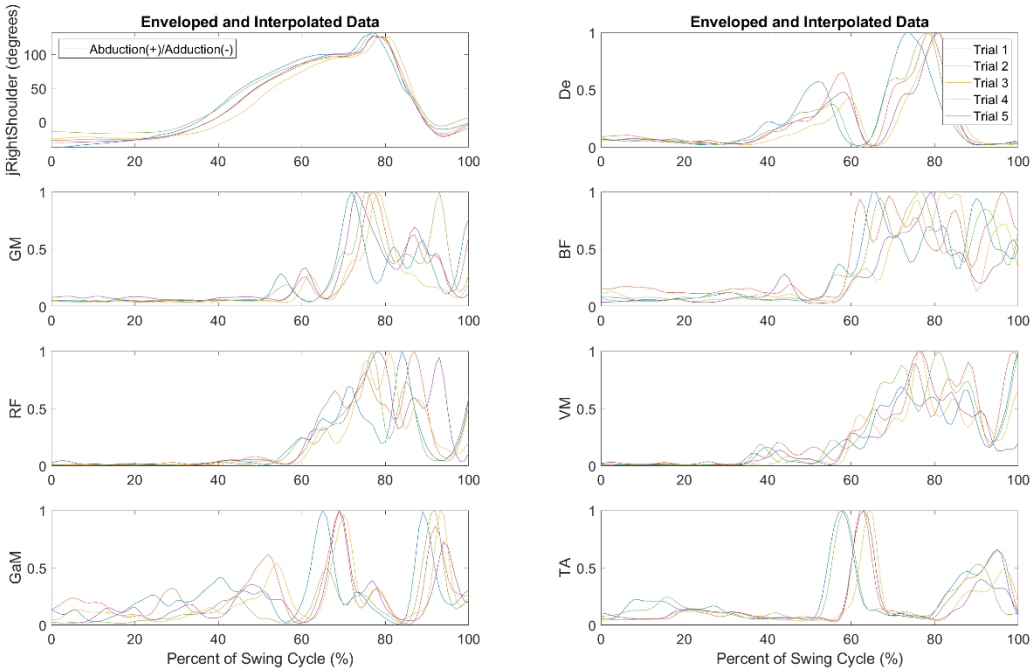

Figure B-33. TX11 individual deuce side serves

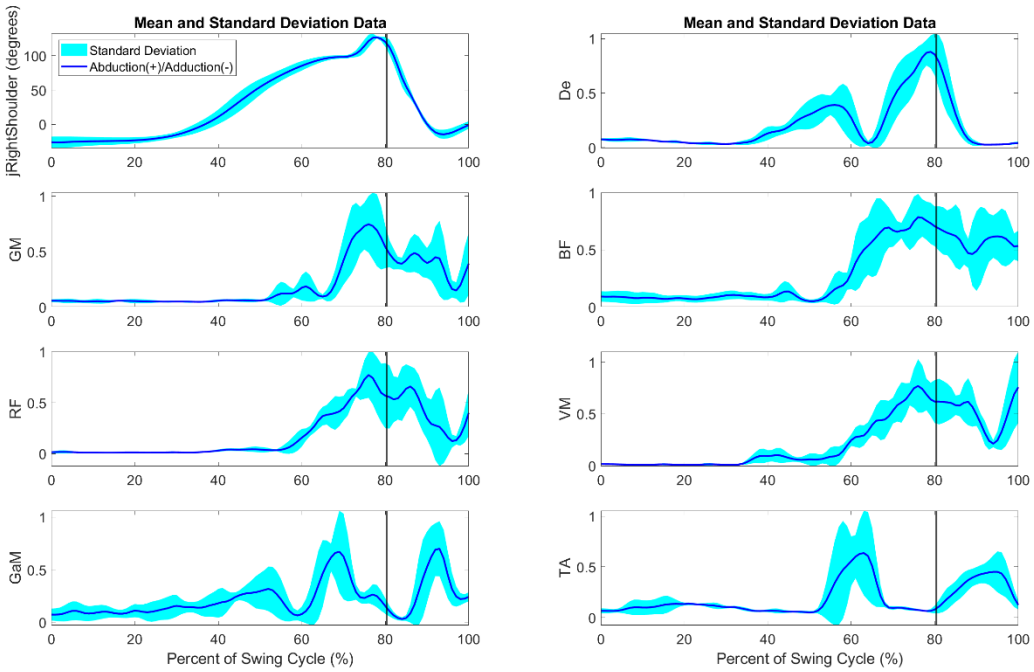

Figure B-34. TX11 averaged deuce side serves with ball contact shown by vertical line

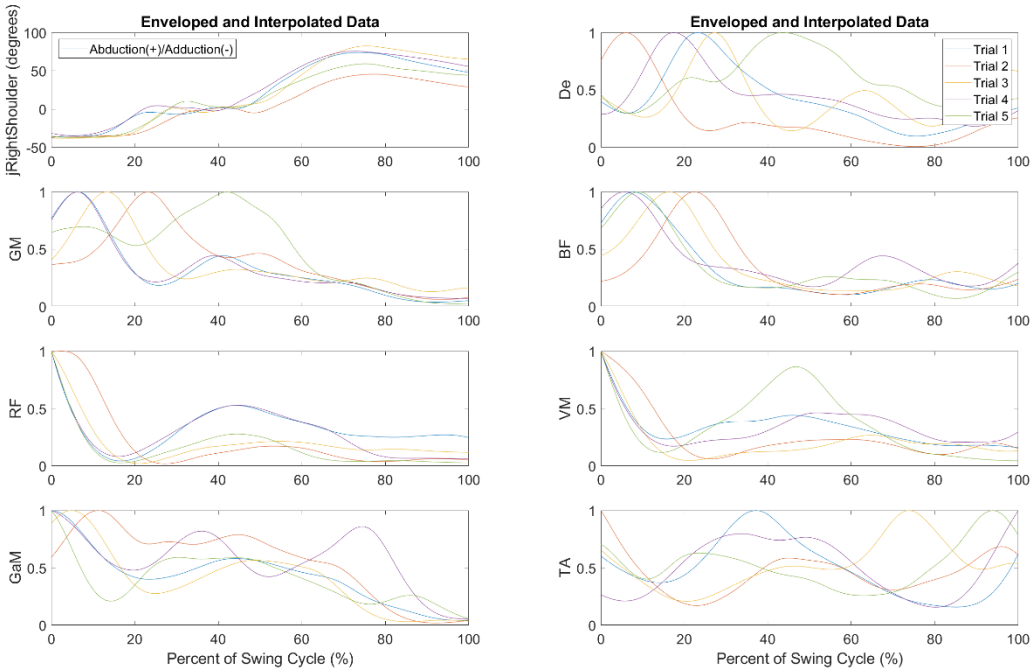

Figure B-35. TX12 individual backhand cross-court groundstrokes

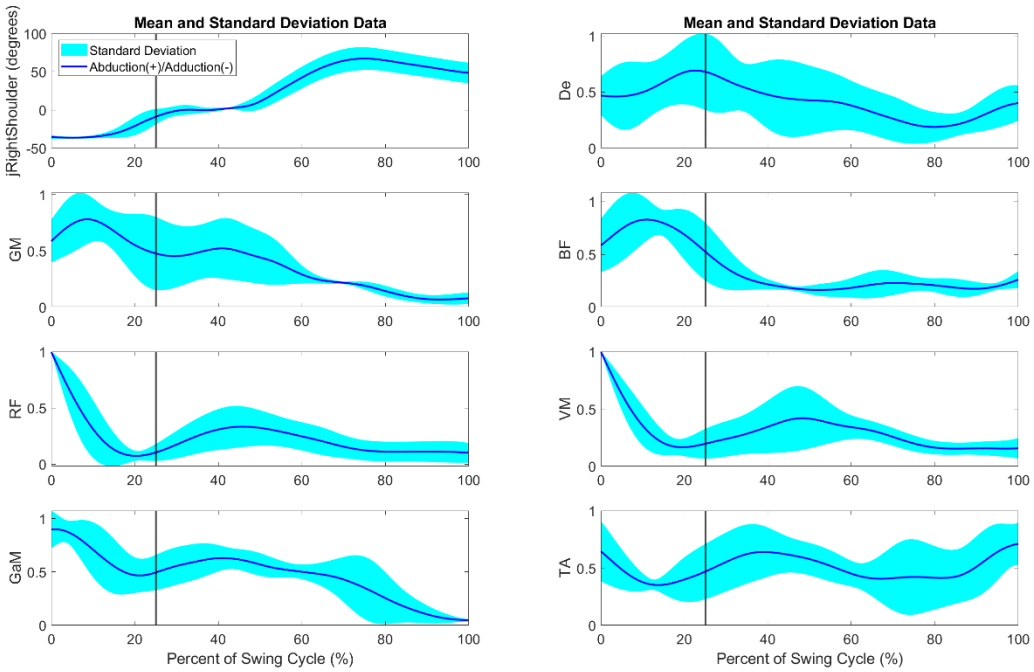

Figure B-36. TX12 averaged backhand cross-court groundstrokes with ball contact shown by vertical line

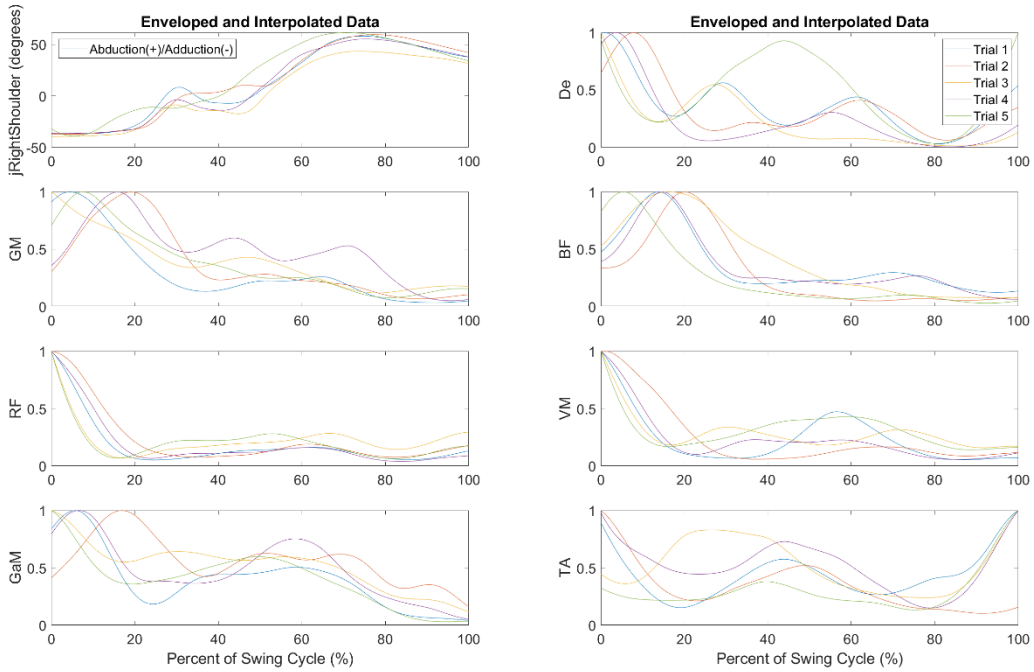

Figure B-37. TX12 individual backhand down-the-line groundstrokes

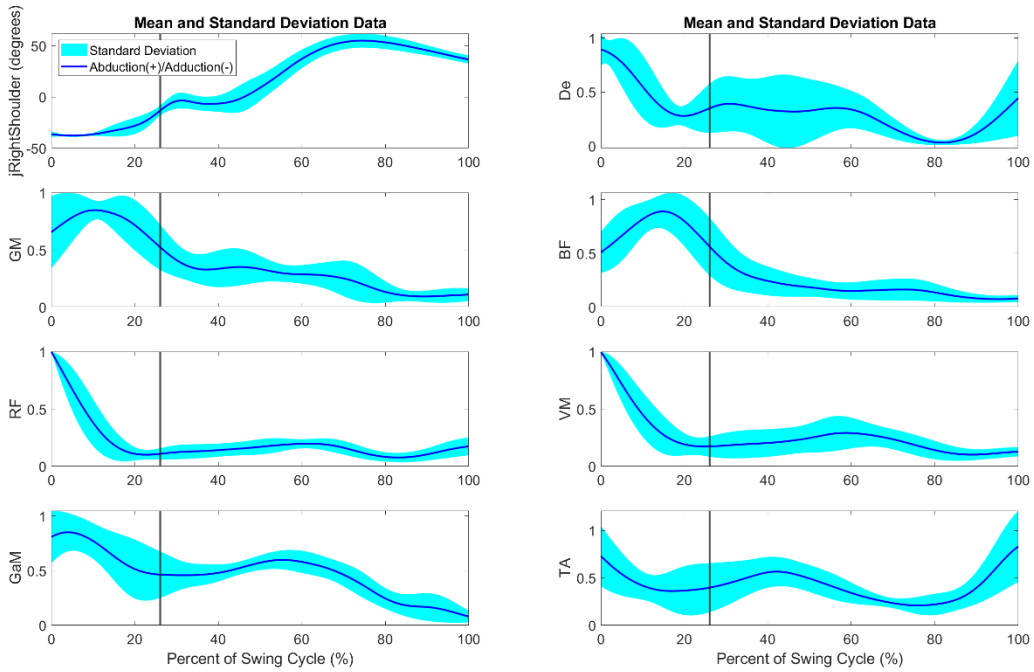

Figure B-38. TX12 averaged backhand down-the-line groundstrokes with ball contact shown by vertical line

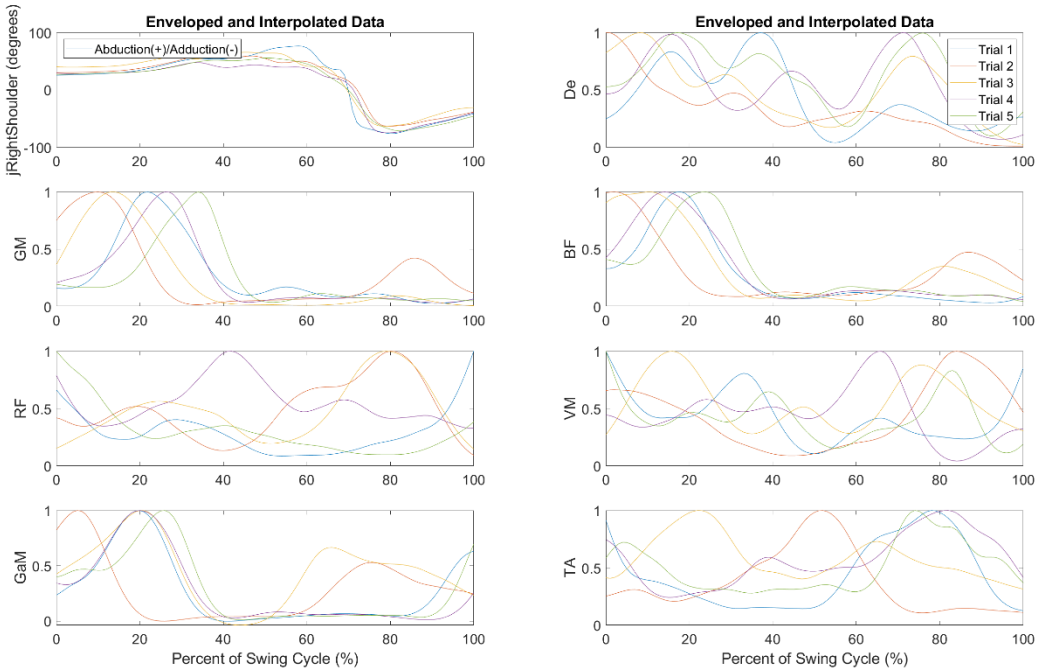

Figure B-39. TX12 individual forehand cross-court groundstrokes

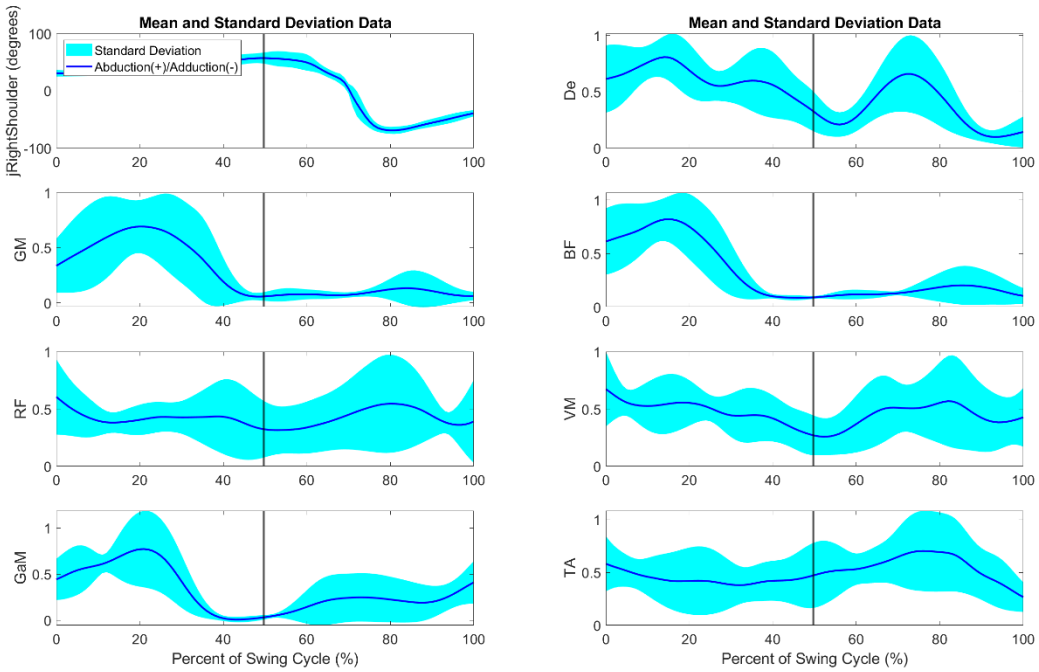

Figure B-40. TX12 averaged forehand cross-court groundstrokes with ball contact shown by vertical line

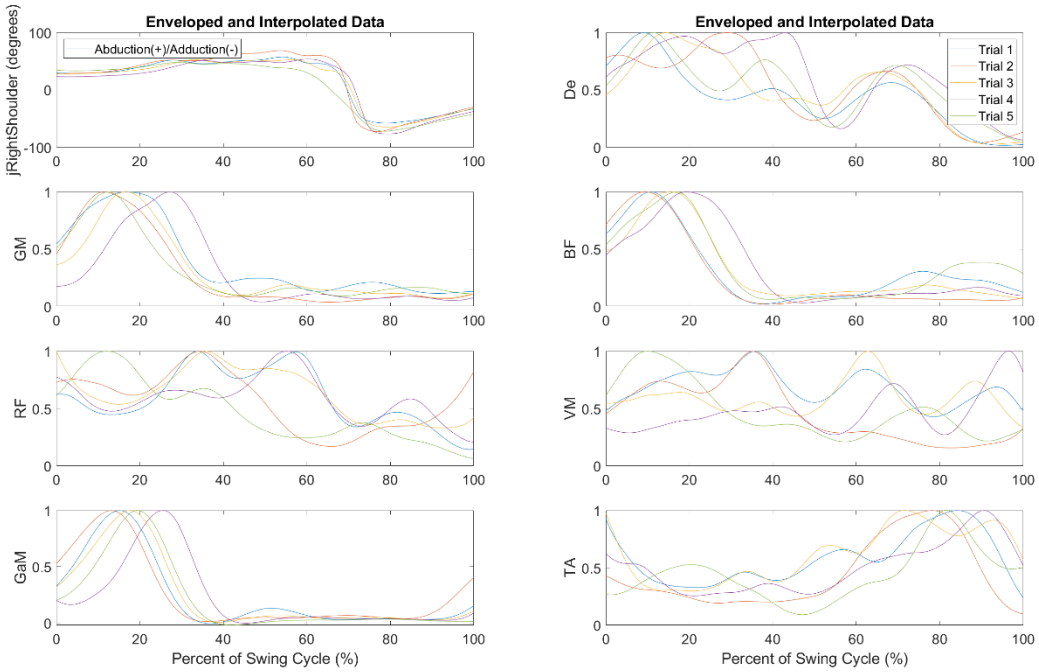

Figure B-41. TX12 individual forehand down-the-line groundstrokes

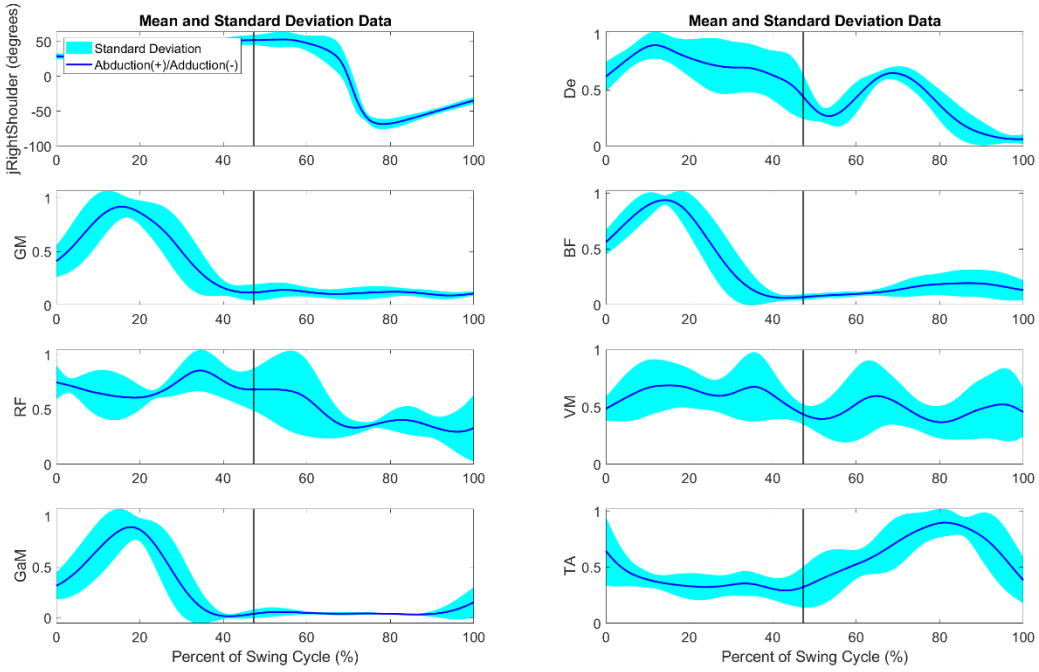

Figure B-42. TX12 averaged forehand down-the-line groundstrokes with ball contact shown by vertical line

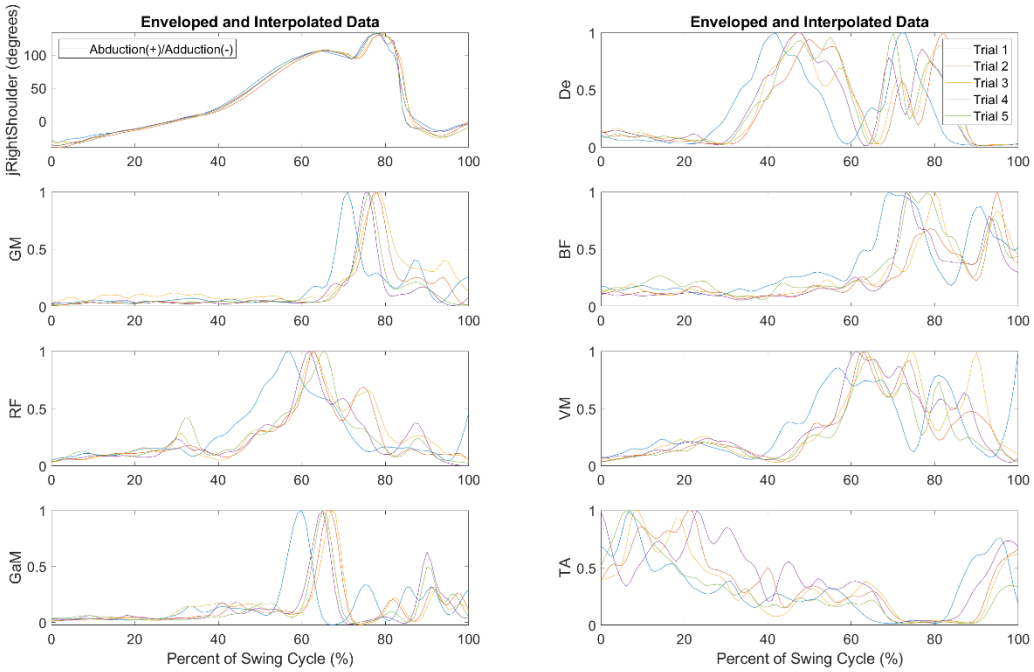

Figure B-43. TX12 individual advantage side serves

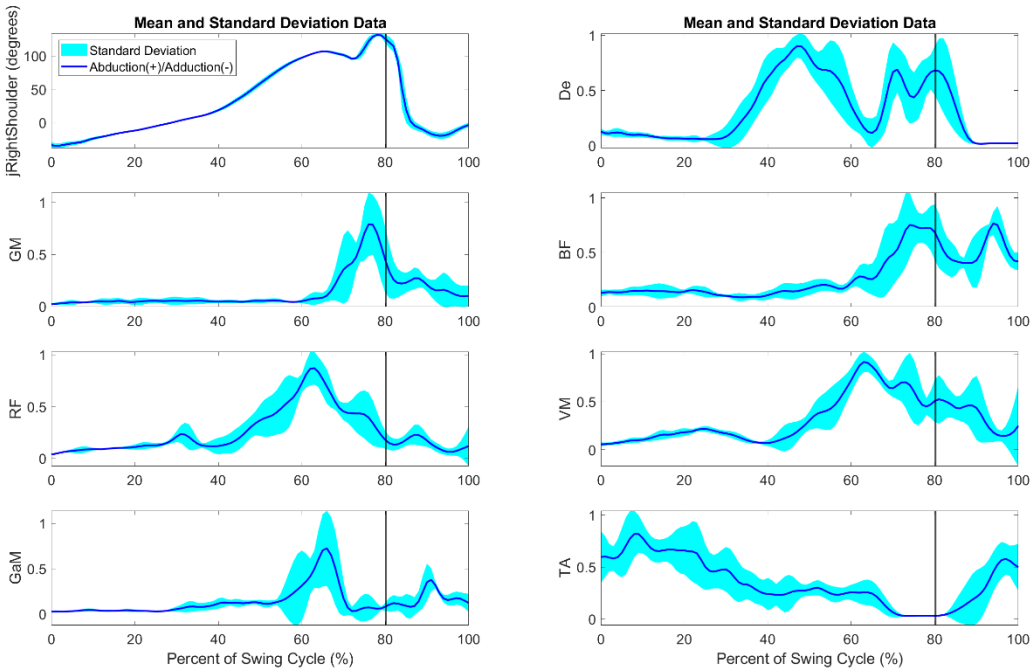

Figure B-44. TX12 averaged advantage side serves with ball contact shown by vertical line

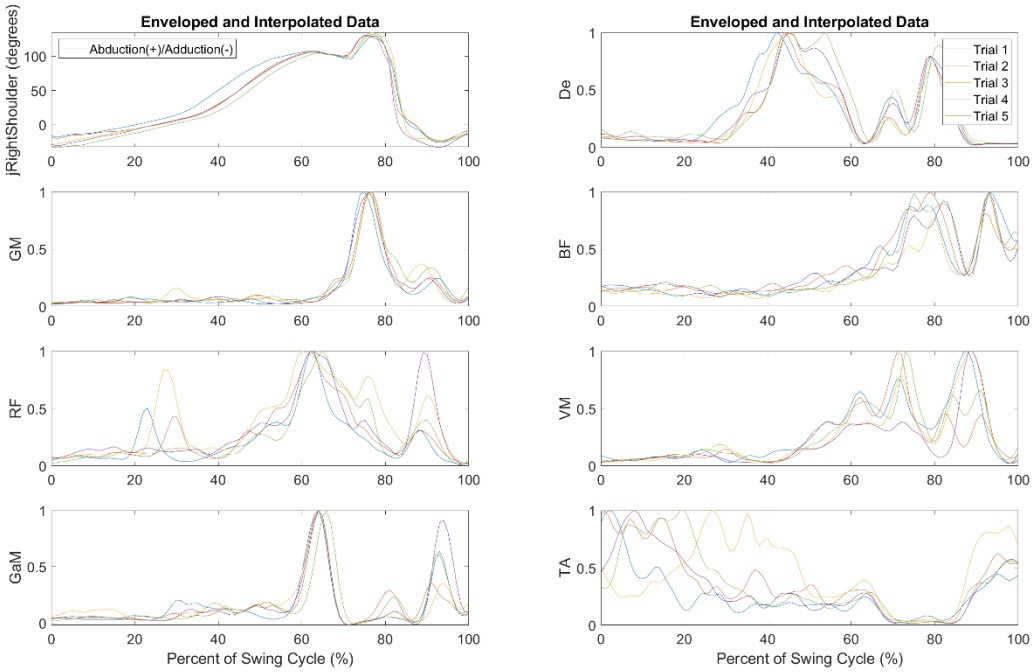

Figure B-45. TX12 individual deuce side serves

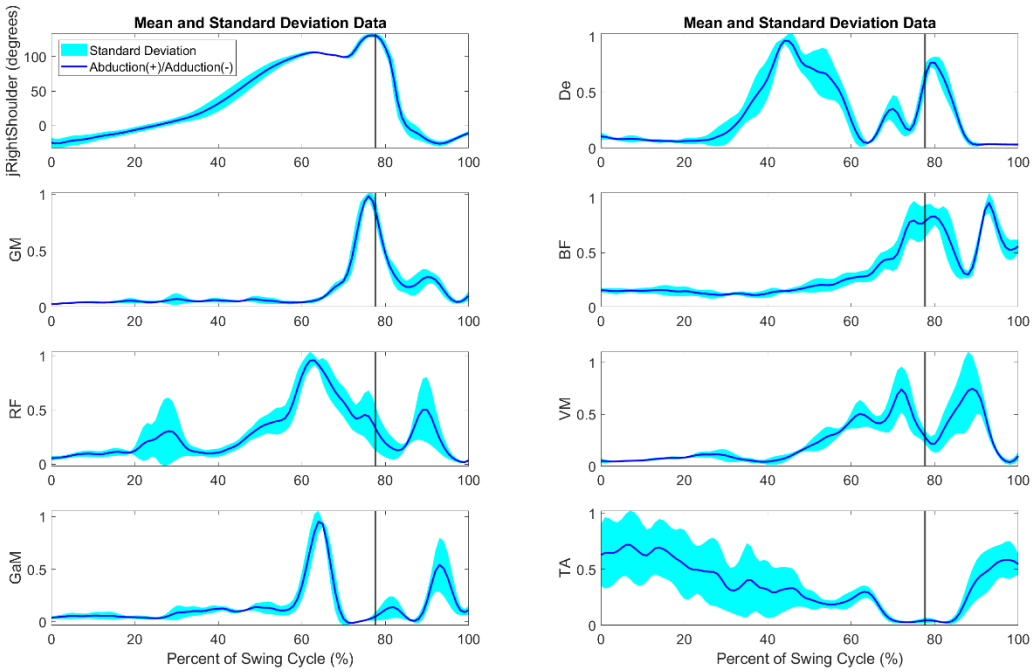

Figure B-46. TX12 averaged deuce side serves with ball contact shown by vertical line

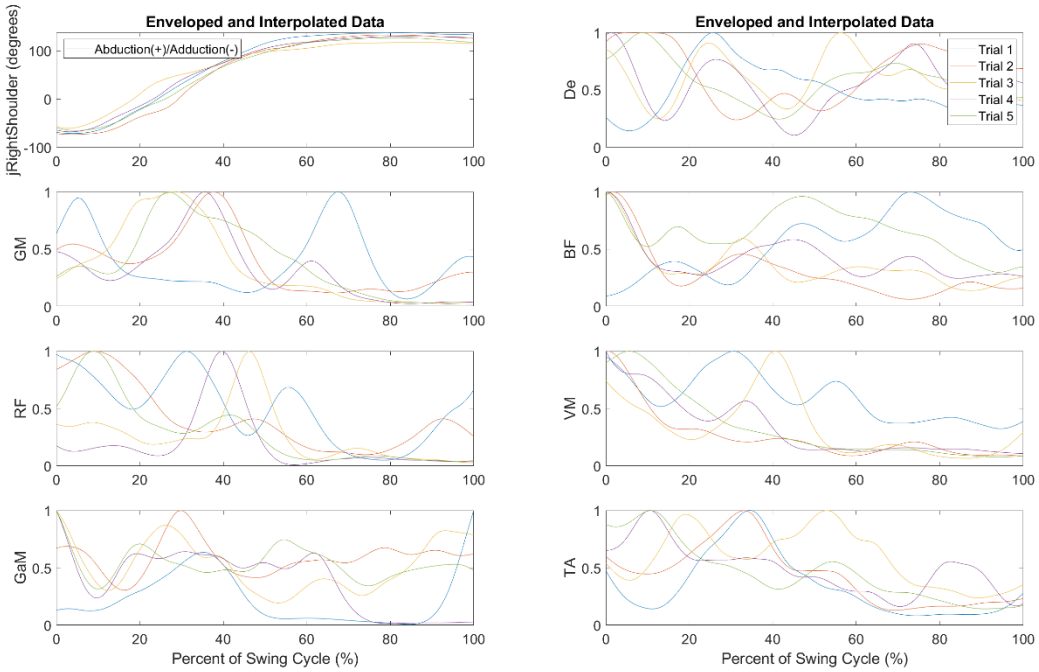

Figure B-47. TX13 individual backhand cross-court groundstrokes

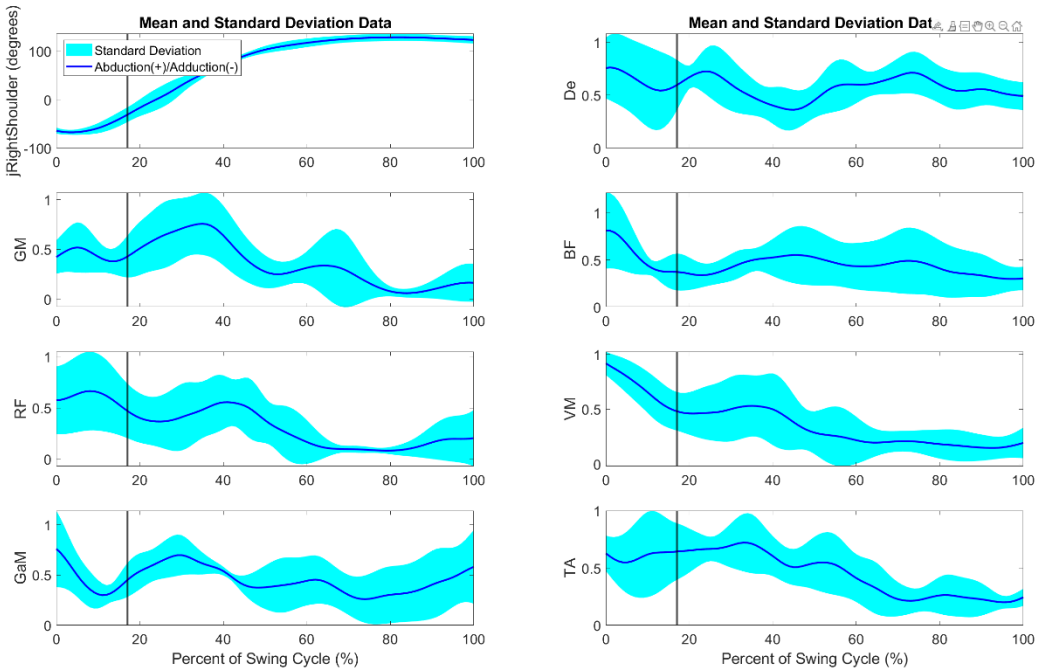

Figure B-48. TX13 averaged backhand cross-court groundstrokes with ball contact shown by vertical line

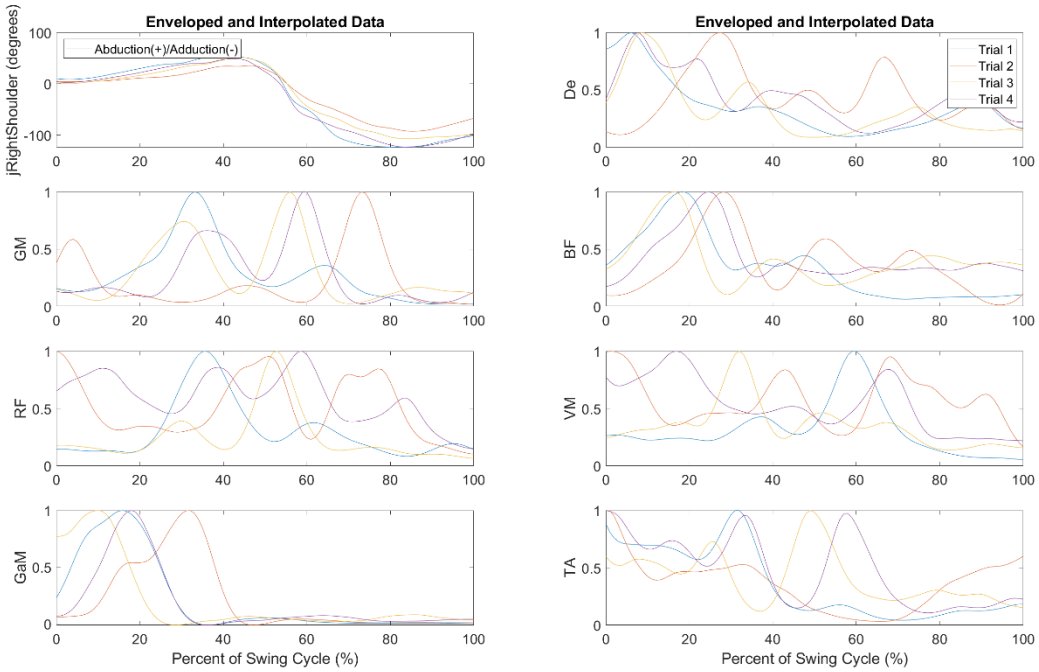

Figure B-49. TX13 individual forehand cross-court groundstrokes

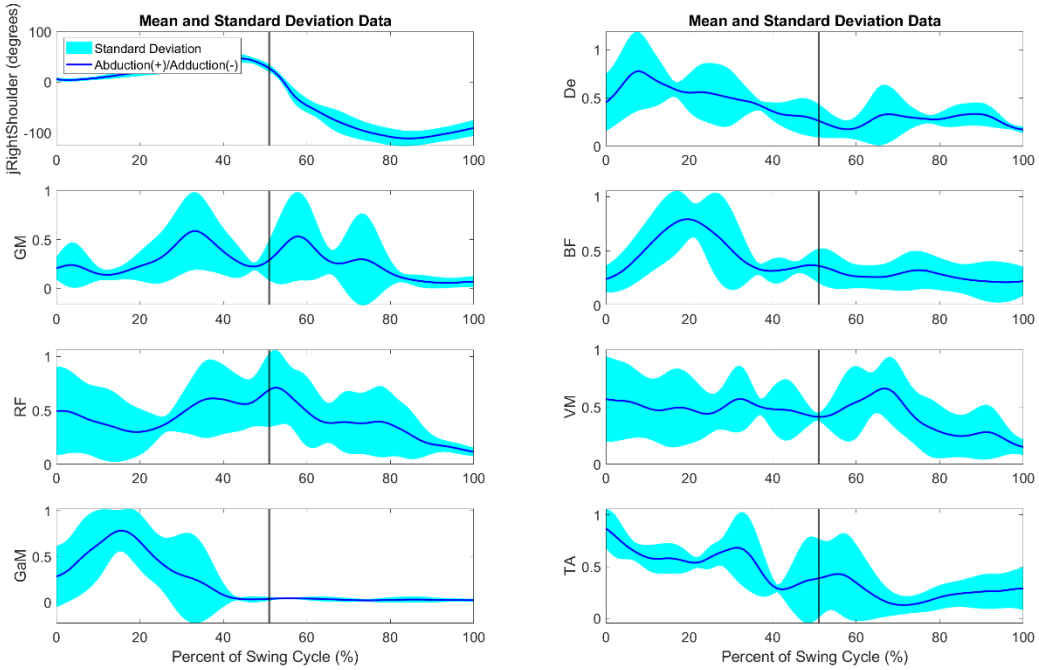

Figure B-50. TX13 averaged forehand cross-court groundstrokes with ball contact shown by vertical line

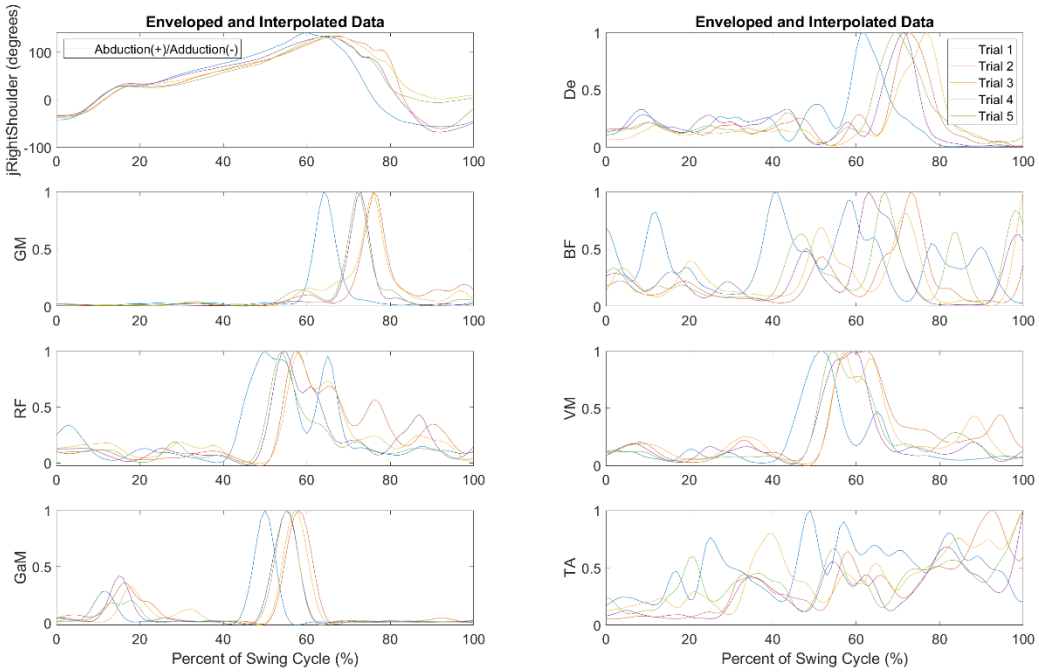

Figure B-51. TX13 individual advantage side serves

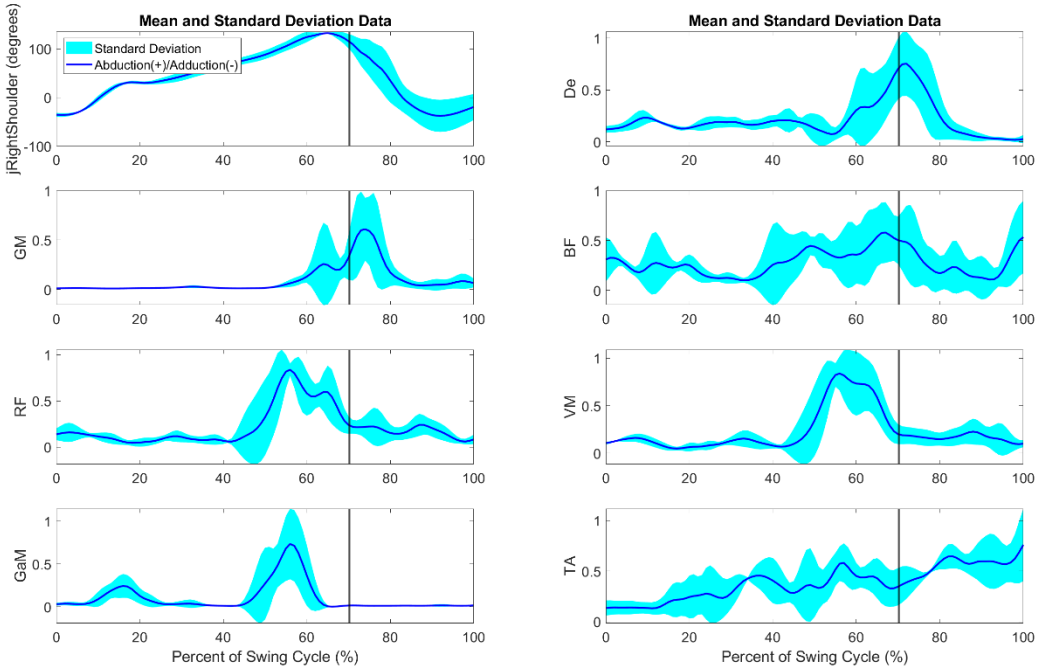

Figure B-52. TX13 averaged advantage side serves with ball contact shown by vertical line

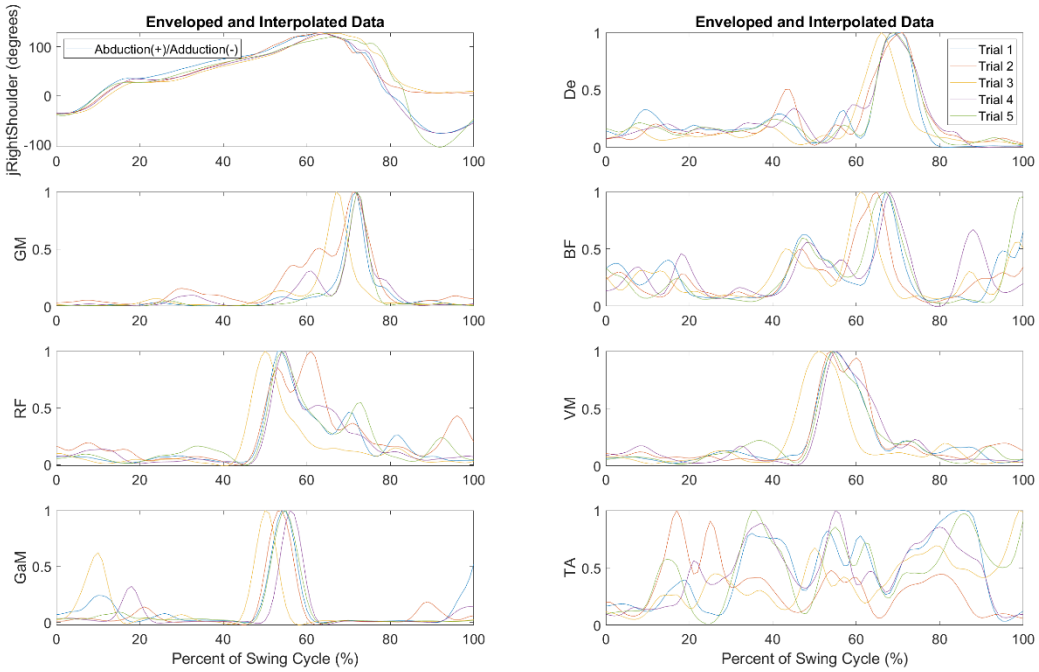

Figure B-53. TX08 individual deuce side serves

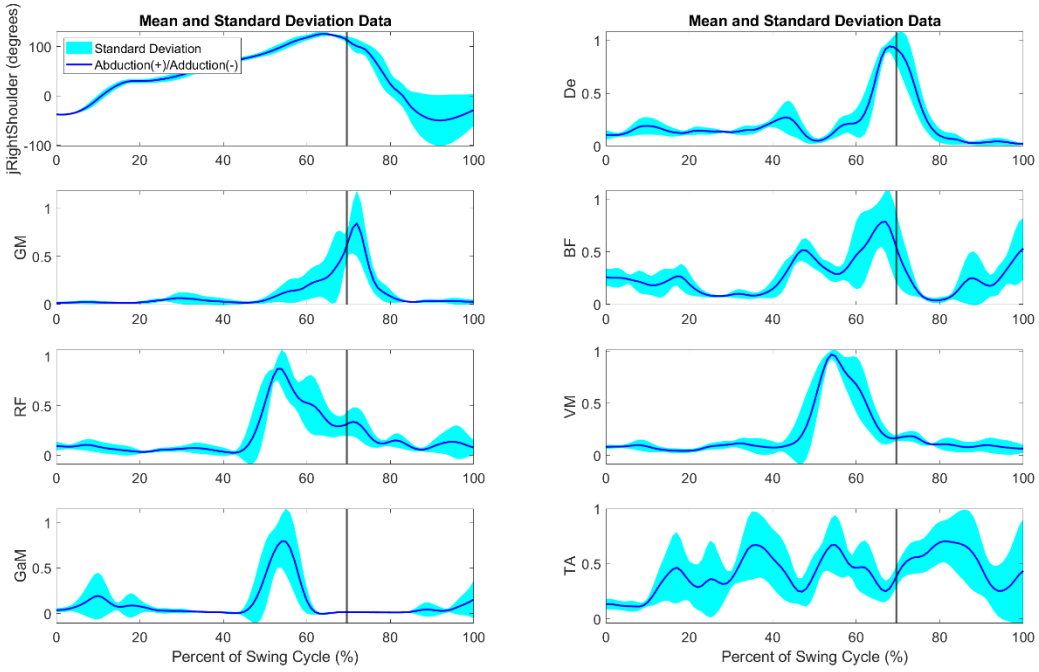

Figure B-54. TX13 averaged deuce side serves with ball contact shown by vertical line

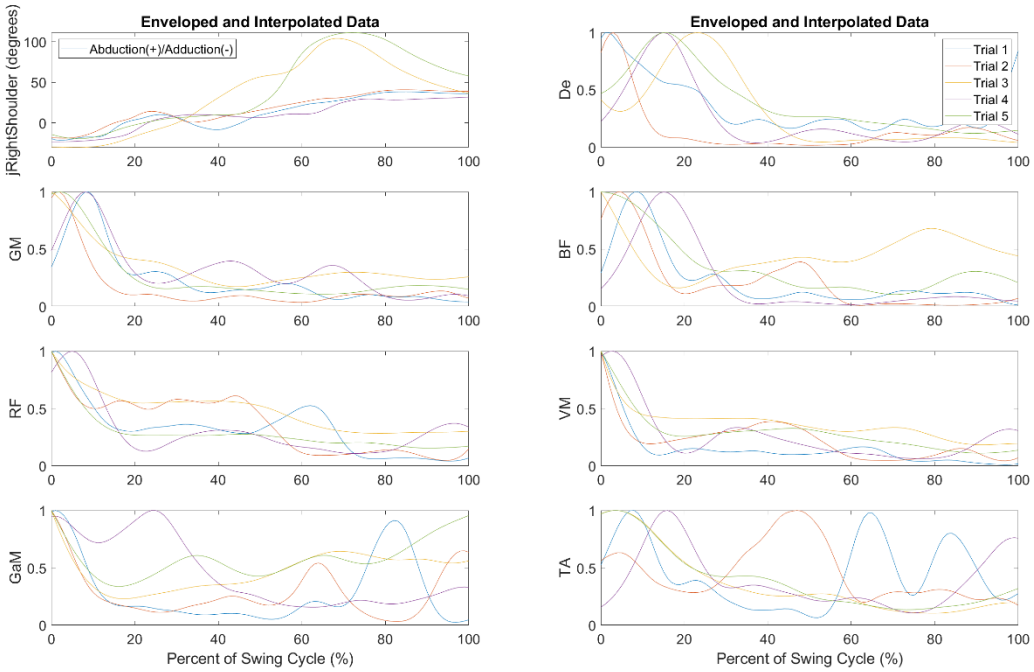

Figure B-55. TX14 individual backhand cross-court groundstrokes

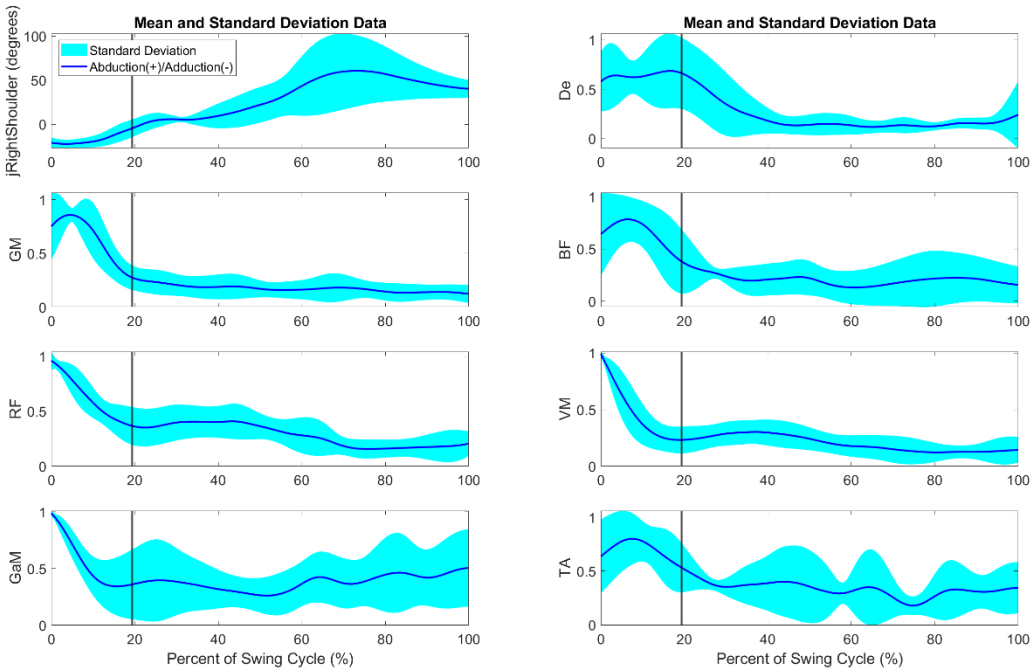

Figure B-56. TX14 averaged backhand cross-court groundstrokes with ball contact shown by vertical line

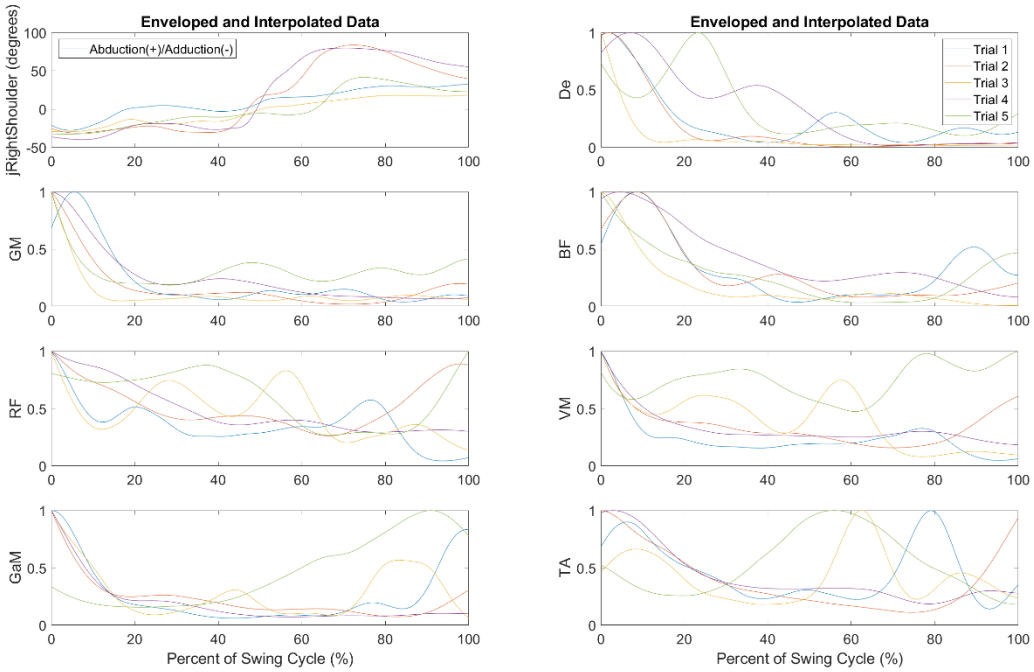

Figure B-57. TX14 individual backhand down-the-line groundstrokes

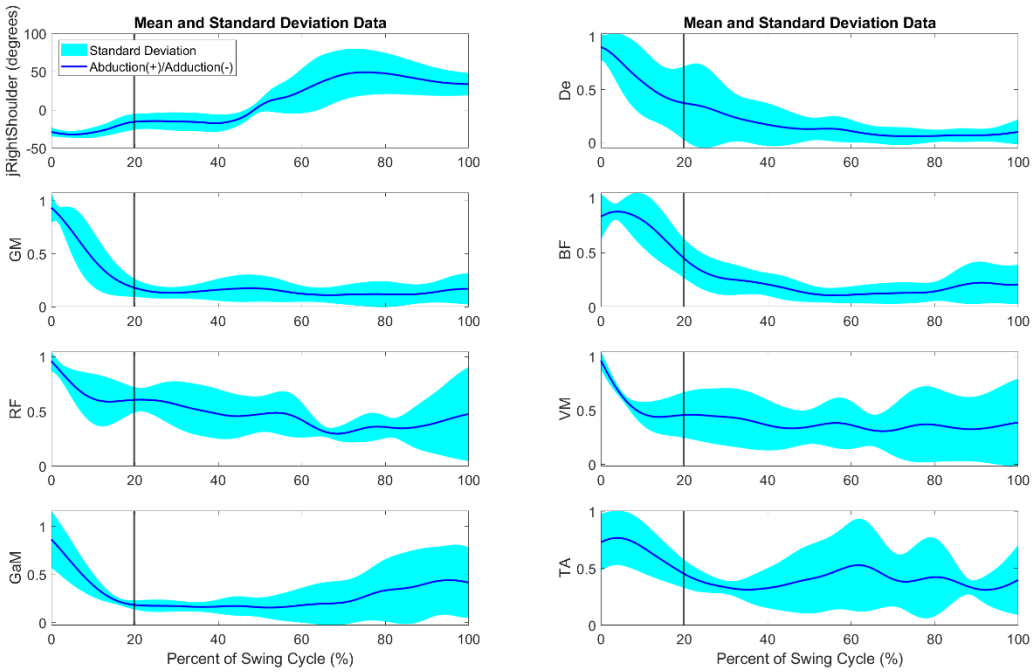

Figure B-58. TX14 averaged backhand down-the-line groundstrokes with ball contact shown by vertical line

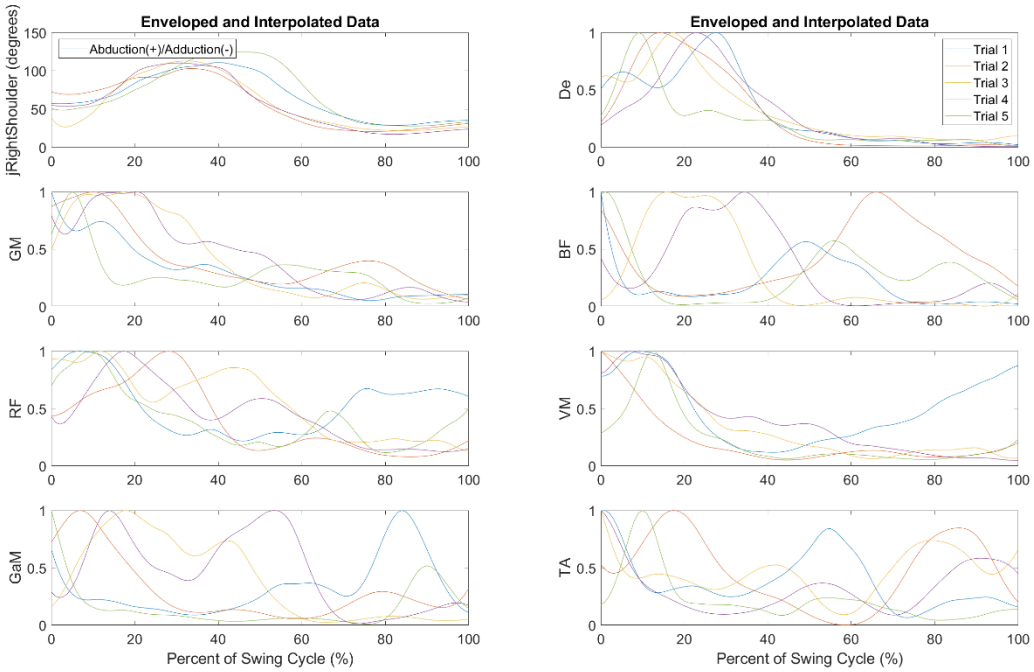

Figure B-59. TX14 individual forehand cross-court groundstrokes

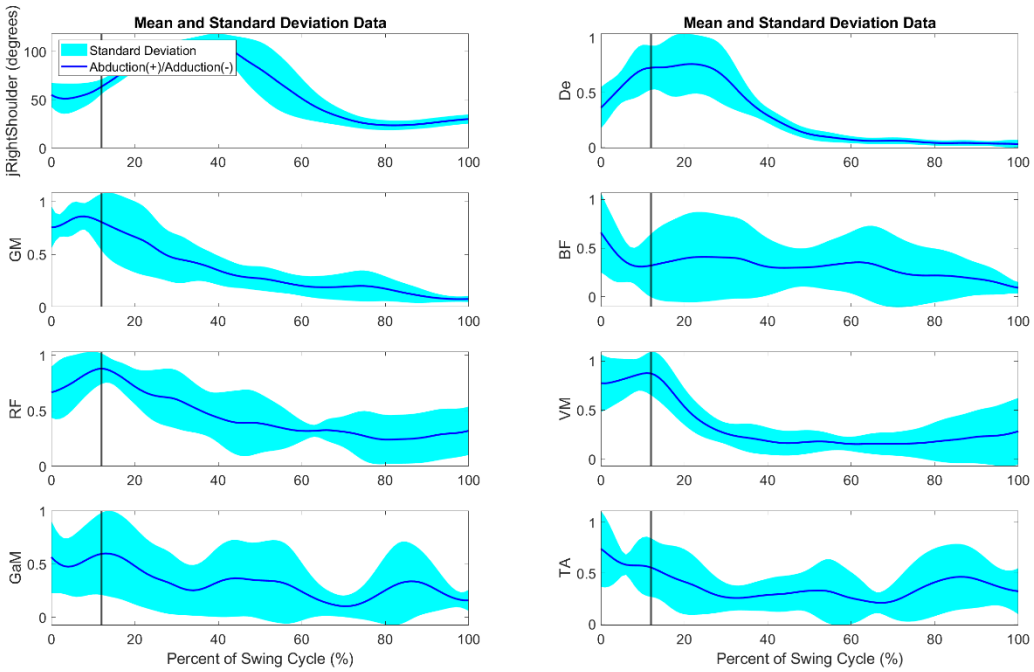

Figure B-60. TX14 averaged forehand cross-court groundstrokes with ball contact shown by vertical line

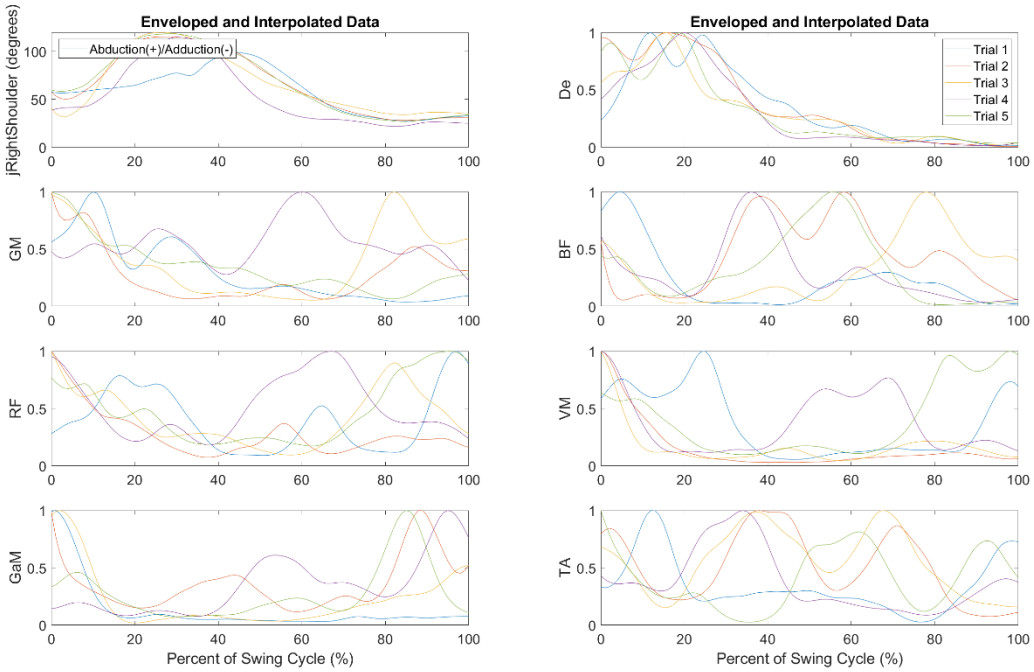

Figure B-61. TX14 individual forehand down-the-line groundstrokes

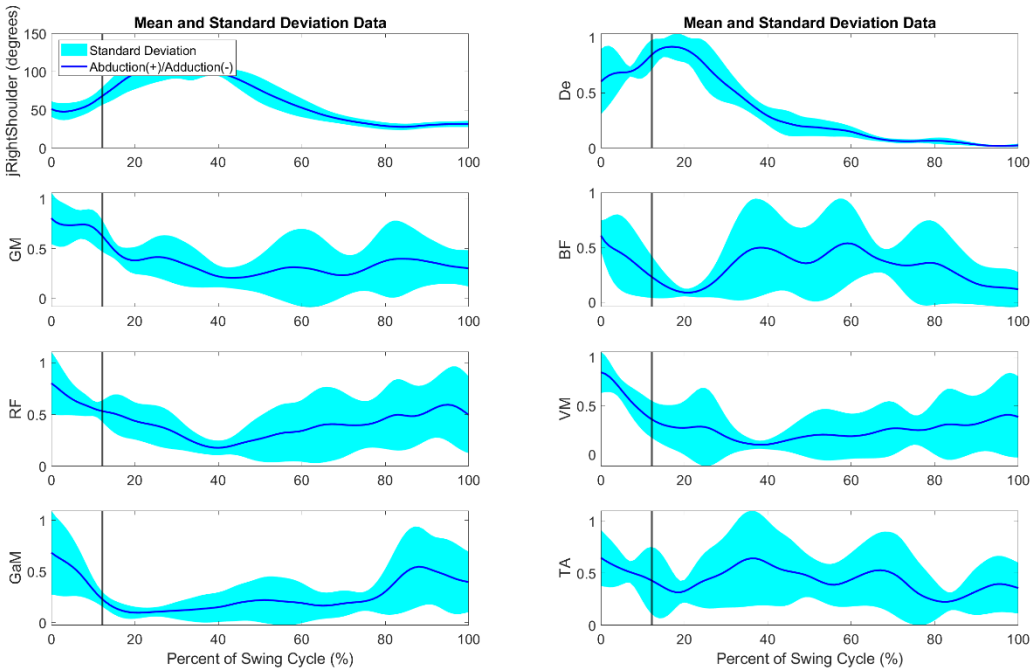

Figure B-62. TX14 averaged forehand down-the-line groundstrokes with ball contact shown by vertical line

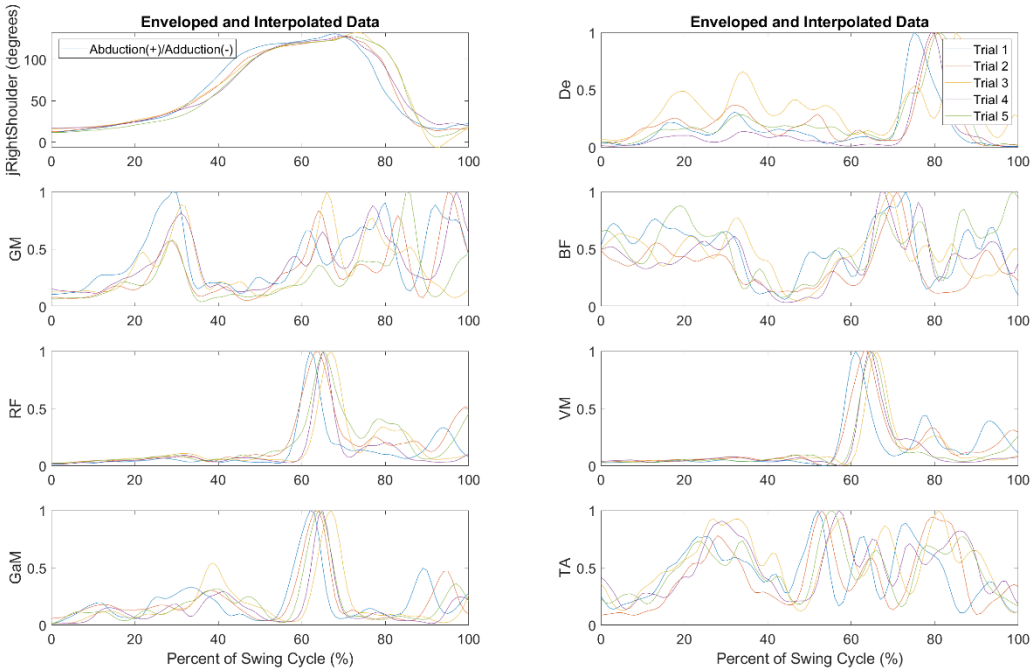

Figure B-63. TX14 individual advantage side serves

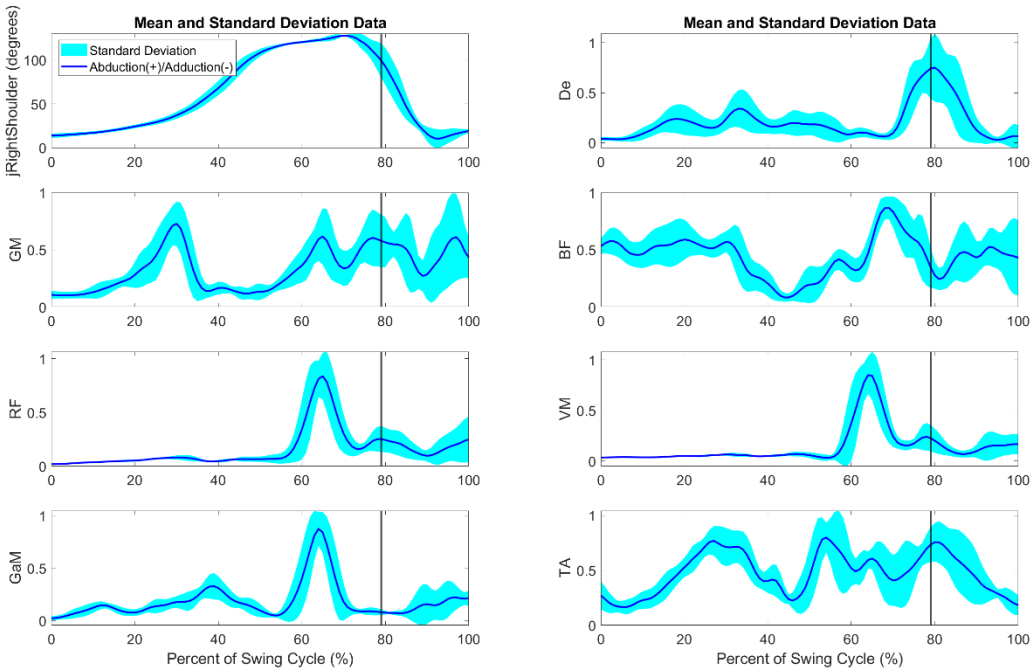

Figure B-64. TX14 averaged advantage side serves with ball contact shown by vertical line

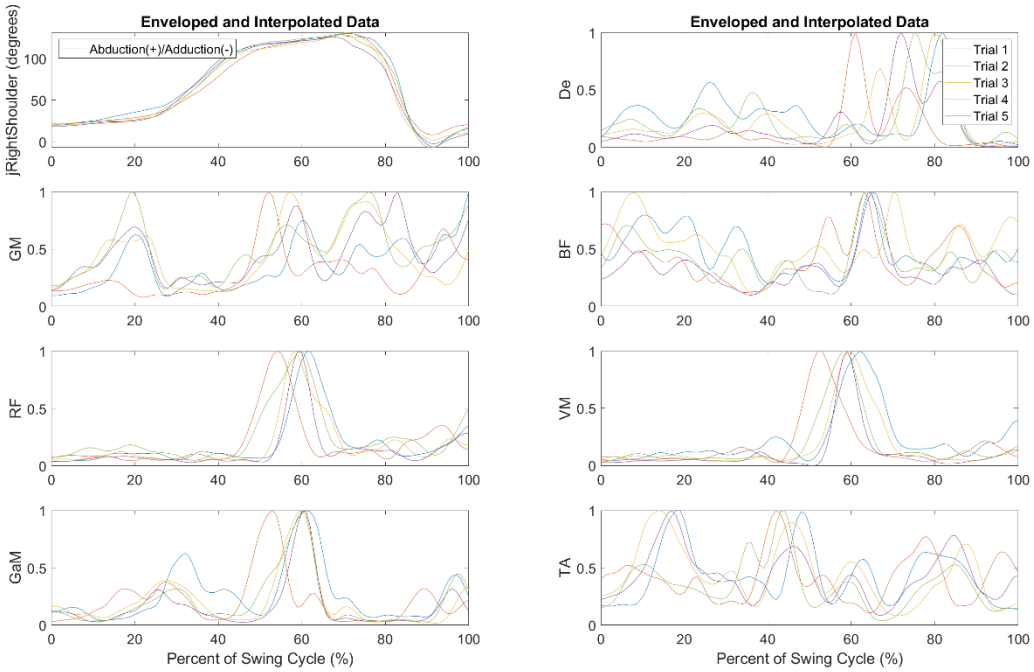

Figure B-65. TX14 individual deuce side serves

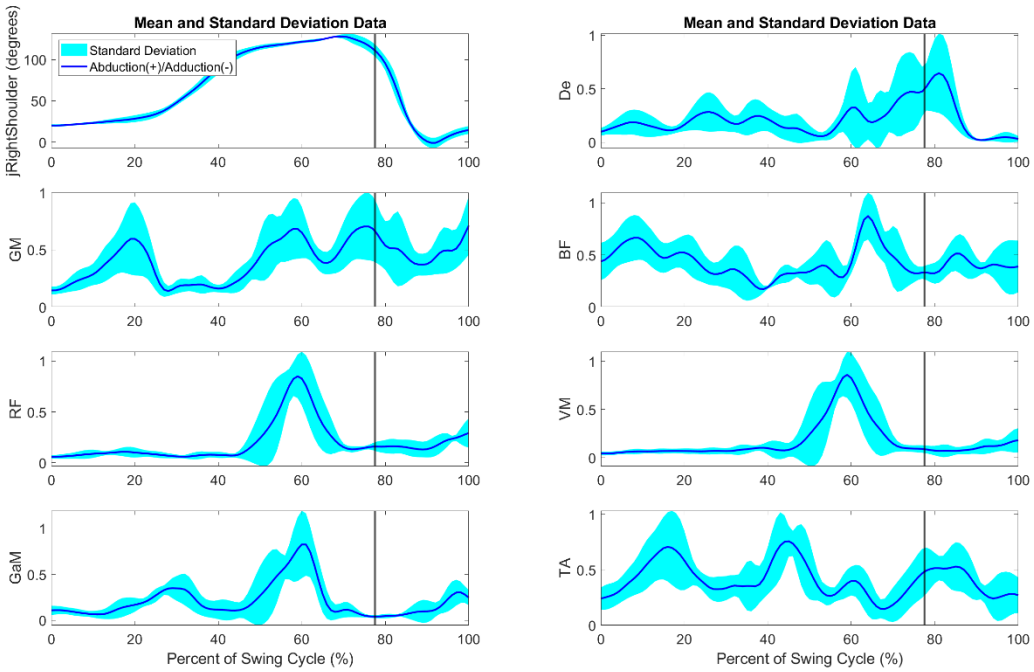

Figure B-66. TX14 averaged deuce side serves with ball contact shown by vertical line

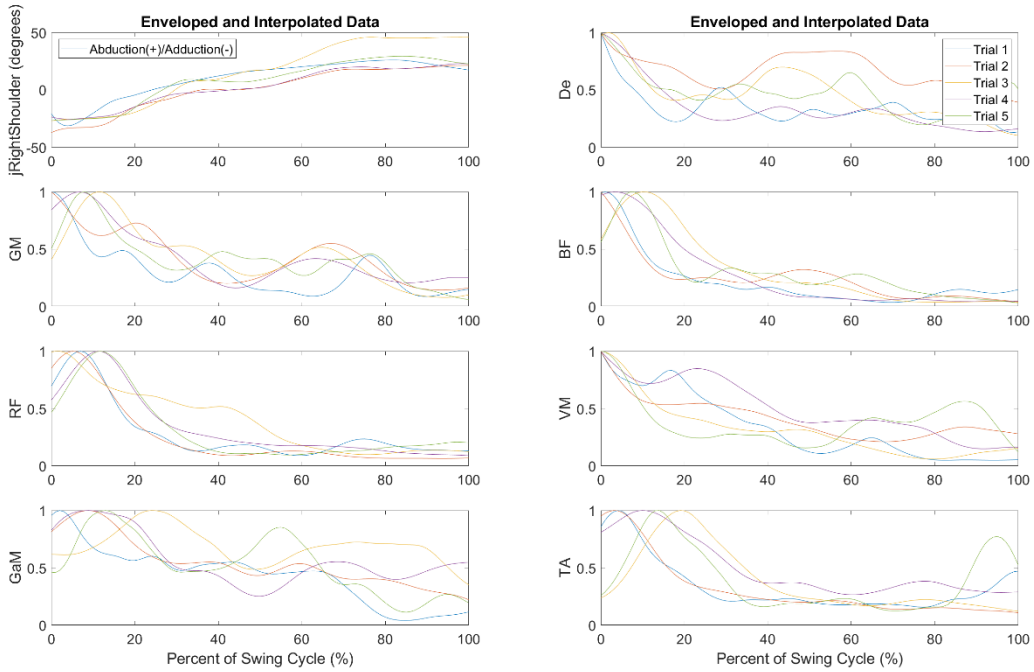

Figure B-67. TX15 individual backhand cross-court groundstrokes

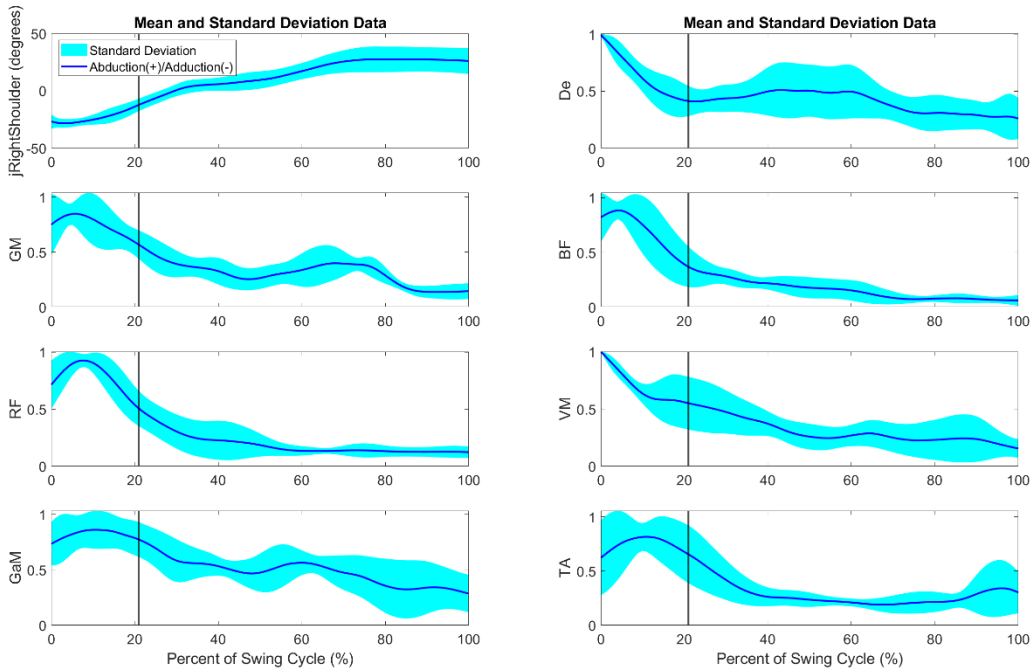

Figure B-68. TX15 averaged backhand cross-court groundstrokes with ball contact shown by vertical line

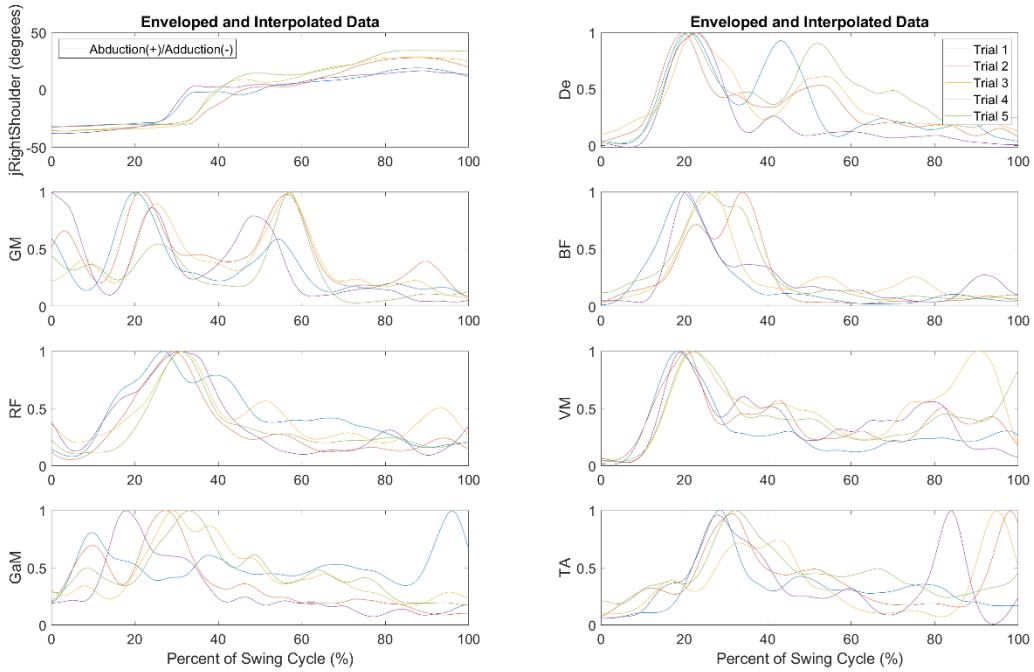

Figure B-69. TX15 individual backhand down-the-line groundstrokes

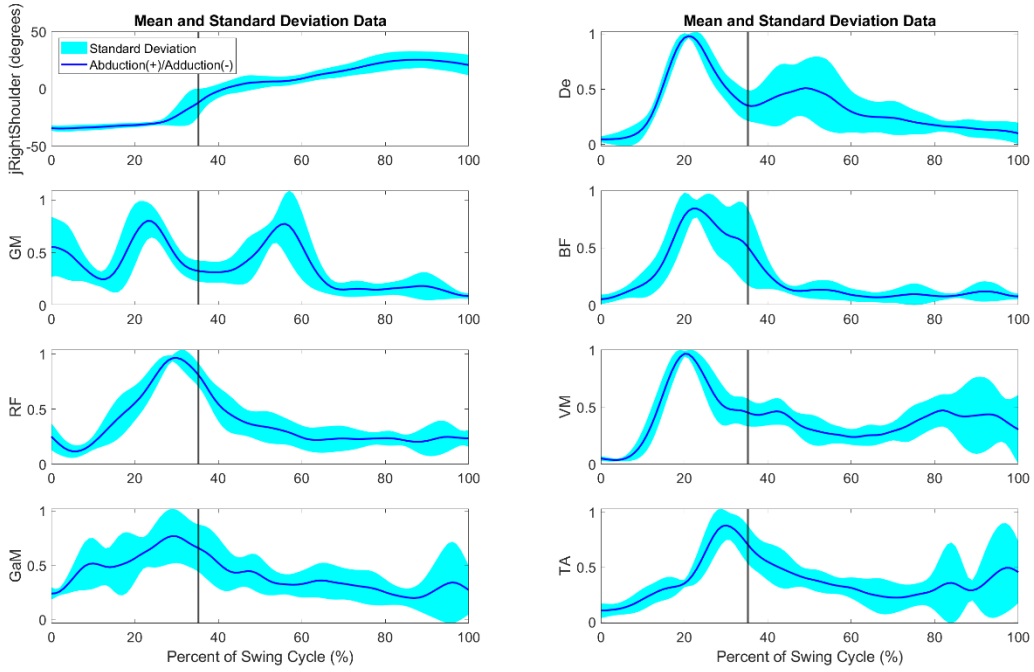

Figure B-70. TX15 averaged backhand down-the-line groundstrokes with ball contact shown by vertical line

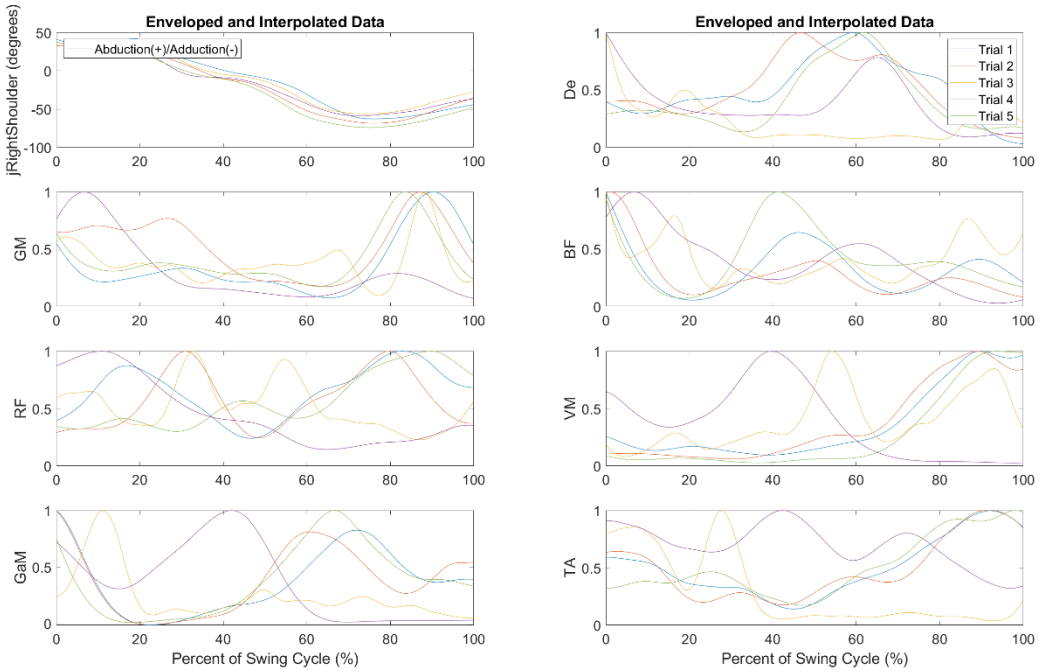

Figure B-71. TX15 individual forehand cross-court groundstrokes

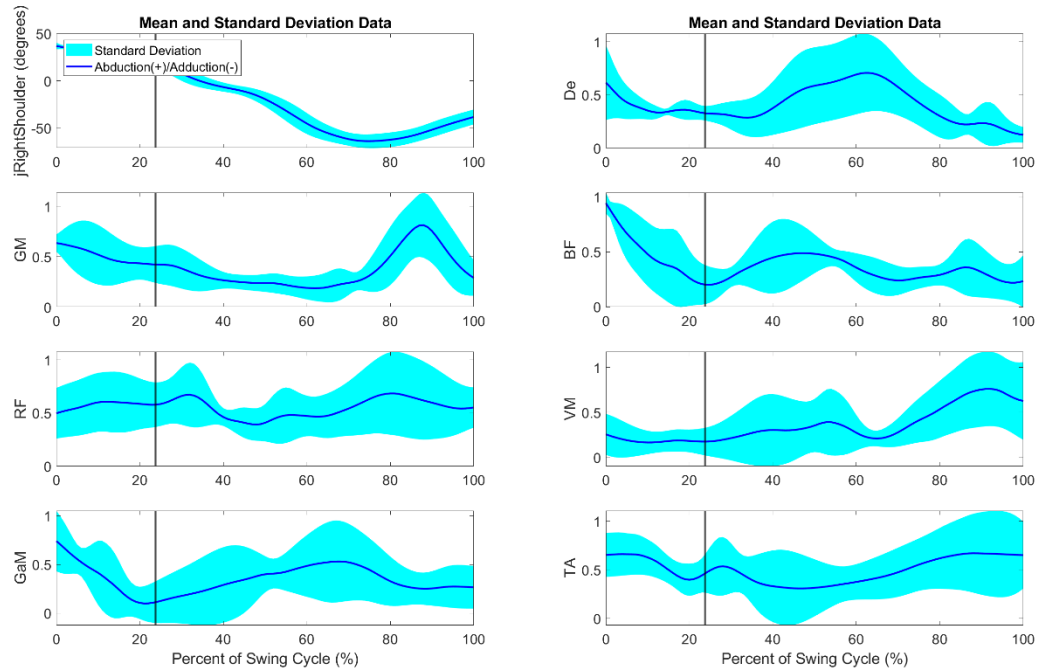

Figure B-72. TX15 averaged forehand cross-court groundstrokes with ball contact shown by vertical line

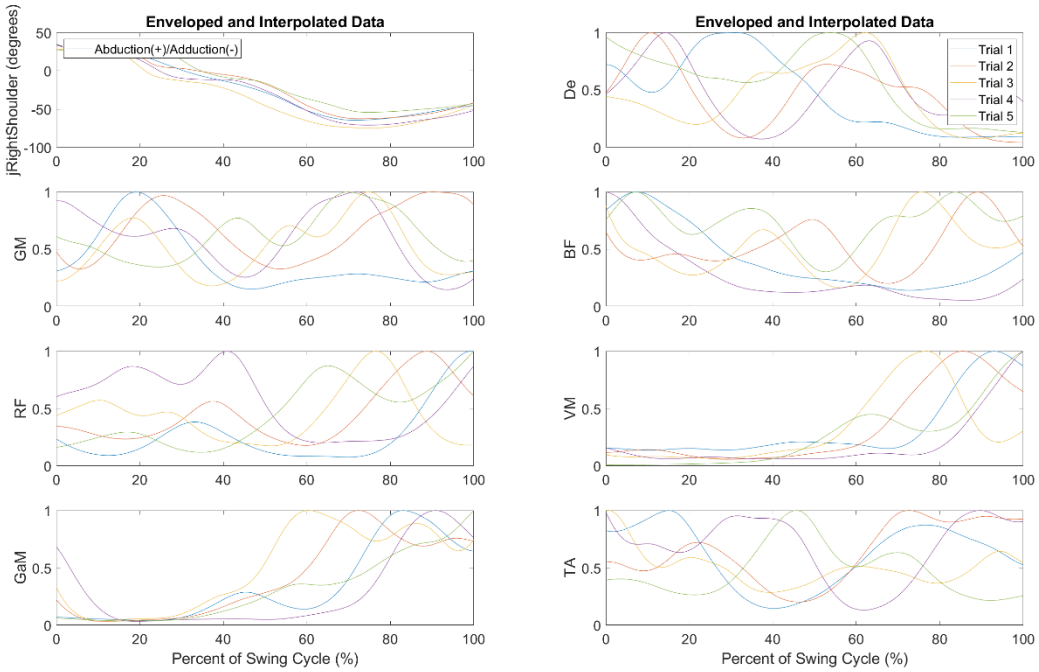

Figure B-73. TX15 individual forehand down-the-line groundstrokes

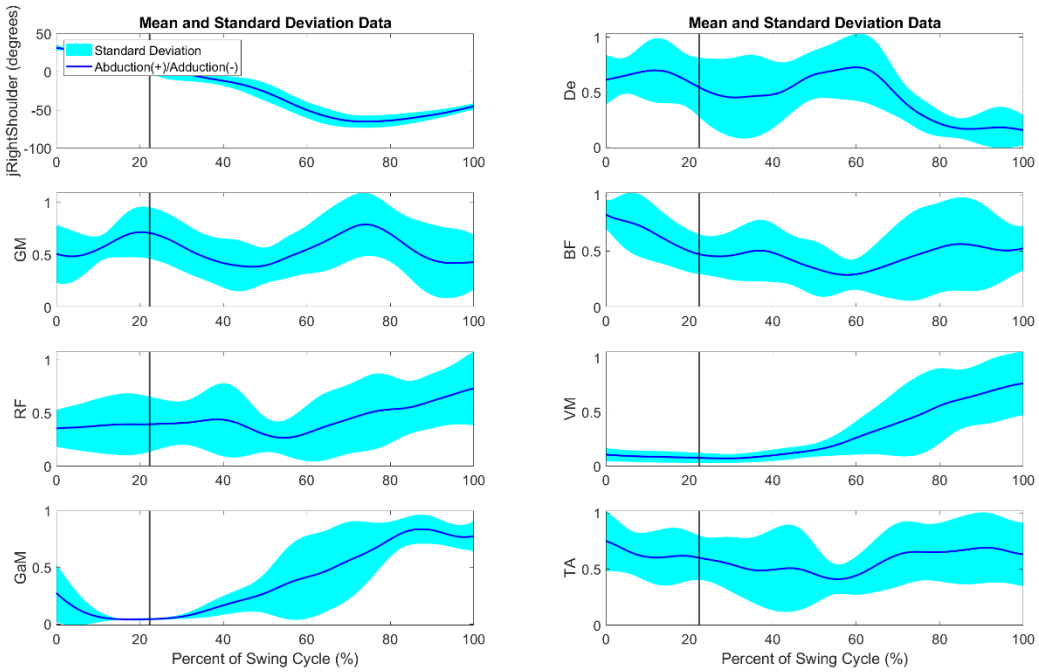

Figure B-74. TX15 averaged forehand down-the-line groundstrokes with ball contact shown by vertical line

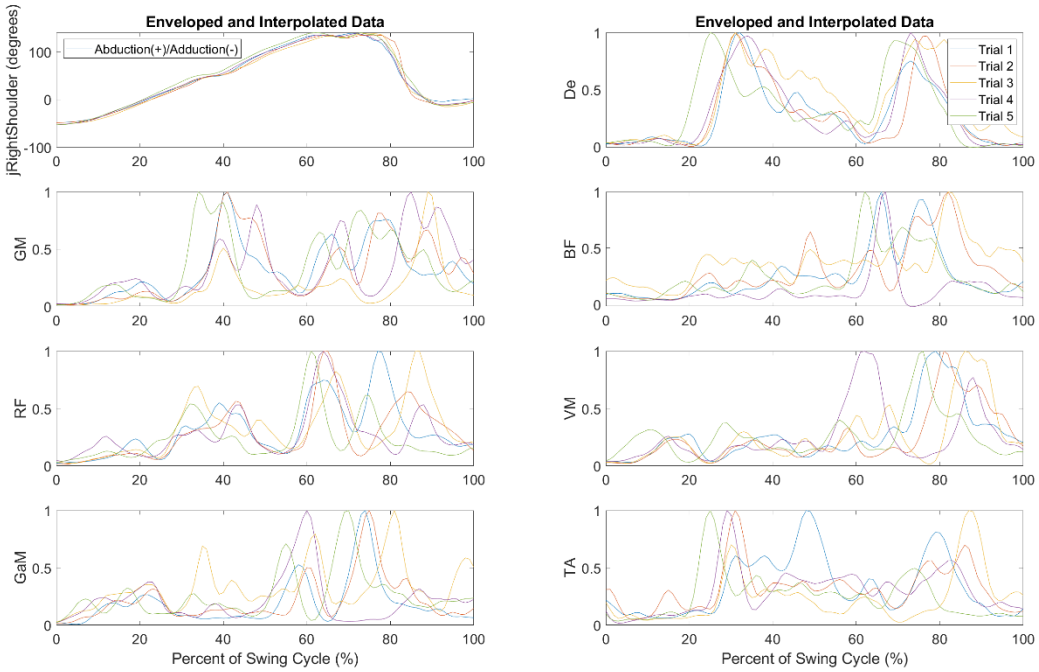

Figure B-75. TX15 individual advantage side serves

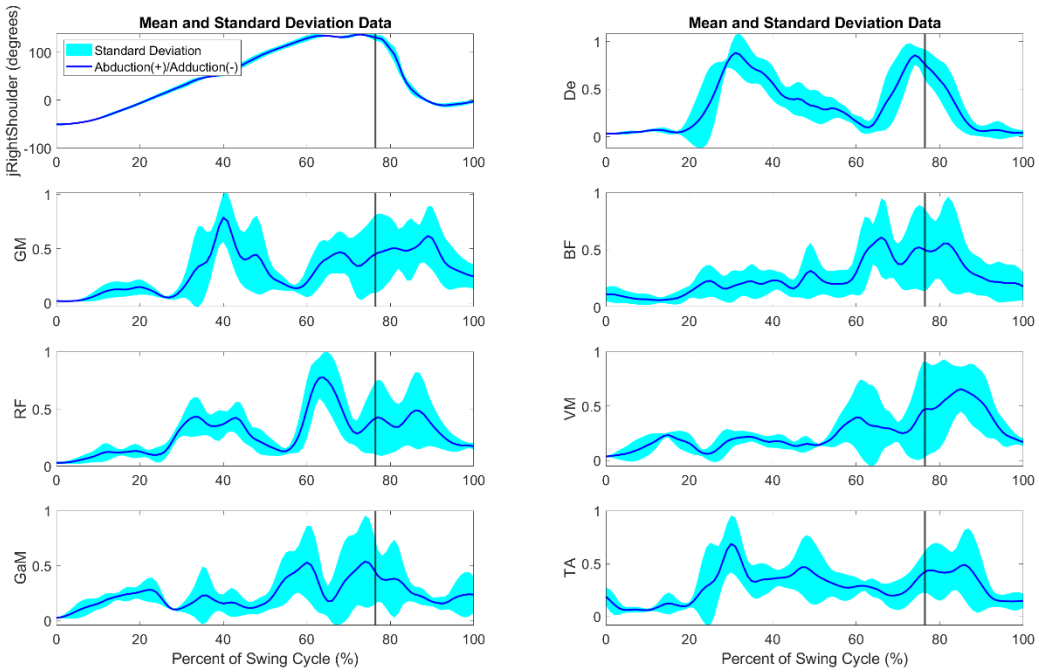

Figure B-76. TX15 averaged advantage side serves with ball contact shown by vertical line

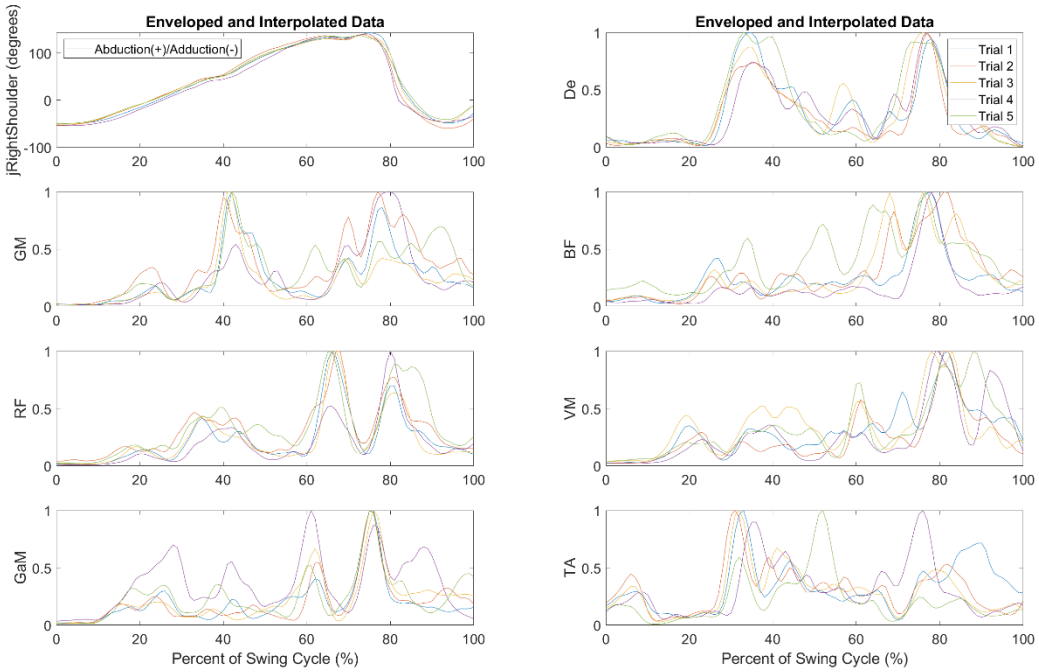

Figure B-77. TX15 individual deuce side serves

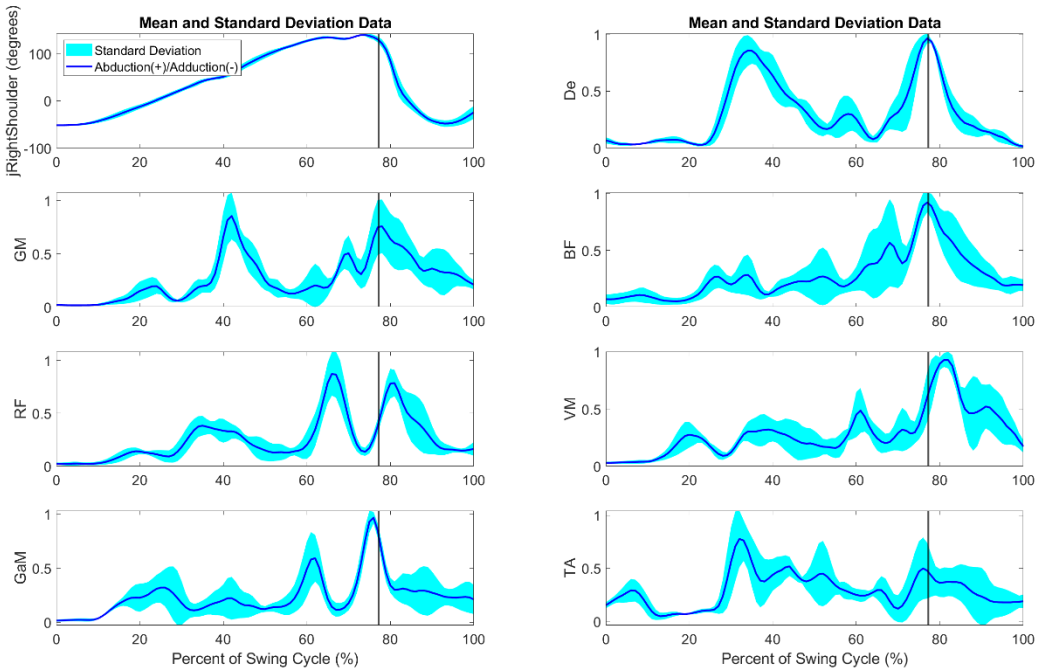

Figure B-78. TX15 averaged deuce side serves with ball contact shown by vertical line

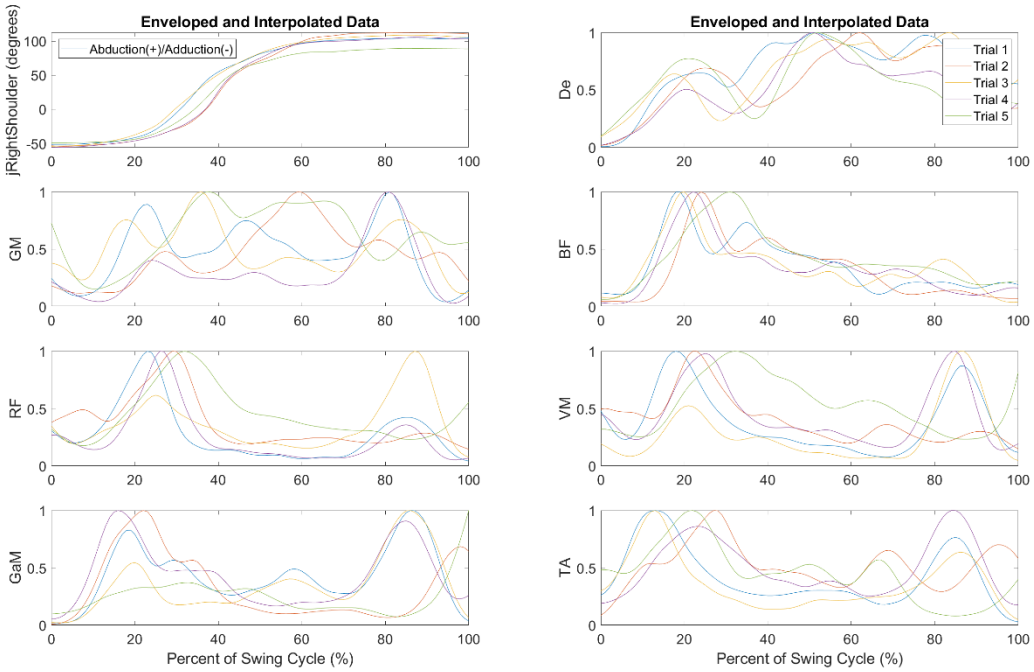

Figure B-79. TX16 individual backhand cross-court groundstrokes

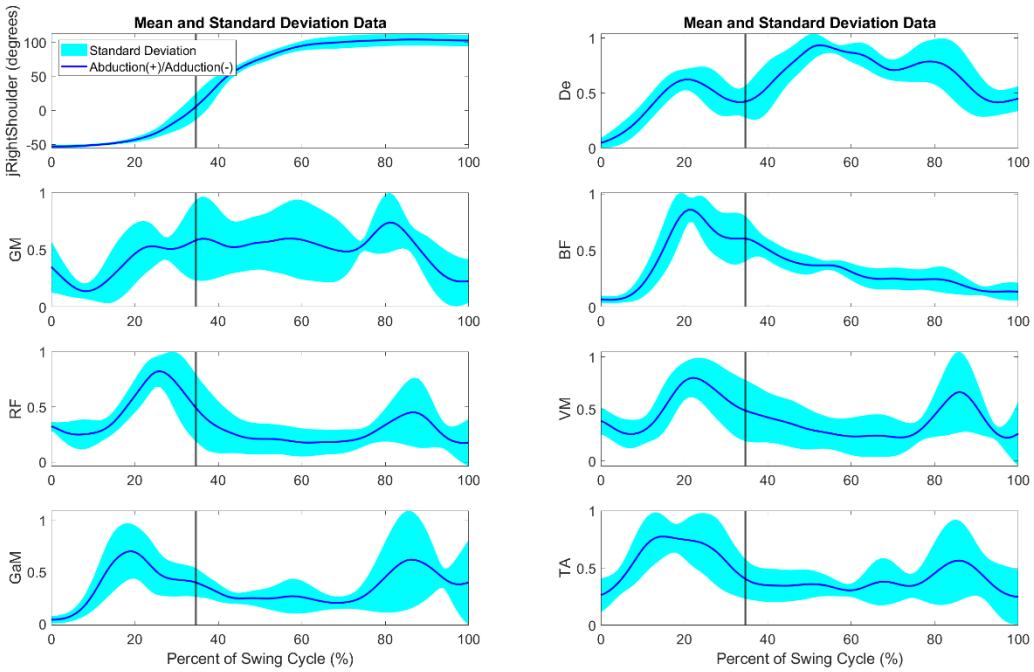

Figure B-80. TX16 averaged backhand cross-court groundstrokes with ball contact shown by vertical line

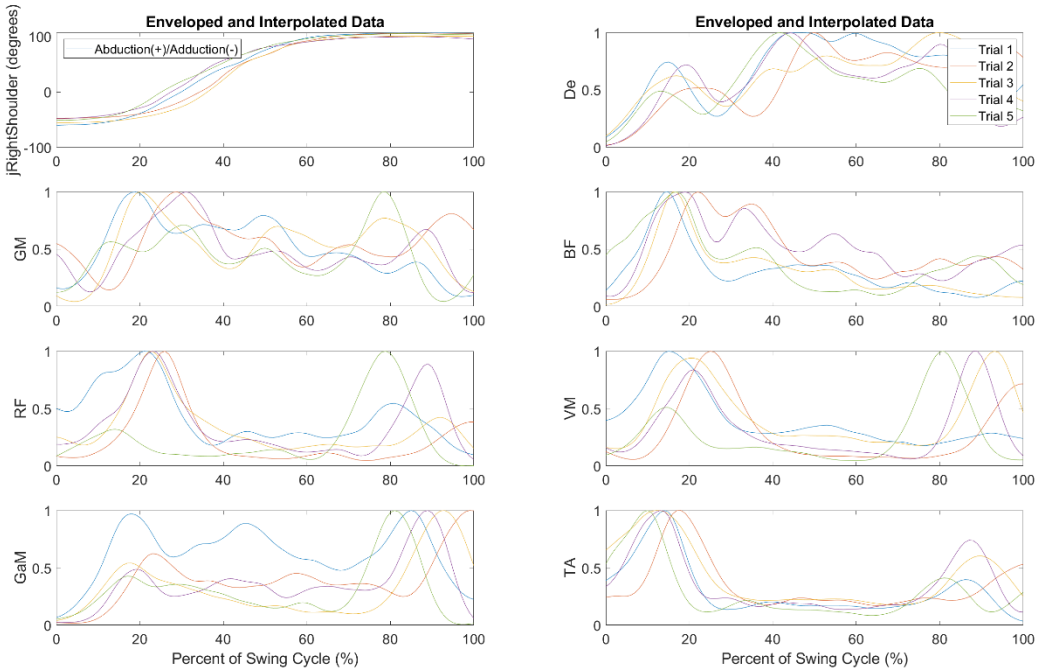

Figure B-81. TX16 individual backhand down-the-line groundstrokes

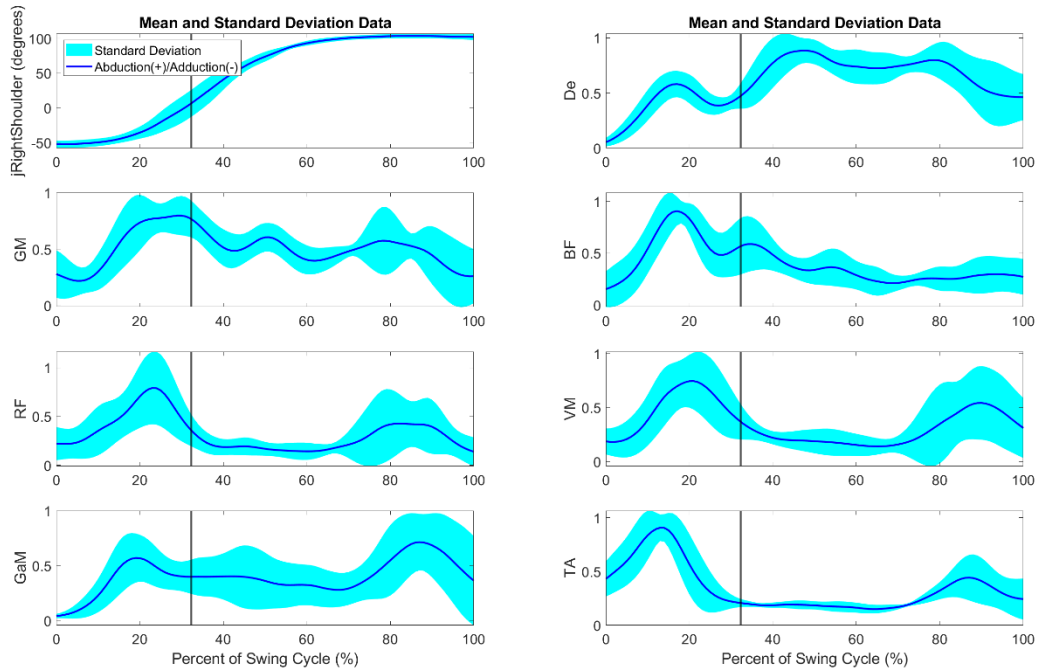

Figure B-82. TX16 averaged backhand down-the-line groundstrokes with ball contact shown by vertical line

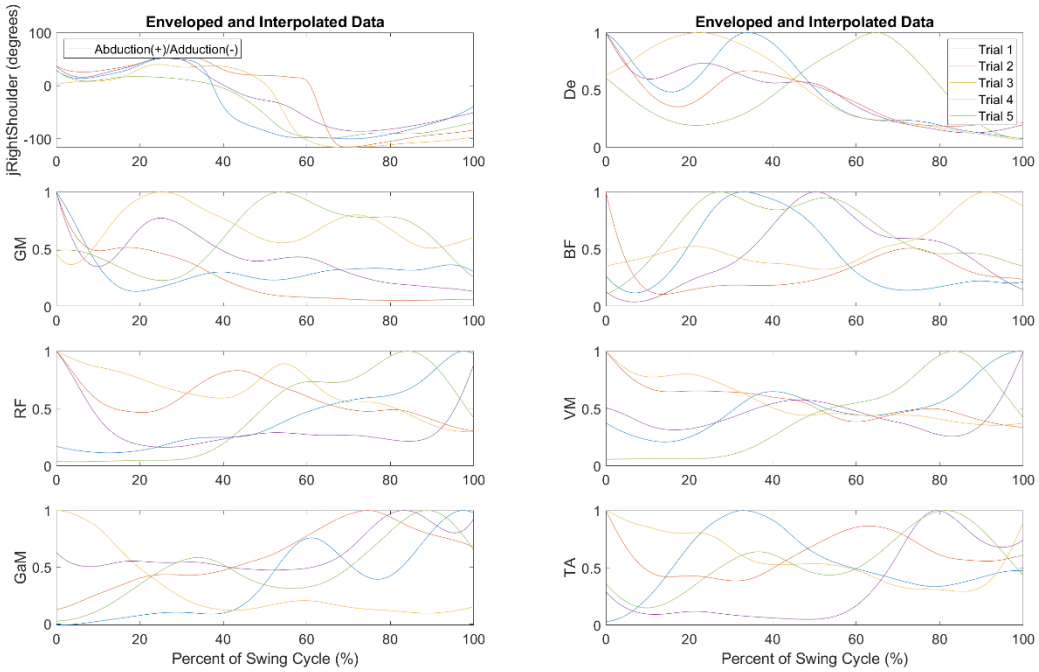

Figure B-83. TX16 individual forehand cross-court groundstrokes

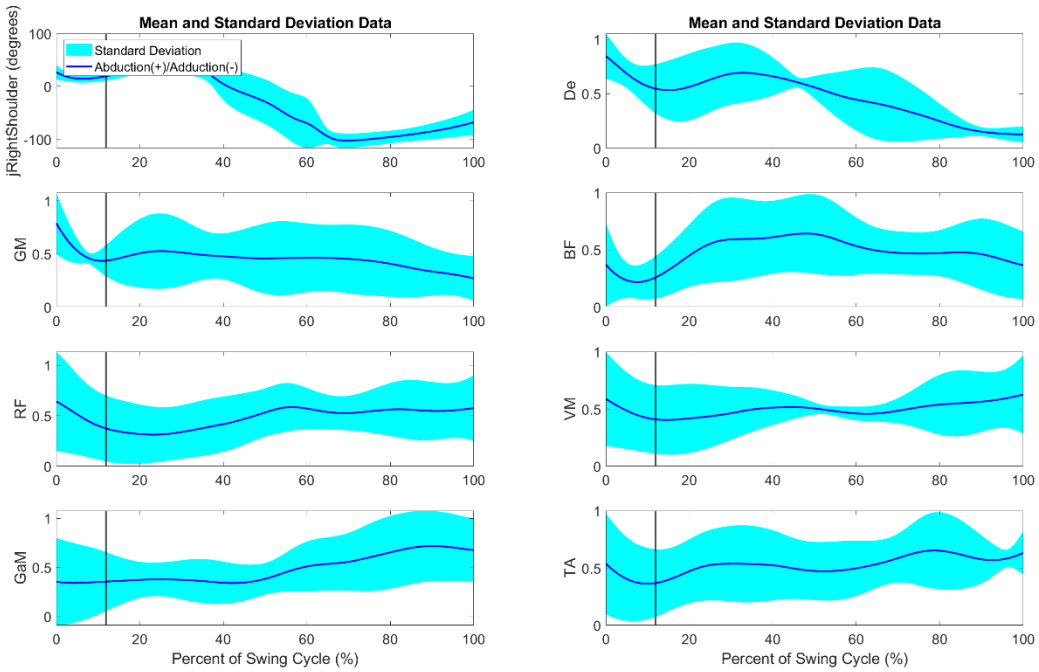

Figure B-84. TX16 averaged forehand cross-court groundstrokes with ball contact shown by vertical line

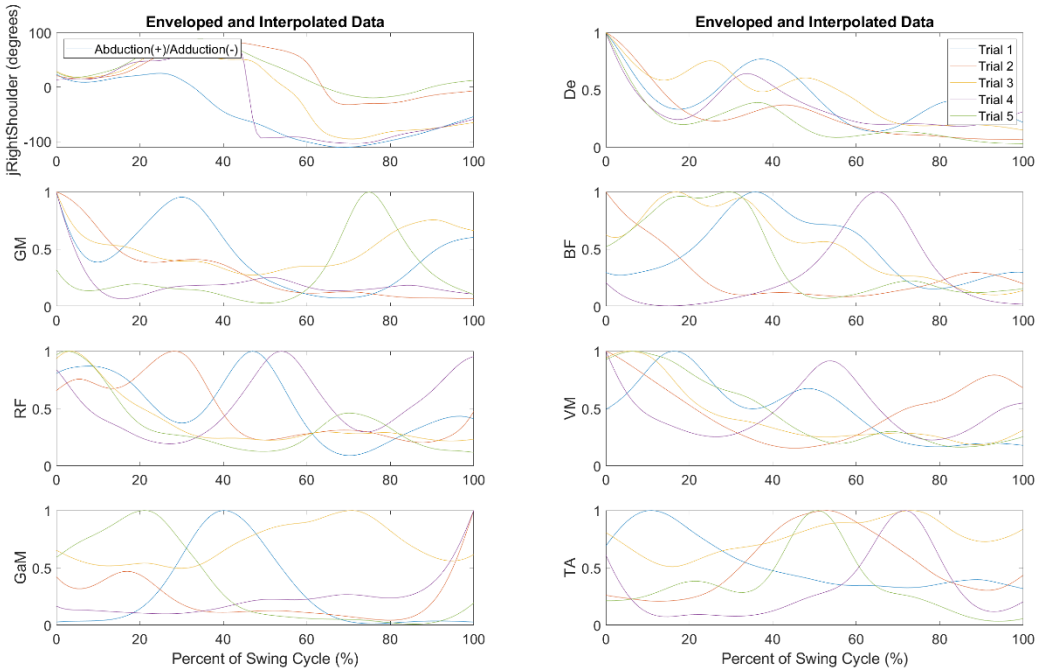

Figure B-85. TX16 individual forehand down-the-line groundstrokes

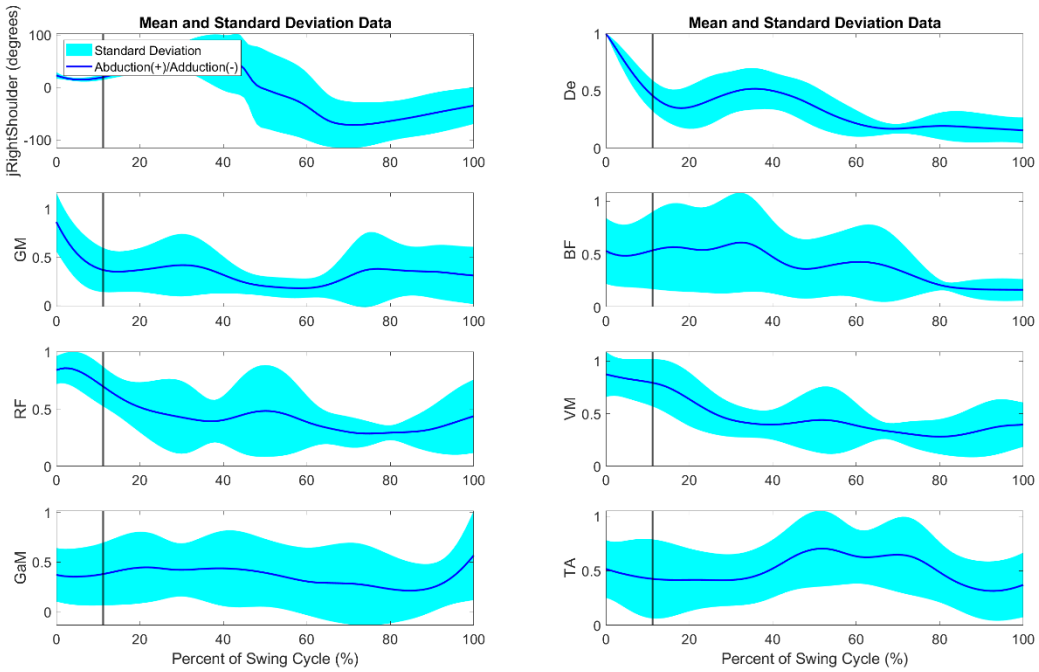

Figure B-86. TX16 averaged forehand down-the-line groundstrokes with ball contact shown by vertical line

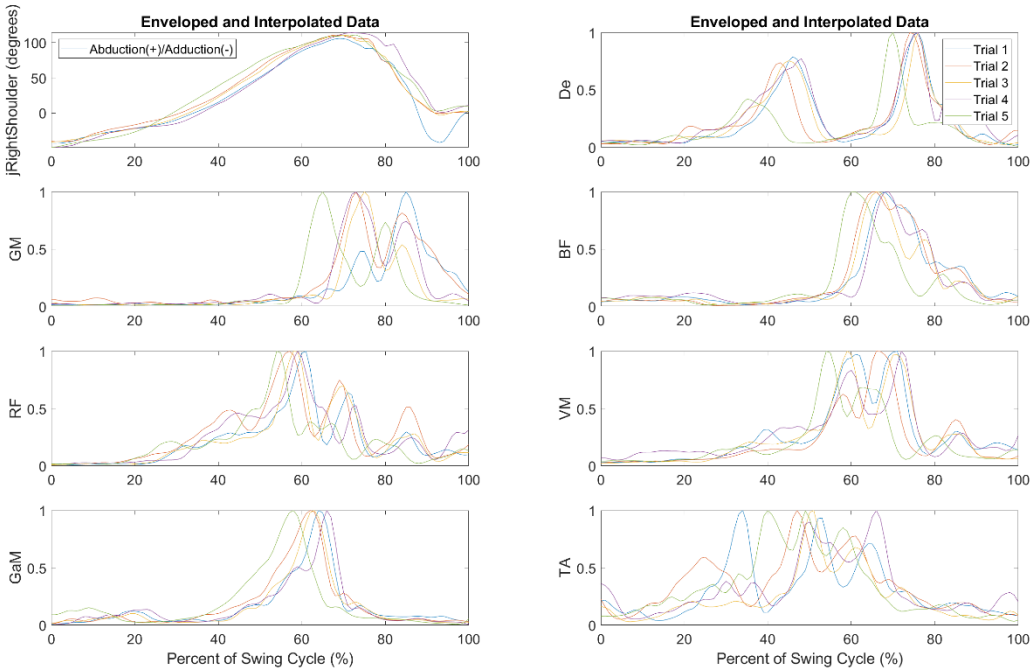

Figure B-87. TX16 individual advantage side serves

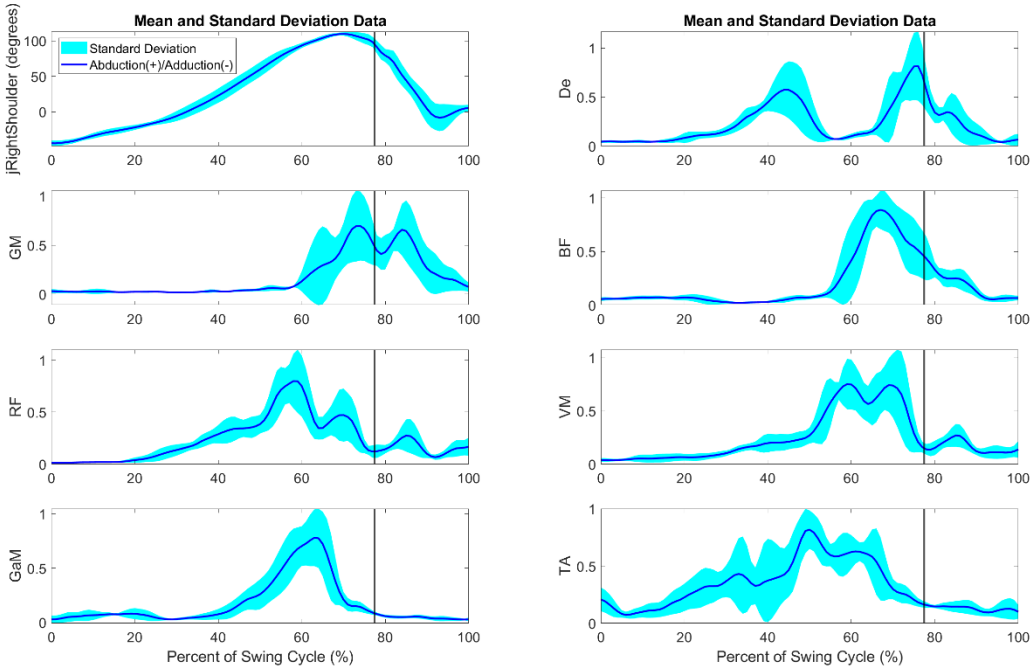

Figure B-88. TX16 averaged advantage side serves with ball contact shown by vertical line

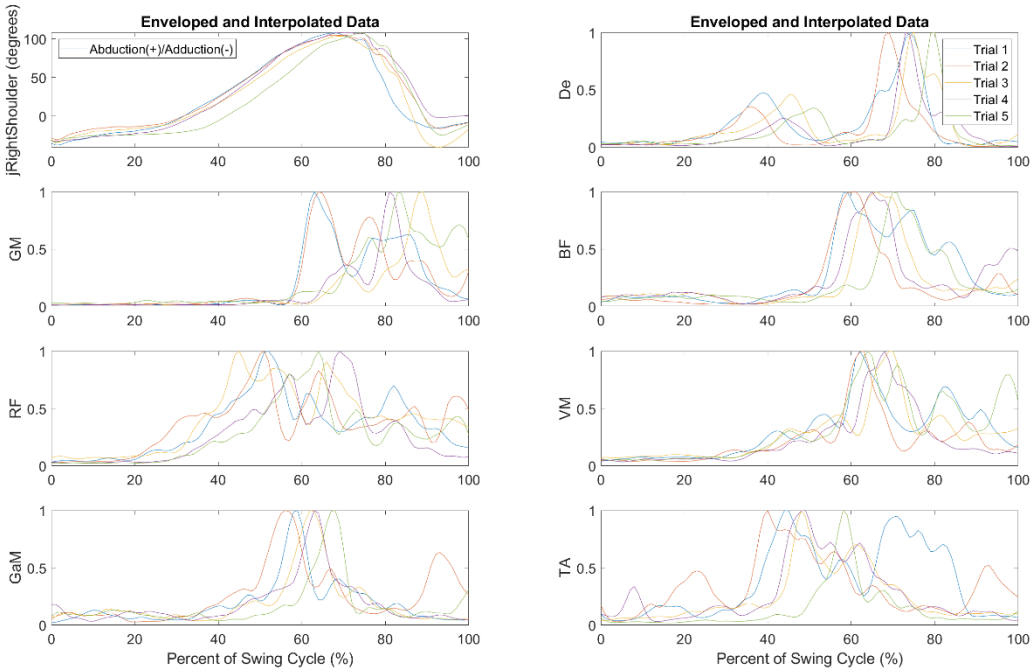

Figure B-89. TX16 individual deuce side serves

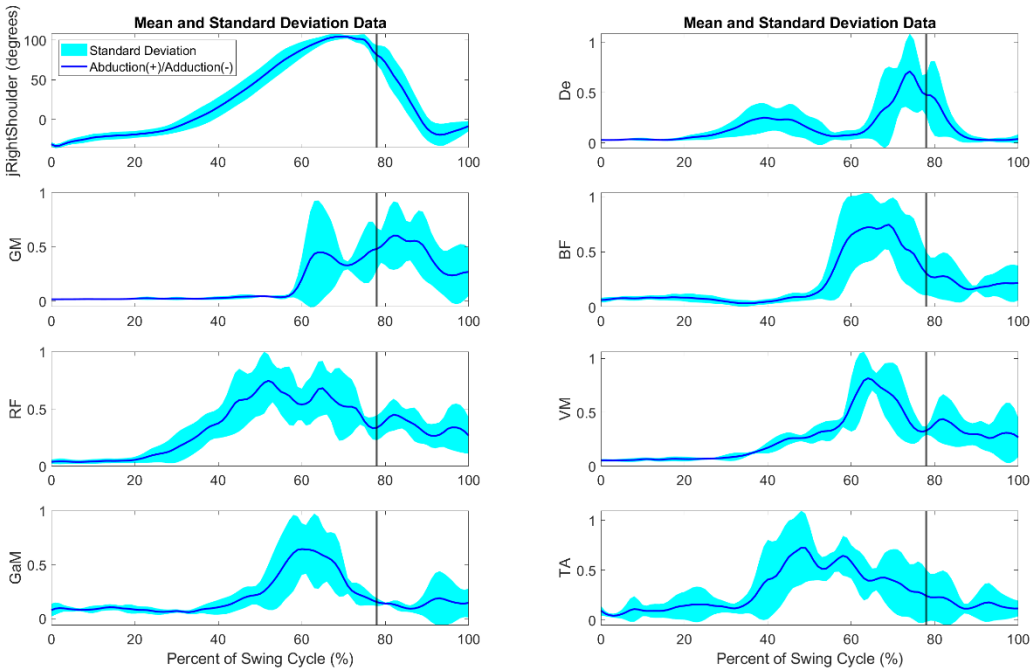

Figure B-90. TX16 averaged deuce side serves with ball contact shown by vertical line

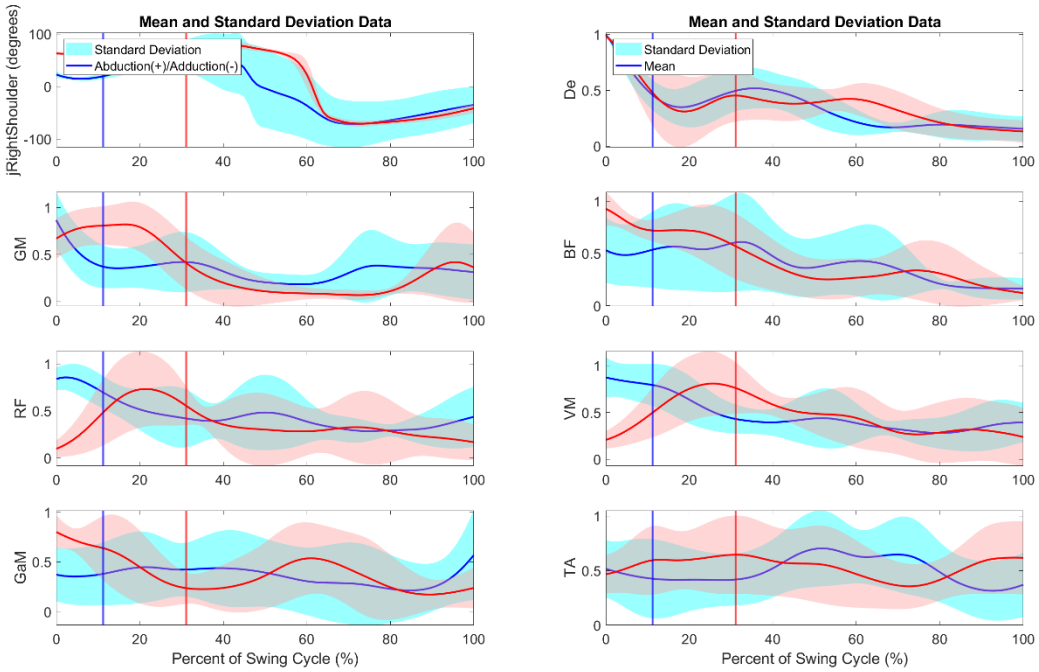

Figure B-91. Professional and non-professional forehand down-the-line groundstrokes. The professional is represented by the red line while the non-professional is represented by the blue line.

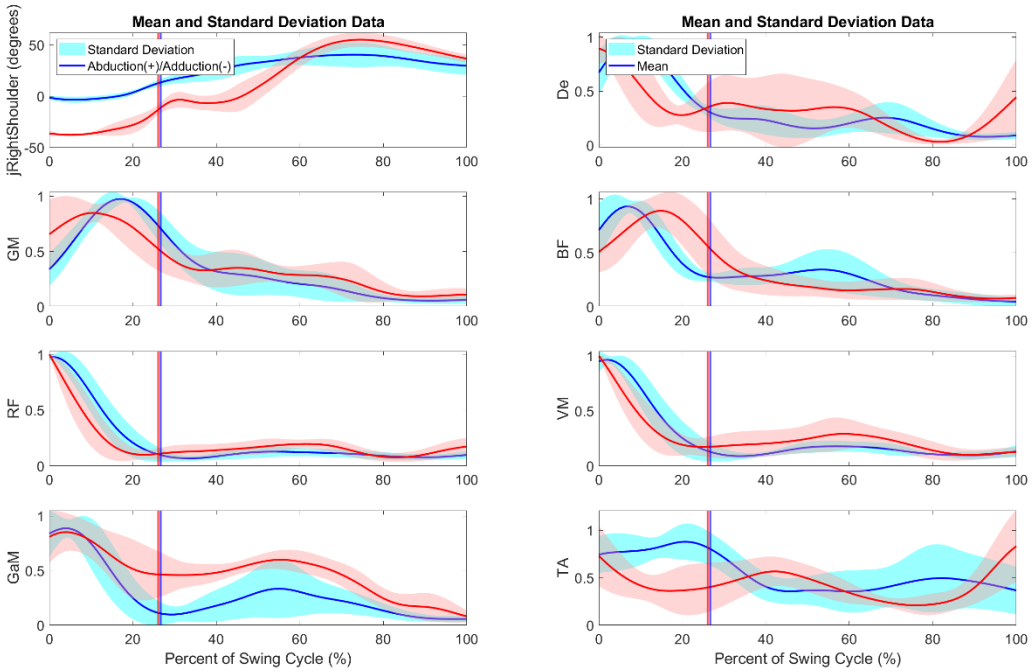

Figure B-92. Professional and non-professional backhand down-the-line groundstrokes. The professional is represented by the red line while the non-professional is represented by the blue line.

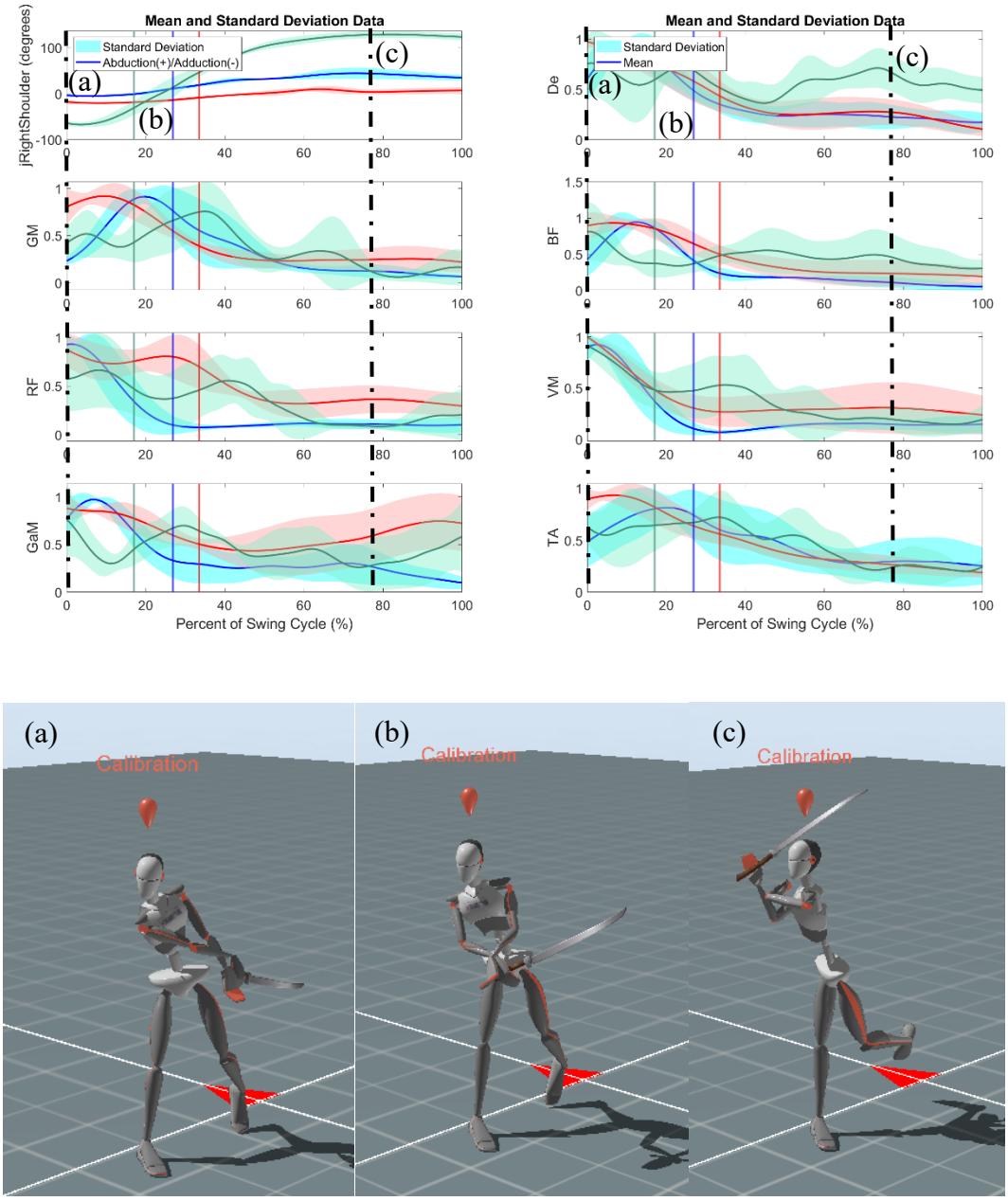

Figure B-93. The graphs depict shoulder abduction and adduction, alongside sEMG data, recorded from non-professionals executing backhand cross-court groundstrokes. Vertical lines in the graphs indicate various stages of the groundstroke, as demonstrated by XSENS MoCap figurines. Three distinct colors denote three different subjects. The solid line represents the average of five trials, while the shaded region indicates the standard deviation across the same five trials.

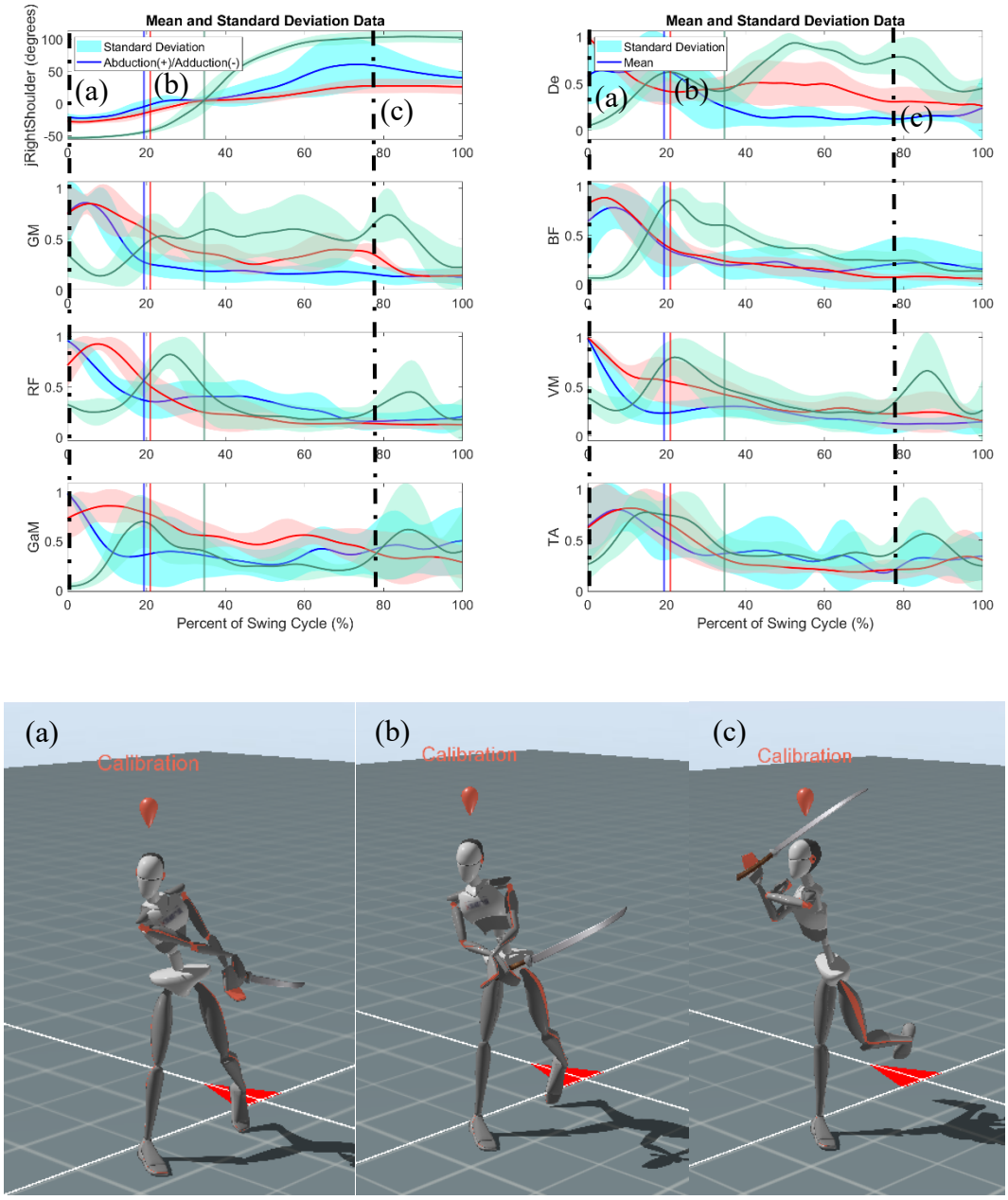

Figure B-94. The graphs depict shoulder abduction and adduction, alongside sEMG data, recorded from non-professionals executing backhand cross-court groundstrokes. Vertical lines in the graphs indicate various stages of the groundstroke, as demonstrated by XSENS MoCap figurines. Three distinct colors denote three different subjects. The solid line represents the average of five trials, while the shaded region indicates the standard deviation across the same five trials.

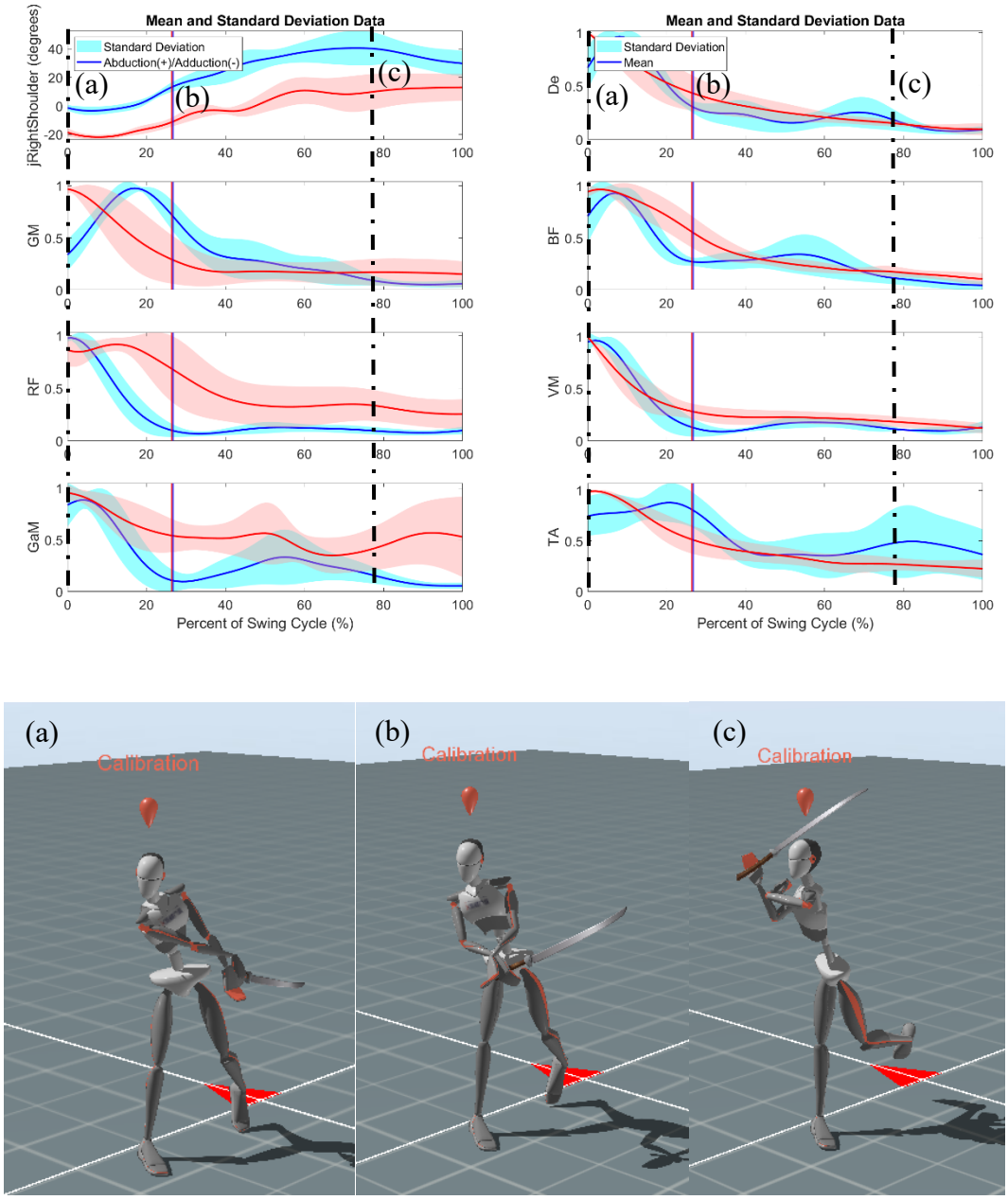

Figure B-95. The graphs depict shoulder abduction and adduction, alongside sEMG data, recorded from non-professionals executing backhand down-the-line groundstrokes. Vertical lines in the graphs indicate various stages of the groundstroke, as demonstrated by XSENS MoCap figurines. Two distinct colors denote two different subjects. The solid line represents the average of five trials, while the shaded region indicates the standard deviation across the same five trials.

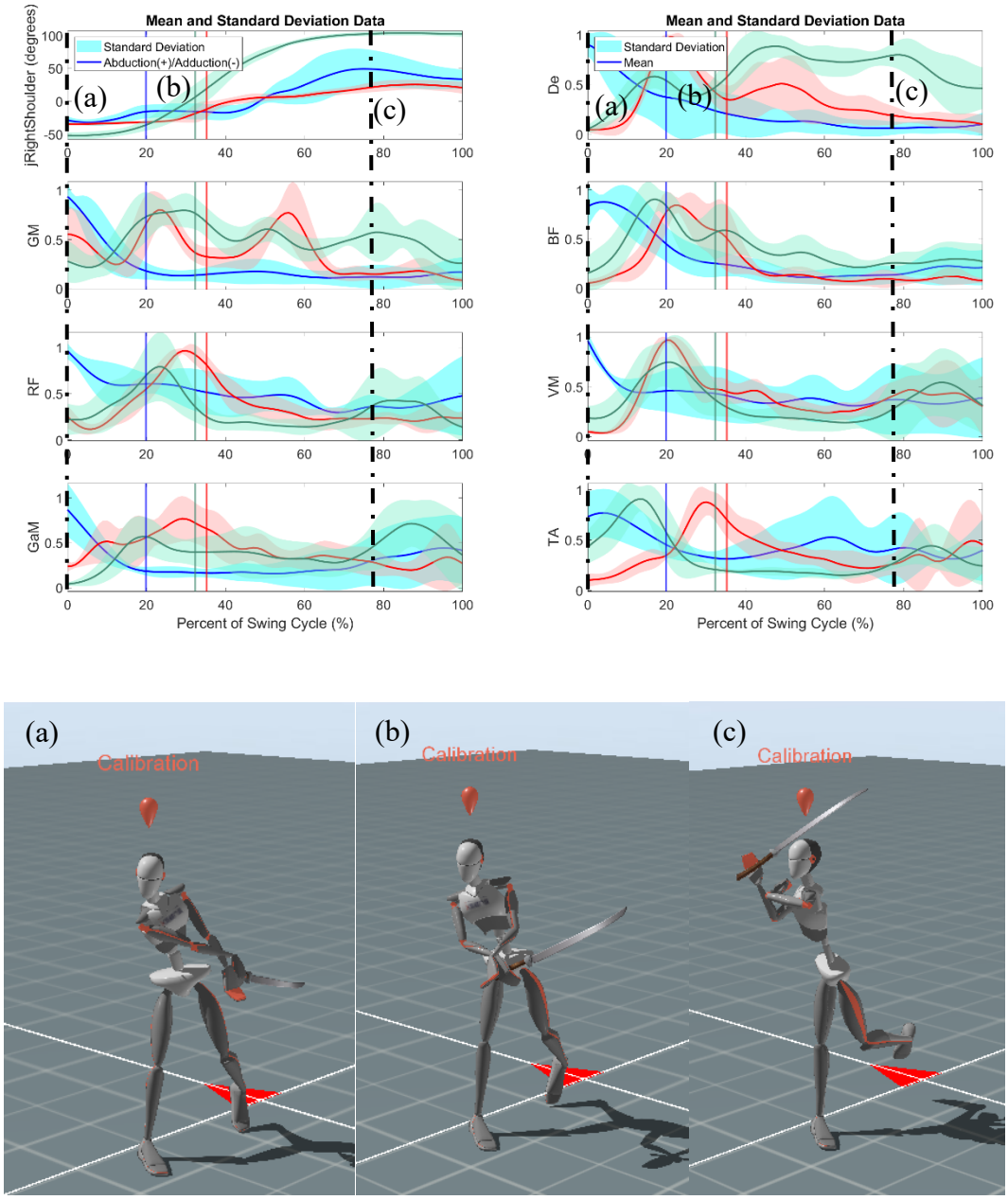

Figure B-96. The graphs depict shoulder abduction and adduction, alongside sEMG data, recorded from non-professionals executing backhand down-the-line groundstrokes. Vertical lines in the graphs indicate various stages of the groundstroke, as demonstrated by XSENS MoCap figurines. Three distinct colors denote three different subjects. The solid line represents the average of five trials, while the shaded region indicates the standard deviation across the same five trials.

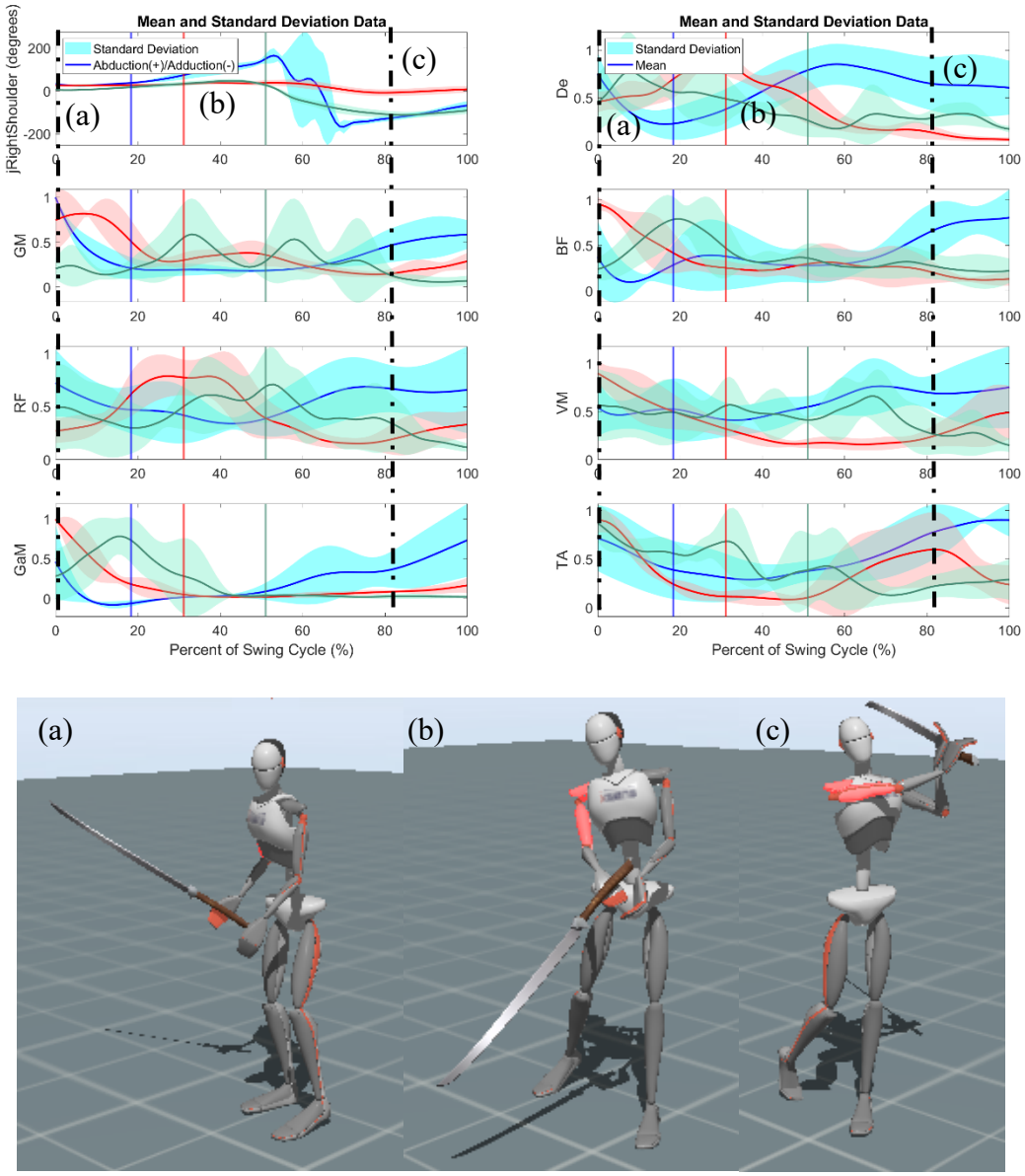

Figure B-97. The graphs depict shoulder abduction and adduction, alongside sEMG data, recorded from non-professionals executing forehand cross-court groundstrokes. Vertical lines in the graphs indicate various stages of the groundstroke, as demonstrated by XSENS MoCap figurines. Three distinct colors denote three different subjects. The solid line represents the average of five trials, while the shaded region indicates the standard deviation across the same five trials.

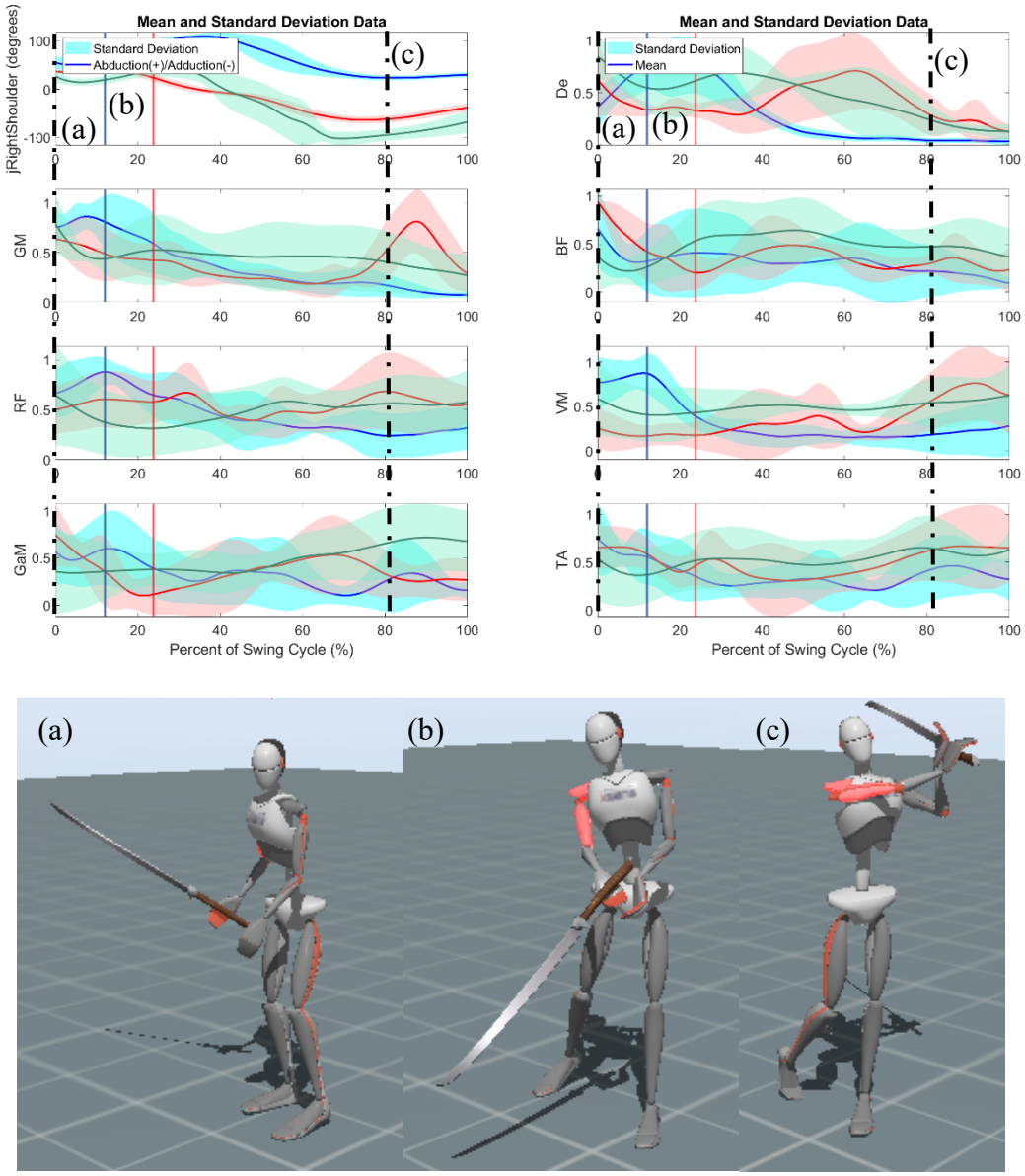

Figure B-98. The graphs depict shoulder abduction and adduction, alongside sEMG data, recorded from non-professionals executing forehand cross-court groundstrokes. Vertical lines in the graphs indicate various stages of the groundstroke, as demonstrated by XSENS MoCap figurines. Three distinct colors denote three different subjects. The solid line represents the average of five trials, while the shaded region indicates the standard deviation across the same five trials.

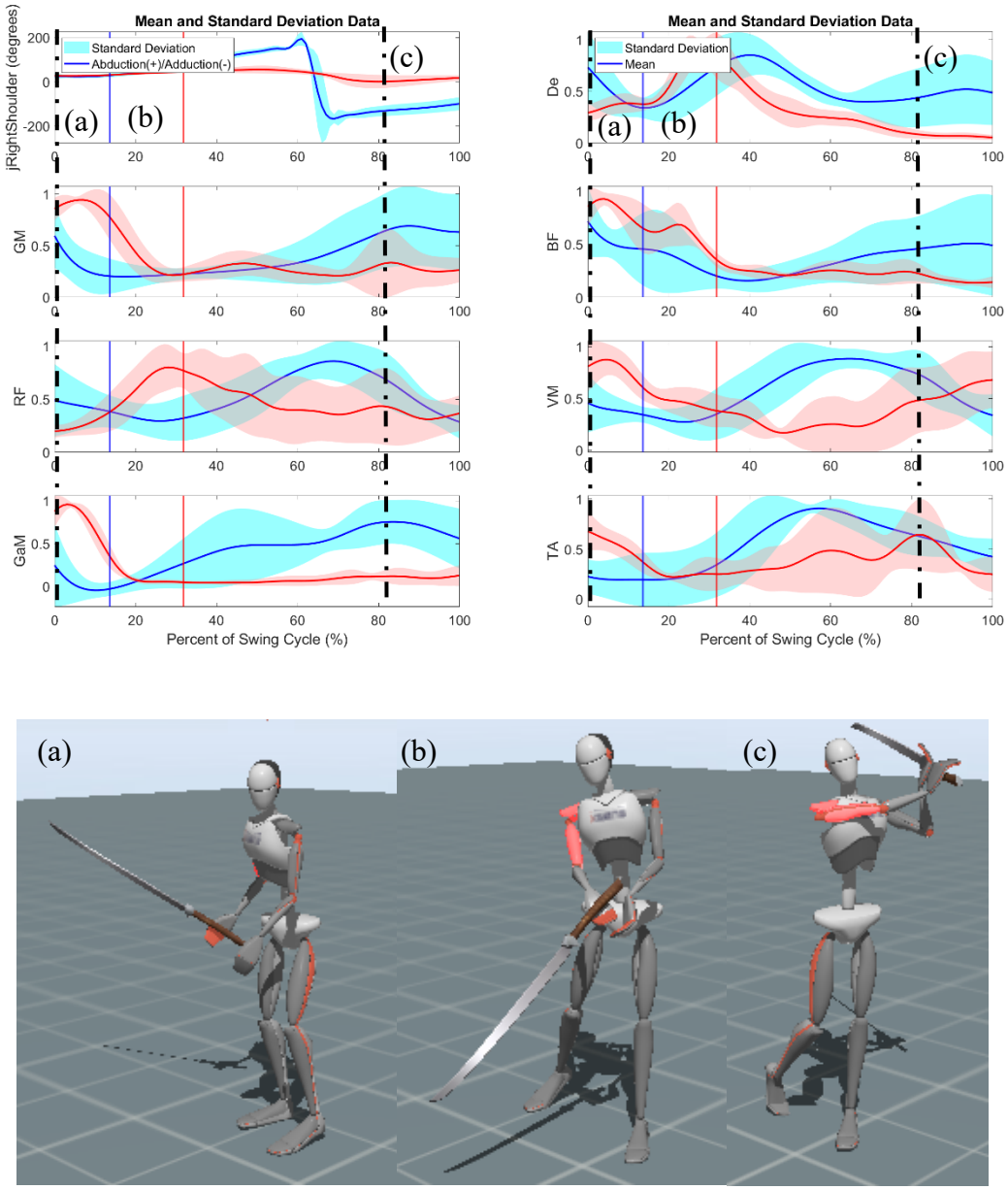

Figure B-99. The graphs depict shoulder abduction and adduction, alongside sEMG data, recorded from non-professionals executing forehand down-the-line groundstrokes. Vertical lines in the graphs indicate various stages of the groundstroke, as demonstrated by XSENS MoCap figurines. Two distinct colors denote two different subjects. The solid line represents the average of five trials, while the shaded region indicates the standard deviation across the same five trials.

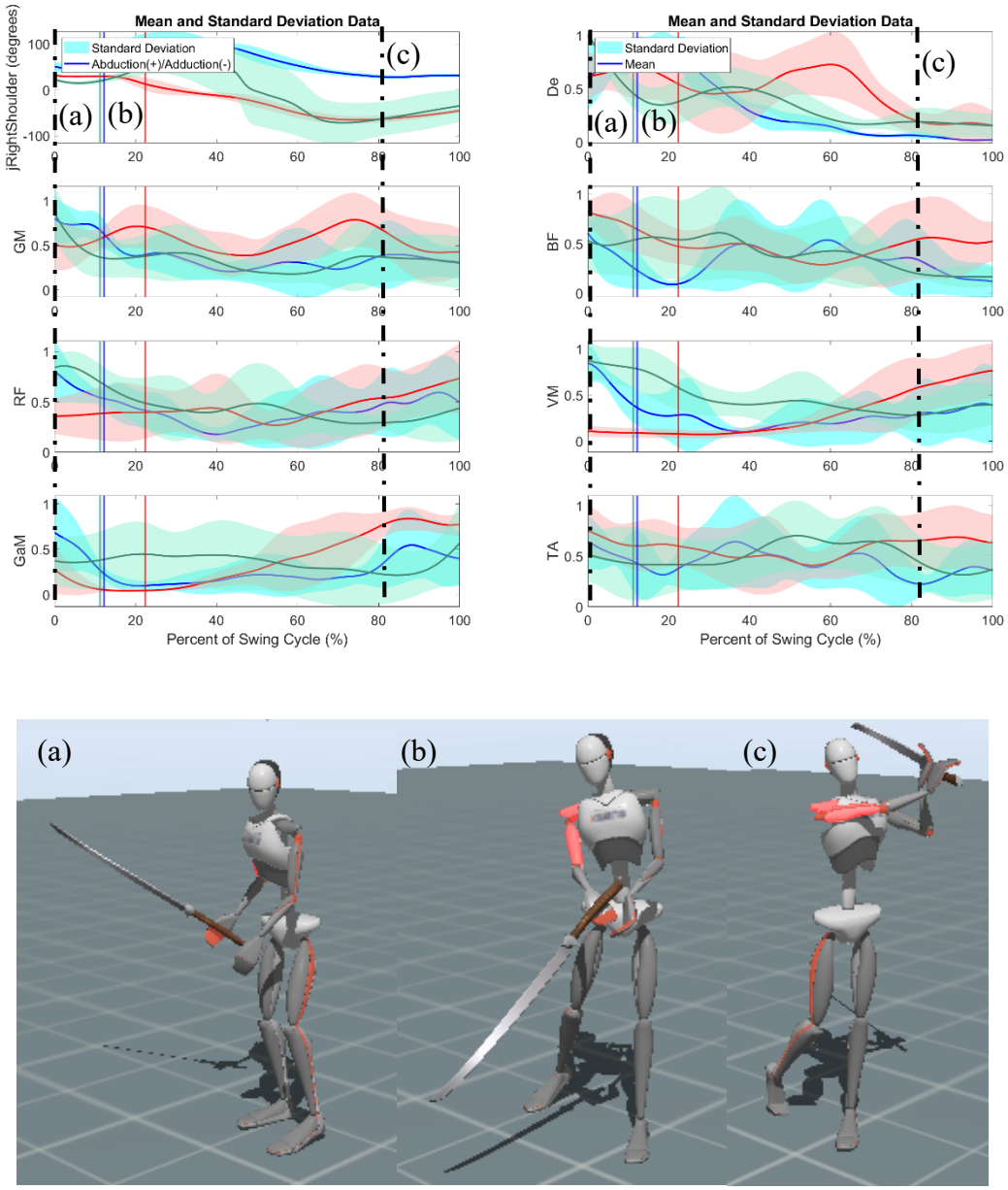

Figure B-100. The graphs depict shoulder abduction and adduction, alongside sEMG data, recorded from non-professionals executing forehand down-the-line groundstrokes. Vertical lines in the graphs indicate various stages of the groundstroke, as demonstrated by XSENS MoCap figurines. Three distinct colors denote three different subjects. The solid line represents the average of five trials, while the shaded region indicates the standard deviation across the same five trials.

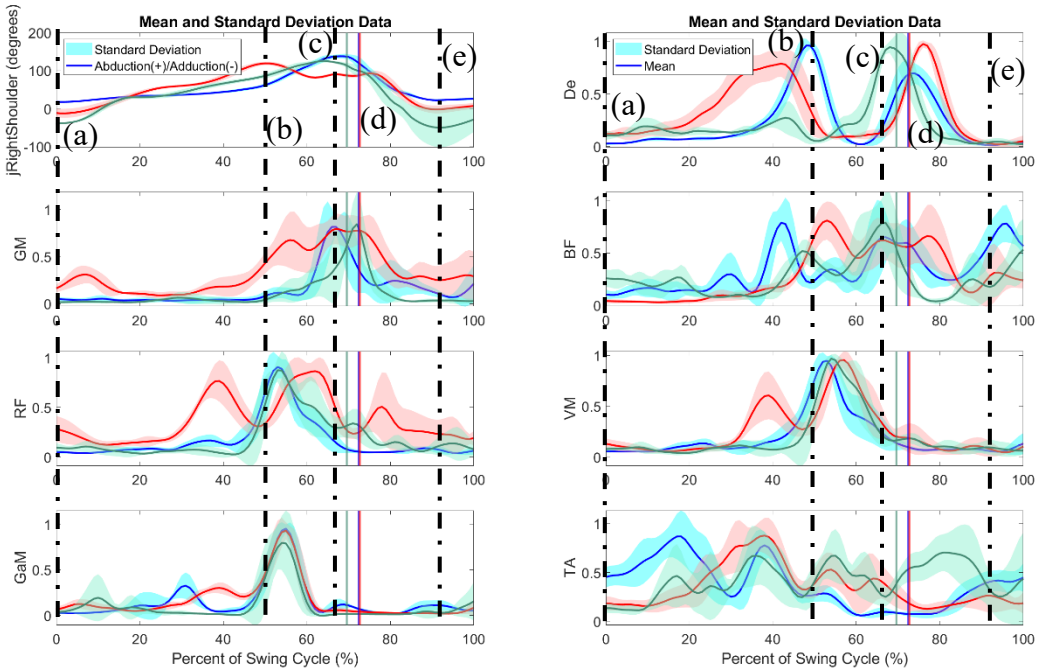

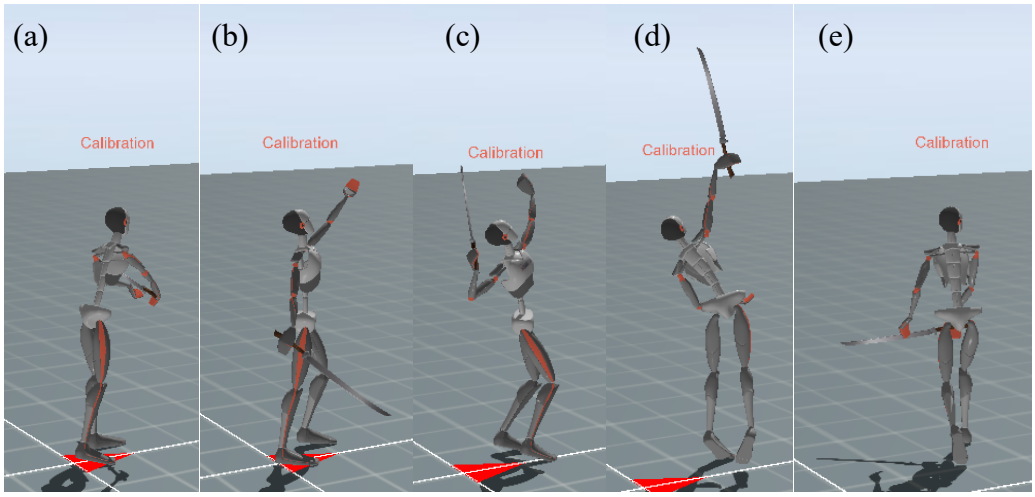

Figure B-101. The graphs depict shoulder abduction and adduction, alongside sEMG data, recorded from non-professionals executing deuce-side serve. Vertical lines in the graphs indicate various stages of the serve, as demonstrated by XSENS MoCap figurines. Three distinct colors denote three different subjects. The solid line represents the average of five trials, while the shaded region indicates the standard deviation across the same five trials.

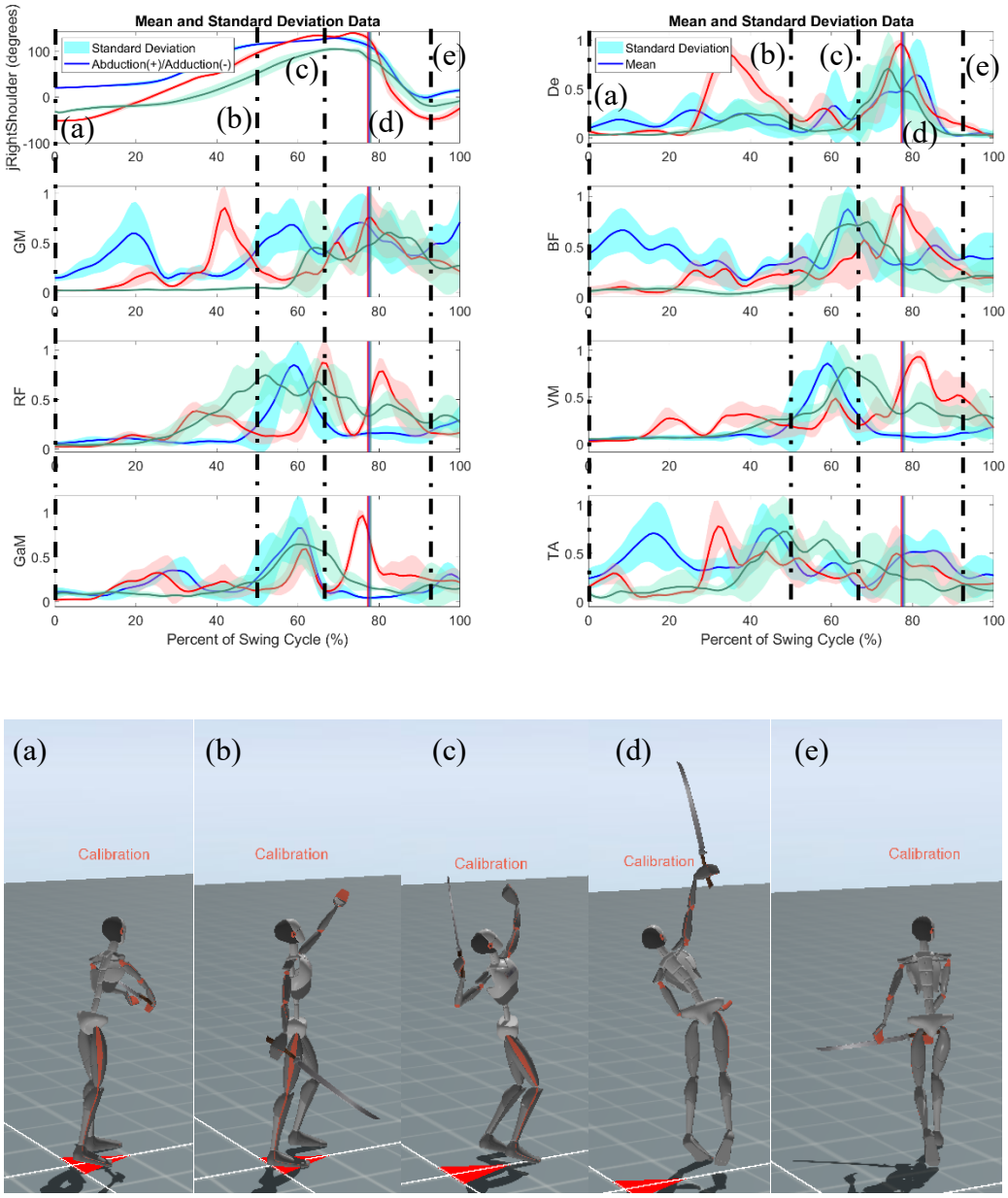

Figure B-102. The graphs depict shoulder abduction and adduction, alongside sEMG data, recorded from non-professionals executing deuce-side serve. Vertical lines in the graphs indicate various stages of the serve, as demonstrated by XSENS MoCap figurines. Three distinct colors denote three different subjects. The solid line represents the average of five trials, while the shaded region indicates the standard deviation across the same five trials.

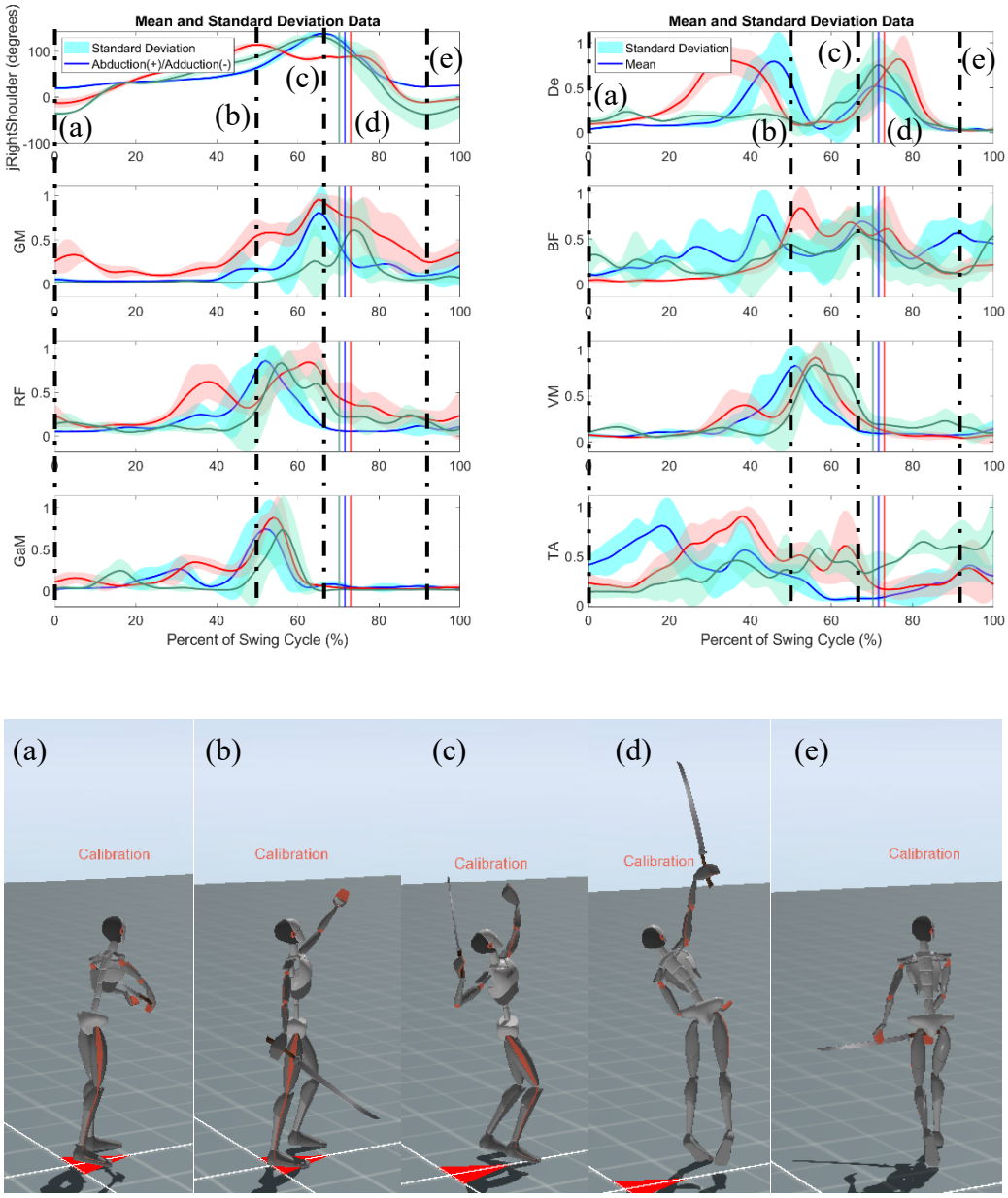

Figure B-103. The graphs depict shoulder abduction and adduction, alongside sEMG data, recorded from non-professionals executing advantage-side serve. Vertical lines in the graphs indicate various stages of the serve, as demonstrated by XSENS MoCap figurines. Three distinct colors denote three different subjects. The solid line represents the average of five trials, while the shaded region indicates the standard deviation across the same five trials.

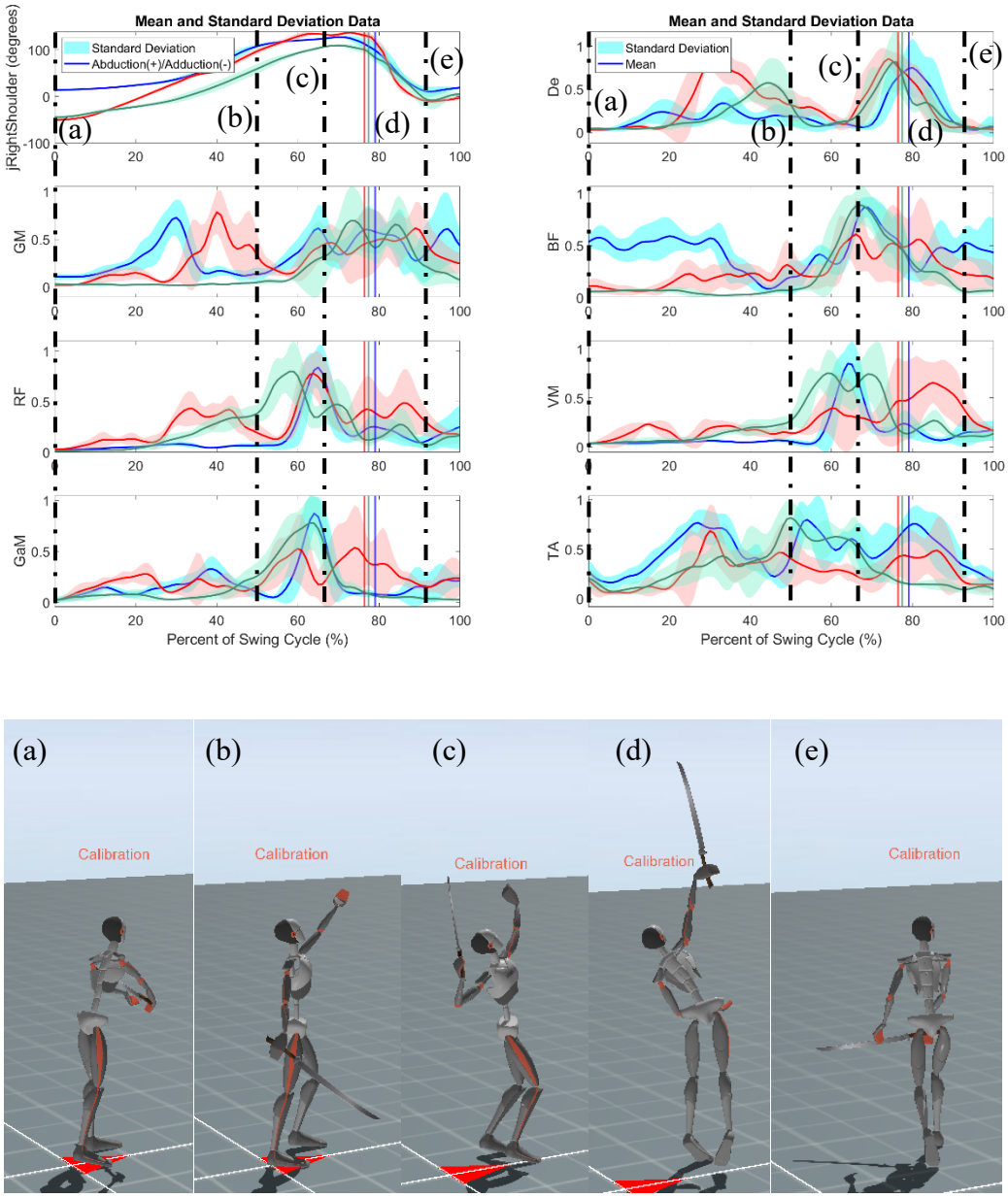

Figure B-104. The graphs depict shoulder abduction and adduction, alongside sEMG data, recorded from non-professionals executing advantage-side serve. Vertical lines in the graphs indicate various stages of the serve, as demonstrated by XSENS MoCap figurines. Three distinct colors denote three different subjects. The solid line represents the average of five trials, while the shaded region indicates the standard deviation across the same five trials.

Appendix C: Code

Main Code 1

```
%%%%%%%%%%%%%%%%%%%%%%%%%%%%%%%%%%%%%%%%%%%%%%%%
% Created on 09-23-2023
% Modified on 1-31-2024
% @ Author: Dr. Yunju Lee & Anton Petrenko
% Description: This script file reads in XSENS and EMG data from ".mvnx'
% and ".xlsx" file types, respectively. The shoulder joint is plotted first
% and the user is prompted to choose the two lowest points of shoulder
% abduction/adduction to find the start and stop times. From there, 20
% seconds are added on to the end time. Using the new start and stop
% time, shoulder joint angle and seven muscles' EMGs are plotted across a
% normalized time scale.
%%%%%%%%%%%%%%%%%%%%%%%%%%%%%%%%%%%%%%%%%%%%%%%%

%% Clearing previous variables
clc;
clear;

%% Reading in XSENS and EMG data
addpath('E:\XSENS data\Tennis Study\TX Analysis - AP')
addpath('E:\XSENS data\Tennis Study\TX Analysis - AP\EMG Files')
addpath('E:\XSENS data\Tennis Study\TX Analysis - AP\Xsens Files')

list = readcell('SubID_Tennis 03-25-2024.xlsx');    % Reading in from the master
spreadsheet

i = 16;     % "i" should be equal to the subject number
            % e.g. if subject is TX08, then "i" should be 8
subID = strcat(cell2mat(list(2,i*2)));

increment = 10;
k = 1;
for j=3:7 % FH-CC01 to FH-CC05
% for j=8:12 % FH-DL01 to FH-DL05
% for j=13:17 % BH-CC01 to BH-CC05
% for j=18:22 % BH-DL01 to BH-DL05
% for j=23:27 % SV-RL01 to SV-RL05
% for j=28:32 % SV-LR01 to SV-LR05

    if (j >= 3 && j <= 7)
        task = 'FH_CC';
    elseif (j >= 8 && j <= 12)
        task = 'FH_DL';
    elseif (j >= 13 && j <= 17)
        task = 'BH_CC';
    elseif (j >= 18 && j <= 22)
        task = 'BH_DL';
    elseif (j >= 23 && j <= 27)
        task = 'SV_RL';
    elseif (j >= 28 && j <= 32)
        task = 'SV_LR';
    end
    name1{1,k} = strcat(subID, '-',cell2mat(list(j,i*2)), '.mvnx');
```

```
    name2{1,k} = strcat(subID, '_',cell2mat(list(j,i*2+1)), '.xlsx');
    k = k + 1;
end

numloops = length(name1);
n = 101;        % Number of points for interpolation

for i=1:numloops
    tree = load_mvnx(name1{1,i});
    figure(1);plot(tree.jointData(8).jointAngleXZY(:,1));
    xlim([0 300]);
    set(gcf,'units','normalized','outerposition',[0 0 1 1])
    ylabel(strcat(tree.jointData(8).label, ' (degrees)')); xlabel('Time (seconds)')
    legend('Abduction(+)/Adduction(-)')

    % Finding highest and lowest points of shoulder ad/abduction
    [x,~]=ginput(2);
    close all;

    % Getting start and end frames
    start_frame{:,i} = round(x(1)); end_frame{:,i} = round(x(2)) + increment;

    %% Declaring time in seconds and XSENS sampling rate for which the trial was
run
    sec = 5;
    XSENS_fs = str2double(tree.metaData.subject_frameRate);

    %% Reading in data
    [t,De1,GM1,BF1,RF1,VM1,GaM1,TA1] = parsePlot(readtable(name2{1,i}));

    % Plotting XSENS data
    % Standard that works
    % figure(2);subplot(8,1,1);plot(tree.jointData(8).jointAngleXZY(:,1));
    % xlim([start_frame end_frame]);
    % set(gcf,'units','normalized','outerposition',[0 0 1 1])
    % ylabel(strcat(tree.jointData(8).label, ' (degrees)')); xlabel('Time
(seconds)')
    % legend('Abduction(+)/Adduction(-)')

    %% Normalizing time and data
    % Either method for choosing time will give the same results
    % t1 = t(start_frame:end_frame);
    % t1 = rescale(t1,0,100);
    t1{:,i} = linspace(0,100,(end_frame{:,i}-start_frame{:,i}+1));

    % Creating start and end times for EMG data
    start_frame_EMG = round((start_frame{:,i}/XSENS_fs) * (length(t)/sec));
    end_frame_EMG = round((end_frame{:,i}/XSENS_fs) * (length(t)/sec));

    % Creating time scale for EMG data
    % Either method for choosing time will give the same results
    % t2 = t(start_frame_EMG:end_frame_EMG);
    % t2 = rescale(t2,0,100);
    t2{:,i} = linspace(0,100,(end_frame_EMG-start_frame_EMG+1));
```

```
    % Extracting desired shoulder joint angle data
    jShoulder = tree.jointData(8).jointAngleXZY(:,1);
    jShoulder1{:,i} = jShoulder(start_frame{:,i}:end_frame{:,i});

    % Extracting desired EMG data
    De2{:,i} = De1(start_frame_EMG:end_frame_EMG);
    GM2{:,i} = GM1(start_frame_EMG:end_frame_EMG);
    BF2{:,i} = BF1(start_frame_EMG:end_frame_EMG);
    RF2{:,i} = RF1(start_frame_EMG:end_frame_EMG);
    VM2{:,i} = VM1(start_frame_EMG:end_frame_EMG);
    GaM2{:,i} = GaM1(start_frame_EMG:end_frame_EMG);
    TA2{:,i} = TA1(start_frame_EMG:end_frame_EMG);

    %% Lowpass filter 500Hz
    [t,De_lf1,GM_lf1,BF_lf1,RF_lf1,VM_lf1,GaM_lf1,TA_lf1] = ...
        lowpass(t,De1,GM1,BF1,RF1,VM1,GaM1,TA1);

    %% Highpass filter 10Hz
    [t,De_hf1,GM_hf1,BF_hf1,RF_hf1,VM_hf1,GaM_hf1,TA_hf1] = ...
        highpass(t,De_lf1,GM_lf1,BF_lf1,RF_lf1,VM_lf1,GaM_lf1,TA_lf1);

    %% Full wave rectification of EMG
    [t,De_filt1,GM_filt1,BF_filt1,RF_filt1,VM_filt1,GaM_filt1,TA_filt1] = ...
        rect(t,De_hf1,GM_hf1,BF_hf1,RF_hf1,VM_hf1,GaM_hf1,TA_hf1);

    %% Linear envelope (2Hz lowpass)
    [t,De_lin1,GM_lin1,BF_lin1,RF_lin1,VM_lin1,GaM_lin1,TA_lin1] = ...
        linEnv(t,De_filt1,GM_filt1,BF_filt1,RF_filt1,VM_filt1,GaM_filt1,TA_filt1);

    %% Extracting desired EMG data
    De_lin2{:,i} = De_lin1(start_frame_EMG:end_frame_EMG);
    GM_lin2{:,i} = GM_lin1(start_frame_EMG:end_frame_EMG);
    BF_lin2{:,i} = BF_lin1(start_frame_EMG:end_frame_EMG);
    RF_lin2{:,i} = RF_lin1(start_frame_EMG:end_frame_EMG);
    VM_lin2{:,i} = VM_lin1(start_frame_EMG:end_frame_EMG);
    GaM_lin2{:,i} = GaM_lin1(start_frame_EMG:end_frame_EMG);
    TA_lin2{:,i} = TA_lin1(start_frame_EMG:end_frame_EMG);
end

%% Finding ball contact point
if (strcmp(task,'SV_RL') | strcmp(task,'SV_LR'))
    for ii=1:numloops
        tree = load_mvnx(name1{1,ii});
        figure(1);plot(tree.segmentData(24).angularVelocity(:,3));
        xlim([start_frame{ii} end_frame{ii}]);
        set(gcf,'units','normalized','outerposition',[0 0 1 1])
        ylabel(strcat(tree.segmentData(24).label, ' (degrees/s)')); xlabel('Time')
        % legend('Abduction(+)/Adduction(-)')

        [contact{ii},~] = ginput(1);
        contact{ii} = round(contact{ii});
        close all;
    end
elseif (strcmp(task,'BH_CC') | strcmp(task,'BH_DL'))
    for ii=1:numloops
```

```
        tree = load_mvnx(name1{1,ii});
        figure(1);plot(tree.segmentData(24).angularVelocity(:,3));
        xlim([start_frame{ii} end_frame{ii}]);
        set(gcf,'units','normalized','outerposition',[0 0 1 1])
        ylabel(strcat(tree.segmentData(24).label, ' (degrees/s)')); xlabel('Time')
        % legend('Abduction(+)/Adduction(-)')

        [contact{ii},~] = ginput(1);
        contact{ii} = round(contact{ii});
        close all;
    end
elseif (strcmp(task,'FH_CC') | strcmp(task,'FH_DL'))
    for ii=1:numloops
        tree = load_mvnx(name1{1,ii});
        figure(1);plot(tree.segmentData(24).angularVelocity(:,3));
        xlim([start_frame{ii} end_frame{ii}]);
        set(gcf,'units','normalized','outerposition',[0 0 1 1])
        ylabel(strcat(tree.segmentData(24).label, ' (degrees/s)')); xlabel('Time')
        % legend('Abduction(+)/Adduction(-)')

        [contact{ii},~] = ginput(1);
        contact{ii} = round(contact{ii});
        close all;
    end
end

% Normalizing the contact to be between 0 - 100
for ii=1:numloops
    contact_norm{ii} = (contact{ii} - start_frame{ii}) / (end_frame{ii} -
start_frame{ii}) * 100;
end

% Averaging the normalized contact points
contact_norm_ave = mean(cat(3,contact_norm{:}),3);

%% Plotting data
% Plotting XSENS data
% for i=1:numloops
%     figure(2);
%     subplot(4,2,1);set(gca,'FontSize',16);plot(t1{:,i},jShoulder1{:,i});
%     set(gcf,'units','normalized','outerposition',[0 0 1 1])
%     title('Raw Data')
%     ylabel(strcat(tree.jointData(8).label, ' (degrees)')); xlabel('Percent of
Serve (%)')
%     legend('Abduction(+)/Adduction(-)')
%     hold on
%     % Plotting raw EMG data in same time frame
%     subplot(4,2,2)
%     set(gca,'FontSize',16)
%     plot(t2{:,i},De2{:,i})
%     title('Raw Data')
%     ylabel('De')
%     hold on
%     % Method that worked previously
%     % subplot(8,1,2)
```

```
%     % plot(t,De1)
%     % xlim([start_frame end_frame])
%     % ylabel('De')
%     subplot(4,2,3)
%     set(gca,'FontSize',16)
%     plot(t2{:,i},GM2{:,i})
%     ylabel('GM')
%     hold on
%     subplot(4,2,4)
%     plot(t2{:,i},BF2{:,i})
%     set(gca,'FontSize',16)
%     ylabel('BF')
%     hold on
%     subplot(4,2,5)
%     set(gcf,'units','normalized','outerposition',[0 0 1 1])
%     set(gca,'FontSize',16)
%     plot(t2{:,i},RF2{:,i})
%     ylabel('RF')
%     hold on
%     subplot(4,2,6)
%     set(gca,'FontSize',16)
%     plot(t2{:,i},VM2{:,i})
%     ylabel('VM')
%     hold on
%     subplot(4,2,7)
%     set(gca,'FontSize',16)
%     plot(t2{:,i},GaM2{:,i})
%     ylabel('GaM')
%     hold on
%     subplot(4,2,8)
%     set(gca,'FontSize',16)
%     plot(t2{:,i},TA2{:,i})
%     ylabel('TA')
%     hold on
%
%     % Plotting XSENS data
%     figure(3);
%     % subplot(8,1,1);plot(tree.jointData(8).jointAngleXZY(:,1));
%     % xlim([start_frame end_frame]);
%     % set(gcf,'units','normalized','outerposition',[0 0 1 1])
%     % ylabel(strcat(tree.jointData(8).label, ' (degrees)')); xlabel('Time
(seconds)')
%     % legend('Abduction(+)/Adduction(-)')
%     subplot(4,2,1);set(gca,'FontSize',16);plot(t1{:,i},jShoulder1{:,i});
%     set(gcf,'units','normalized','outerposition',[0 0 1 1])
%     title('Enveloped Data')
%     ylabel(strcat(tree.jointData(8).label, ' (degrees)')); xlabel('Percent of
Serve (%)')
%     legend('Abduction(+)/Adduction(-)')
%     hold on
%     % Plotting rectified EMG data in same time frame
%     subplot(4,2,2)
%     set(gca,'FontSize',16)
%     plot(t2{:,i},De_lin2{:,i})
%     title('Enveloped Data')
```

```
%     ylabel('De')
%     hold on
%     subplot(4,2,3)
%     set(gca,'FontSize',16)
%     plot(t2{:,i},GM_lin2{:,i})
%     ylabel('GM')
%     hold on
%     subplot(4,2,4)
%     set(gca,'FontSize',16)
%     plot(t2{:,i},BF_lin2{:,i})
%     ylabel('BF')
%     hold on
%     subplot(4,2,5)
%     set(gcf,'units','normalized','outerposition',[0 0 1 1])
%     set(gca,'FontSize',16)
%     plot(t2{:,i},RF_lin2{:,i})
%     ylabel('RF')
%     hold on
%     subplot(4,2,6)
%     set(gca,'FontSize',16)
%     plot(t2{:,i},VM_lin2{:,i})
%     ylabel('VM')
%     hold on
%     subplot(4,2,7)
%     set(gca,'FontSize',16)
%     plot(t2{:,i},GaM_lin2{:,i})
%     ylabel('GaM')
%     hold on
%     subplot(4,2,8)
%     set(gca,'FontSize',16)
%     plot(t2{:,i},TA_lin2{:,i})
%     ylabel('TA')
%     hold on
% end

%% Interpolation
for i = 1:numloops
    x1 = 1:length(jShoulder1{1,i});
    xi1 = linspace(-1,length(jShoulder1{1,i}),n);

    x2 = 1:length(De_lin2{1,i});
    xi2 = linspace(1,length(De_lin2{1,i}),n);

    jShoulder2{1,i} = interp1(x1,jShoulder1{1,i},xi1,'spline');
    De3{1,i} = interp1(x2,De_lin2{1,i},xi2,'spline');
    GM3{1,i} = interp1(x2,GM_lin2{1,i},xi2,'spline');
    BF3{1,i} = interp1(x2,BF_lin2{1,i},xi2,'spline');
    RF3{1,i} = interp1(x2,RF_lin2{1,i},xi2,'spline');
    VM3{1,i} = interp1(x2,VM_lin2{1,i},xi2,'spline');
    GaM3{1,i} = interp1(x2,GaM_lin2{1,i},xi2,'spline');
    TA3{1,i} = interp1(x2,TA_lin2{1,i},xi2,'spline');
end

%% Normalizing the interpolated data
for i = 1:numloops
```

```
    De3{1,i} = De3{1,i}/max(De3{1,i});
    GM3{1,i} = GM3{1,i}/max(GM3{1,i});
    BF3{1,i} = BF3{1,i}/max(BF3{1,i});
    RF3{1,i} = RF3{1,i}/max(RF3{1,i});
    VM3{1,i} = VM3{1,i}/max(VM3{1,i});
    GaM3{1,i} = GaM3{1,i}/max(GaM3{1,i});
    TA3{1,i} = TA3{1,i}/max(TA3{1,i});
end

t3 = 0:100;     % New time scale for interpolated data

%% Plotting interpolated data
for i = 1:numloops
    figure(4)
    subplot(4,2,1)
    set(gca,'FontSize',16)
    plot(t3,jShoulder2{1,i})
    set(gcf,'units','normalized','outerposition',[0 0 1 1])
    title('Enveloped and Interpolated Data')
    ylabel(strcat(tree.jointData(8).label, ' (degrees)')); xlabel('Percent of Serve
(%)')
    legend('Abduction(+)/Adduction(-)','Location','northwest')
    xlim([0 100])
    hold on
    subplot(4,2,2)
    set(gca,'FontSize',16)
    plot(t3,De3{1,i})
    title('Enveloped and Interpolated Data')
    ylabel('De')
    xlim([0 100])
    legend('Trial 1','Trial 2','Trial 3','Trial 4','Trial 5')
    hold on
    subplot(4,2,3)
    set(gca,'FontSize',16)
    plot(t3,GM3{1,i})
    ylabel('GM')
    xlim([0 100])
    hold on
    subplot(4,2,4)
    set(gca,'FontSize',16)
    plot(t3,BF3{1,i})
    ylabel('BF')
    xlim([0 100])
    hold on
    subplot(4,2,5)
    set(gcf,'units','normalized','outerposition',[0 0 1 1])
    set(gca,'FontSize',16)
    plot(t3,RF3{1,i})
    ylabel('RF')
    xlim([0 100])
    hold on
    subplot(4,2,6)
    set(gca,'FontSize',16)
    plot(t3,VM3{1,i})
    ylabel('VM')
```

```
    xlim([0 100])
    hold on
    subplot(4,2,7)
    set(gca,'FontSize',16)
    plot(t3,GaM3{1,i})
    ylabel('GaM')
    xlim([0 100])
    hold on
    subplot(4,2,8)
    set(gca,'FontSize',16)
    plot(t3,TA3{1,i})
    ylabel('TA')
    xlim([0 100])
    hold on
end

%% Finding average and standard deviation of data
jShoulder3_M = mean(cat(3,jShoulder2{:}),3);
jShoulder3_SD = std(cat(3,jShoulder2{:}),[],3);
jShoulder3_UL = jShoulder3_M + jShoulder3_SD;
jShoulder3_LL = jShoulder3_M - jShoulder3_SD;
jShoulder3_IB = [jShoulder3_UL, fliplr(jShoulder3_LL)];

De4_M = mean(cat(3,De3{:}),3);
De4_SD = std(cat(3,De3{:}),[],3);
De4_UL = De4_M + De4_SD;
De4_LL = De4_M - De4_SD;
De4_IB = [De4_UL, fliplr(De4_LL)];

GM4_M = mean(cat(3,GM3{:}),3);
GM4_SD = std(cat(3,GM3{:}),[],3);
GM4_UL = GM4_M + GM4_SD;
GM4_LL = GM4_M - GM4_SD;
GM4_IB = [GM4_UL, fliplr(GM4_LL)];

BF4_M = mean(cat(3,BF3{:}),3);
BF4_SD = std(cat(3,BF3{:}),[],3);
BF4_UL = BF4_M + BF4_SD;
BF4_LL = BF4_M - BF4_SD;
BF4_IB = [BF4_UL, fliplr(BF4_LL)];

RF4_M = mean(cat(3,RF3{:}),3);
RF4_SD = std(cat(3,RF3{:}),[],3);
RF4_UL = RF4_M + RF4_SD;
RF4_LL = RF4_M - RF4_SD;
RF4_IB = [RF4_UL, fliplr(RF4_LL)];

VM4_M = mean(cat(3,VM3{:}),3);
VM4_SD = std(cat(3,VM3{:}),[],3);
VM4_UL = VM4_M + VM4_SD;
VM4_LL = VM4_M - VM4_SD;
VM4_IB = [VM4_UL, fliplr(VM4_LL)];

GaM4_M = mean(cat(3,GaM3{:}),3);
GaM4_SD = std(cat(3,GaM3{:}),[],3);
```

```
GaM4_UL = GaM4_M + GaM4_SD;
GaM4_LL = GaM4_M - GaM4_SD;
GaM4_IB = [GaM4_UL, fliplr(GaM4_LL)];

TA4_M = mean(cat(3,TA3{:}),3);
TA4_SD = std(cat(3,TA3{:}),[],3);
TA4_UL = TA4_M + TA4_SD;
TA4_LL = TA4_M - TA4_SD;
TA4_IB = [TA4_UL, fliplr(TA4_LL)];

t4 = [t3, fliplr(t3)];

%% Plotting the average and standard deviation data
figure(5)
subplot(4,2,1)
fill(t4,jShoulder3_IB,'c','LineStyle','none');
hold on;
plot(t3,jShoulder3_M,'b','LineWidth',2)
xline(contact_norm_ave,'LineWidth',2,'Color','black')
set(gca,'FontSize',16)
set(gcf,'units','normalized','outerposition',[0 0 1 1])
title('Mean and Standard Deviation Data')
ylabel(strcat(tree.jointData(8).label, ' (degrees)')); xlabel('Percent of Serve
(%)')
legend('Standard Deviation','Abduction(+)/Adduction(-)','Location','northwest')
% hold off;
subplot(4,2,2)
fill(t4,De4_IB,'c','LineStyle','none');
hold on;
plot(t3,De4_M,'b','LineWidth',2)
xline(contact_norm_ave,'LineWidth',2,'Color','black')
set(gca,'FontSize',16)
title('Mean and Standard Deviation Data')
ylabel('De')
% hold off;
subplot(4,2,3)
fill(t4,GM4_IB,'c','LineStyle','none');
hold on;
plot(t3,GM4_M,'b','LineWidth',2)
xline(contact_norm_ave,'LineWidth',2,'Color','black')
set(gca,'FontSize',16)
ylabel('GM')
% hold off;
subplot(4,2,4)
fill(t4,BF4_IB,'c','LineStyle','none');
hold on;
plot(t3,BF4_M,'b','LineWidth',2)
xline(contact_norm_ave,'LineWidth',2,'Color','black')
set(gca,'FontSize',16)
ylabel('BF')
% hold off;
subplot(4,2,5)
fill(t4,RF4_IB,'c','LineStyle','none');
hold on;
plot(t3,RF4_M,'b','LineWidth',2)
```

```
xline(contact_norm_ave,'LineWidth',2,'Color','black')
set(gca,'FontSize',16)
ylabel('RF')
% hold off;
subplot(4,2,6)
fill(t4,VM4_IB,'c','LineStyle','none');
hold on;
plot(t3,VM4_M,'b','LineWidth',2)
xline(contact_norm_ave,'LineWidth',2,'Color','black')
set(gca,'FontSize',16)
ylabel('VM')
% hold off;
subplot(4,2,7)
fill(t4,GaM4_IB,'c','LineStyle','none');
hold on;
plot(t3,GaM4_M,'b','LineWidth',2)
xline(contact_norm_ave,'LineWidth',2,'Color','black')
set(gca,'FontSize',16)
ylabel('GaM')
% hold off;
subplot(4,2,8)
fill(t4,TA4_IB,'c','LineStyle','none');
hold on;
plot(t3,TA4_M,'b','LineWidth',2)
xline(contact_norm_ave,'LineWidth',2,'Color','black')
set(gca,'FontSize',16)
ylabel('TA')
% hold off;

%% Saving workspace into command window
save(strcat(subID,'_',task,'.mat'))
```

Main Code 2

```
clc;
clear;

% Name inside () will need to change based on desired subject and task
load("TimePerTrial.mat")
load("TX16_SV_RL.mat")

%% Finding average length of time for task
for i = 1:length(start_frame)
    time(i) = (end_frame{:,i} - start_frame{:,i} + 1)/XSENS_fs;
end

%% Saving data into a struct file
% Trials = ['Trial 1';'Trial 2';'Trial 3';'Trial 4';'Trial 5'];
if (length(start_frame) == 1)
    Trials = ['Trial 1'];
    Time = [time(1)];
elseif (length(start_frame) == 2)
    Trials = ['Trial 1';'Trial 2'];
    Time = [time(1);time(2)];
```

```
elseif (length(start_frame) == 3)
    Trials = ['Trial 1';'Trial 2';'Trial 3'];
    Time = [time(1);time(2);time(3)];
elseif (length(start_frame) == 4)
    Trials = ['Trial 1';'Trial 2';'Trial 3';'Trial 4'];
    Time = [time(1);time(2);time(3);time(4)];
elseif (length(start_frame) == 5)
    Trials = ['Trial 1';'Trial 2';'Trial 3';'Trial 4';'Trial 5'];
    Time = [time(1);time(2);time(3);time(4);time(5)];
end

% msg = sprintf('Average length of time for task = %.2f seconds',ave_length);
% msgbox(msg);
varnames = ["Trials","Time"];
TimePerTrial.(subID).(task) = table(Trials,Time,'VariableNames',varnames);
TimePerTrial = orderfields(TimePerTrial);
% TimePerTrial = orderfields(TimePerTrial.(subID));
save("TimePerTrial.mat","TimePerTrial");

%% Plotting interpolated data
for i = 1:numloops
    figure(1)
    subplot(4,2,1)
    set(gca,'FontSize',16)
    plot(t3,jShoulder2{1,i})
    set(gcf,'units','normalized','outerposition',[0 0 1 1])
    title('Enveloped and Interpolated Data')
    ylabel(strcat(tree.jointData(8).label, ' (degrees)'));
    legend('Abduction(+)/Adduction(-)','Location','northwest')
    xlim([0 100])
    hold on
    subplot(4,2,2)
    set(gca,'FontSize',16)
    plot(t3,De3{1,i})
    title('Enveloped and Interpolated Data')
    ylabel('De')
    xlim([0 100])
    legend('Trial 1','Trial 2','Trial 3','Trial 4','Trial 5')
    hold on
    subplot(4,2,3)
    set(gca,'FontSize',16)
    plot(t3,GM3{1,i})
    ylabel('GM')
    xlim([0 100])
    hold on
    subplot(4,2,4)
    set(gca,'FontSize',16)
    plot(t3,BF3{1,i})
    ylabel('BF')
    xlim([0 100])
    hold on
    subplot(4,2,5)
    set(gcf,'units','normalized','outerposition',[0 0 1 1])
    set(gca,'FontSize',16)
    plot(t3,RF3{1,i})
```

```
    ylabel('RF')
    xlim([0 100])
    hold on
    subplot(4,2,6)
    set(gca,'FontSize',16)
    plot(t3,VM3{1,i})
    ylabel('VM')
    xlim([0 100])
    hold on
    subplot(4,2,7)
    set(gca,'FontSize',16)
    plot(t3,GaM3{1,i})
    ylabel('GaM')
    xlabel('Percent of Swing Cycle (%)')
    xlim([0 100])
    hold on
    subplot(4,2,8)
    set(gca,'FontSize',16)
    plot(t3,TA3{1,i})
    ylabel('TA')
    xlabel('Percent of Swing Cycle (%)')
    xlim([0 100])
    hold on
end

%% Plotting the average and standard deviation data
figure(2)
subplot(4,2,1)
fill(t4,jShoulder3_IB,'c','LineStyle','none');
hold on;
plot(t3,jShoulder3_M,'b','LineWidth',2)
xline(contact_norm_ave,'LineWidth',2,'Color','black')
set(gca,'FontSize',16)
set(gcf,'units','normalized','outerposition',[0 0 1 1])
title('Mean and Standard Deviation Data')
ylabel(strcat(tree.jointData(8).label, ' (degrees)'));
legend('Standard Deviation','Abduction(+)/Adduction(-)','Location','northwest')
% hold off;
subplot(4,2,2)
fill(t4,De4_IB,'c','LineStyle','none');
hold on;
plot(t3,De4_M,'b','LineWidth',2)
xline(contact_norm_ave,'LineWidth',2,'Color','black')
set(gca,'FontSize',16)
title('Mean and Standard Deviation Data')
ylabel('De')
% hold off;
subplot(4,2,3)
fill(t4,GM4_IB,'c','LineStyle','none');
hold on;
plot(t3,GM4_M,'b','LineWidth',2)
xline(contact_norm_ave,'LineWidth',2,'Color','black')
set(gca,'FontSize',16)
ylabel('GM')
% hold off;
```

```
subplot(4,2,4)
fill(t4,BF4_IB,'c','LineStyle','none');
hold on;
plot(t3,BF4_M,'b','LineWidth',2)
xline(contact_norm_ave,'LineWidth',2,'Color','black')
set(gca,'FontSize',16)
ylabel('BF')
% hold off;
subplot(4,2,5)
fill(t4,RF4_IB,'c','LineStyle','none');
hold on;
plot(t3,RF4_M,'b','LineWidth',2)
xline(contact_norm_ave,'LineWidth',2,'Color','black')
set(gca,'FontSize',16)
ylabel('RF')
% hold off;
subplot(4,2,6)
fill(t4,VM4_IB,'c','LineStyle','none');
hold on;
plot(t3,VM4_M,'b','LineWidth',2)
xline(contact_norm_ave,'LineWidth',2,'Color','black')
set(gca,'FontSize',16)
ylabel('VM')
% hold off;
subplot(4,2,7)
fill(t4,GaM4_IB,'c','LineStyle','none');
hold on;
plot(t3,GaM4_M,'b','LineWidth',2)
xline(contact_norm_ave,'LineWidth',2,'Color','black')
set(gca,'FontSize',16)
ylabel('GaM')
xlabel('Percent of Swing Cycle (%)')
% hold off;
subplot(4,2,8)
fill(t4,TA4_IB,'c','LineStyle','none');
hold on;
plot(t3,TA4_M,'b','LineWidth',2)
xline(contact_norm_ave,'LineWidth',2,'Color','black')
set(gca,'FontSize',16)
ylabel('TA')
xlabel('Percent of Swing Cycle (%)')
% hold off;

% Saving figure 1
% figdir = 'E:\XSENS\XSENS data\Tennis Study\TX Analysis - PT\Matlab Figures\PNG';
figdir = 'E:\XSENS data\Tennis Study\TX Analysis - AP\Matlab Figures\(.png)
Figures';
filename1 = strcat(subID,'_',task,'_Raw.png');
saveas(figure(1),fullfile(figdir,filename1));

% Saving figure 2
filename2 = strcat(subID,'_',task,'_M_SD.png');
saveas(figure(2),fullfile(figdir,filename2));
```

parsePlot Function

```
% This function separates individual muscle data from a matrix of muscle
% contractions.
function [t,De,GM,BF,RF,VM,GaM,TA] = parsePlot(data)
    t = table2array(data(:,1)) * 60;
    De = table2array(data(:,4));
    GM = table2array(data(:,5));
    BF = table2array(data(:,6));
    RF = table2array(data(:,7));
    VM = table2array(data(:,8));
    GaM = table2array(data(:,9));
    TA = table2array(data(:,10));
end
```

lowpass Function

```
% This function performs a lowpass filter at 400 Hz
function [t,De_lf,GM_lf,BF_lf,RF_lf,VM_lf,GaM_lf,TA_lf] =
lowpass(t,De,GM,BF,RF,VM,GaM,TA)
    Freq = 1200;
    NyqFreq = Freq/2;
    Lowpass = 400;
    Wn = Lowpass/NyqFreq;
    [B,A] = butter(2,Wn,'low');

    De_lf = filtfilt(B,A,De);
    GM_lf = filtfilt(B,A,GM);
    BF_lf = filtfilt(B,A,BF);
    RF_lf = filtfilt(B,A,RF);
    VM_lf = filtfilt(B,A,VM);
    GaM_lf = filtfilt(B,A,GaM);
    TA_lf = filtfilt(B,A,TA);
end
```

highpass Function

```
% This function performs a highpass filter at 20 Hz
function [t,De_hf,GM_hf,BF_hf,RF_hf,VM_hf,GaM_hf,TA_hf] =
highpass(t,De_lf,GM_lf,BF_lf,RF_lf,VM_lf,GaM_lf,TA_lf)
    Freq = 1200;
    NyqFreq = Freq/2;
    Highpass = 20;
    Wo = Highpass/NyqFreq;
    [D,C] = butter(2,Wo,'high');

    De_hf = filtfilt(D,C,De_lf);
    GM_hf = filtfilt(D,C,GM_lf);
    BF_hf = filtfilt(D,C,BF_lf);
    RF_hf = filtfilt(D,C,RF_lf);
    VM_hf = filtfilt(D,C,VM_lf);
    GaM_hf = filtfilt(D,C,GaM_lf);
    TA_hf = filtfilt(D,C,TA_lf);
end
```

rect Function

```
% This function rectifies the EMG
function [t,De_filt,GM_filt,BF_filt,RF_filt,VM_filt,GaM_filt,TA_filt] =
rect(t,De_hf,GM_hf,BF_hf,RF_hf,VM_hf,GaM_hf,TA_hf)
    De_filt = abs(De_hf);
    GM_filt = abs(GM_hf);
    BF_filt = abs(BF_hf);
    RF_filt = abs(RF_hf);
    VM_filt = abs(VM_hf);
    GaM_filt = abs(GaM_hf);
    TA_filt = abs(TA_hf);
end
```

linEnv Function

```
% This function performs a linear envelope at 2 Hz
function [t,De_lin,GM_lin,BF_lin,RF_lin,VM_lin,GaM_lin,TA_lin] =
linEnv(t,De_filt,GM_filt,BF_filt,RF_filt,VM_filt,GaM_filt,TA_filt)
    Freq = 1200;
    NyqFreq = Freq/2;
    LP = 5;
    Wp = LP/NyqFreq;
    [F,E] = butter(2,Wp,'low');

    De_lin = filtfilt(F,E,De_filt);
    GM_lin = filtfilt(F,E,GM_filt);
    BF_lin = filtfilt(F,E,BF_filt);
    RF_lin = filtfilt(F,E,RF_filt);
    VM_lin = filtfilt(F,E,VM_filt);
    GaM_lin = filtfilt(F,E,GaM_filt);
    TA_lin = filtfilt(F,E,TA_filt);
end
```

Overlaying Professional Data

```
%%%%%%%%%%%%%%%%%%%%%%%%%%%%%%%%%%%%%%%%%%%%%%%%
% Created on 03-28-2024
% Modified on 03-28-2024
% @ Author: Anton Petrenko
% Description: This script file reads in previously recorded and processed
% XSENS data and creates figures in comparison.
%%%%%%%%%%%%%%%%%%%%%%%%%%%%%%%%%%%%%%%%%%%%%%%%

clc;
clear;

% Name inside () will need to change based on desired subject and task
load("TX11_FH_DL.mat")

alpha_num = 0.4;

figure(1)
subplot(4,2,1)
fill(t4,jShoulder3_IB,'c','LineStyle','none');
hold on;
```

```
plot(t3,jShoulder3_M,'b','LineWidth',2)
xline(contact_norm_ave,'LineWidth',2,'Color','blue')
set(gca,'FontSize',16)
set(gcf,'units','normalized','outerposition',[0 0 1 1])
title('Mean and Standard Deviation Data')
ylabel(strcat(tree.jointData(8).label, ' (degrees)'));
% hold off;
subplot(4,2,2)
fill(t4,De4_IB,'c','LineStyle','none');
hold on;
plot(t3,De4_M,'b','LineWidth',2)
xline(contact_norm_ave,'LineWidth',2,'Color','blue')
set(gca,'FontSize',16)
title('Mean and Standard Deviation Data')
ylabel('De')
% hold off;
subplot(4,2,3)
fill(t4,GM4_IB,'c','LineStyle','none');
hold on;
plot(t3,GM4_M,'b','LineWidth',2)
xline(contact_norm_ave,'LineWidth',2,'Color','blue')
set(gca,'FontSize',16)
ylabel('GM')
% hold off;
subplot(4,2,4)
fill(t4,BF4_IB,'c','LineStyle','none');
hold on;
plot(t3,BF4_M,'b','LineWidth',2)
xline(contact_norm_ave,'LineWidth',2,'Color','blue')
set(gca,'FontSize',16)
ylabel('BF')
% hold off;
subplot(4,2,5)
fill(t4,RF4_IB,'c','LineStyle','none');
hold on;
plot(t3,RF4_M,'b','LineWidth',2)
xline(contact_norm_ave,'LineWidth',2,'Color','blue')
set(gca,'FontSize',16)
ylabel('RF')
% hold off;
subplot(4,2,6)
fill(t4,VM4_IB,'c','LineStyle','none');
hold on;
plot(t3,VM4_M,'b','LineWidth',2)
xline(contact_norm_ave,'LineWidth',2,'Color','blue')
set(gca,'FontSize',16)
ylabel('VM')
% hold off;
subplot(4,2,7)
fill(t4,GaM4_IB,'c','LineStyle','none');
hold on;
plot(t3,GaM4_M,'b','LineWidth',2)
xline(contact_norm_ave,'LineWidth',2,'Color','blue')
set(gca,'FontSize',16)
ylabel('GaM')
```

```
xlabel('Percent of Swing Cycle (%)')
% hold off;
subplot(4,2,8)
fill(t4,TA4_IB,'c','LineStyle','none');
hold on;
plot(t3,TA4_M,'b','LineWidth',2)
xline(contact_norm_ave,'LineWidth',2,'Color','blue')
set(gca,'FontSize',16)
ylabel('TA')
xlabel('Percent of Swing Cycle (%)')
hold on;

load("TX12_FH_DL.mat")

subplot(4,2,1)
fill(t4,jShoulder3_IB,[1 0.6 0.6],'LineStyle','none');
hold on;
plot(t3,jShoulder3_M,'r','LineWidth',2)
xline(contact_norm_ave,'LineWidth',2,'Color','red')
set(gca,'FontSize',16)
set(gcf,'units','normalized','outerposition',[0 0 1 1])
title('Mean and Standard Deviation Data')
ylabel(strcat(tree.jointData(8).label, ' (degrees)'));
legend('Standard Deviation','Abduction(+)/Adduction(-)','Location','northwest')
hold off;
alpha(alpha_num)
subplot(4,2,2)
fill(t4,De4_IB,[1 0.6 0.6],'LineStyle','none');
hold on;
plot(t3,De4_M,'r','LineWidth',2)
xline(contact_norm_ave,'LineWidth',2,'Color','red')
set(gca,'FontSize',16)
title('Mean and Standard Deviation Data')
ylabel('De')
legend('Standard Deviation','Mean','Location','northwest')
hold off;
alpha(alpha_num)
subplot(4,2,3)
fill(t4,GM4_IB,[1 0.6 0.6],'LineStyle','none');
hold on;
plot(t3,GM4_M,'r','LineWidth',2)
xline(contact_norm_ave,'LineWidth',2,'Color','red')
set(gca,'FontSize',16)
ylabel('GM')
hold off;
alpha(alpha_num)
subplot(4,2,4)
fill(t4,BF4_IB,[1 0.6 0.6],'LineStyle','none');
hold on;
plot(t3,BF4_M,'r','LineWidth',2)
xline(contact_norm_ave,'LineWidth',2,'Color','red')
set(gca,'FontSize',16)
ylabel('BF')
hold off;
alpha(alpha_num)
```

```
subplot(4,2,5)
fill(t4,RF4_IB,[1 0.6 0.6],'LineStyle','none');
hold on;
plot(t3,RF4_M,'r','LineWidth',2)
xline(contact_norm_ave,'LineWidth',2,'Color','red')
set(gca,'FontSize',16)
ylabel('RF')
hold off;
alpha(alpha_num)
subplot(4,2,6)
fill(t4,VM4_IB,[1 0.6 0.6],'LineStyle','none');
hold on;
plot(t3,VM4_M,'r','LineWidth',2)
xline(contact_norm_ave,'LineWidth',2,'Color','red')
set(gca,'FontSize',16)
ylabel('VM')
hold off;
alpha(alpha_num)
subplot(4,2,7)
fill(t4,GaM4_IB,[1 0.6 0.6],'LineStyle','none');
hold on;
plot(t3,GaM4_M,'r','LineWidth',2)
xline(contact_norm_ave,'LineWidth',2,'Color','red')
set(gca,'FontSize',16)
ylabel('GaM')
xlabel('Percent of Swing Cycle (%)')
hold off;
alpha(alpha_num)
subplot(4,2,8)
fill(t4,TA4_IB,[1 0.6 0.6],'LineStyle','none');
hold on;
plot(t3,TA4_M,'r','LineWidth',2)
xline(contact_norm_ave,'LineWidth',2,'Color','red')
set(gca,'FontSize',16)
ylabel('TA')
xlabel('Percent of Swing Cycle (%)')
hold off;
alpha(alpha_num)

figdir = 'E:\XSENS data\Tennis Study\TX Analysis - AP\Matlab Figures\Pros
Overlayed';
filename1 = strcat('Pros','_',task,'.png');
saveas(figure(1),fullfile(figdir,filename1));
```

Overlaying Non-Professional Data

```
%%%%%%%%%%%%%%%%%%%%%%%%%%%%%%%%%%%%%%%%%%%%%%%%
% Created on 03-28-2024
% Modified on 03-28-2024
% @ Author: Anton Petrenko
% Description: This script file reads in previously recorded and processed
% XSENS data and creates figures in comparison.
%%%%%%%%%%%%%%%%%%%%%%%%%%%%%%%%%%%%%%%%%%%%%%%%

clc;
```

```
clear;

% Name inside () will need to change based on desired subject and task
load("TX08_SV_LR.mat")

alpha_num = 0.4;

figure(1)
subplot(4,2,1)
fill(t4,jShoulder3_IB,'c','LineStyle','none');
hold on;
plot(t3,jShoulder3_M,'b','LineWidth',2)
xline(contact_norm_ave,'LineWidth',2,'Color','blue')
set(gca,'FontSize',16)
set(gcf,'units','normalized','outerposition',[0 0 1 1])
title('Mean and Standard Deviation Data')
ylabel(strcat(tree.jointData(8).label, ' (degrees)'));
% hold off;
subplot(4,2,2)
fill(t4,De4_IB,'c','LineStyle','none');
hold on;
plot(t3,De4_M,'b','LineWidth',2)
xline(contact_norm_ave,'LineWidth',2,'Color','blue')
set(gca,'FontSize',16)
title('Mean and Standard Deviation Data')
ylabel('De')
% hold off;
subplot(4,2,3)
fill(t4,GM4_IB,'c','LineStyle','none');
hold on;
plot(t3,GM4_M,'b','LineWidth',2)
xline(contact_norm_ave,'LineWidth',2,'Color','blue')
set(gca,'FontSize',16)
ylabel('GM')
% hold off;
subplot(4,2,4)
fill(t4,BF4_IB,'c','LineStyle','none');
hold on;
plot(t3,BF4_M,'b','LineWidth',2)
xline(contact_norm_ave,'LineWidth',2,'Color','blue')
set(gca,'FontSize',16)
ylabel('BF')
% hold off;
subplot(4,2,5)
fill(t4,RF4_IB,'c','LineStyle','none');
hold on;
plot(t3,RF4_M,'b','LineWidth',2)
xline(contact_norm_ave,'LineWidth',2,'Color','blue')
set(gca,'FontSize',16)
ylabel('RF')
% hold off;
subplot(4,2,6)
fill(t4,VM4_IB,'c','LineStyle','none');
hold on;
plot(t3,VM4_M,'b','LineWidth',2)
```

```
xline(contact_norm_ave,'LineWidth',2,'Color','blue')
set(gca,'FontSize',16)
ylabel('VM')
% hold off;
subplot(4,2,7)
fill(t4,GaM4_IB,'c','LineStyle','none');
hold on;
plot(t3,GaM4_M,'b','LineWidth',2)
xline(contact_norm_ave,'LineWidth',2,'Color','blue')
set(gca,'FontSize',16)
ylabel('GaM')
xlabel('Percent of Swing Cycle (%)')
% hold off;
subplot(4,2,8)
fill(t4,TA4_IB,'c','LineStyle','none');
hold on;
plot(t3,TA4_M,'b','LineWidth',2)
xline(contact_norm_ave,'LineWidth',2,'Color','blue')
set(gca,'FontSize',16)
ylabel('TA')
xlabel('Percent of Swing Cycle (%)')
hold on;

load("TX10_SV_LR.mat")

subplot(4,2,1)
fill(t4,jShoulder3_IB,[1 0.6 0.6],'LineStyle','none');
hold on;
plot(t3,jShoulder3_M,'r','LineWidth',2)
xline(contact_norm_ave,'LineWidth',2,'Color','red')
set(gca,'FontSize',16)
set(gcf,'units','normalized','outerposition',[0 0 1 1])
title('Mean and Standard Deviation Data')
ylabel(strcat(tree.jointData(8).label, ' (degrees)'));
legend('Standard Deviation','Abduction(+)/Adduction(-)','Location','northwest')
hold on;
alpha(alpha_num)
subplot(4,2,2)
fill(t4,De4_IB,[1 0.6 0.6],'LineStyle','none');
hold on;
plot(t3,De4_M,'r','LineWidth',2)
xline(contact_norm_ave,'LineWidth',2,'Color','red')
set(gca,'FontSize',16)
title('Mean and Standard Deviation Data')
ylabel('De')
legend('Standard Deviation','Mean','Location','northwest')
hold on;
alpha(alpha_num)
subplot(4,2,3)
fill(t4,GM4_IB,[1 0.6 0.6],'LineStyle','none');
hold on;
plot(t3,GM4_M,'r','LineWidth',2)
xline(contact_norm_ave,'LineWidth',2,'Color','red')
set(gca,'FontSize',16)
ylabel('GM')
```

```
hold on;
alpha(alpha_num)
subplot(4,2,4)
fill(t4,BF4_IB,[1 0.6 0.6],'LineStyle','none');
hold on;
plot(t3,BF4_M,'r','LineWidth',2)
xline(contact_norm_ave,'LineWidth',2,'Color','red')
set(gca,'FontSize',16)
ylabel('BF')
hold on;
alpha(alpha_num)
subplot(4,2,5)
fill(t4,RF4_IB,[1 0.6 0.6],'LineStyle','none');
hold on;
plot(t3,RF4_M,'r','LineWidth',2)
xline(contact_norm_ave,'LineWidth',2,'Color','red')
set(gca,'FontSize',16)
ylabel('RF')
hold on;
alpha(alpha_num)
subplot(4,2,6)
fill(t4,VM4_IB,[1 0.6 0.6],'LineStyle','none');
hold on;
plot(t3,VM4_M,'r','LineWidth',2)
xline(contact_norm_ave,'LineWidth',2,'Color','red')
set(gca,'FontSize',16)
ylabel('VM')
hold on;
alpha(alpha_num)
subplot(4,2,7)
fill(t4,GaM4_IB,[1 0.6 0.6],'LineStyle','none');
hold on;
plot(t3,GaM4_M,'r','LineWidth',2)
xline(contact_norm_ave,'LineWidth',2,'Color','red')
set(gca,'FontSize',16)
ylabel('GaM')
xlabel('Percent of Swing Cycle (%)')
hold on;
alpha(alpha_num)
subplot(4,2,8)
fill(t4,TA4_IB,[1 0.6 0.6],'LineStyle','none');
hold on;
plot(t3,TA4_M,'r','LineWidth',2)
xline(contact_norm_ave,'LineWidth',2,'Color','red')
set(gca,'FontSize',16)
ylabel('TA')
xlabel('Percent of Swing Cycle (%)')
hold on;
alpha(alpha_num)

load("TX13_SV_LR.mat")
color_1 = [69 139 116] / 255;
color_2 = [118 238 198]/255;

subplot(4,2,1)
```

```
fill(t4,jShoulder3_IB,color_2,'LineStyle','none');
hold on;
plot(t3,jShoulder3_M,'Color',color_1,'LineWidth',2)
xline(contact_norm_ave,'LineWidth',2,'Color',color_1)
set(gca,'FontSize',16)
set(gcf,'units','normalized','outerposition',[0 0 1 1])
title('Mean and Standard Deviation Data')
ylabel(strcat(tree.jointData(8).label, ' (degrees)'));
legend('Standard Deviation','Abduction(+)/Adduction(-)','Location','northwest')
hold on;
alpha(alpha_num)
subplot(4,2,2)
fill(t4,De4_IB,color_2,'LineStyle','none');
hold on;
plot(t3,De4_M,'Color',color_1,'LineWidth',2)
xline(contact_norm_ave,'LineWidth',2,'Color',color_1)
set(gca,'FontSize',16)
title('Mean and Standard Deviation Data')
ylabel('De')
legend('Standard Deviation','Mean','Location','northwest')
hold on;
alpha(alpha_num)
subplot(4,2,3)
fill(t4,GM4_IB,color_2,'LineStyle','none');
hold on;
plot(t3,GM4_M,'Color',color_1,'LineWidth',2)
xline(contact_norm_ave,'LineWidth',2,'Color',color_1)
set(gca,'FontSize',16)
ylabel('GM')
hold on;
alpha(alpha_num)
subplot(4,2,4)
fill(t4,BF4_IB,color_2,'LineStyle','none');
hold on;
plot(t3,BF4_M,'Color',color_1,'LineWidth',2)
xline(contact_norm_ave,'LineWidth',2,'Color',color_1)
set(gca,'FontSize',16)
ylabel('BF')
hold on;
alpha(alpha_num)
subplot(4,2,5)
fill(t4,RF4_IB,color_2,'LineStyle','none');
hold on;
plot(t3,RF4_M,'Color',color_1,'LineWidth',2)
xline(contact_norm_ave,'LineWidth',2,'Color',color_1)
set(gca,'FontSize',16)
ylabel('RF')
hold on;
alpha(alpha_num)
subplot(4,2,6)
fill(t4,VM4_IB,color_2,'LineStyle','none');
hold on;
plot(t3,VM4_M,'Color',color_1,'LineWidth',2)
xline(contact_norm_ave,'LineWidth',2,'Color',color_1)
set(gca,'FontSize',16)
```

```
ylabel('VM')
hold on;
alpha(alpha_num)
subplot(4,2,7)
fill(t4,GaM4_IB,color_2,'LineStyle','none');
hold on;
plot(t3,GaM4_M,'Color',color_1,'LineWidth',2)
xline(contact_norm_ave,'LineWidth',2,'Color',color_1)
set(gca,'FontSize',16)
ylabel('GaM')
xlabel('Percent of Swing Cycle (%)')
hold on;
alpha(alpha_num)
subplot(4,2,8)
fill(t4,TA4_IB,color_2,'LineStyle','none');
hold on;
plot(t3,TA4_M,'Color',color_1,'LineWidth',2)
xline(contact_norm_ave,'LineWidth',2,'Color',color_1)
set(gca,'FontSize',16)
ylabel('TA')
xlabel('Percent of Swing Cycle (%)')
hold on;
alpha(alpha_num)

figure(2)
load("TX14_SV_LR.mat")
color_1 = 'b';
color_2 = 'c';

subplot(4,2,1)
fill(t4,jShoulder3_IB,color_2,'LineStyle','none');
hold on;
plot(t3,jShoulder3_M,'Color',color_1,'LineWidth',2)
xline(contact_norm_ave,'LineWidth',2,'Color',color_1)
set(gca,'FontSize',16)
set(gcf,'units','normalized','outerposition',[0 0 1 1])
title('Mean and Standard Deviation Data')
ylabel(strcat(tree.jointData(8).label, ' (degrees)'));
legend('Standard Deviation','Abduction(+)/Adduction(-)','Location','northwest')
hold on;
alpha(alpha_num)
subplot(4,2,2)
fill(t4,De4_IB,color_2,'LineStyle','none');
hold on;
plot(t3,De4_M,'Color',color_1,'LineWidth',2)
xline(contact_norm_ave,'LineWidth',2,'Color',color_1)
set(gca,'FontSize',16)
title('Mean and Standard Deviation Data')
ylabel('De')
legend('Standard Deviation','Mean','Location','northwest')
hold on;
alpha(alpha_num)
subplot(4,2,3)
fill(t4,GM4_IB,color_2,'LineStyle','none');
hold on;
```

```
plot(t3,GM4_M,'Color',color_1,'LineWidth',2)
xline(contact_norm_ave,'LineWidth',2,'Color',color_1)
set(gca,'FontSize',16)
ylabel('GM')
hold on;
alpha(alpha_num)
subplot(4,2,4)
fill(t4,BF4_IB,color_2,'LineStyle','none');
hold on;
plot(t3,BF4_M,'Color',color_1,'LineWidth',2)
xline(contact_norm_ave,'LineWidth',2,'Color',color_1)
set(gca,'FontSize',16)
ylabel('BF')
hold on;
alpha(alpha_num)
subplot(4,2,5)
fill(t4,RF4_IB,color_2,'LineStyle','none');
hold on;
plot(t3,RF4_M,'Color',color_1,'LineWidth',2)
xline(contact_norm_ave,'LineWidth',2,'Color',color_1)
set(gca,'FontSize',16)
ylabel('RF')
hold on;
alpha(alpha_num)
subplot(4,2,6)
fill(t4,VM4_IB,color_2,'LineStyle','none');
hold on;
plot(t3,VM4_M,'Color',color_1,'LineWidth',2)
xline(contact_norm_ave,'LineWidth',2,'Color',color_1)
set(gca,'FontSize',16)
ylabel('VM')
hold on;
alpha(alpha_num)
subplot(4,2,7)
fill(t4,GaM4_IB,color_2,'LineStyle','none');
hold on;
plot(t3,GaM4_M,'Color',color_1,'LineWidth',2)
xline(contact_norm_ave,'LineWidth',2,'Color',color_1)
set(gca,'FontSize',16)
ylabel('GaM')
xlabel('Percent of Swing Cycle (%)')
hold on;
alpha(alpha_num)
subplot(4,2,8)
fill(t4,TA4_IB,color_2,'LineStyle','none');
hold on;
plot(t3,TA4_M,'Color',color_1,'LineWidth',2)
xline(contact_norm_ave,'LineWidth',2,'Color',color_1)
set(gca,'FontSize',16)
ylabel('TA')
xlabel('Percent of Swing Cycle (%)')
hold on;
alpha(alpha_num)

load("TX15_SV_LR.mat")
```

```
color_1 = 'r';
color_2 = [1 0.6 0.6];

subplot(4,2,1)
fill(t4,jShoulder3_IB,color_2,'LineStyle','none');
hold on;
plot(t3,jShoulder3_M,'Color',color_1,'LineWidth',2)
xline(contact_norm_ave,'LineWidth',2,'Color',color_1)
set(gca,'FontSize',16)
set(gcf,'units','normalized','outerposition',[0 0 1 1])
title('Mean and Standard Deviation Data')
ylabel(strcat(tree.jointData(8).label, ' (degrees)'));
legend('Standard Deviation','Abduction(+)/Adduction(-)','Location','northwest')
hold on;
alpha(alpha_num)
subplot(4,2,2)
fill(t4,De4_IB,color_2,'LineStyle','none');
hold on;
plot(t3,De4_M,'Color',color_1,'LineWidth',2)
xline(contact_norm_ave,'LineWidth',2,'Color',color_1)
set(gca,'FontSize',16)
title('Mean and Standard Deviation Data')
ylabel('De')
legend('Standard Deviation','Mean','Location','northwest')
hold on;
alpha(alpha_num)
subplot(4,2,3)
fill(t4,GM4_IB,color_2,'LineStyle','none');
hold on;
plot(t3,GM4_M,'Color',color_1,'LineWidth',2)
xline(contact_norm_ave,'LineWidth',2,'Color',color_1)
set(gca,'FontSize',16)
ylabel('GM')
hold on;
alpha(alpha_num)
subplot(4,2,4)
fill(t4,BF4_IB,color_2,'LineStyle','none');
hold on;
plot(t3,BF4_M,'Color',color_1,'LineWidth',2)
xline(contact_norm_ave,'LineWidth',2,'Color',color_1)
set(gca,'FontSize',16)
ylabel('BF')
hold on;
alpha(alpha_num)
subplot(4,2,5)
fill(t4,RF4_IB,color_2,'LineStyle','none');
hold on;
plot(t3,RF4_M,'Color',color_1,'LineWidth',2)
xline(contact_norm_ave,'LineWidth',2,'Color',color_1)
set(gca,'FontSize',16)
ylabel('RF')
hold on;
alpha(alpha_num)
subplot(4,2,6)
fill(t4,VM4_IB,color_2,'LineStyle','none');
```

```
hold on;
plot(t3,VM4_M,'Color',color_1,'LineWidth',2)
xline(contact_norm_ave,'LineWidth',2,'Color',color_1)
set(gca,'FontSize',16)
ylabel('VM')
hold on;
alpha(alpha_num)
subplot(4,2,7)
fill(t4,GaM4_IB,color_2,'LineStyle','none');
hold on;
plot(t3,GaM4_M,'Color',color_1,'LineWidth',2)
xline(contact_norm_ave,'LineWidth',2,'Color',color_1)
set(gca,'FontSize',16)
ylabel('GaM')
xlabel('Percent of Swing Cycle (%)')
hold on;
alpha(alpha_num)
subplot(4,2,8)
fill(t4,TA4_IB,color_2,'LineStyle','none');
hold on;
plot(t3,TA4_M,'Color',color_1,'LineWidth',2)
xline(contact_norm_ave,'LineWidth',2,'Color',color_1)
set(gca,'FontSize',16)
ylabel('TA')
xlabel('Percent of Swing Cycle (%)')
hold on;
alpha(alpha_num)

load("TX16_SV_LR.mat")
color_1 = [69 139 116] / 255;
color_2 = [118 238 198]/255;

subplot(4,2,1)
fill(t4,jShoulder3_IB,color_2,'LineStyle','none');
hold on;
plot(t3,jShoulder3_M,'Color',color_1,'LineWidth',2)
xline(contact_norm_ave,'LineWidth',2,'Color',color_1)
set(gca,'FontSize',16)
set(gcf,'units','normalized','outerposition',[0 0 1 1])
title('Mean and Standard Deviation Data')
ylabel(strcat(tree.jointData(8).label, ' (degrees)'));
legend('Standard Deviation','Abduction(+)/Adduction(-)','Location','northwest')
hold on;
alpha(alpha_num)
subplot(4,2,2)
fill(t4,De4_IB,color_2,'LineStyle','none');
hold on;
plot(t3,De4_M,'Color',color_1,'LineWidth',2)
xline(contact_norm_ave,'LineWidth',2,'Color',color_1)
set(gca,'FontSize',16)
title('Mean and Standard Deviation Data')
ylabel('De')
legend('Standard Deviation','Mean','Location','northwest')
hold on;
alpha(alpha_num)
```

```
subplot(4,2,3)
fill(t4,GM4_IB,color_2,'LineStyle','none');
hold on;
plot(t3,GM4_M,'Color',color_1,'LineWidth',2)
xline(contact_norm_ave,'LineWidth',2,'Color',color_1)
set(gca,'FontSize',16)
ylabel('GM')
hold on;
alpha(alpha_num)
subplot(4,2,4)
fill(t4,BF4_IB,color_2,'LineStyle','none');
hold on;
plot(t3,BF4_M,'Color',color_1,'LineWidth',2)
xline(contact_norm_ave,'LineWidth',2,'Color',color_1)
set(gca,'FontSize',16)
ylabel('BF')
hold on;
alpha(alpha_num)
subplot(4,2,5)
fill(t4,RF4_IB,color_2,'LineStyle','none');
hold on;
plot(t3,RF4_M,'Color',color_1,'LineWidth',2)
xline(contact_norm_ave,'LineWidth',2,'Color',color_1)
set(gca,'FontSize',16)
ylabel('RF')
hold on;
alpha(alpha_num)
subplot(4,2,6)
fill(t4,VM4_IB,color_2,'LineStyle','none');
hold on;
plot(t3,VM4_M,'Color',color_1,'LineWidth',2)
xline(contact_norm_ave,'LineWidth',2,'Color',color_1)
set(gca,'FontSize',16)
ylabel('VM')
hold on;
alpha(alpha_num)
subplot(4,2,7)
fill(t4,GaM4_IB,color_2,'LineStyle','none');
hold on;
plot(t3,GaM4_M,'Color',color_1,'LineWidth',2)
xline(contact_norm_ave,'LineWidth',2,'Color',color_1)
set(gca,'FontSize',16)
ylabel('GaM')
xlabel('Percent of Swing Cycle (%)')
hold on;
alpha(alpha_num)
subplot(4,2,8)
fill(t4,TA4_IB,color_2,'LineStyle','none');
hold on;
plot(t3,TA4_M,'Color',color_1,'LineWidth',2)
xline(contact_norm_ave,'LineWidth',2,'Color',color_1)
set(gca,'FontSize',16)
ylabel('TA')
xlabel('Percent of Swing Cycle (%)')
hold on;
```

```
alpha(alpha_num)

figdir = 'E:\XSENS data\Tennis Study\TX Analysis - AP\Matlab Figures\Non Pros
Overlayed';
filename1 = strcat('Non-Pros1','_',task,'.png');
saveas(figure(1),fullfile(figdir,filename1));
filename2 = strcat('Non-Pros2','_',task,'.png');
saveas(figure(2),fullfile(figdir,filename2));
```

Arduino Code

```
enum switch_states {
  OFF,
  ON
} state = OFF;

// Setting pins
const byte delay_s = 5;         // Number that can be changed for delay
const byte Xsens = 7;
const byte EMG = 8;             // Plug into odd side of backpack unit. Toe or #1.
const byte not_recording = 9;
const byte recording = 10;
const byte interruptPin = 3;
// int first, second;
// volatile byte state = LOW;

void setup() {
  Serial.begin(9600);
  pinMode(not_recording, OUTPUT);
  pinMode(recording, OUTPUT);
  pinMode(Xsens, OUTPUT);
  pinMode(EMG, OUTPUT);
  pinMode(interruptPin, INPUT_PULLUP);  // Making the input pin high == 5 V
  // Attaching interrupt to pin 3 to look for the falling edge
  attachInterrupt(digitalPinToInterrupt(interruptPin), switch_status, FALLING);
}

void loop() {
  if(state == OFF)
  {
    digitalWrite(recording, LOW);
    digitalWrite(Xsens, LOW);
    digitalWrite(EMG, HIGH);
    digitalWrite(not_recording, HIGH);

    // Serial.println("Off");
  }
  else if(state == ON)
  {
```

```
    digitalWrite(recording, HIGH);
    digitalWrite(not_recording, LOW);
    digitalWrite(Xsens, HIGH);
    digitalWrite(EMG, LOW);
    // Serial.println("On");
    // first = millis();
    delay(1000*delay_s);
    // second = millis();
    // Serial.println(second-first);
    state = OFF;
  }
}

void switch_status() {
  if(state == OFF)
  {
    state = ON;
  }
  // else if(state == ON)
  // {
  //   state = OFF;
  // }
}
```

References

[1] Menolotto, M., Komaris, D.-S., Tedesco, S., O'Flynn, B., & Walsh, M. (2020). Motion Capture Technology in Industrial Applications: A Systematic Review. Sensors, 20(19), 5687. MDPI AG. Retrieved from http://dx.doi.org/10.3390/s20195687

[2] Zhang, Z. (2012). Microsoft kinect sensor and its effect. IEEE multimedia, 19(2), 4-10.

[3]Roetenberg, D., Luinge, H., & Slycke, P. (2009). Xsens MVN: Full 6DOF human motion tracking using miniature inertial sensors. Xsens Motion Technologies BV, Tech. Rep, 1, 1-7.

[4] Bohannon, R. W., Harrison, S., & Kinsella-Shaw, J. (2009). Reliability and validity of pendulum test measures of spasticity obtained with the Polhemus tracking system from patients with chronic stroke. Journal of neuroengineering and rehabilitation, 6, 1-7.

[5] Tamir, M.; Oz, G. Real-Time Objects Tracking and Motion Capture in Sports Events. U.S. Patent Application No. 11/909,080, 14 August 2008.

[6] Pueo, B., & Jimenez-Olmedo, J. M. (2017). Application of motion capture technology for sport performance analysis. RETOS. Nuevas Tendencias en Educación Fısica, Deporte y Recreación,(32).

[7] Adesida, Y., Papi, E., & McGregor, A. H. (2019). Exploring the Role of Wearable Technology in Sport Kinematics and Kinetics: A Systematic Review. Sensors, 19(7), 1597. MDPI AG. Retrieved from http://dx.doi.org/10.3390/s19071597

[8] Hornestam, J. F., Souza, T. R., Magalhães, F. A., Begon, M., Santos, T. R. T., & Fonseca, S. T. (2021). The effects of knee flexion on tennis serve performance of intermediate level tennis players. Sensors, 21(16), 5254.

[9] Pedro, B., João, F., Lara, J. P., Cabral, S., Carvalho, J., & Veloso, A. P. (2022). Evaluation of upper limb joint contribution to racket head speed in elite tennis players using imu sensors: Comparison between the cross-court and inside-out attacking forehand drive. Sensors, 22(3), 1283.

[10] Büthe, L., Blanke, U., Capkevics, H., & Tröster, G. (2016, June). A wearable sensing system for timing analysis in tennis. In 2016 IEEE 13th International Conference on Wearable and Implantable Body Sensor Networks (BSN) (pp. 43-48). IEEE.

[11] Farina, D., Merletti, R., & Enoka, R. M. (2014). The extraction of neural strategies from the surface EMG: an update. Journal of Applied Physiology, 117(11), 1215-1230.

[12] Chow, J. W., Shim, J. H., & Lim, Y. T. (2003). Lower trunk muscle activity during the tennis serve. Journal of science and medicine in sport, 6(4), 512-518.

[13] Knudson, D., & Blackwell, J. (2000). Trunk muscle activation in open stance and square stance tennis forehands. International journal of sports medicine, 21(05), 321-324.

[14] Girard, O. L. I. V. I. E. R., Micallef, J. P., & Millet, G. P. (2005). Lower-limb activity during the power serve in tennis: effects of performance level. Medicine and science in sports and exercise, 37(6), 1021-1029.

[15] Chow, J. W., Park, S. A., & Tillman, M. D. (2009). Lower trunk kinematics and muscle activity during different types of tennis serves. BMC Sports Science, Medicine and Rehabilitation, 1, 1-14.

[16] Fenter, B., Marzilli, T. S., Wang, Y. T., & Dong, X. N. (2017). Effects of a Three-Set Tennis match on knee kinematics and leg muscle activation during the tennis serve. Perceptual and Motor Skills, 124(1), 214-232.

[17] Hermens, H. J., Freriks, B., Disselhorst-Klug, C., & Rau, G. (2000). Development of recommendations for SEMG sensors and sensor placement procedures. Journal of electromyography and Kinesiology, 10(5), 361-374.

[18] Schepers, M., Giuberti, M., & Bellusci, G. (2018). Xsens MVN: Consistent tracking of human motion using inertial sensing. Xsens Technol, 1(8), 1-8.

[19] Manual, M. U., & Enschede, N. (2021). Available online: https://www. xsens. com/hubfs/Downloads/usermanual. MVN_User_Manual. pdf (accessed on 13 December 2022).

[20] Shafizadeh, M., Bonner, S., Barnes, A., & Fraser, J. (2020). Effects of task and environmental constraints on axial kinematic synergies during the tennis service in expert players. European Journal of Sport Science, 20(9), 1178–1186.

[21] Williams, J. (n.d.). *Vicon Motion Capture: Perceiving Systems*. Max Planck Institute for Intelligent Systems. https://ps.is.mpg.de/pages/motion-capture

[22] Abu-Faraj, Ziad & Harris, Gerald & Smith, Peter & Hassani, Sahar. (2015). Human Gait and Clinical Movement Analysis. 10.1002/047134608X.W6606.pub2.

[23] All about EMG. Noraxon USA. (2021, June 15). https://www.noraxon.com/all-about-emg/

[24] Motion Lab Systems Inc. (n.d.). https://www.motion-labs.com/pdf/ma400_user_manual.pdf